TECHNISCHE UNIVERSITÄT MÜNCHEN
WACKER-Lehrstuhl für Makromolekulare Chemie

CO_2 ACTIVATION USING NITROGEN-BEARING DONORS: CAPTURING OF CO_2 USING [*n*]-OLIGOUREAS AS NOVEL GREEN SORBENTS

ABDUSSALAM KAYED YOUSEF QAROUSH

Vollständiger Abdruck der von der Fakultät für Chemie der Technischen Universität München zur Erlangung des akademischen Grades eines

Doktors der Naturwissenschaften (Dr. rer. nat.)

genehmigten Dissertation.

Vorsitzender:	Univ.-Prof. Dr. Tom Nilges
Prüfer der Dissertation:	1. Univ.-Prof. Dr. Dr. h. c. Bernhard Rieger
	2. Jun.-Prof. Dr. Konrad Tiefenbacher

Die Dissertation wurde am 11.07.2014 bei der Technischen Universität München eingereicht und durch die Fakultät für Chemie am 05.08.2014 angenommen.

DEDICATION

"O MY LORD! ADVANCE ME IN KNOWLEDGE" Taha (20:114)

To my late Grandmother 'Aziza H. Saleh', with her unforgettable "Whole-family in one" character. I have always been impressed by her way of life and thinking and by her constant encouragement to me ever since I was a preschooler. Sadly, she passed away while I was pursuing my PhD in October, 2012. I could never do her right by my humble words, only that may God have mercy upon her soul.

To my beloved supportive father 'Prof. Dr. Kayed Qaroush' **and mother** 'Arifah A. Abdullah', who were truly my guardians, source of inspiration, success, peace and enlightenment. They taught me what I know, and gave me their best in order to deal with real-life problems to be the person I am today. Mom and dad, without your support and encouragement, I would have never proceeded with my studies an inch farther.

To the Qaroushes represented by brothers and sisters, nephews and nieces. Worldwide, they were much more connected to me than simple flesh and blood. *A whole network was established among us along the globe, ranging from Asia (Jordan and KSA), North America (USA), South America (Venezuela) to include me in Europe (Germany).*

To the Abdullahs, Othmans, and Nakhlehs, who gave me all the hope, support and respect I needed wherever I went. I was extremely happy with their presence. I would never be what I am without their encouragement.

To Mr. Mohammed Abu-Khaira and his respectful family as well, who were and still the guardians and consultants that I have always resorted to since I established to start my PhD degree in Germany.

To whom it may concern, thank you all for your great support and trust.

Abdussalam K. Qaroush

August, 2014

ACKNOWLEDGEMENT

Firstly, I would like to thank Prof. Dr. Dr. h.c Bernhard Rieger, My PhD advisor and mentor who has really given me the driving force and the full thrust to finish my thesis. I was extremely happy to be in his Chair, as well as accompanying him to different conferences and scientific events, *viz.* "October, 2010, Dead Sea, Jordan", "December, 2010, Thuwal, Saudi Arabia", together with "October, 2012, Essen, Germany". Moreover, I would like to thank the committee members represented by Prof. Dr. Tom Nilges and Prof. Dr. Konrad Tiefenbacher. They really enlightened me with their knowledge and expertise that I would be ungrateful if I do not express my sincere thanks and gratitude to them. I am really looking forward to working with them in the near future.

Thanks also to my PhD sponsor 'King Abdullah University of Science and Technology' (**KAUST**), without its support this work would not be feasible. Furthermore, I should pay my respects to the 'Technical University of Munich's Graduate School' (**TUM-GS**), for its contribution as a *2012-travelling grant* to the "*243rd American Chemical Society (ACS) national meeting*" that was held in Philadelphia, USA, 2012. In addition, being an active member in this respective organization flourished my soft skills and increased my package of high-impact, task-oriented training courses. New horizons and perspectives have been paved for me throughout their collaborative efforts and keen search for 'top-quality' PhD researchers in all fields. Thanks also are paid to *German Chemical Society* (**GDCh**), for funding my *2014-travelling grant* to the "*Gordon Research Conference on Green Chemistry-2014*" that will be held in Hong Kong, China.

As well, thanks are to be paid to our Jordanian research partners and their respected universities, *viz.*, German Jordan University (**GJU**) represented by Dr. Malyuba A. Abu-Daabes, Jordan University (**JU**) represented by Dr. Hatem M. Alsyouri and the Hashemite University (**HU**) represented by Prof. Dr. Adnan S. Abu-Surrah, who I was extremely happy to share some of our research activities with.

Thanks also are paid to colleagues and research partners in the Technical University of Munich (**TUM**), *viz.* Dr. Carsten Troll my PhD co-supervisor, Dr. Sergei I. Vagin, Dr. Dante A. Castillo-

Molina, my B. Sc. and M. Sc. students, along the staff of the “WACKER-Chair for Macromolecular Chemistry” especially, MSc, Andriy Pliktha. They truly were helpful with their fruitful discussions, and provided me with the kinetic energy and driving force that was sufficient to get me to my goal.

Thanks also to the four musketeers of the WACKER-Chair, *viz.*, Mrs. Sabine Saul-Hubrich, Mrs. Annette Bauer, Mrs. Gabriele Uruk, and Mrs. Sabine Martinetz-Groβe. They really made my presence in the chair to be so smooth, comfortable and time- and work-efficient. I really thank them from the bottom of my heart.

To Mr. Mahmoud Kayari with his thriving character and good manners, who I used to spend some time with during the rush hour.

Thanks also to my colleagues and friends, Dr. Ahmad Habbaba, Dr. Marwan Radi, Dr. Mahmoud Hassouneh, Mr. Timo Hawamdeh, and Mr. Muhammad Sheikh-Ali together their supporting families. In addition, thanks to all of my friends and students in Germany and Jordan. They were extremely caring, passionate and helpful. Once you need them, you find them. They truly embody ‘*a friend in need is a friend indeed*’.

LIST OF PUBLICATIONS

A. Publications

Herein, a brief summary for the scientific disseminations and achievements is given while performing my PhD work in the WACKER-Chair for Macromolecular Chemistry, at the Technische Universität München (TUM), Germany.

1. **A. K. Qaroush**, A. S. Al-Hamayda, Y. K. Khashman, S. I. Vagin, C. Troll, and B. Rieger. "Highly Efficient Isocyanate-Free Microwave-Assisted Synthesis of [*6*]-Oligourea". *Catal. Sci Technol.*, ***Hot Article***, **2013**, *3*, 2221-2226.
2. **A. K. Qaroush**, A. S. Al-Hamayda, Y. K. Khashman, S. I. Vagin, C. Troll, and B. Rieger. *Catal. Sci. Technol.*, ***Cover Page***, ***inside front cover***, **2013**, *3*, 2150-2150, DOI: 10.1039/C3CY90028B.
3. **A. K. Qaroush**, D. A. Castillo-Molina, C. Troll, M. A. Abu-Daabes, H. M. Alsyouri, A. S. Abu-Surrah, and B. Rieger. Towards the design of robust [*n*]-oligourea-based CO_2-sorbents following green chemistry protocols, *ChemSusChem*, ***to be submitted***.
4. **A. K. Qaroush**, M. I. Saleh, H. M. Alsyouri, M. A. Abu-Daabes, D. A. Castillo-Molina, C. Troll, and B. Rieger. New Insights into [*n*]-Oligourea-Based Sorbents: *In-situ* Formation of New Active Sites for CO_2 Chemisorption during activation. *ChemSusChem*, ***to be submitted***.
5. **A. K. Qaroush**, C. Troll, and B. Rieger. "A New Synthetic Route for the Preparation of Highly Pure, Imidazolium-Based Task-Specific Ionic Liquids: From Synthesis to CO_2 capture", *RSC Adv.*, ***to be submitted***.

- **Side project**

6. **A. K. Qaroush**, D. A. Castillo-Molina, M. Wehrle, M. Winnacker, C. Troll, M. and B. Rieger. Incorporation of secondary and tertiary amines into [*n*]-Oligoureas backbone: A green protocol and CO_2 capture, *CARBON*, ***In preparation***.

B. Oral Presentations

7. **A. K. Qaroush**, Schiff Base Containing Late Transition Metal Based Complexes as Chemoselective Catalysts for the Synthesis of Styrene Carbonate. ***Oral Presentation***, International Conference on Sciences-2012 (ICS), Al al-Bayt University, Mafraq, Jordan, November, (20^{th} – 22^{nd}), **2012**.
8. **A. K. Qaroush**, Cyclic Carbonates as Valuable Carbonylating Agents: From Synthesis to Application, ***Oral Presentation***, ***Invited speaker***, Hashemite University, Zarqa, Jordan, 29^{th}, November, **2012**.
9. **A. K. Qaroush**, D. A. Castillo-Molina, C. Troll, and B. Rieger, "[*n*]-Oligoureas as Novel Green Solid Sorbents for the Capturing of CO_2", ***Accepted Oral presentation***, *Gordon Research Conference on Green Chemistry*, Hong Kong, China, (27^{th} July – 1^{st} August), **2014**.

C. Posters in international conferences

10. **A. K. Qaroush**, Y. Li, C. E. Anderson, S. Y. T. Lee, K. Salmeia, A. Monassier, C. Troll, M. Cokoja, F. E. Kühn, and B. Rieger. CO_2 as a Building Block for the Synthesis of Cyclic Urea/Urethanes, *Poster*, European-Asian Chemical conference of chemical Sciences, (***Eu-AsC$_2$S-11***), Deadsea, Jordan, October, (6^{th} – 10^{th}), **2010**. ***Best Poster Presentation for all sections of chemistry***.
11. **A. K. Qaroush**, A. S. Al-Hamayda, Y. K. Khashman, V. D'Elia, S. I. Vagin, C. Troll, and B. Rieger. A New Organocatalyzed Microwave-Assisted Isocyanate-Free Synthesis of [*n*]-Oligourea: A New energy-saving, eco-friendly method generating Oligourea Using Green Chemistry Approaches, *Poster*, *244^{th} ACS national meeting*, Philadelphia, Pennsylvania, United States. August, (19^{th} – 23^{rd}), **2012**.
12. **A. K. Qaroush**, C. Troll, and B. Rieger. "Novel Task Specific Ionic Liquids as Sorbents for the Capture of CO_2", *Poster*, "Carbon Dioxide as Feedstock for Chemistry and Polymers", Essen, Germany, October, (10^{th} – 11^{th}), **2012**.
13. **A. K. Qaroush,** C. Troll, and B. Rieger. "Propylene Carbonate as a Green Carbonylating Agent: A Novel Methodology for the Synthesis of [*n*]-Oligourea", *Poster*, International

Conference on Sciences-2012 (ICS), Al al-Bayt University, Mafraq, Jordan, November, ($20^{th} – 22^{nd}$), **2012**.

14. **A. K. Qaroush**, D. A. Castillo-Molina, C. Troll, and B. Rieger, "[*n*]-Oligoureas as Novel Green Solid Sorbents for the Capturing of CO_2", ***Accepted Poster***, Gordon Research Conference on Green Chemistry, Hong Kong, China, (27^{th} July – 1^{st} August), **2014**.

- ***Further co-authored posters***

15. K. Salmeia, C. E. Anderson, **A. K. Qaroush**, A. Monassier, S. Y. T. Lee, C. Troll, M. Cokoja, F. E. Kühn, and B. Rieger. Poly(propylene carbonate): Physical Properties and Microstructure". *Poster,* European-Asian Chemical conference of chemical Sciences, Eu-AsC_2S-11, Deadsea, Jordan, October, ($6^{th} – 10^{th}$), **2010**.
16. A. Monassier, S. Y. T. Lee, Y. Li, **A. K. Qaroush**, K. Salmeia, C. E. Anderson, C. Troll, M. Cokoja, F. E. Kühn, and B. Rieger. "Molecular Activation of CO_2: Synthetic Routes towards New Activating Complexes". *Poster,* European-Asian Chemical conference of chemical Sciences, Eu-AsC_2S-11, Deadsea, Jordan, October, ($6^{th} – 10^{th}$), **2010**.
17. S. Y. T. Lee, A. Monassier, Y. Li, **A. K. Qaroush**, K. Salmeia, C. E. Anderson, C. Troll, M. Cokoja, F. E. Kühn, and B. Rieger. "Formation of Methyl Acrylate from CO_2 and Ethylene *via* Methylation of Nickelalactones". *Poster,* European-Asian Chemical conference of chemical Sciences, Eu-AsC_2S-11, Deadsea, Jordan, October, ($6^{th} – 10^{th}$), **2010**.

TABLE OF CONTENTS

LIST OF FIGURES

LIST OF SCHEMES

LIST OF TABLES

LIST OF ABBREVIATIONS

1,10-DAD	1,10-diaminododecane
AMP	2-amino-2- methyl-1-propanol
ATR-FTIR	Attenuated Total Reflectance-Fourier Transform Infra-Red Spectroscopy
BET	Brunauer-Emmett-Teller
BHDC	Dibutyl hexamethylenedicarbamate
CCR	CO_2 capture and Recycling
CCS	CO_2 capture and storage/sequestration
CCU	CO_2 capture, and utilization
CO_2	Carbon dioxide
CP-MAS	Cross Polarization-Magic Angle Spin
CRU	Constitutional repeating unit
DABCO	1,4-diazabicyclo[2.2.2]octane
DBN	1,5-diazabicyclo[4.3.0]non-5-ene
DBU	1,8-diazabicyclo[5.4.0]undec-7-ene
DEA	Diethanolamine
DMAP	4-dimethylaminopyridine
DMC	Dimethyl carbonate
DME	Dimethyl ether

DPC	Diphenyl carbonate
DSC	Differential scanning calorimetry
DTBC	di-*tert*-butyl dicarbonate
ΔH_{fus}	Enthalpy of fusion
EA	Elemental analysis
EC	Ethylene carbonate
GHGs	Greenhouse gases
Gt	Gega ton
GWP	Global warming potential
HFC-23	Fluoroform, CHF_3
HMDA	Hexamethylenediamine
HFIP	1,1,1,3,3,3-Hexafluoroisopropanol
HPP	Hybrid porous polymers
HP-TGA	High pressure- Thermogravimetric Analysis
IGCC	Integrated Gasification Combine Cycle
ILs	Ionic Liquids
MOF	Metal-organic frameworks
MMM	Mixed matrix membrane
MOP	Microporous organic polymers

m.p.	Melting point
*mp*PIL	Mesoporous poly(ionic liquid)
[*n*]-OU	[*n*]-Oligourea
MEA	Monoethanolamine
Mt	Mega ton
2-MP	2-methyl-2-pyrrolidone
MW	Microwave
PC	Propylene Carbonate
PEI	Poly(ethyleneimine)
PCCC	Post-combustion carbon capture process
PEO	Poly(ethyleneoxide)
PILs	Poly(ionic liquids)
ppm	Parts per million
p-TSOH	*para*-Toluenesulfonic acid
Recitsol®	-40°C-chilled MeOH
S_{BET}	Apparent Brunauer-Emmett-Teller surface area
SBs	Sacrificial Bases
Selxol®	A mixture of dimethylether of polyethyleneglycol
SF_6	Sulfur hexafluoride

Tan δ	loss tangent (energy dissipation factor)
T_g	Glass transition temperature
TBD	1,5,7-Triazabicyclo[4.4.0]dec-5-ene
TEA	Triethanolamine
TGA	Thermogravimetric Analysis
TGA-MS	Thermogravimetric Analysis-Mass Spectrometry
TMG	1,1,3,3-tetramethylguanidine
THP	1,4,5,6-tetrahydropyrimidine
TR	Thermally-Rearranged
TrCl	Triphenylmethylchloride
TSIL	Task Specific Ionic Liquid
WIPO	World Intellectual Property Organization

CHAPTER 1

INTRODUCTION

1 INTRODUCTION

1.1 CO_2 as a Greenhouse Gas (GHG).

Global warming is still an unresolved problem that everybody can notice since the initial spark of the industrial revolution. Weather changes and severe environmental problems are seen as a result of the increased concentrations of GHGs which disturbs the carbon cycle.[1] One valid option to reduce CO_2 emissions is throughout carbon capture and sequestration (CCS) (Figure 1.1).[2] Excess CO_2 can be sequestered in porous rocks in the deep subsurface.[3]

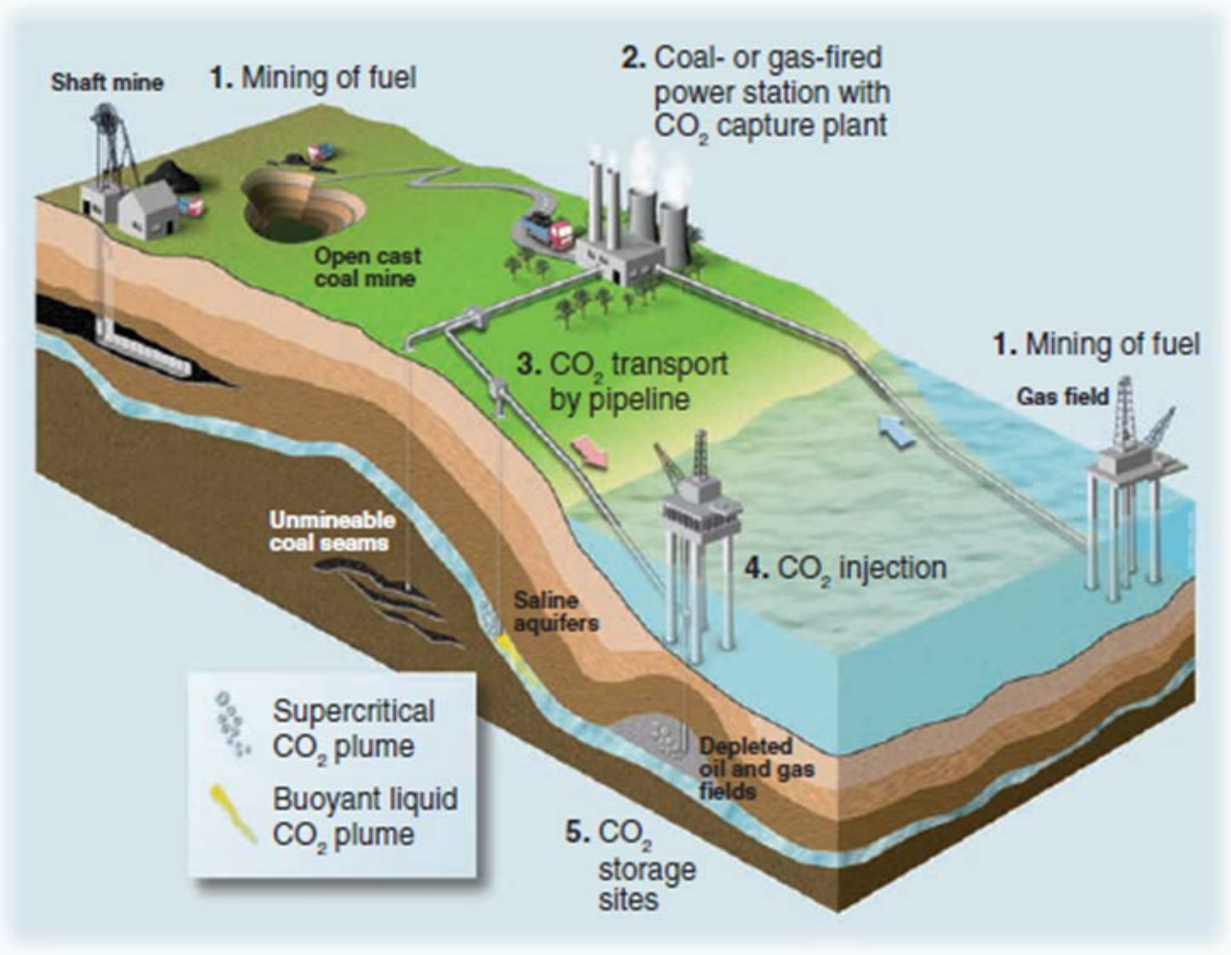

Figure 1.1. CO_2 separation and capture at power plants enables storage of CO_2 in porous rocks deep below ground.[3]

Global greenhouse gas (GHG) emissions have increased by approximately 80% over the period 1970-2004 (from 21 to 38 Gt/year). Approximately, 77% are from CO_2 emissions of which the

majority (55.6%) came from fossil fuels, 17.3% from deforestation and agriculture, 2.8% from other sources, with a further contribution from methane and N_2O with an estimate of 14.3% and 7.9%, respectively. as shown in Figure 1.2.[4]

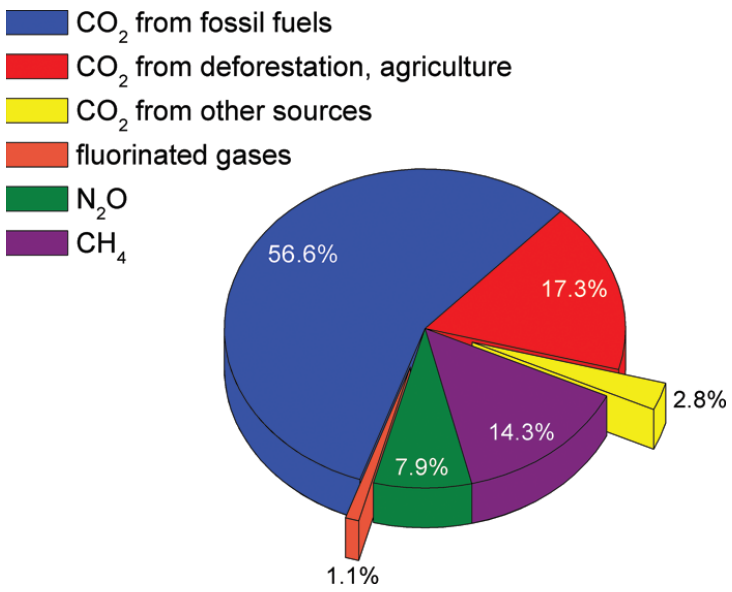

Figure 1.2. Global greenhouse gas emission sources in 2004 of which approximately 77% are represented by CO_2 emissions.[4]

The most noticeable GHG that is made by man-made "anthropogenic" emission is CO_2. Due to the increased utilization of energy and its production from fossil- or oil-based fuels, it left behind a negative impact on the overall ecosystem as what we call today an anthropogenic effect. Figure 1.3 summarizes examples of such emissions such as those from electricity generation in coal-run power plants, cement industry, or even those coming from naturally-occurring phenomena (volcanoes, ocean temperature oscillations, fires, *etc.*) during the industrialization period.[5]

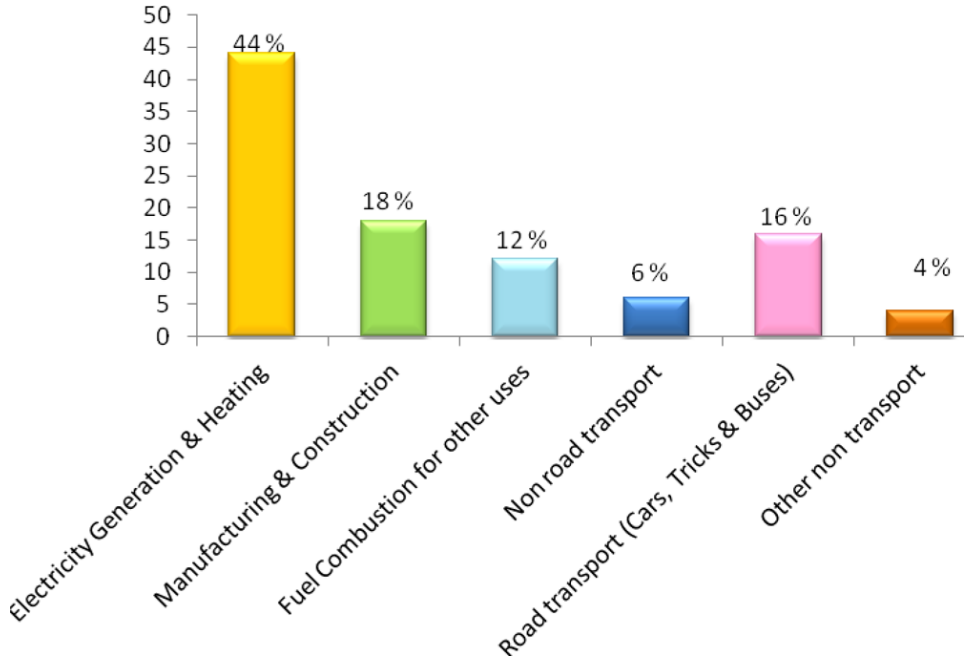

Figure 1.3. Emission of CO_2 by activity sector.[5]

Allan *et al.*[6] predicted that total anthropogenic emissions of one trillion tons of carbon (3.67 trillion tones of CO_2), about half of which has already been emitted since the beginning of the industrial revolution. The concentration of CO_2 in the atmosphere has increased significantly from about 280 ppm in 1750 (pre-industrial era) to 367 ppm in 1999 and to 379 ppm in 2005.[7] Moreover, the **I**nternational **P**anel on **C**limate **C**hange (**IPCC**) anticipated that the atmospheric levels of CO_2 would increase up to 570 ppm in 2100, leading to a global temperature rise of 1.9 °C and a sea level increase of 38 cm.[8] The concentration is still estimated to increase by 1.4 ppm/year unless strict regulations and extreme precautions are not taken into consideration. Thus, CO_2 management is a global demand and continuous challenge to be met by a collaborative action of humankind rather than individual efforts. Many efforts have been gathered to effectively capture CO_2 from the atmosphere to reduce its enormous effects on the environement.[9] Among the top industrial countries, the United States and China are considered the main producers of CO_2 with more than 40.0% (Figure 1.4).

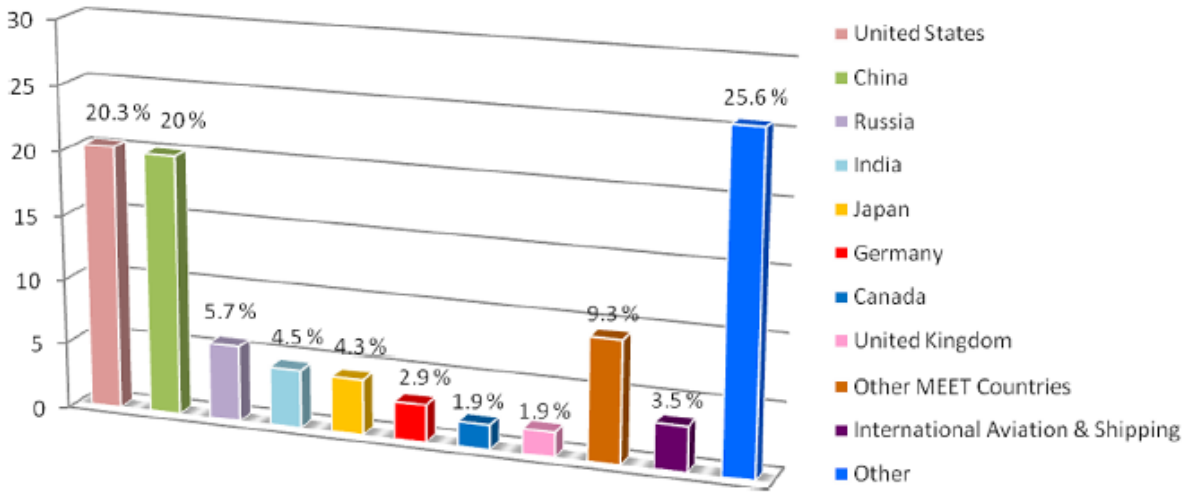

Figure 1.4. Emission of CO_2 per country (% of the total) and from the avio-sector.[5]

1.2 Industrially-Applied Separation Methods

In brief, CCS is mainly carried out by three industrially-applied methods which facilitate the separation and capture of CO_2, they include: postcombustion, precombustion, oxyfuel, and many others like membranes, cryogenic distillation, algal and microbial systems, (Scheme 1.1).[1] It is noteworthy that this thesis will focus on a novel green sorbent that would be feasible and applicable to be used in postcombustion and explains its highlight in terms of CO_2 capture from a chemical point of view.

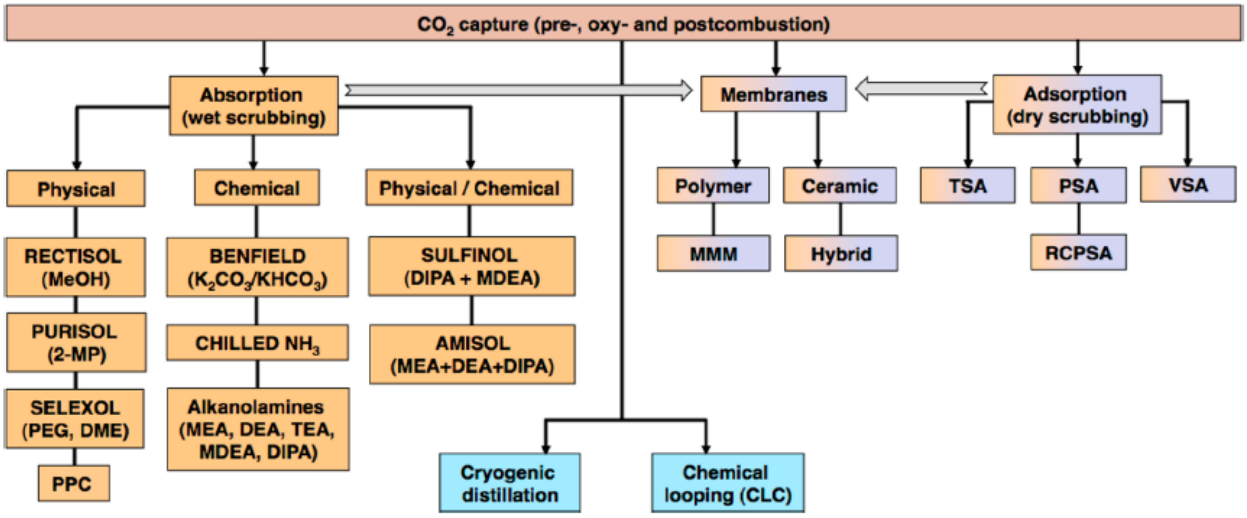

Scheme 1.1. Different CO_2 capturing technologies. (*Orange, postcombustion; violet, precombustion; and blue, oxy-combustion*). **MMM**: Mixed matrix membrane. **PPC**: Polypropylene carbonate. **2-MP**: 2-methyl-2-pyrrolidone. **TSA**: Temperature swing adsorption, **VSA**: Vacuum swing adsorption **PSA**: Pressure swing adsorption; **RCPSA**: rapid cycle pressure swing adsorption. **MDEA**: N-methyldiethanolamine; **MEA**: Monoethanolamine; **DEA**: Diethanolamine; **DIPA**: Diisopropanolamine.[10]

A brief explanation of each one of these terminologies will be indexed briefly within the context accordingly (*vide infra*).

1.2.1 Post-Combustion Process

In order to successfully deploy the concept of sequestration, recycling or utilization of CO_2, first CO_2 has to be efficiently captured from different anthropogenic resources. The removal and capture of CO_2 can be achieved by a range of conventional separation techniques; they are based on different physical and chemical processes, including absorption into liquid solution systems *e.g.* amines, bases, and so on. Moreover, adsorption can be enhanced using solid materials, Adsorption into a solid material as in MOFs and zeolites, or O_2/CO_2 recycles combustion system, cryogenic separation, and permeation through membranes.[11] Generally, in CCS systems[12] capture of CO_2 from a flue gas must be in an efficient, reversible fashion. Table 1.1 shows the composition of a flue gas in a typical postcombustion process. Moreover, Scheme 1.2 shows block diagram for typical postcombustion, based plants.

Table 1.1. Typical postcombustion flue gas composition for a coal-fired power plant.[13]

Molecule	Concentration (by volume)
N_2	73-77%
CO_2	15-16%
H_2O	5-7%
O_2	3-4%
SO_2	800 ppm
SO_3	10 ppm
NOx	500 ppm
HCl 100 ppm	100 ppm
CO	20 ppm
hydrocarbons	10 ppm
Hg	1 ppb

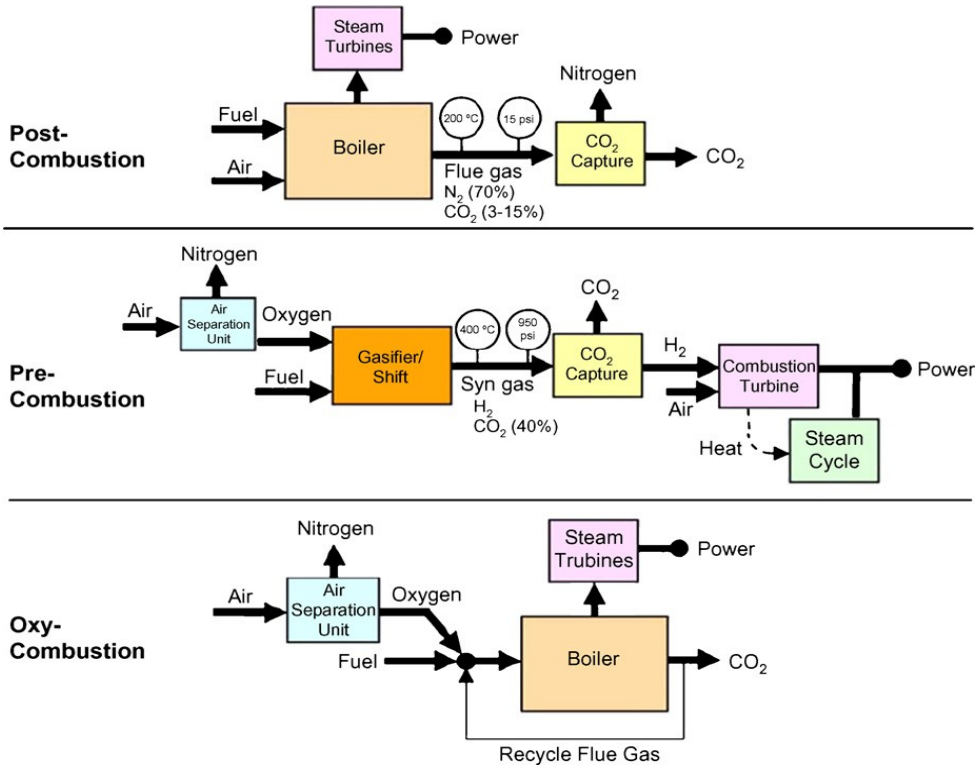

Scheme 1.2. Block diagram illustrating post-combustion, pre-combustion, and oxy-combustion systems.[16]

1.2.1.1 Chemical Absorption

In a chemical-based absorption process, *e.g.*, strong bases such as sodium hydroxide and potassium hydroxide are used. The primary disadvantage of such sorbents is the regeneration, as it is a highly energy-intensive process. but according to the intensive energy needed during their regeneration, and the high energy required, absorption technology utilizing amine-based solvents has been known on an industrial scale for decades and therefore promising candidates, such as monoethanolamine (**MEA**) and diethanolamine (**DEA**), which form carbamates and bicarbonates with CO_2 have been fully explored and studied.[19,14] Wet scrubbing using amine solutions of MEA have been introduced and patented in the literature since the early work of Bottoms in 1930.[15] This is the most common method in capturing of CO_2 as a well-known mature technology, through the use of solvents and subsequent solvent regeneration.[16] However, this procedure has several shortcomings. For instance, the efficiency is decreased due to evaporative losses of MEA or crosslinking at high temperatures to form urea. In addition, the regeneration of the utilized amine[17] (CO_2-stripping) requires high energy consumption and it causes severe corrosion to the facility pipelines. Consequently, more practical and economical approaches have been sought to overcome these limitations.

The main challenge still to achieve is to recover the CO_2 with a minimum energy penalty provided with an acceptable cost.[16] In this sense, strong bases are less used than amines due to much lower temperatures needed for their regeneration.[18] Nevertheless, limited concentration of amines due to corrosion problems and amine degradation are major drawbacks warranting the development of more efficient, and robust CO_2 sorbents.[19]

1.2.1.2 Physical Adsorbents

Physical separation process mainly depends on absorption using non-reactive polar solvents with an acid affinity.[19] Examples of such materials are Recitsol® (-40°C-chilled MeOH), Selxol® (a mixture of dimethylether of polyethyleneglycol), and Purisol® (2-MP: 2-methyl-2-pyrrolidone).[10] The key step for their utilization in CO_2 capturing is the low regeneration temperature which can be driven by either heating or lowering pressure.[14] Moreover, due to vaporization of the amine-based scrubbing agents, ionic liquids (ILs, Section 1.4) have been

proposed as another alternative with a partial solution to some of the associated problems in amine-based solutions.[14]

1.2.2 Pre-combustion Process

In general, most of facilities that apply precombustion methods are natural gas plants where CO_2 capture is entrapped at high partial pressure. Two noticeable advantages are involved in a precombustion process: Firstly, the lower energy capture penalty once compared to postcombustion (10-16%) which is almost half of that in latter process. Secondly, production of hydrogen (H_2) which can be used as a chemical feedstock. Precombustion is found in an **I**ntegrated **G**asification **C**ombine **C**ycle (**IGCC**) plants which involve three steps (stages): Firstly, a fuel is reacted at high pressure and temperature to form the syngas containing a mixture of CO, CO_2, and H_2, Secondly, CO is converted into CO_2 *via* a water gas shift reactor (Scheme 1.2, Section 1.2.1).[2] Thirdly, the separation is carried out by the use of an adsorbent (physisorption) which is considered a much cheaper process for follow-up and separation. Physical-sorption based solvents can be used in **IGCC** because of the relatively high partial pressure of CO_2 in the syngas exiting the shift converter. Moreover, **RTI** developed a highly active lithium silicate (Li_4SiO_4) for the high temperature, it was reported that it is highly effective in the range of 250 to 550 °C, along with pressures ranging 0 to 20 atm, CO_2 concentrations of 2 to 20% in the presence of contaminants such as hydrogen sulfide (H_2S).[20]

1.2.3 Oxy-Combustion Process

Another alternative to capture CO_2 from flue gas is simply by increasing the CO_2 levels to higher concentrations (greater than 95.0 %). This can be achieved by supplying the flue gas with oxygen, by which the latter can be efficiently produced provided that a cryogenic air separation unit (ASU) is available (Scheme 1.2, Section 1.2.1). The disadvantages in this process are the extra cost for the ASU unit as well as the flue gas recirculation. Therefore, to sum the advantages and disadvantages of the three approaches mentioned (*vide supra*), which might give a clear perspective for the pros and cons of each one of them. It is noteworthy, that the first oxy-fuel technology, pilot-plant was inaugurated in September 2008 by the European energy company Vattenfall, at “Schwarze Pumpe” located in Germany.[21]

1.2.4 Advantages and disadvantages of the industrially applied separation methods.

Table 1.2. Advantages and disadvantages of CO_2 capturing technologies.[16]

	Advantages	**Barriers to implementation**
Post-combustion	- Applicable to the majority of existing coal-fired power plants - Retrofit technology option	Flue gas is … - Dilute in CO_2 - At ambient pressure … resulting in … - Low CO_2 partial pressure - Significantly higher performance or circulation volume required for high capture levels - CO_2 produced at low pressure compared to sequestration requirements
Pre-combustion	Synthesis gas is … - Concentrated in CO_2 - High pressure … resulting in … - High CO_2 partial pressure - Increased driving force for separation - More technologies available for separation - Potential for reduction in compression costs/loads	- Applicable mainly to new plants, as few gasification plants are currently in operation - Barriers to commercial application of gasification are common to pre-combustion capture - Availability - Cost of equipment - Expensive supporting systems requirements
Oxy-combustion	- Very high CO_2 concentration in flue gas - Retrofit and repowering technology option	- Large cryogenic O_2 production requirement may be cost prohibitive - Cooled CO_2 recycle required to maintain temperatures within limits of combustor materials - Decreased process efficiency - Added auxiliary load

A summary of the advantages and disadvantages is already given (*vide supra*). Therefore, search for more candidates is still valid. In the current work, *Postcombustion is the main process of interest to be considered for the capturing of CO_2.*

1.3 Bicarbonate *vs.* Carbamates; 1:1 Mechanism versus 1:2 Mechanism

A milestone that needs to be addressed when dealing with different sorbents *e.g.*, amines, the **CO_2:amine** ratio involved during absorption is a *condition-dependent* process; *viz.*, different mechanisms are evolved depending on wet/dry conditions and type of amine used. Two main mechanisms can be evolved depending on stoichiometric amount of CO_2 captured. Firstly, a **1:2 mechanism**, in this mechanism, one mole of CO_2 reacts with two molecules of the reactive species, *e.g.* the reaction of primary and secondary amines with CO_2 to form carbamates, (dry conditions, upper, Scheme 1.3). Secondly, **1:1 mechanism**, in which one mole of CO_2 can be captured by one mole of sorbent. *e.g.* amidine, guanidine, carbenes, tertiary amines in aqueous solutions. (wet conditions, lower, Scheme 1.3) are considered to be cost-effective due to its energy consumption on regeneration.

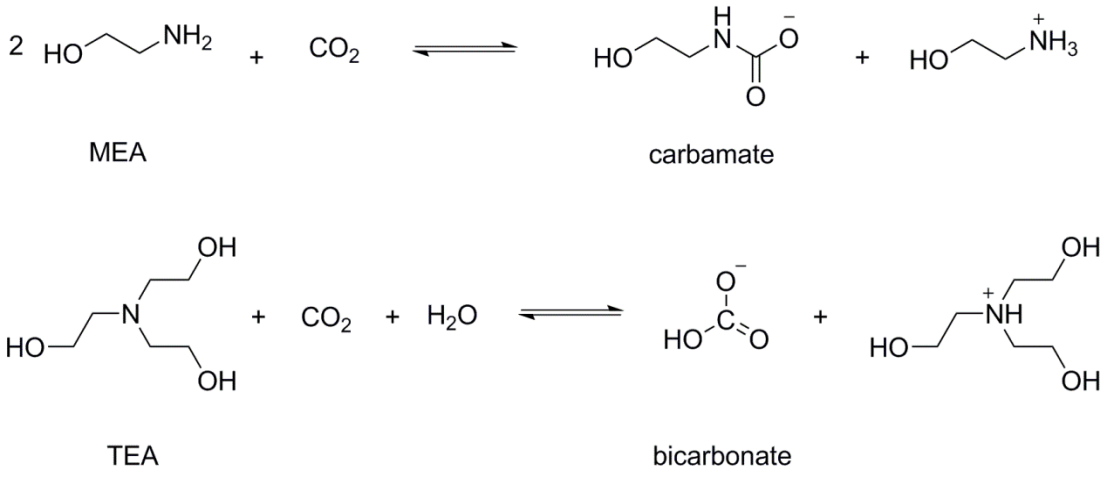

Scheme 1.3. The interaction of CO_2 with monoethanolamine (**MEA**) and triethanolamine (**TEA**) to form carbamates (Upper, dry conditions) and bicarbonate anions (Lower, wet conditions,), respectively.

In 2012, a very important study was reported by Liu *et al*[22] regarding steric-hindered-controlled CO_2 absorption followed a **1:1 mechanism** through the formation of carbamic acid rather than ammonium carbamate (Scheme 1.4). The reason behind such discrepancy is due to intramolecular hydrogen bonding; it was proved by both NMR (1H & 13C) and IR using sodium N-alkylglycinates and alaninates in the presence of PEG, the function of the latter is to enhance the counterion capacity towards CO_2. It is noteworthy that the cost effectiveness of energy for regeneration for of the materials produced was less than that for bicarbonate based systems, regeneration was either under 40.0 °C or 90.0 °C in the presence or absence of nitrogen, respectively.

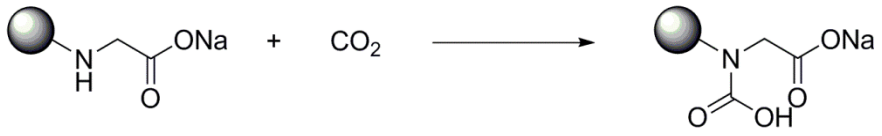

Scheme 1.4. CO_2 capture through the formation of carbamic acid rather than ammonium carbamates.[22]

1.4 Ionic Liquids and their Feasibility for Gas Separation

Ionic Liquids (ILs) are inorganic or organic salts with a melting or glass transition temperature (T_g) below the boiling point of water.[23] IL's have a surprisingly long history, which started with Gabriel and Weiner who were the first to report on the production of ethanol ammonium nitrate (*m.p.* 52.0-55.0 °C) in 1888.[24] Afterwards, in 1970s and 1980s ILs based on alkyl substituted imidazolium and pyridinium cations, with halide or tetrahalogenoaluminate anions, were initially developed for use as electrolytes.[25] New classes of ILs that consist of dialkylimidazolium chloroaluminate were reported by Wilkes *et al*. in 1982.[26] Notable interests of ionic liquids have been increased during the last two decades; many studies were done by the research community,[27] ILs have distinctive properties such as high thermal and chemical stability and low flammability. Moreover, they are considered to be an excellent material for recyclability and ionic conductivity.[28] They have a wide liquids range, ranging from 75.0 °C to 300.0 °C, which allows better kinetic control on reactions. On the other hand, they have the potential to be used as novel solvents or fluids for a diverse range of applications.[29] ILs play an important role as organocatalysts,[30] electrolyte materials,[31] and many other applications such

as liquid–liquid extractions,[32] mass spectrometric applications,[33,34] IR, Raman and fluorescence spectroscopy.[35] They have the potential to be used as liquid absorbents since they have shown to exhibit high CO_2 solubility.[36] The desirable properties of IL solvents as described above make them remarkable candidates as new materials in well-known CO_2 capturing processes.[37] They present many opportunities to reassess and optimize existing technologies and processes. Several studies have shown that the gas solubility in ionic liquids increases when the pressure is increased and decreases with an increment in temperature. The absorption of CO_2 into standard ionic liquids is controlled exclusively by physical mechanisms.[38] Obviously, the use of ILs gained more importance, this importance is focused in changing the ILs properties; by varying the cations and anions or by functionalization of ILs "task specific ionic liquids, TSIL" which can be produced by grafting functional groups onto the ions. The design and synthesis of ILs for special applications or to enhance the efficiency of different processes using functional ILs is a very interesting topic.[39]

Organic cations such as imidazolium (**A**), pyridinium (**B**), ammonium (**C**), phosphonium (**D**) and pyrrolidinium (**E**), Figure 1.5, can be easily combined with a variety of anions (halides, PF_6^-, BF_4^-, Tf_2N^-), leading to a myriad of possibilities for the modification of their physicochemical properties, this special feature is not possible for organic compounds.[40]

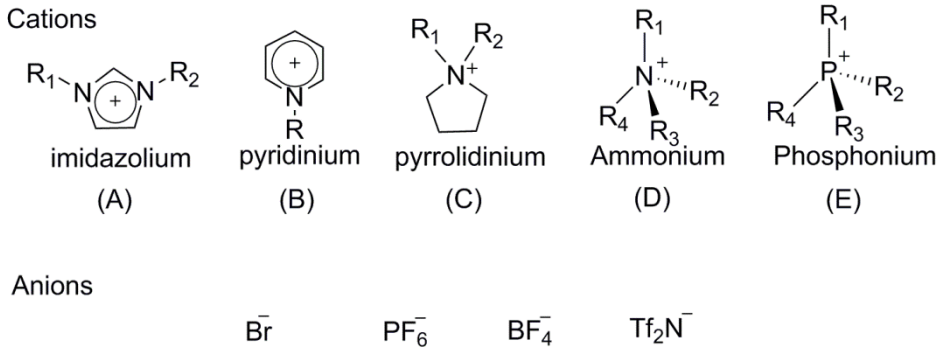

Figure 1.5. The structures of common cations and anions of ILs

Selected properties, such as thermal stability and miscibility, mainly depend on the anion, while others, such as viscosity and density, depend on the length of the alkyl chain in the cation, shape,

and symmetry. However, the use of ILs also has some disadvantages; the physical properties are not always known, their viscosity is usually higher than that of common solvents and their toxicity effects are still unknown.[29]

1.4.1 Task Specific Ionic Liquids (TSILs)

ILs are tailor-made solvents this means that their properties can be adjusted to suit the requirements of a particular process, so it is almost possible to tune a particular IL associating an anion with a cation adapted for a specific reaction.[41] These named solvents, *viz.* TSIL mainly take a place as 'green' alternatives to several volatile organic solvents and welcome environmentally friendly technologies.[42] In 1999, Davis and co-workers[43] were the first to demonstrate the concept of designing IL to interact with a solute in a specific fashion for applications other than CO_2 absorption. Followed by another consecutive work in which he focused and outlined the concept briefly in a mini-review by introducing the term TSILs.[44] Progress and advancement in the field of TSIL and their use in organic chemistry is already well reviewed in literature, which is beyond the scope of the thesis.[45] Therefore, the work is focused on TSIL for the capture of CO_2. In terms of CO_2 absorption, and in contrast to standard ILs as pointed above, TSILs have chemical absorption which makes the selectivity towards capturing CO_2 easier, among other gases.

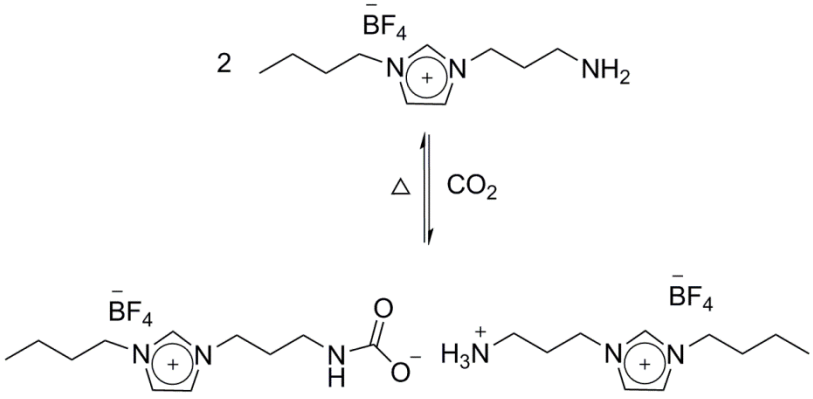

Scheme 1.5. Proposed reaction between TSIL and CO_2

For the use of TSIL and their utilization for the capture of CO_2, a breakthrough took place in 2002 by Davis and coworkers,[46] who synthesized a novel IL containing an amine-tethered, imidazolium-based IL that can absorb CO_2 with an efficiency of 7.4 wt%, (Scheme 1.5).

Compared to an earlier literature that was preceded by Brennecke[47a] with a *1-hexyl-3-methyl imidazolium hexafluorophosphate*, [6-mim]PF_6, (Figure 1.6), the increase in mass was due to the purely physical absorption, with an increase in mass by 0.0881 wt% of the IL.

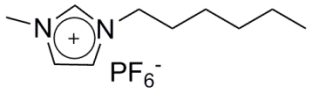

Figure 1.6. *1-hexyl-3-methyl imidazolium hexafluorophosphate*

Zhang *et al.*,[48] synthesized a new type of TSIL based on tetrabutylphosphonium amino acid $[P(C_4)_4][OH]$ [AA], it was synthesized by the reaction of tetrabutylphosphonium hydroxide $[P(C_4)_4][OH]$ with amino acids, including glycine, L-alanine, L-*β*-alanine, L-serine, and L-lysine, (Figure 1.7). They showed that the CO_2 absorption capacity at equilibrium was 50.0 mol% of the used IL. In the presence of water (1.0 wt%), the ionic liquids could absorb 1 mole of CO_2. The CO_2 absorption mechanisms of the ionic liquids with and without water were different.

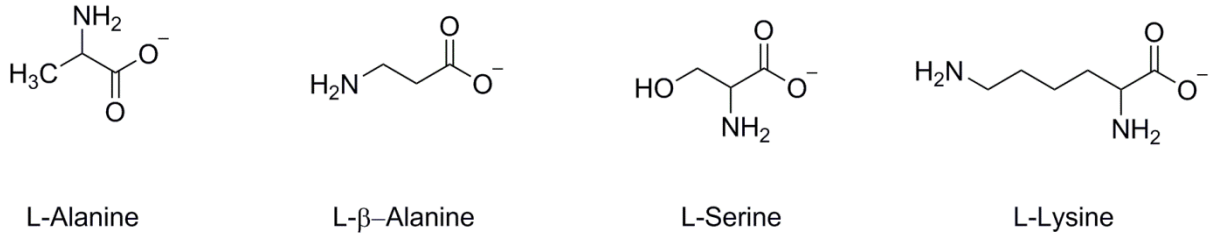

Figure 1.7. Structural representation for the anionic amino acids [AA] used in the study

In 2009, as an unprecedented step in TSIL regarding the modification of both cation and anion at the same time, Zhang *et al.*[49] synthesized a new series of 20 dual amino-functionalized Phosphonium ILs based on *(3-aminopropyl)tributylphosphonium* amino acid salts $[aP_{4443}][AA]$. It was found that the $[aP_{4443}][AA]$ ILs have excellent thermal properties, such as low T_g values that range from -69.7 to -29.7 °C and thermal decomposition temperatures all above 200.0 °C.

Supported by porous SiO_2, the CO_2 absorption by $[aP_{4443}][Gly]$, $[aP_{4443}][Ala]$, $[aP_{4443}][Val]$ and $[aP_{4443}][Leu]$ almost reaches equilibrium within 80.0 min. 1 mol CO_2 per mol IL, which is a factor of two greater than that reported before. The $[aP_{4443}][AA]$ ILs (Figure 1.8) can be repeatedly recycled for CO_2 uptake. For $[aP_{4443}][Gly]$, the durability or loss of absorption rate and capacity are almost not significant and lasts for five absorption cycles.

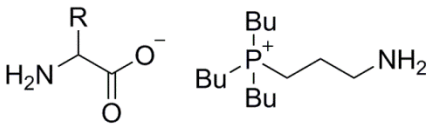

Figure 1.8. Structure of the dual amino-functionalized phosphonium ILs ($[aP_{4443}][AA]$). $[AA]^-$ = $[Ala]^-$, $[Arg]^-$, $[Asn]^-$, $[Asp]^-$, $[Cys]^-$, $[Gln]^-$, $[Glu]^-$, $[Gly]^-$, $[His]^-$, $[Ile]^-$, $[Leu]^-$, $[Lys]^-$, $[Met]^-$, $[Phe]^-$, $[Pro]^-$, $[Ser]^-$, $[Thr]^-$, $[Trp]^-$, $[Tyr]^-$, and $[Val]^-$.

Wang *et al.*[50] managed to synthesize a binary system consisting of an equimolar ratio of an alcohol-functionalized IL together with a superbase. The system was found to be effective for CO_2 capture under atmospheric pressure. What was advantageous in their system is that no dry conditions are needed, and the system follows a typical **1:1 Mechanism** (Figure 1.9). The novelty of the applied system is to be considered one alternative to replace volatile amine solutions.

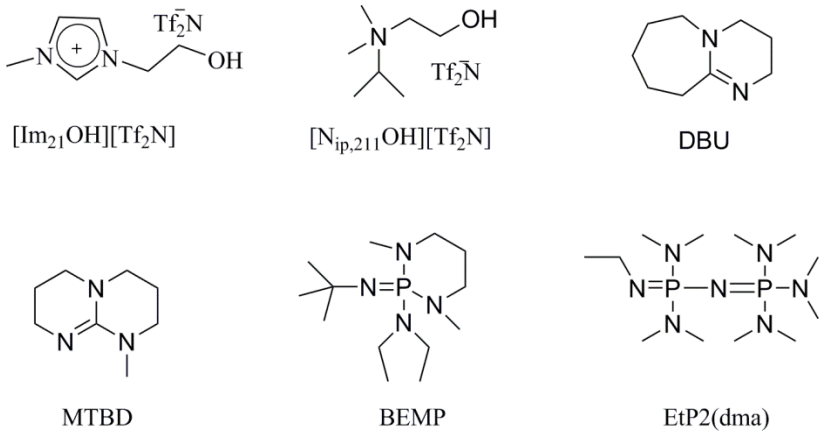

Figure 1.9. The chemical structures of the RTILs and superbases used and their designation.[50]

In 2011, Xue *et al.*[51] synthesized a TSIL with a first-time synthesis of a dual-functionalized imidazolium-based IL with amine functionality on both cation and anion (Figure 1.10). Absorption isotherm of CO_2 showed that absorption capacity is about 0.9 mol CO_2/IL. The absorption is due to a chemical process as verified by both NMR and IR.

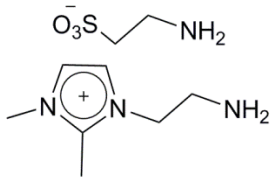

Figure 1.10. Chemical Structure of [aemmim][Tau]

For more closer look on the field of TSIL, Yang *et al.*,[52] gave a brief review for the use of TSIL for CO_2 capture/activation and subsequent conversion. Also, Zhang and coworkers [53] gave another review on carbon capture using ILs. It is up to now in competitive race to give the best solution for the capture of CO_2 using such systems.

1.4.2 Poly (Ionic Liquids) (PILs)

Very recently, significant progress has been made in the application of ILs as absorbents for CO_2 separation.[47a] As previously mentioned, one of these applications was based on a TSIL for CO_2 capture, which was developed by introducing an amine group to ILs, causing the CO_2 solubility to increase substantially.[54] On the other hand, Poly(ionic liquids) (PILs) or polymerized ionic liquids have emerged recently as a research focus attracting steadily growing interest in the fields of polymer and material science as another successful application.[55]

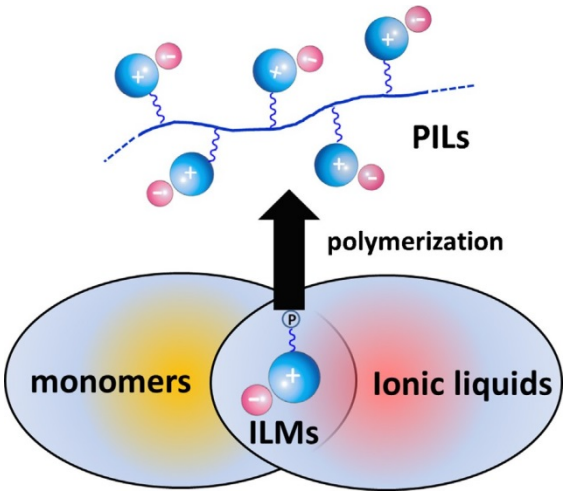

Figure 1.11. Illustration of the relationship between ILs and PILs. **ILMs**: ionic liquid monomers. "**P**": polymerizable group.[55]

It should be mentioned that initial research on PILs or back then named as polyelectrolytes was back-dated to 1970's.[56] The major advantages of using a PIL instead of an IL are not only the enhanced mechanical stability, improved processability, durability over the IL species, but also much faster CO_2 absorption and desorption rates than ILs.[57]

PILs refer to a special type of polyelectrolytes which carry an IL moiety in the constitutional repeating unit (CRU), providing them with a combination of unique properties of ILs with the flexibility and properties of macromolecular architectures as well as enhancing novel properties and functions that are of huge potential in a multitude of applications as in the case of absorption of CO_2.[55] They are heavily used as carbon materials,[58] thermo-responsive materials,[59] energy harvesting and storage[60], and many others such as bio-related application.[61]

In 2005, the first report to describe the use of PILs as sorbent-based materials was given by Tang *et al.*[62] Unexpectedly, they reported several imidazolium-based PILs that exhibited significantly higher CO_2 absorption capacities than the corresponding ILs. Most importantly, CO_2 absorption and desorption of PILs are much faster and are completely reversible. All of these factors indicate that PILs are more suitable than ILs for industrial CO_2 capture, storage, or conversion.

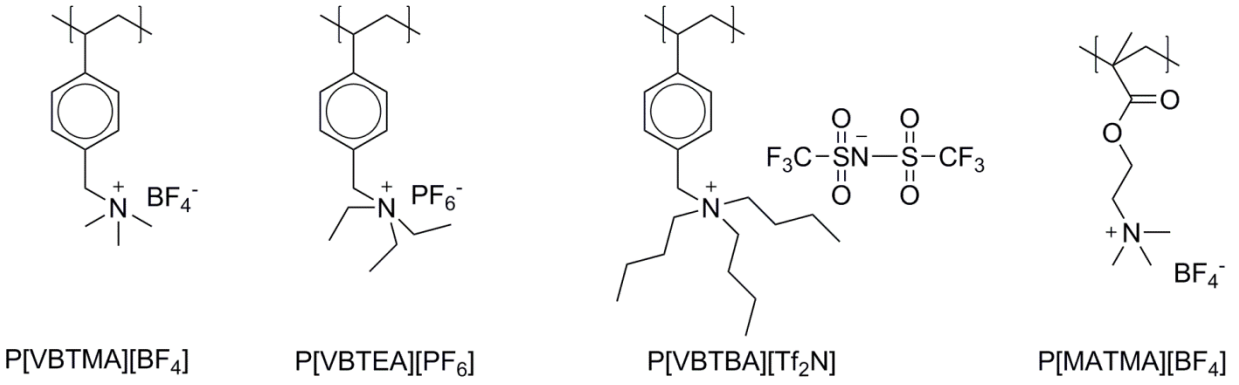

Figure 1.12. Structural representation of PILs reported in the study.[62]

Consecutively, Tang *et al.*[63] reported on the use of another set PILs where he compared ammonium-based PIL relative imidazolium-based ones (Figure 1.13).

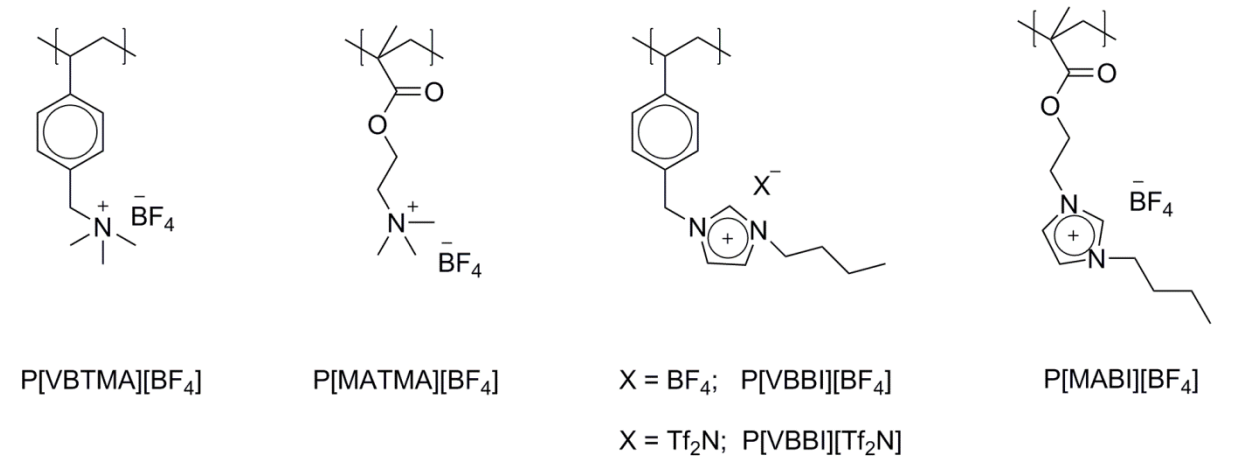

Figure 1.13. The structures of the PILs reported in the study.[63]

Synthesized materials, *viz.*, poly[p-vinylbenzyltrimethyl ammonium tetrafluoroborate] (**P[VBTMA][BF$_4$]**) and poly[2-(methacryloyloxy)ethyltrimethylamnonium tetrafluoroborate] (**P[MATMA][BF$_4$**]) have absorption capacities of almost eight- and six-fold of those of RTILs, *e.g.* [bmim][BF_4], respectively, with reversible and fast sorption and desorption.

J. Yuan *et al.*,[55a] reported on the CO_2 absorption capacities of PILs containing different cations have been observed to decrease in the order of ammonium [**(NR$_4$)]$^+$** > pyridinium [**Py**]$^+$ > phosphonium [**(PR$_4$)]$^+$**> imidazolium [**Im]$^+$**. While PILs containing different anions decrease in

the order of BF_4^- > PF_6^- > Tf_2N^-. Moreover, PIL membranes are physically resistant to higher pressures (overcoming blowing out problems faced when dealing with supported ILs). Furthermore, the IL moieties in PILs provide good CO_2/light gas selectivity. The current drawback to PIL membranes is their CO_2 permeabilities, which are still orders of magnitude, lower than its IL-monomeric analogous.

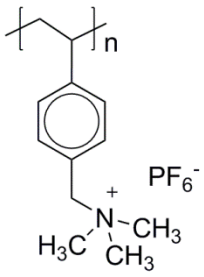

Figure 1.14. Poly[(*p*-vinylbenzyl)trimethylammonium) hexafluorophosphate P[VBTMA][PF_6].[36]

Unexpectedly, Supasitmongkol and Styring[36] reported a similar PIL that was reported by Tang et al. (P[VBTMA][PF_6]) the discrepancy was in the amount adsorbed, *viz.*, up to 77.0 wt%, upon the use of a Radley's carousel synthesizer (scaled-up adsorber unit). However, under TGA conditions, this material absorbed only 2.47 wt% (gravimetrical technique).

1.5 Microwave-Assisted Reactions

Microwave-assisted reactions are considered to be one of the most important methodologies which has been used for more than over two decades.[64] It has been widely used in organic,[65, 66] inorganic,[67] and polymer synthesis[68] as well as in chemical modification.[69] Since 1986 the attention towards microwave-assisted reactions has grown exponentially. Advantages for microwave-assisted reaction as compared to conventional heating applying conduction phenomena, such as rapid and directed uniform heating (Table 1.3).[70] In some cases, it has been shown to reduce polymerization reaction times from hours to few minutes,[71] as well as from minutes to seconds scale for simple organic reactions,[72] thus, saving energy and time.

Table 1.3. Characteristics of microwave and conventional heating.[65]

Microwave heating	Conventional heating
Energetic coupling	Conduction/convection
Coupling at the molecular level	Superficial heating
Rapid	Slow
Volumetric	Superficial
Selective	Non selective
Dependent on the properties of the material	Less dependent

Regarding the synthesis of polyureas using a microwave-assisted reaction, there was a sole pioneering study in 2004.[73]

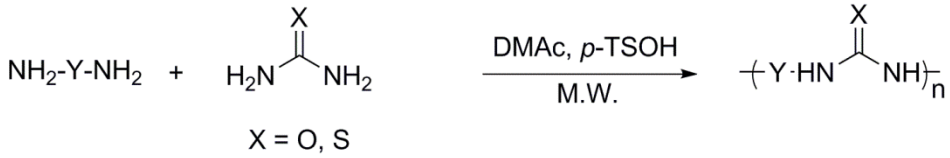

Scheme 1.6. Schematic representation for the general synthesis of polyureas /polythioureas organocatalyzed by *p*-TSOH.

Interestingly, Banihashemi *et al.* was the first to describe an efficient and rapid microwave-assisted synthesis of polyureas and polythioureas (Scheme 1.6). Upon the reaction of an equimolar ratio of urea or thiourea with diamines catalyzed by 10.0 mol% *p*-toluenesulfonic acid (*p*-TSA) in the presence of 5.0 mL DMAc as a solvent. In his report, a domestic microwave oven was used; the reaction period was an overall of 15.0 minutes, it was divided into two intervals with two different power inputs, for the first interval, microwave energy of 220.0 W for 7.0 minutes and then 400.0 W for 8.0 minutes to control the evolution of ammonia. In our method, milder reaction conditions as in a solvent-free, lower catalyst loading, shorter overall reaction times, as well as lower microwave power are used. Furthermore, in some cases; more efficient and almost quantitative yields were obtained. In contrast to our method, the use of aromatic diamines for the synthesis of the presumed polyurea/polythioureas was not successful.

1.6 Large-Scale Sorbents for CO_2 Capture:

1.6.1 Amine-Scrubbing-, Impregnation-, and Grafting-based Process.

Amine based scrubbing agents (solvent-based) are the most well-known, developed technologies with a mature knowledge of both chemical and engineering aspects regarding capturing of CO_2. Other candidates to replace MEA that might be suggested or tailored, *e.g.*, sterically-hindered amines such as 2-amino-2- methyl-1-propanol (AMP), this solvent is considered to be the most promising absorption solvent among others due to its lower stability carbamate-formed (carbamate stability constant: AMP, 0.1 < DEA, 2.0 < MEA, 12.5 at 303 K).[74] The sterically-hindered amines allow higher CO_2 loadings in excess of 0.5 mol equivalents to be reached, with higher regeneration rates (process-effective with minimal regeneration costs) compared with the conventional alkanolamines (*e.g.*, the CO_2 regeneration rate ratio for AMP/MEA is 1.83[75]).[76]

In 2002, the first amine-impregnated silica used to capture CO_2 was reported by Song and coworkers.[77] MCM-41 was impregnated with low molecular weight poly(ethyleneimine) (PEI), a high-surface-area mesoporous silica with cylindrical pores of relatively small diameter was obtained, a CO_2 adsorption capacity as high as 215 mg_{CO2}/g_{PEI} was obtained with MCM-41-PEI-50 at 75.0 °C. Further reports regarding impregnation can be seen elsewhere.[81] To minimize costs and increase the efficiency of capturing/separation, other advances regarding the use of templated polymeric materials as adsorbents for postcombustion capture (PCC) are also reported.[78]

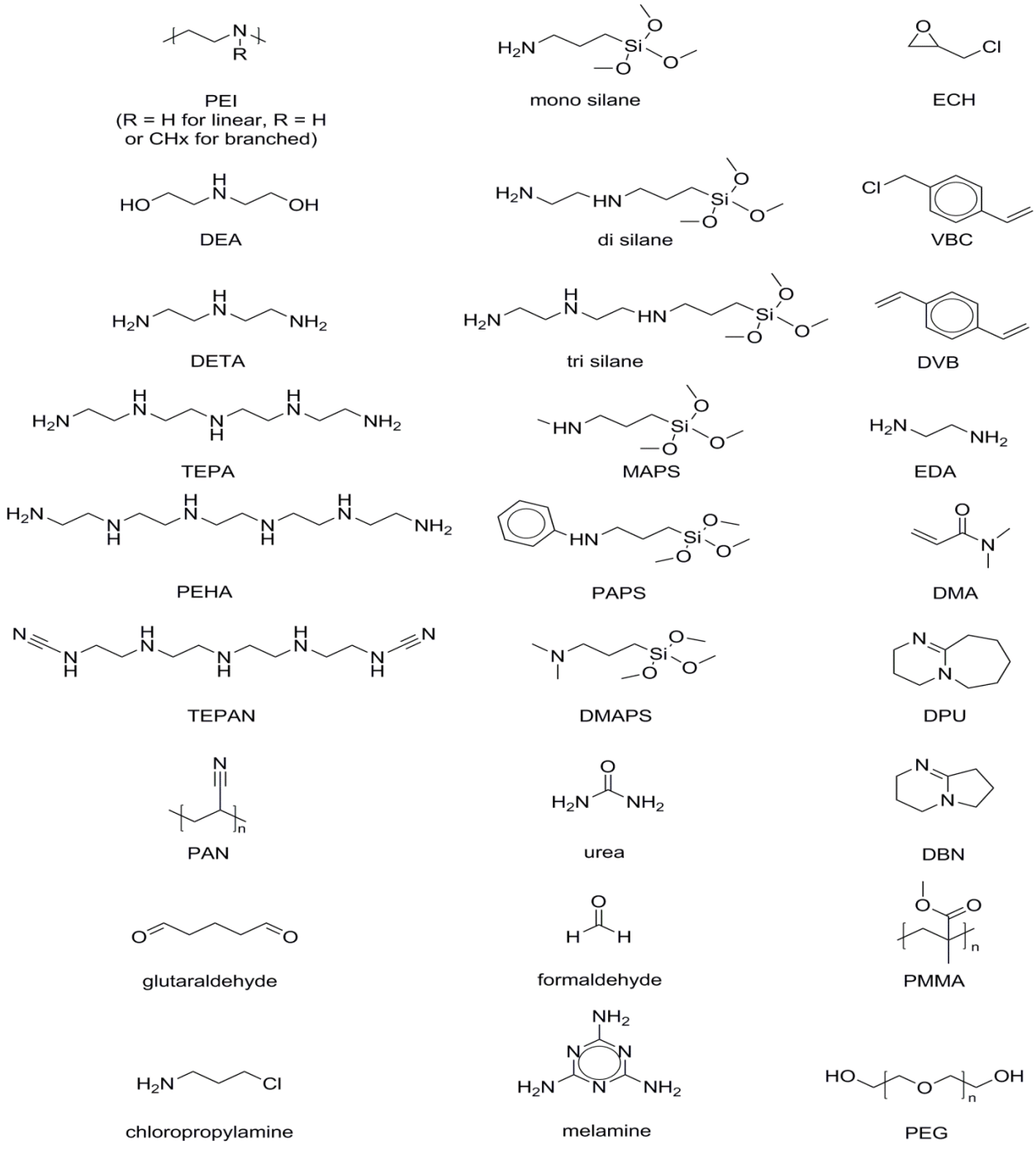

Figure 1.15. Amines, silanes monomers and polymers used in the synthesis of solid supported amine adsorbents.[81]

1.6.2 Membrane-Based Process.

Membranes suited for CO_2 capturing purposes possess certain merits that make them successful

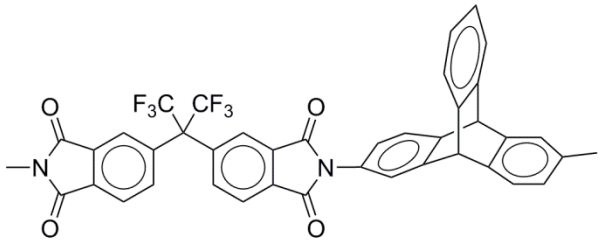

Polyimide

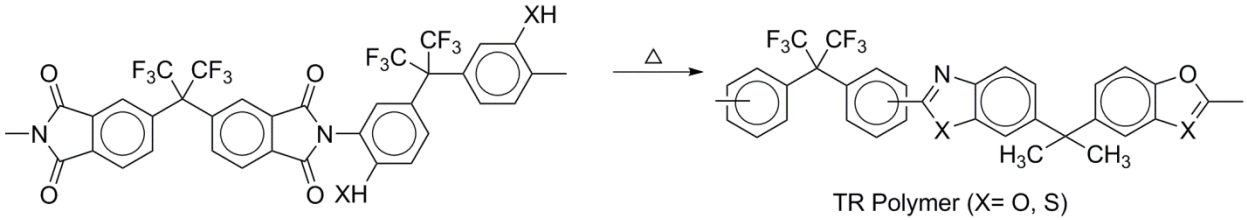

TR Polymer (X= O, S)

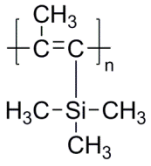

PTMSP (Polyacetylenes)

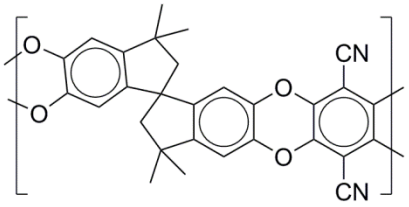

PIM

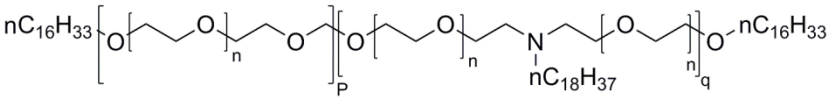

PEO

Scheme 1.7. Representative chemical structures of polymers with high CO_2 permeability. TR: Thermally-rearranged; PTMSP: Poly(trimethylsilylpropyne), (a derivative of polyactylene); PIM: Polymer with intrinsic microporosity; PEO: a derivative of Poly(ethyleneoxide).[80]

candidates for the separation of CO_2 from other gases, these characteristics include: cost effectiveness high CO_2 permeability, aging resistance, high CO_2/N_2 selectivity, thermal and chemical resistance, plasticization resistance, and ability to be cheaply processed and manufactured into different membrane modules.[79] Further, Membrane-based processes offer the opportunity to efficiently save energy alternative for CO_2 capture due to having no phase transformation. However, they lack the high permeability for massive volumes processing of flue gas, which would result in a high CO_2 capture (*If successful*). Some examples that are heavily used in the industry for suitable applications are summarized below, *viz.*, Thermally-rearranged polymers (TR), polyactylene and its derivatives, *e.g.* Poly(trimethylsilylpropyne) (PTMSP), Polymer with intrinsic microporosity (PIM), or even Poly(ethyleneoxide) (PEO) and its derivatives (Scheme 1.7).[80]

1.6.3 Adsorbent-Based Process.

Many factors affect the use of sorbents (liquids or solids) to adsorb CO_2. Among the other candidates, they should generally have large adsorption capacity, fast adsorption/desorption kinetics, multitude of regenerability and stability.[81] Examples of liquid adsorbents include Rectisol®, Selexol® (Section 1.2.1.2), and ionic liquids (Section 1.4).

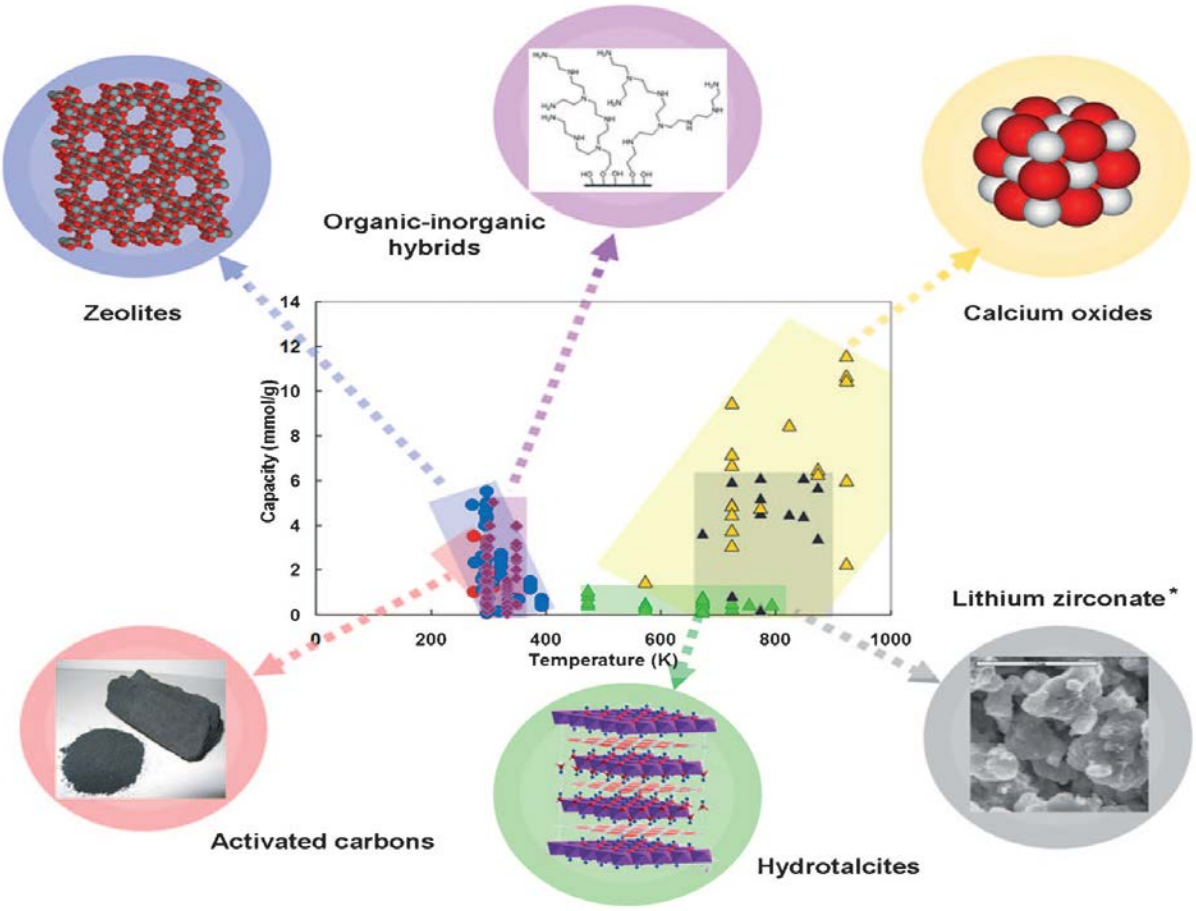

Figure 1.16. Different types of solid adsorbents applied for the capturing of CO_2.[81]

1.6.4 Solvents, Sorbents, and Membranes, Which is Which?

Li *et al.*[82] reviewed the recent advances in CO_2 capture technologies from a patent point of view. Among them, emphasis has been placed on patenting (1297 patents from 1980 to March, 2012) solvent- (37.5%), sorbent- (35.5%), or membrane-based technologies (27.0%). Indeed, more than a quarter of the patents were documented in the last 2 years (*i.e.* 2010–2011). Most probably, the authors referred the major increase of patenting in the 1990s due to the realization of the Sleipner project in 1996 (environmental concern), the early adoption of the Kyoto Protocol in 1997, as well as the prospective benefit of CO_2 injection for enhanced oil recovery (commercial purposes), (Figure 1.17).[82]

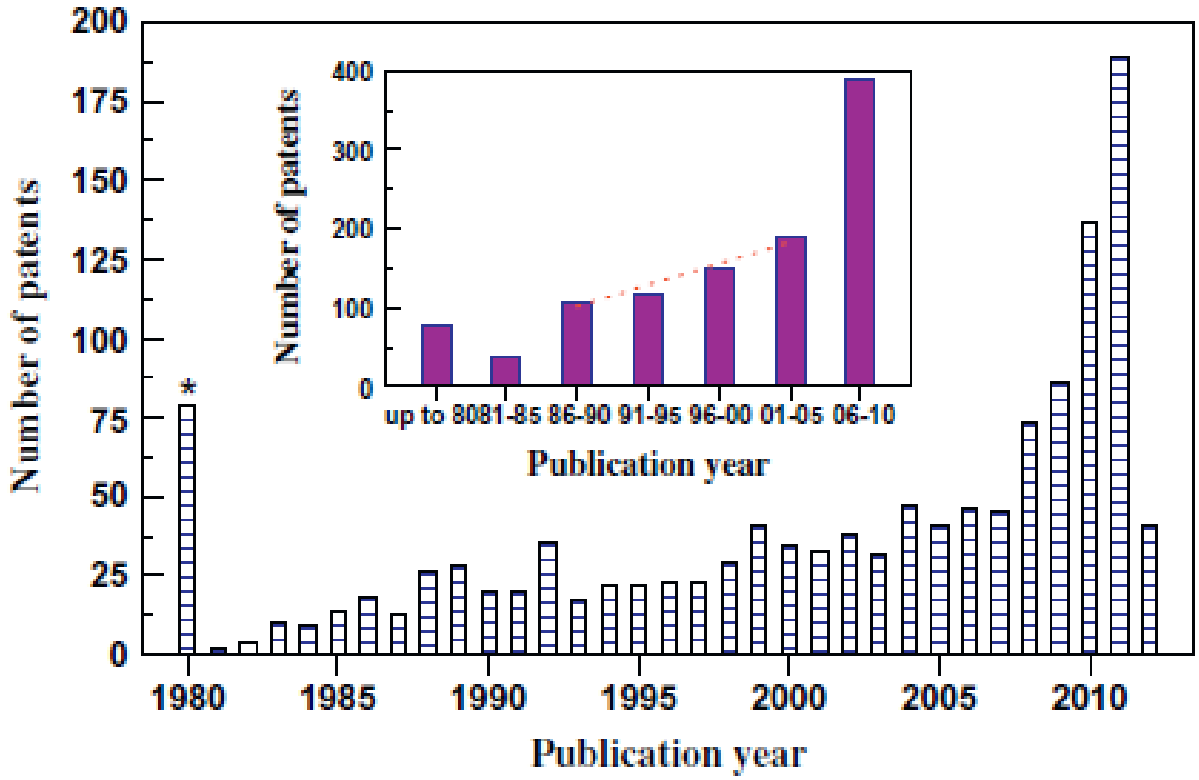

Figure 1.17. Number of publications *vs.* publication year./Total patents published by 1980.[82]

Further, according to the patent type (*i.e.* the country or organization where the patent application was filed or granted), Japan (JP), the United States (US), World Intellectual Property Organization (WIPO), and China (CN) are the top four types of patents found, making up approximately 71% of the overall number of patents. Each one of the main four contributors for the different types of patents (*i.e.* JP, US, WO, and CN) possesses more than 100 patents on CO_2 capture (Figure 1.18 **A**) corresponding to 26.5%, 22.5%, 11.6%, and 10.6% of the overall number of patents, respectively (Figure 1.18 **B**). Interestingly, *for the JP patent type, substantially more technologies were patented as sorbent- (192 patents) or membrane-based (139 patents) compared to those as solvents-based ones (53 patents).* On the other hand, for the Australia (AU), Germany (DE), European Patent Office (EP), France (FR), and United Kingdom (GB) patent types, solvent patents dominated (Figure 1.18 **A**).[82]

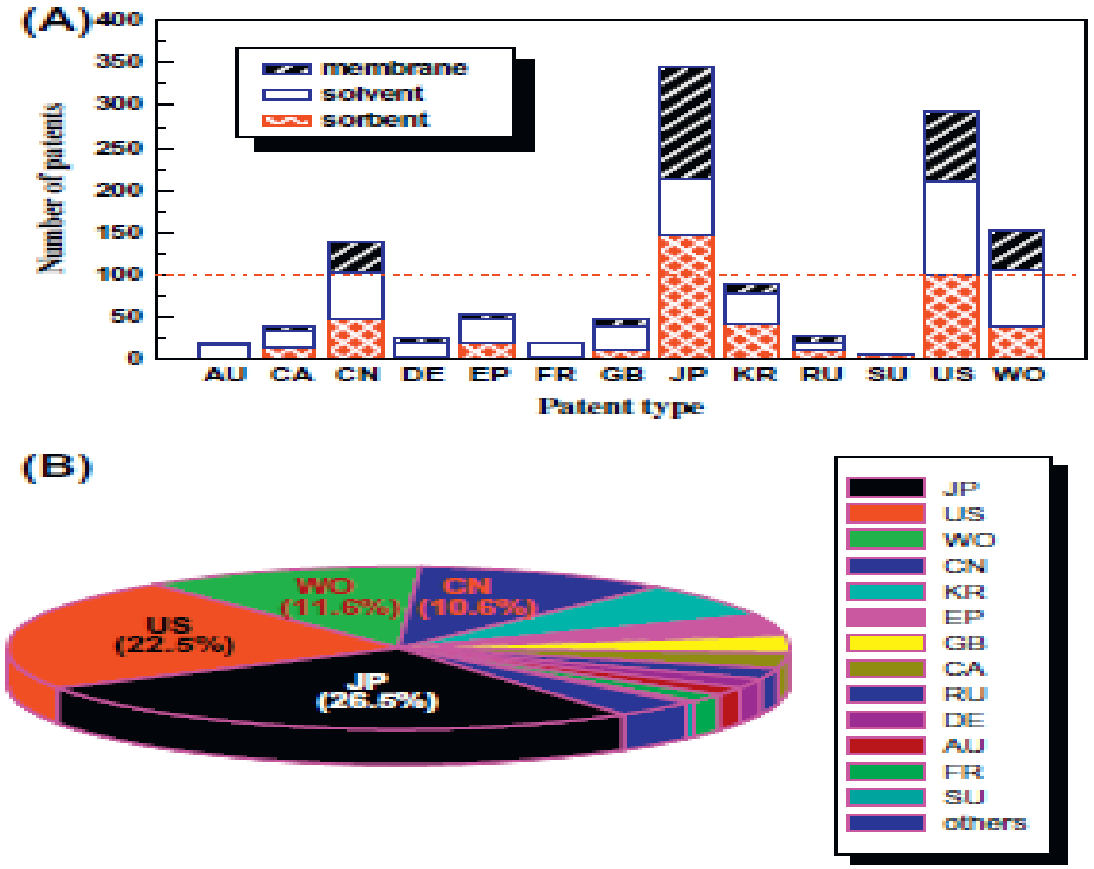

Figure 1.18. (**A**) Number of patents in solvent, sorbent, and membrane *vs.* patent type. (**B**) Distribution of patent type. Country codes: **AU** (Australia); **CA** (Canada); **CN** (China); **DE** (Germany); **EP** (European Patent Office); **FR** (France); **GB** (United Kingdom); **JP** (Japan); **KR** (Korea); **RU** (Russian Federation); **SU** (Soviet Union, USSR); **US** (United States); **WO** (World Intellectual Property Organization, WIPO).[82]

1.7 Sorbents Used for the Capture of CO_2

Several advanced solid CO_2 sorbents like organic–inorganic hybrid materials,[83] metal–organic frameworks (MOF) materials,[84] microporous organic polymers (MOPs),[85] hydrotalcites,[86] calcium oxides[16] and micro- and/or mesoporous sorbents (activated carbon[87] and zeolites[2]) have been reported in the literature. The latter two substances, *viz.*, activated carbon and zeolites have been preferred worldwide due to their ability to tailor their sorption behavior by simple modification of their surface/structural properties and low cost. This is important considering that physisorption of activated carbon and zeolite is dramatically reduced at high temperatures.[10] In this respect, amine grafting [88] or impregnation of samples with amines/polyamines[89] have shown to enhance the CO_2 sorption at high temperatures through chemisorption. The first type of amine functionalization of solid sorbents reduces the leaching and improves the reuse performance. Nevertheless, the addition of the amino groups to the sorbent surface is usually conducted by using toxic amine-containing silanes. Therefore, more benign/green methods to immobilize amines or to fabricate nitrogen-containing CO_2 sorbents are of extreme importance. In addition, the development of an optimal CO_2-sorbents has also been motivated by the aim of finding a capturing material that meets several criteria in order to enable a fair competition/replacement with other industrially applied processes. Consequently, nitrogen-containing, chemically-stable quests with a high sorption capacity (at least 3.0 $mmol_{CO2}/g_{sorbent}$) at temperatures in the range of 40.0 to 80.0 ºC at 1.0 bar have been searched.[85]

1.8 Polyureas: Synthesis, Development, and Green Chemistry Perspectives.

Polyureas are defined as ureylene containing polymers –NHCONH– in the polymer backbone, (Figure 1.19). They are well synthesized and characterized since the early times of polymer chemistry itself, which is based on the condensation reactions that were initiated by the pioneering work of both Carothers[90] and Bayer.[91]

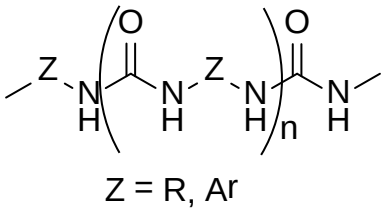

Figure 1.19. General structural formula for polyurea, R: Aliphatic. Ar: Aromatic.

In medicinal chemistry, urea bonds are used as critical structural elements in enzyme inhibitors, (Figure 1.20).[92] In addition, whether as a polyurea or poly(urea-urethane) copolymers, it has many uses. They are widely used in foams, films and membranes, molding, fibers, biomedical applications and coatings.[93,94]

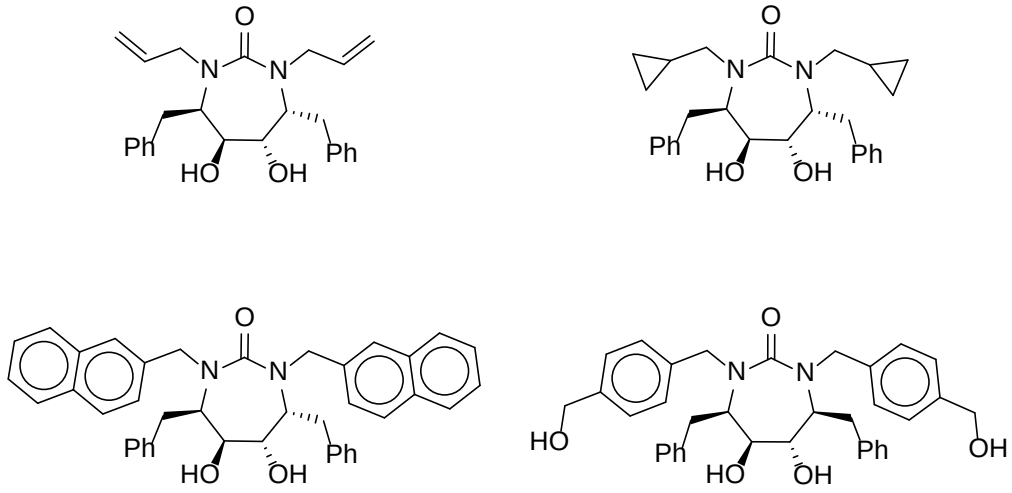

Figure 1.20. Structural representation for some non-peptide, urea-based HIV protease inhibitors

The production of polyurea is based on the reaction of the diamine with phosgene,[95] diisocyanates,[96] triphosgene,[97] biscarbamyl chlorides[98] and dimethyl carbonate (**DMC**),[99] or di-*tert*-butyl dicarbonate (**DTBC**).[100] Furthermore, it was produced using CO_2[101] or *s*CO_2[102], (Figure 1.21).

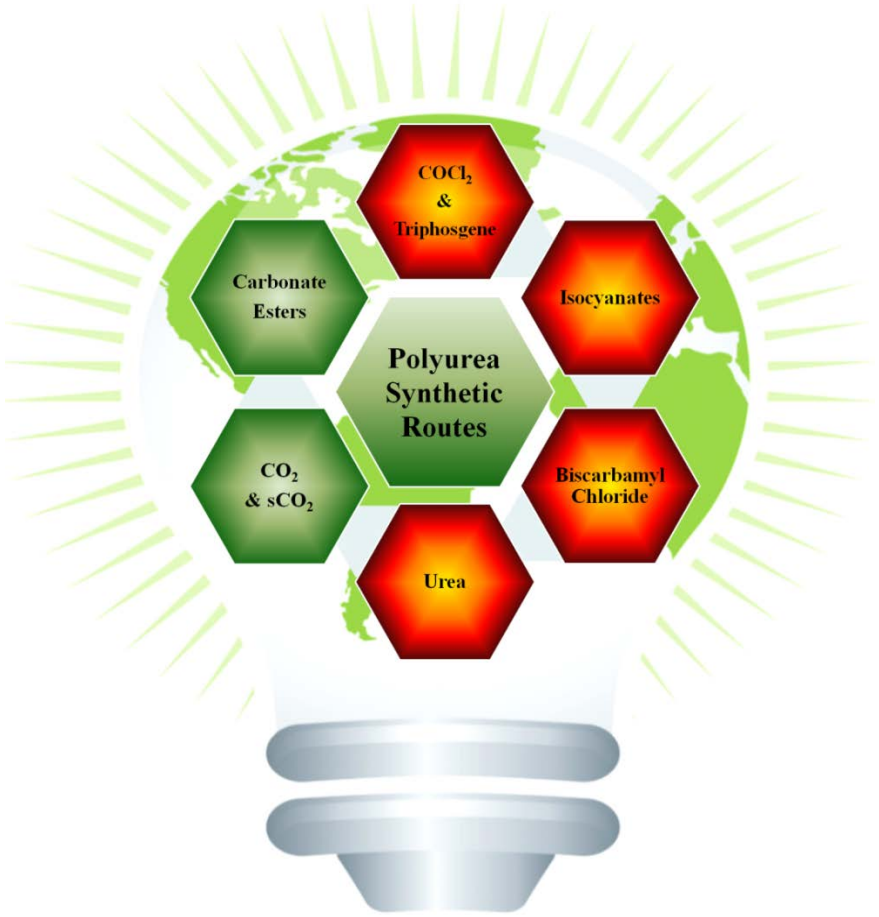

Figure 1.21. Different synthetic routes for the preparation of Polyureas

Industrially, due to the fact that the use of toxic *carbonylating agents* such as phosgene, isocyanate or corrosive alternatives, *e.g.*, biscarbamyl chlorides has environmental and hazardous problems, they are no longer a motivating target to be used. Consequently, much more benign eco-friendly carbonylating agents; *e.g.* alkylene carbonates with high yield reactions to replace the above mentioned toxic and corrosive reagents for the synthesis of polyurea is of great interest to industry and of global demand. On the other hand, oligoureas have biological properties as they are considered to be an attractive class of synthetic oligomers.[103]

Besides urea, among the most important carbonylating agents that can be derived from CO_2 are carbonates (Figure 1.22), *e.g.* DMC, (**A**), ethylene carbonate (**EC**, **B**), propylene carbonate (**PC**, **C**), and diphenyl carbonate (**DPC**, **D**). Due to toxicity of the phenol which is formed as a

byproduct of the latter, green chemistry utilizes EC, DMC and PC as 'benign' carbonylating agents.

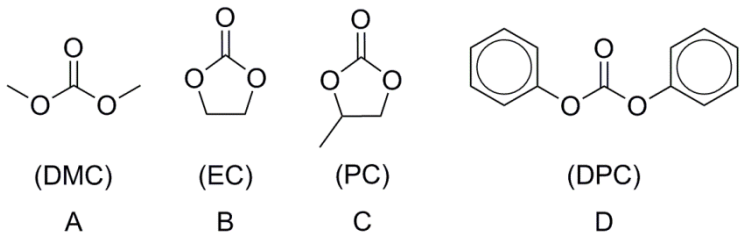

Figure 1.22. Structural representation of some common carbonates.

Furthermore, the formation of liquefied byproducts of the aforementioned carbonylating agents such as methanol, ethylene glycol, and propylene glycol, respectively, makes use of a solvent free process much more feasible and interesting acting as a cosolvent. PC can be synthesized from CO_2[104] in almost quantitave yields,[105] which makes it more interesting to be used as a carbonylating agent that can be used in a pilot or plant scale. Furthermore, the search for benign materials and catalysts that can be recycled and recovered is also considered to be one of the leading goals in industrial plants, such that our work and others for the production of fine chemicals using transition-metal free processes or simply the use of organocatalysis [106] is a must. Therefore, this perspective of green sorbents' generation through an organocatalyzed microwave-assisted, solvent-free, and isocyanate-free synthesis of aliphatic **[*n*]-OU** starting from PC and the aliphatic diamines still a motivation that needs to be fulfilled. Furthermore, the aim of this thesis is to emphasize the use of green chemistry approaches to minimize the hazards of the starting materials and byproducts afterwards to have the most efficient eco-friendly approach for the synthesis of title oligoureas, therefore, PC is used as a carbonylating agent rather than ethylene carbonate due to the fact that propylene glycol is being less toxic than its ethylene homologue.[107] Moreover, the produced **[*n*]-OU**-based sorbents might be easily recycled to yield N-substituted carbamates (Scheme 1.8), as reported for similar substances by Shang *et al*.[108]

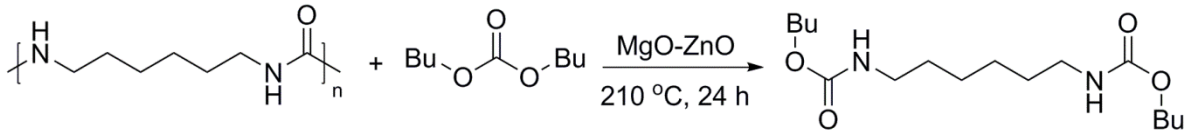

Scheme 1.8. The results of dibutyl hexamethylenedicarbamate (**BHDC**) synthesis from dibutylcarbonate (**DBC**) and **[*6*]-PU**.[108]

1.9 Oligoureas/Polyureas and CO_2 Capture

Simple (oligo)urea-based organic structures have shown to be able to capture CO_2 from air (*vide infra*). These H-bond receptors can absorb CO_2 in the form of carbonate anions forming a 2:1 (host/guest) complex. In 2009, Gale[109] and coworkers reported on the synthesis of some substituted ureas, in which they used to stabilize the formation of alkyl carbamate through their H-bond receptors. This glimpse gave a better understanding for a later study, they showed the interaction with either alkylcarbamate anions formed by the reaction of carbon dioxide with primary aliphatic amines and the zwitterionic amidinium carbamate formed by the reaction of carbon dioxide with 1,4,5,6-tetrahydropyrimidine (THP, Scheme 1.9).[110] By applying both solution and solid state investigations, significant downfield chemical shifts regarding the NH of the urea, which is consistent with a host:guest coordination; *viz.*, anion hydrogen bonding interactions, confirmed the interaction with bound-carbon dioxide species.

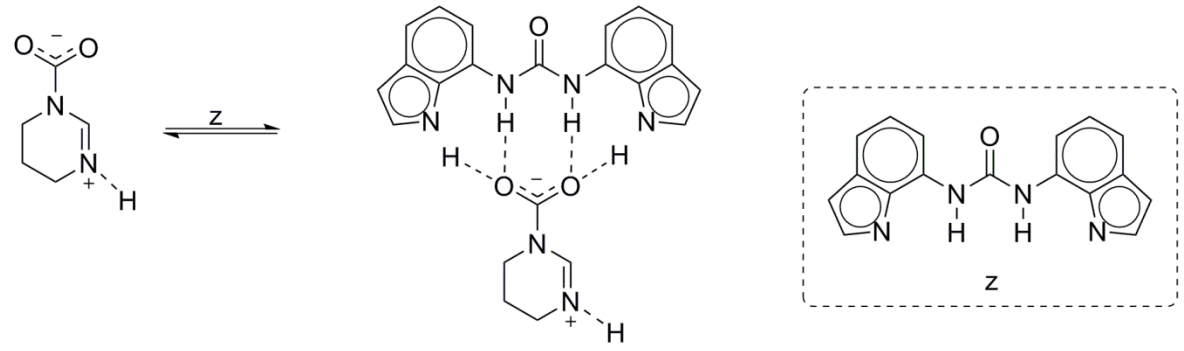

Scheme 1.9. Expected binding mode between the urea derivative and THP-CO_2 complex.[110]

Incorporation of more functionalized groups, *e.g. tren*-based tris-ureas/thioureas, such as phenyl-substituted *tris*-thiourea,[111] *m*-nitrophenyl-substituted *tris*-urea,[112] *p*-cyanophenyl-substituted tris-thiourea,[113] pentafluorophenyl-substituted *tris*-urea,[114] and recently, Pramanik *et al.*[115] synthesized a new tripodal hexaurea derivative in a three-step synthesis, and showed the interactions of a bound CO_3^{2-} with urea motifs, by which each oxygen of the carbonate anion was bound to two ureas (four bound NH···O). In the previous examples, the overall interaction was shown to bind carbonate anions, forming 2:1 (host/guest) complexes as evidenced by single-crystal X-ray diffraction, (Figure 1.23).

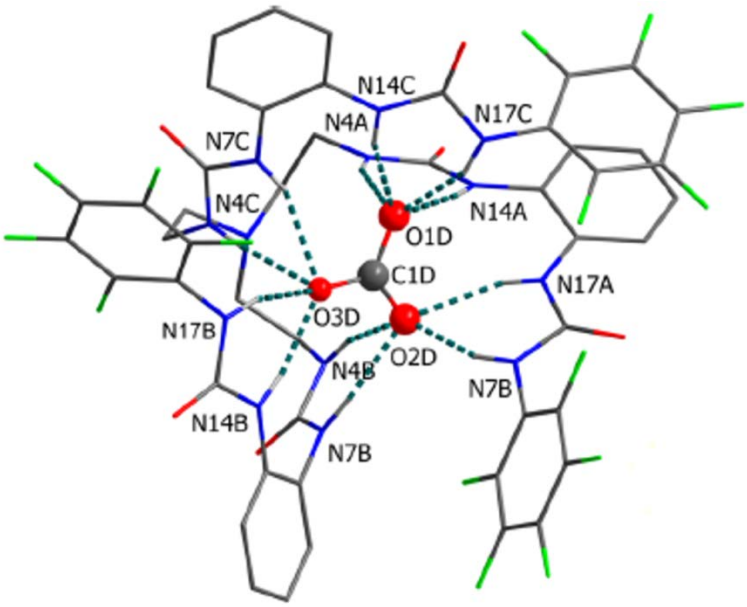

Figure 1.23. Single-crystal X-ray structure of the carbonate complex (countercations and hydrogen atoms on carbons are omitted for clarity).[115]

Interestingly, polyureas have not been intensively explored as CO_2 sorbents. For the first time, this type of sorbent was addressed only in one recent publication [116] where organic molecular networks were formed by crosslinking of multifunctional monomers *via* organic sol-gel polymerization to yield 3D-networks. However, the properties of the products were governed by maintaining the networks as colloidal dispersions below their critical gelation concentration accompanied by the use of highly toxic isocyanates.

Chapter 2

AIM OF THE WORK

2 AIMS OF THE WORK

Aims of the work are explicitly summarized in the following main milestones (**A**, **B**, and **C**). Part **A** which deals with basic concepts when dealing with CO_2 and its corresponding amine interaction. Further, Part **B** deals with synthesis, optimization, and full characterization of [*n*]-oligoureas, (**[*n*]-OU**). Finally, Part **C** gives an insight towards the measurement of CO_2 sorption capacity using a gravimetric method *via* microbalance. Briefly, points are bulleted as follows:

A. Understanding the basic interactions in CO_2-activated nitrogen-bearing donors for the development of an effective system for the capture of CO_2.

1. Investigation on the interaction of diamines and amino alcohols with CO_2.

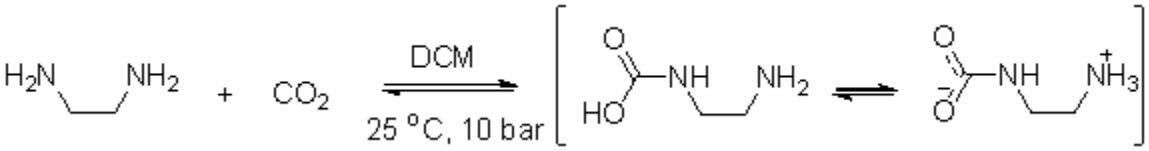

2. Use of *in-situ* techniques to study reversible CO_2 binding reactions of ethylenediamine.

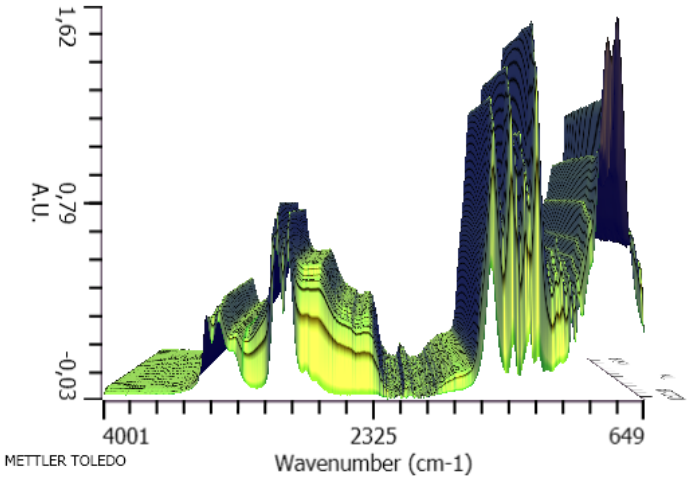

3. Quantification of carbamate, by means spectroscopic techniques, *e.g.* 1H and 13C NMR, HPLC, and GC-MS.

4. Synthesis of organic molecules with multi-arm containing amines.

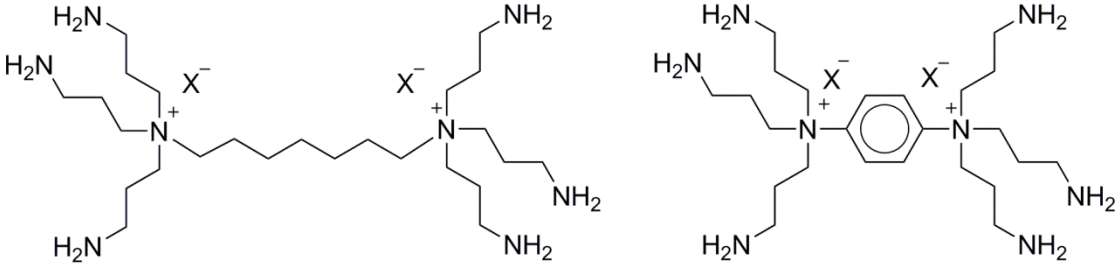

5. Synthesis of other candidates for the capturing of CO_2 using a mono- or bi-tethered imidazolium-based ionic liquids, *viz.*, Task-specific ionic liquids (TSILs) and their presumed polymers/oligomers to capture CO_2.

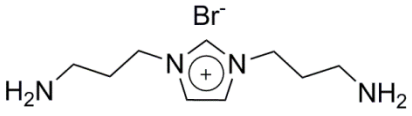

6. Investigation of a newly-developed system for CO_2 capturing, **[*n*]-OUs**.

B. Synthesis, optimization, and full characterization of [*n*]-oligoureas, ([*n*]-OU).

1. Synthesis of aliphatic [*n*]-oligoureas, (**[*n*]-OU; *n* = 4**, **6**, **7**, **10**, and **12**) by a microwave-assisted, organocatalyzed reaction throughout the use of propylene carbonate (**PC**) and aliphatic diamines.

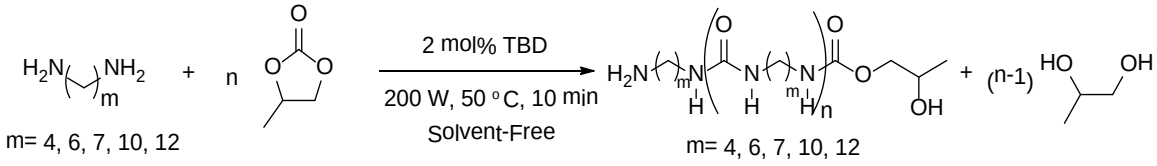

2. Performing optimization reactions to find out the best values to propagate further, using both dynamic and fixed power modes. *viz.*, (organocatalysts used, organocatalyst loading (mol%), microwave power (W), temperature (°C), and time of experiments (min)).

3. Full characterization of the synthesized materials in both solution *via* 1H- & 13C NMR, and solid state using Elemental Analysis (**EA**), **A**ttenuated **T**otal **R**eflectance-**F**ourier **T**ransform **I**nfra-**R**ed Spectroscopy (**ATR-FTIR**).

4. Performing a stability study in acidic solutions of deuterated trifluoroacetic acid (TFA-*d*) as a function of time using 1H NMR over hours to days scale.

5. Performing of a stability study in the solid state, and characterization of thermal properties regarding the synthesized materials *via* **T**hermo-**G**ravimetric **A**nalysis (**TGA**), and **D**ifferential **S**canning **C**alorimetry, (**DSC**). Further testing to confirm crystallinity using **P**owder **X**-**R**ay **D**iffraction (**PXRD**).

C. Performing CO_2 sorption experiments using a gas microbalance.

6. Measurement of CO_2 equilibrium capacities using a TGA-DSC microbalance. Optimization experiments were carried out following the measurement of sorption capacities at 35.0 °C and 1.0 bar of CO_2.

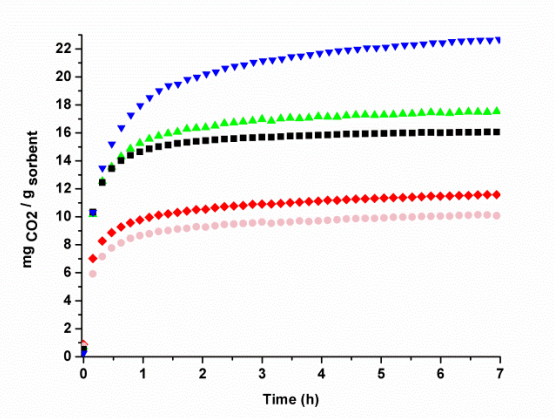

7. Optimization of prepared **[*n*]-OU** based materials at two different activation/desorption temperatures; *viz.*, 60.0 and 100.0 °C (*in vacuuo*).

8. Measurement of the porous character (if any) within the **[*n*]-OU** solid sorbents using a **B**runauer-**E**mmett-**T**eller (**BET**) model.

9. Analysis of the CO_2-sorbed species *via* physi- and/or chemisorption by the means of solid state 13C **C**ross **P**olarization-**M**agic **A**ngle **S**pin (**CP-MAS**) NMR and ATR-FTIR spectroscopy, *i.e.* differentiation of the sorbed materials by confirming the presence of carbamates, carbonates, or bicarbonates.

10. Detection of chemical and thermal stability of the green sorbents *via* TGA.

11. Testing of sorption experiments at different temperatures. *i.e.*, 35.0, 65.0, and 95.0 °C

12. Testing of regenerability of the optimal sorbent at different activation/desorption temperatures, *viz.* 60.0 and 100.0 °C.

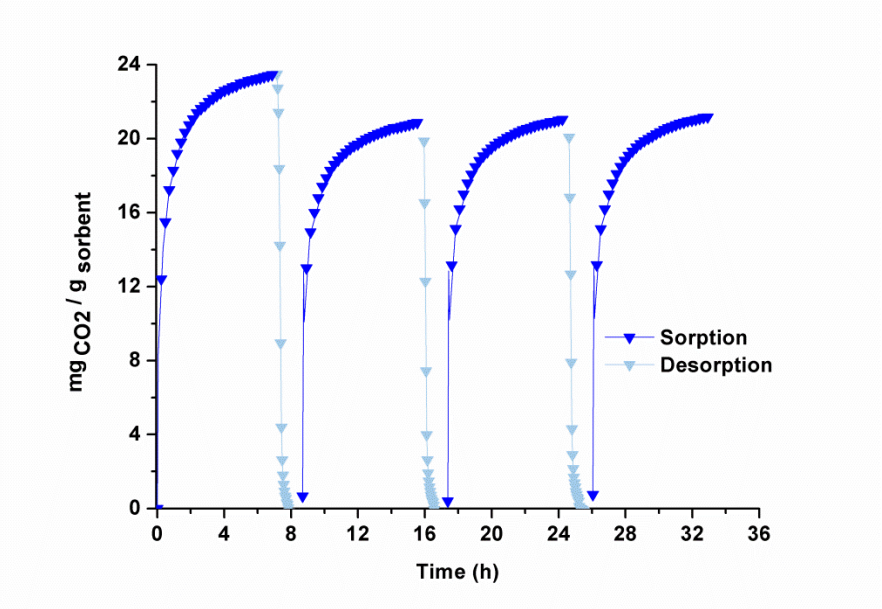

13. Comparison with other well-known technologies.

Chapter 3

RESULTS AND DISCUSSION

3 RESULTS AND DISCUSSION.

3.1 Synthesis of Alkylammonium/Arylammonium Carbamates

Ethylenediamine was set as a model compound to test its interaction with CO_2. Primarily, it shows a very fast sorption kinetics which might be due to the formation of six-membered ring hydrogen bonded product. The product was to isolate and separate out of solution upon contact. The new shift in the IR spectrum was observed for the formation of the carbamate formation RNH---(C=O)O at 1573 cm^{-1}. Carbamates are shown to be affected by water which can undergo further a multi set of equilibria in order to form carbonates and bicarbonates, which was further verified by the use of thermogravimetric analysis (TGA). Due to the insoluble character of the formed carbamates, which hinders their quantification in solution only solid state analyses were feasible to deduce their structures.

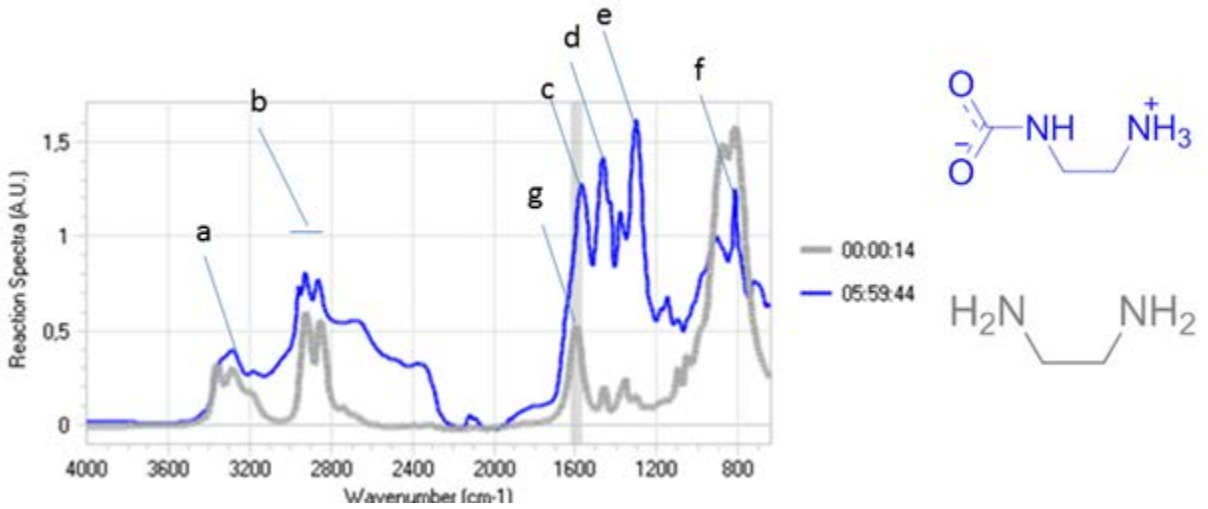

Figure 3.1. *In–situ* ATR-FTIR spectrum of Ethylenediammonium carbamate (**blue**) and its starting material, ethylenediamine (**grey**). **a**: (3282 cm^{-1}) $\boldsymbol{\nu}_{(NH_2)}$; **b**: (2959, 2922 cm^{-1}) $\nu_{as,\ s\ (C\text{-}H)}$; **c**:(1573 cm^{-1}) $\nu_{as\ (COO\text{-})}$; **d**: (1462 cm^{-1}) $\delta_{(NH3+)}$; **e**: (1389 cm^{-1}) $\nu_{s\ (COO\text{-})}$; **f**:(1101 cm^{-1}) $\nu_{(C\text{-}N)}$; **g**: (1595 cm^{-1}) $\omega_{(NH2)}$.

Figure 3.1 shows ATR-FTIR spectra for both the starting material (grey) and the product (blue). The vibrational analysis for the product is already well recognized by the formation of a secondary amine (**a**, ν = 3282 cm^{-1}) as a result of the formation of a carbamate ion, accompanied by the formation of an antisymmetric (**c**, ν_{as} = 1573 cm^{-1}) and symmetric stretching (**e**, ν_s = 1389

cm^{-1}) of the carboxylate group assigned at and (C(=O)-O^-). A broadened band ranging from the 2200-3000 cm^{-1} region was due to intramolecular hydrogen bonding which can be attributed to an ammonium ion. Further peaks are associated with the bending mode of the ammonium (**d**, $\delta_{NH_3^+}$) assigned at 1462 cm^{-1}. A prominent C-N peak, (**f**, ν **C-N**) as a result of the formation of carbamate can be located at 1101 cm^{-1}.[117]

Other candidates were synthesized, *viz.*, 1,3-propylenediamine (**1,3-$C_{3)}$**, 1,6-haxamethylene-diamine (**1,6-C_6**, **HMDA**), and 1,10-decamethylenediamine (**1,10-C_{10}**) and compared relative to ethylenediamine as a function of stability of the presumed carbamates, yields ranged from (78-92) % and well-characterized by elemental analysis and IR spectroscopy which confirmed the presumed structures.

A specially designed TGA experiment to show the stability of a set of series of diammonium carbamates with respect to time was performed. The TGA experiment was carried out starting from room temperature with a ramp of 10.0 °C.min^{-1} up to 60.0 °C, The isotherm at 60.0 °C was kept for 40.0 minutes. After that the temperature was continuously-increased till the evaporation temperature of the parent diamine. The carbamate released CO_2 with time as a result of the reversible character of the system as shown in Figure 3.2 (*vide infra*). To prove the hypothesis, an MS spectrometer was coupled with the outlet of the oven chamber. TGA-MS proved the fact that CO_2, starting materials and unexpectedly the carbamate itself was observed. Hence, sublimation experimnets of carbamates took place but no successful isolation of any crystal was feasible. Interestingly, 10-ammoniodecylcarbamate (**1,10-C_{10} carbamate**) (**d**, Figure 3.2) showed a tangible stability as while an isotherm was applied.

Attempts to quantify the conversion towards the ionic carbamates produced from diamines using GC-MS was not working. Only the parent molecule, *i.e.* ethylenediamine was detected, as a result of a possible decomposition of the carbamate at the high temperature in the injection chamber of the GC.

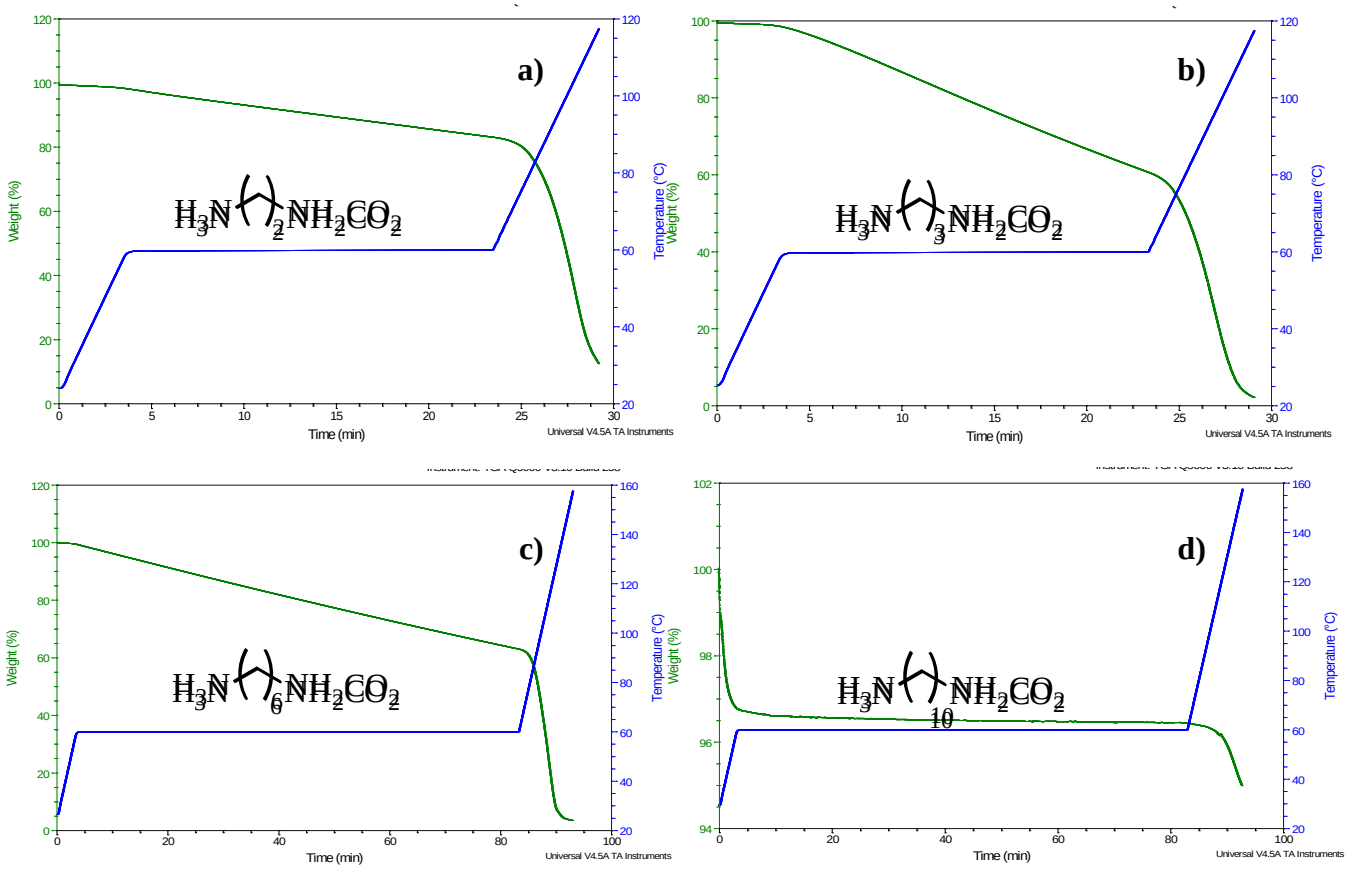

Figure 3.2. TGA diagrams for the carbamates of aliphatic diamines: (**a**): 1,2-C_2 carbamate; (**b**): 1,3-C_3 carbamate; (**c**): 1,6-C_6 carbamate; (**d**): 1,10-C_{10} carbamate.

Further, a theoretical study was carried upon the cooperation of our research group together with scientists from the Theoretical Chemistry Chair to study the stability of the transition state during the absorption of CO_2, *viz.*, carbamate *vs.* carbamic acid, using diamine based solutions to produce cyclic carbonate. Eger *et al.* set ethylenediamine as a model under investigation. In the studied system, where they analyzed the stepwise addition of CO_2 to ethylenediamine, the transition state that mediates the reaction above is either being a carbamate or carbamic acid, depending on the solvent of interest with a value below or above the critical dielectric constant ($\boldsymbol{\varepsilon_{cr}} \approx 18$). Moreover, within high dielectric constant solvents ($\boldsymbol{\varepsilon > \varepsilon_{cr}}$), the direct interaction of **2** with the amino group, yields a betainic ammonium salt, *viz.*, carbamate (**3_15**, 10 kJ•mol^{-1}), and proton transfer (**15_16**) ending with the more favorable betainic carbamate (**16**, 33 kJ•mol^{-1}). On the other hand, When the reversed case is studied ($\boldsymbol{\varepsilon < \varepsilon_{cr}}$), in the mechanism as agents that mediate proton shuttling.[118]

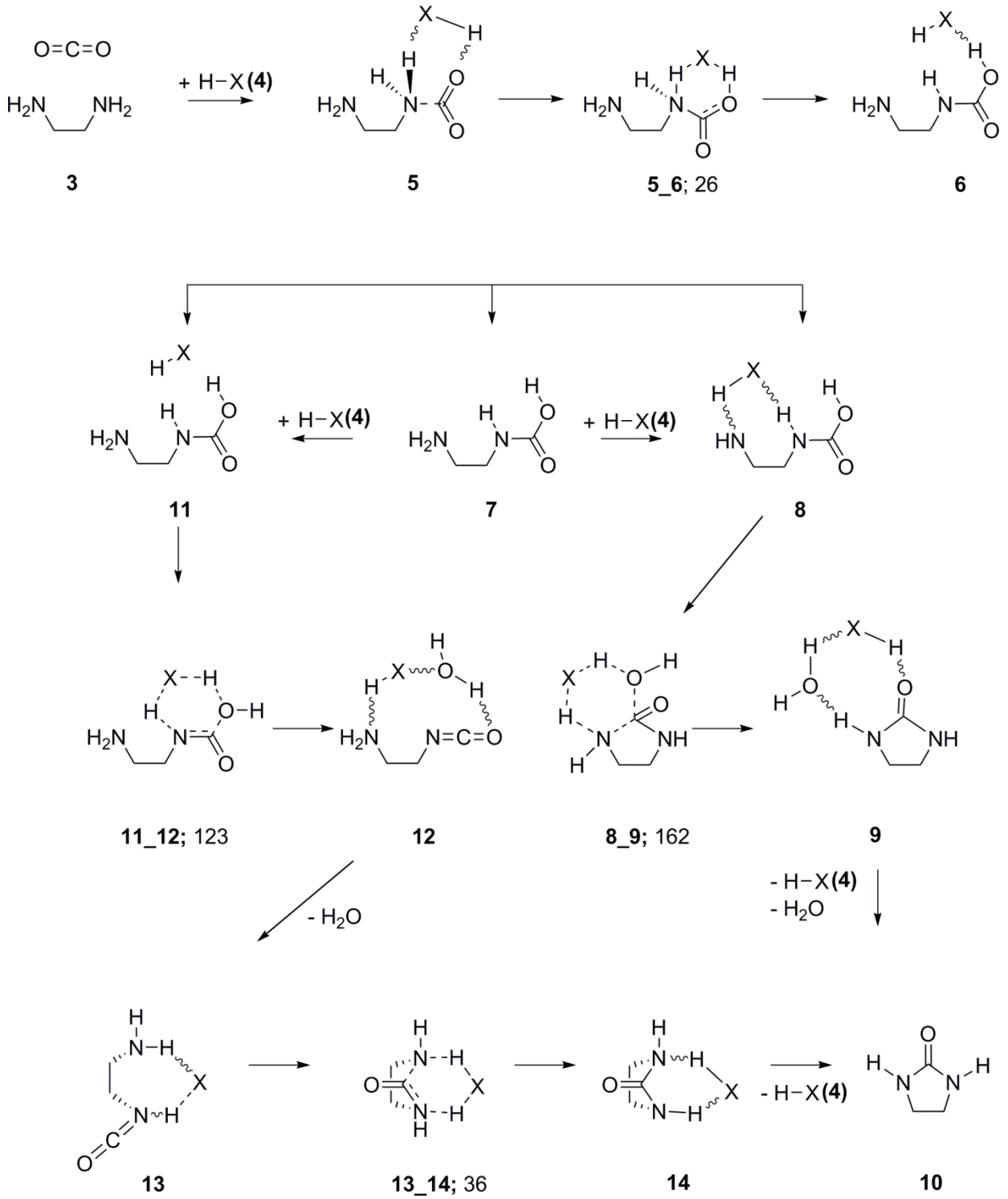

Scheme 3.1. Mechanism of CO_2 (**2**) insertion into a diamine with proton shuttling agent X-H (**4**). The numerical values next to the designators of transition structures indicate the barriers with X-H=$MeNH_2$ (in kJ•mol^{-1}) relative to the immediate precursor. Important hydrogen bonds are indicated by gray wavy lines.[118]

3.2 Substituted Ammonium (alkylamine)-Based Bromides.

One of the disadvantages of using MEA is the use of sacrificial bases (MEA captures 0.5 mol CO_2 per amine group, **1:2 Mechanism**, Section 1.3). Therefore, the synthesis of multi-armed, amine-containing, ammonium bromides (Scheme 3.2) was thought to be a plausible solution to tether as many amine functionalities over one mole of a stable capturing agent. Unfortunately, the synthesis was tedious and showed decomposition products, *e.g.* Olefins as a result of elimination of the alkyl halide under the conditions applied. Moreover, due to having a charged ammonium salt, the presumed syntheses undergo Hoffmann elimination.

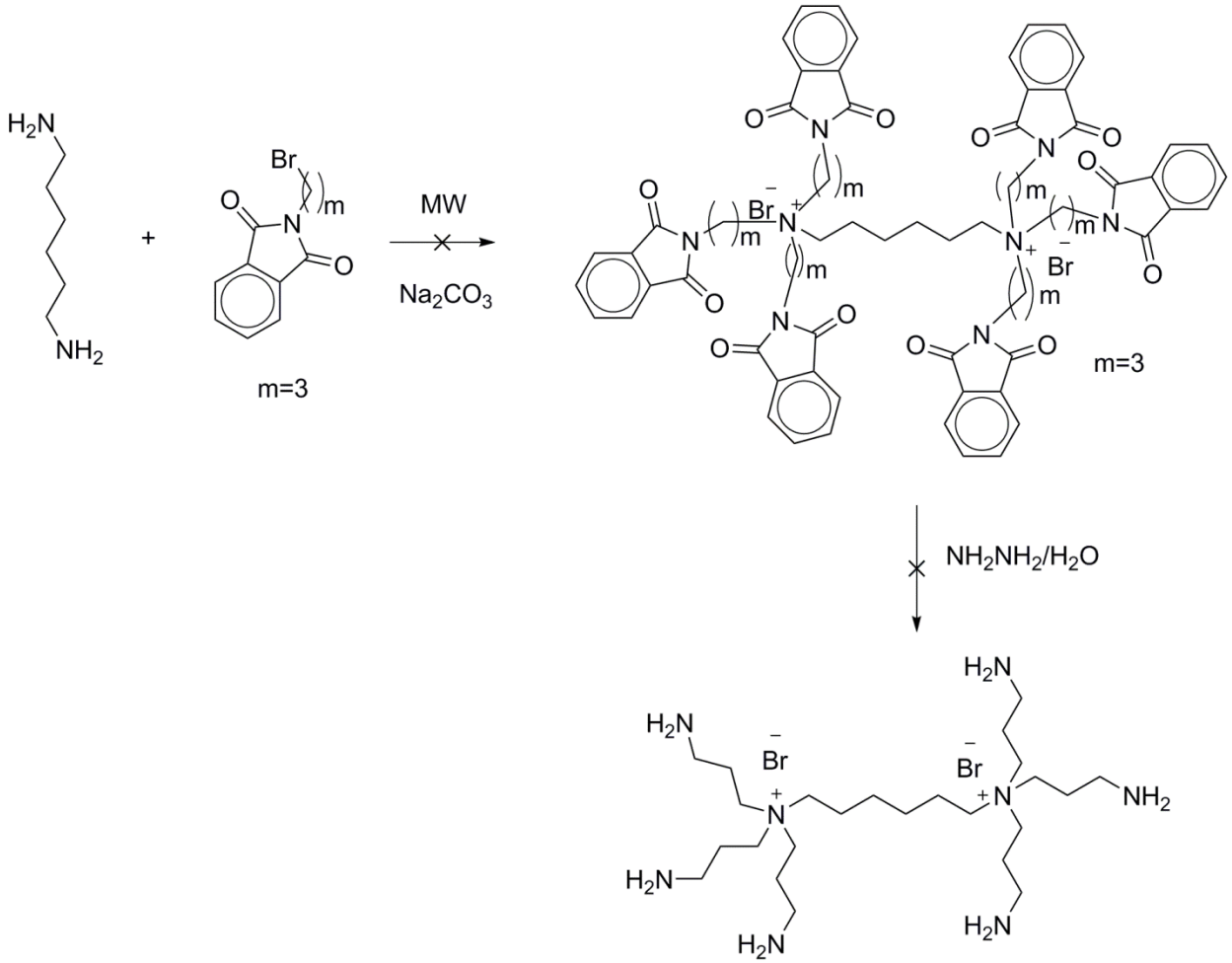

Scheme 3.2. Failed synthesis of the amine-terminated, ammonium bromide-based TSILs

The HMDA substituent was replaced by a *p*-phenylenediamine. The reaction was carried out in DMSO, and followed by 1H NMR measurements. But the same problem took place, no

feasibility for the separation of the product among other byproduct. Therefore, the search for a more stable capturing agent at temperatures for PCC regenerability applications (chemical stability above 150.0 °C) is still on the search (*vide infra*). Hence, TSILs were thought to be a stable solution.

3.3 Task specific ionic liquids (TSILs) and their oligomeric correspondents (OILs)

Briefly, the presumed synthesis as shown in Scheme 3.3 was based on a multistep approach to yield the TSIL with high purity. On a later stage, PILs synthesized will be used as sorbents to effectively capture CO_2. Recently, we discovered a pathway for the synthesis of urea-based OILs using a microwave assisted approach which is based on organocatalyzed, solvent-free synthesis starting from propylene carbonate and diamines.[119] Therefore, our approach was to design a TSIL with a diamine-based imidazolium moiety for the purpose of oligomerization /polymerization to yield their corresponding OILs/PILs, respectively. Imidazolium based ionic liquids and the interaction with the anion to determine CO_2 solubility [120] was chosen among the other candidates due to its high stability and heavily-reported research articles, as it was reported primarily by the pioneering work of Brennecke in 1999.[47a] It should be mentioned that this approach is novel for the synthesis of such PILs. From a synthetic perspective, each of these strategies as well as the polymerization techniques governs different structural parameters of PILs, and demonstrates distinct advantages as well as limitations with respect to the molecular design. Antonietti and coworkers [121] gave the recent update in the production of PILs and their different uses along the multidisciplinary fields.

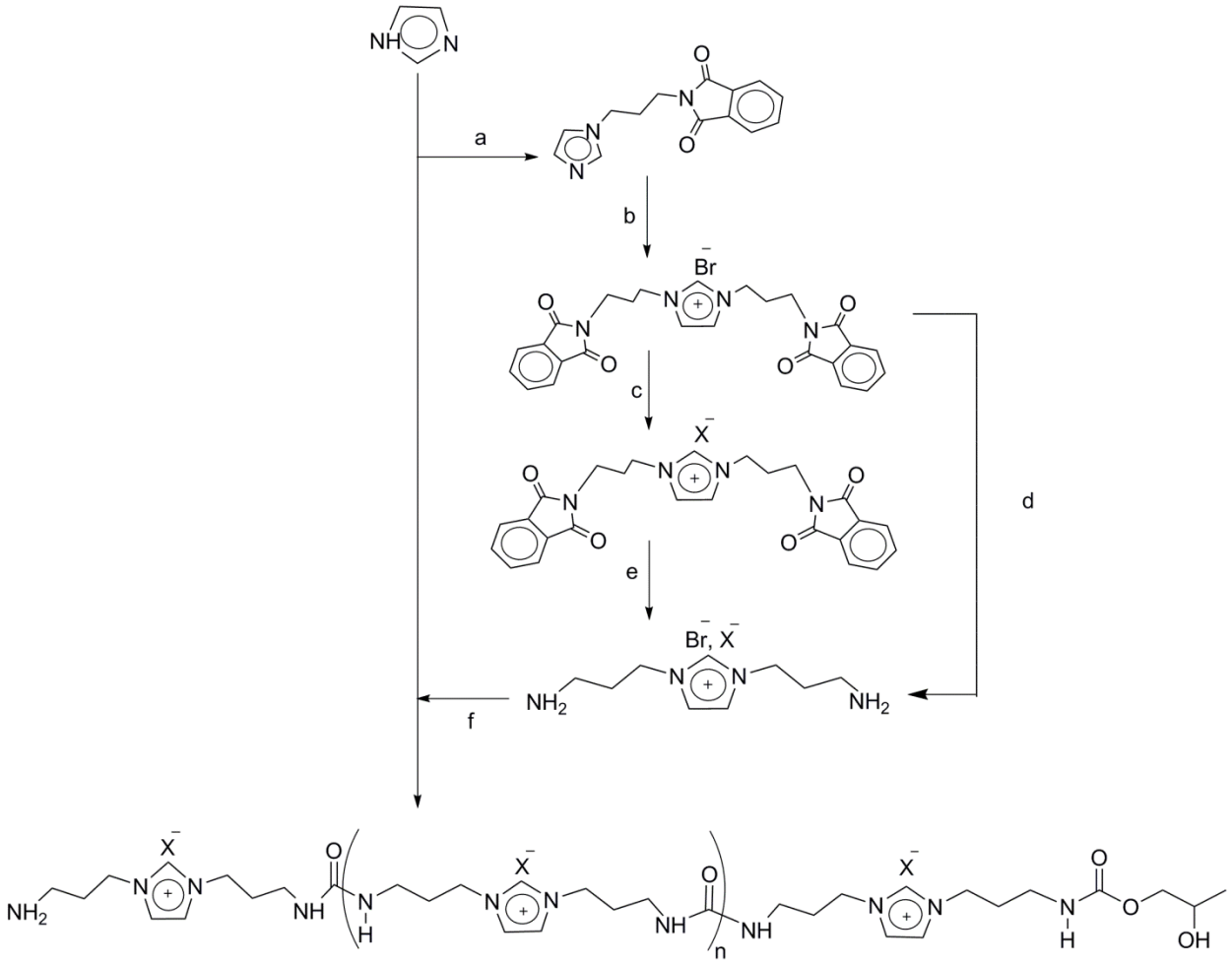

Scheme 3.3. **a)** NaH, THF, $C_{11}H_{10}BrNO_2$, 1 h, r.t., 67.0 °C, 3 h; **b)** $C_{11}H_{10}BrNO_2$, toluene, 60.0 °C,48h; **c)** MX: KPF_6, $NaBF_4$, or $LiTf_2N$ metathesis; **d, e)** $N_2H_4.H_2O$; **f)** TBD, PC, MW.

3.3.1 Synthesis of 2-(3-(1H-imidazol-1-yl)propyl)isoindoline-1,3-dione (3)

Regarding the synthesis of (**3**), a proper protection of the amine terminated alkyl halide of choice is a must. Otherwise, intra- and intermolecular nucleophilic attack occurs, which may give rise to several products that might be difficult to separate. The primary amine group needs to be protected/deprotected to ensure the ease of modification and cleanliness of the target material upon workup. The protecting group was a phthaloyl group. Therefore, *N-(3-bromopropyl)phthalimide* (**2**, Scheme 3.4) was used.

The general procedure for the synthesis of *2-(3-(1H-imidazol-1-yl)propyl)isoindoline-1,3-dione* (**3**, Scheme 3.4), was carried out by Harjani *et al.*[122]

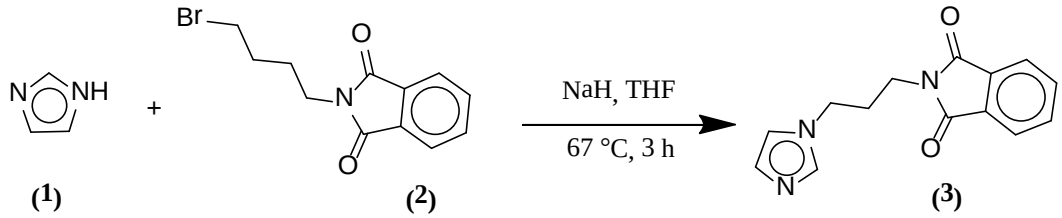

(**1**) (**2**) (**3**)

Scheme 3.4. Ternerization reaction of mono-substituted TSIL-precursor (**3**)

Harjani *et al.* isolated the final product (**3**) as an amorphous white powder with a yield of 80%. A slight modification was carried out concerning the last step, the final product was concentrated and left to crystallize, crystals were formed and collected *ca.* 60%. Furthermore, 1H NMR analysis of (**3**) was performed in deuterated methanol, MeOH-d^4. The 1H NMR of the organic ternerized-imidazole (**3**) is shown in Figure 3.3. A multiplet assigned at (7.76-7.85) ppm, this multiplet region gives a clear indicator towards the presence of the aromatic ring of the phthalimide's phenyl, *viz.*, **7** and **8** (Figure 3.3). A singlet at 7.70 ppm corresponding to an imidazolium **C2** (**1**, Figure 3.3) was observed. Further two more singlets at 7.17 and 6.92 ppm can be ascribed to the hydrogen's **3** and **2**, respectively (Figure 3.3). The aliphatic spacer's hydrogen's **6**, **4** and **5** can be distinguished as two triplets at 4.09, 3.68, and a pentet at 2.17 ppm, respectively. Moreover, Elemental analysis confirmed the proposed structure for both calculated and found molecule for the TSIL precursor (**3**).

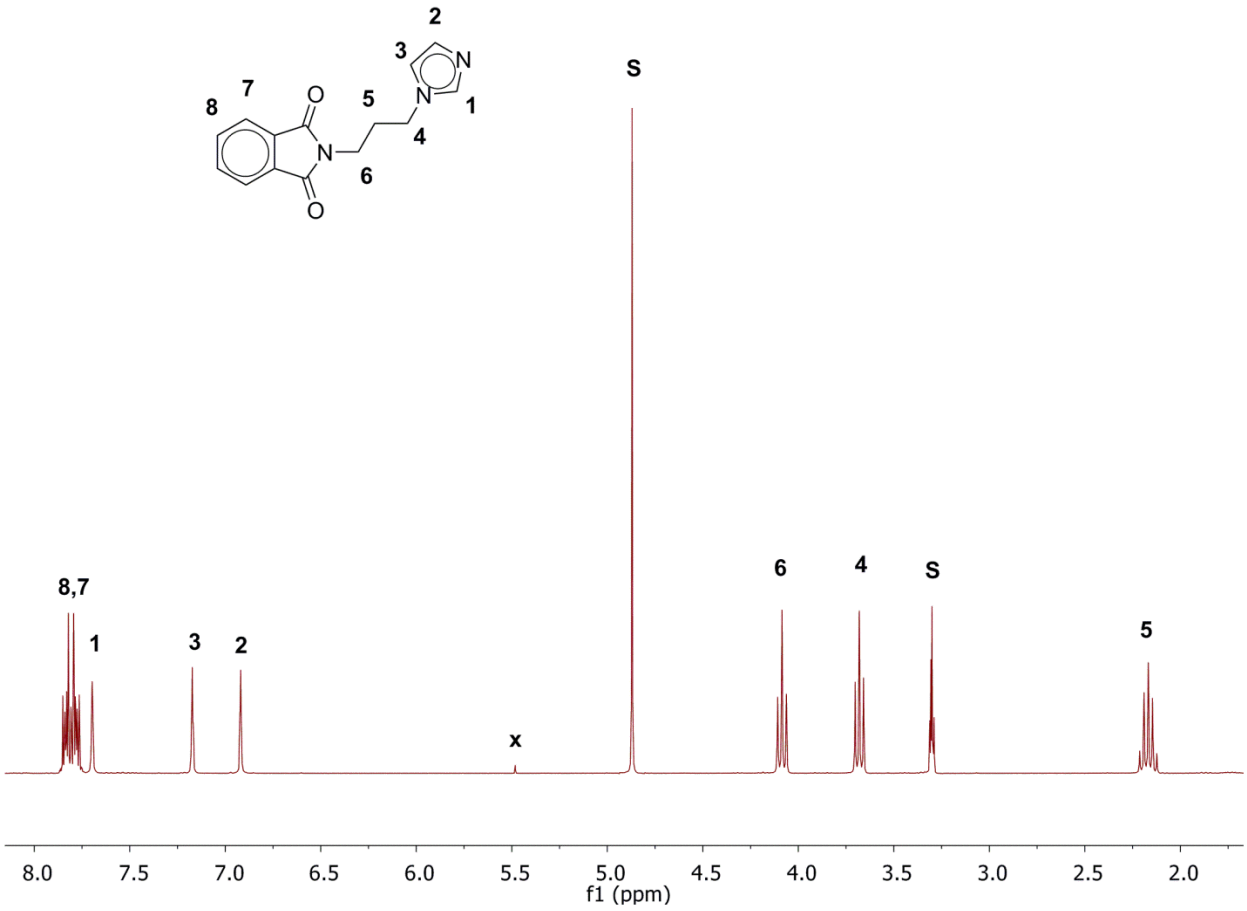

Figure 3.3. 1H NMR in MeOH-d^4 of the organic compound. **S**: solvent; **x**: DCM.

3.3.2 Synthesis of 1,3-bis(3-(1,3-dioxoisoindolin-2-yl)propyl)-1H-imidazol-3-ium bromide (**4**)

Two different pathways were used for the synthesis of the di-substituted TSIL precursor (**4**, Scheme 3.4); *viz.*, Thermal and microwave-assisted pathways. Both pathways gave the same chemoselectivity regarding the product but in different yields, which were 28 and 91% regarding the thermal and microwave-assisted approaches, respectively. Preference was given towards using a microwave reactor due to higher yielding as well as shorter reaction times (20 min *vs.* 48 h).

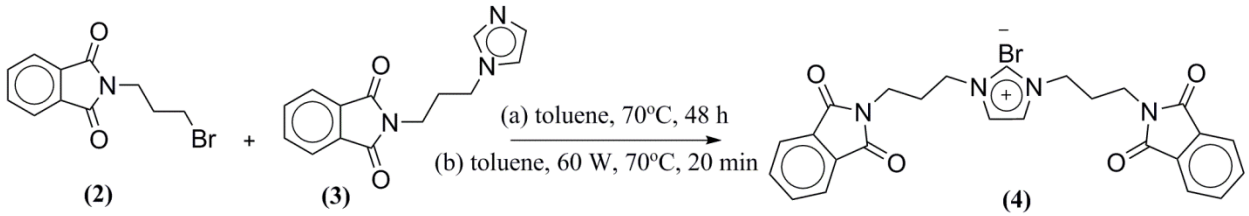

Scheme 3.5. Quaternization reaction of the di-substituted TSIL precursor (**4**)

The use of microwave synthesis has considerably speeded up the TSIL preparation. Furthermore, the 1H NMR analysis for the prepared TSIL precursor (**4**) was shown in Figure 3.4, a singlet at 9.07 ppm, which can be ascribed to the hydrogen at the C2 of the imidazolium ring. (**1**, Figure 3.4). Moreover, a solid evidence for the quaternerization process due to a shift to a more down field position can be seen clearly within the alkylene chain's hydrogens. *i.e.* **3** to **4**, (Figure 3.4**)**. A multiplet observed in the region (7.79-7.91) ppm, which can be ascribed to the aromatic phenyl of the phthalimide moiety, **6** (Figure 3.4). A singlet at 7.74 ppm which corresponds to aromatic hydrogen for the imidazolium ring **2**. The aliphatic arm hydrogen's **5**, **4** and **3** can be distinguished as a triplet at 3.75, pentet at 2.32 and a triplet at 4.30, respectively. Elemental analysis for TSIL-precursor (**4**) confirmed the calculated CHN ratio.

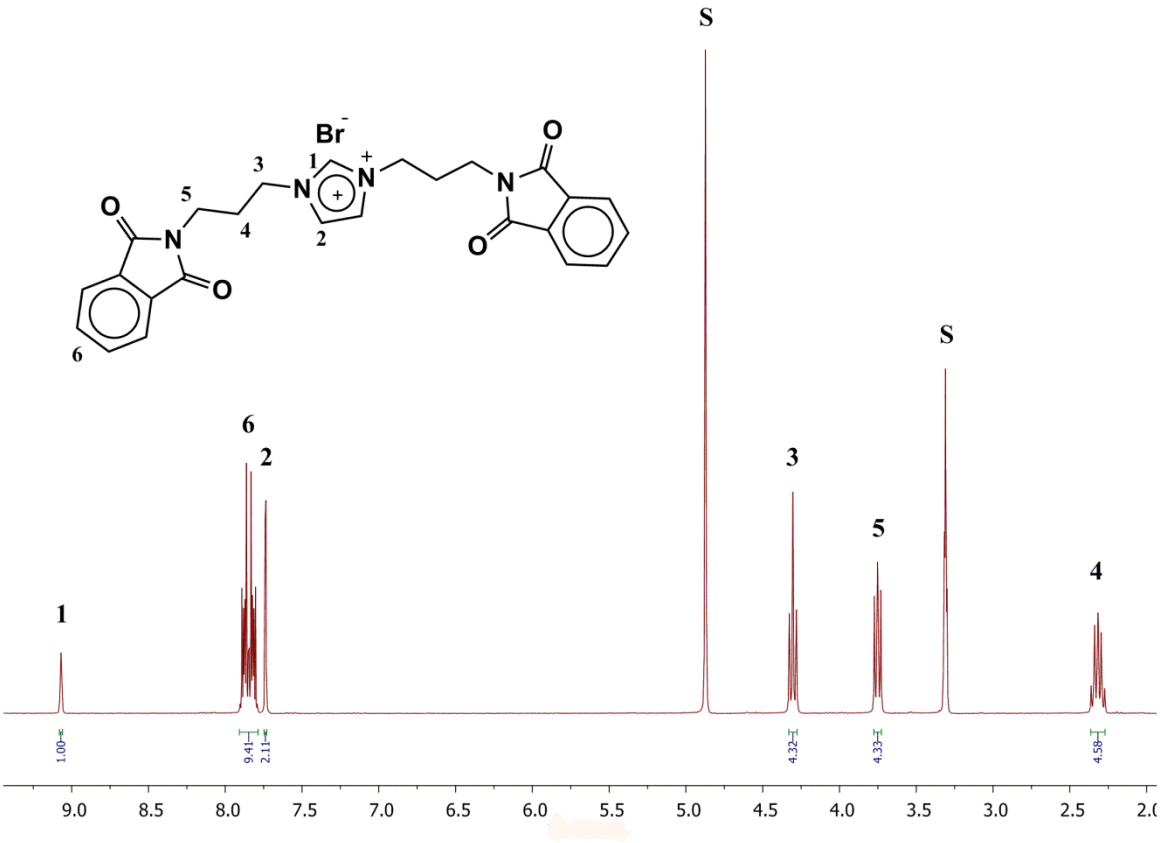

Figure 3.4. 1H NMR in MeOH-d^4 of product (**4**); **S**: Solvent.

3.3.3 Hydrolysis of TSIL-precursor (4) to yield 1,3-bis(3-aminopropyl)-1H-imidazol-3-ium Bromide, TSIL-Br (10)

In the literature, several methods were used for the production of the TSIL (**10**). Instead of working directly with imidazole and *3-bromopropylamine hydrobromide*, it was a problematic issue to clean the final product. This might result in multi nucleophilic attacks due to high nucleophilicity of the resulting secondary and tertiary amines once formed. In order to avoid this problem, it was thought to proceed with a suitable protecting group, *viz.*, the use of phthaloyl group. The hydrolysis of the TSIL-Precursor was carried out in basic solution using ethanolic hydrazine monohydrate solution. The yield was 99.0% (NMR yield, assay: 84.0 %). A singlet shown at 8.35 ppm which is presumably due to the H-2 of the imidazolium ring **1**. A singlet at 7.70 ppm which corresponds to an aromatic hydrogen H-4 for the imidazolium ring **2**, the aliphatic arm hydrogen's **3**, **5** and **4** (Figure 3.5) can be distinguished as a triplet at 4.34, triplet at

2.81 and a pentet at 2.13. The main impurity which can ascribed to two sets of multiplets in the ranges of (8.18-8.24), (7.80-7.84) is attributed to the aromatic hydrogens of the phthalhydrazide, **x**. The reason why for this impurity presumably is due to the partial solubility of the phthalhydrazide hydrolysis byproduct.in the synthesized (**10**).

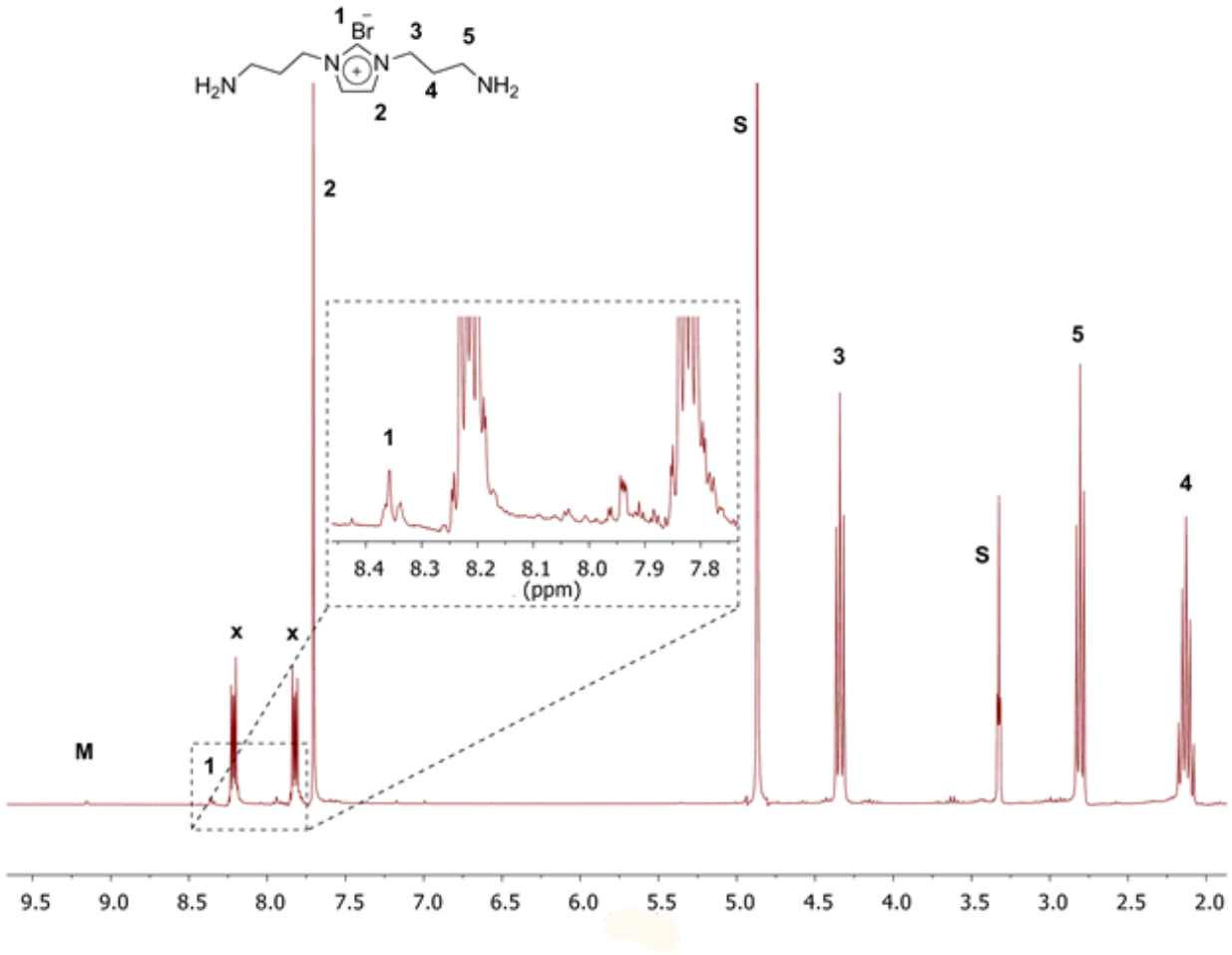

Figure 3.5. 1H NMR of TSIL-Br (**10**) in MeOH-d^4. **M**: Traces of starting material, **x**: hydrogen region showing the aromatic rings of the dissolved byproduct, phthalhydrazide.

3.3.4 Failed Manipulation of Anion Exchange (6-8) and Attempted Hydrolysis of TSILs precursors (**11-13**)

The anion exchange (double replacement) reactions using metals salts (**MX**) of potassium hexafluorophosphate (KPF_6, **5a**) sodium tetrafluoroborate ($NaBF_4$, **5b**), and lithium bis((trifluoro-methyl)sulfonyl)imide ($LiTf_2N$, **5c**) to yield TSIL-precursors with different counter ions of PF_6^- (**6**), BF_4^- (**7**), Tf_2N^- (**8**) was not successful (Scheme 3.6).

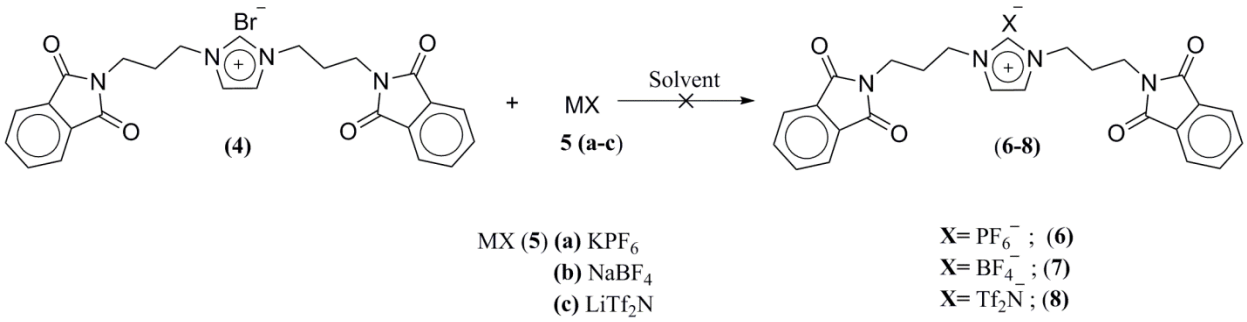

Scheme 3.6. Failed anion exchange of TSIL-precursor (**4**) using different metal salts (**MX**), **5**(**a-c**)

Moreover, the hydrolysis of the TSIL precursors (**6-8**) to yield the TSILs with counter anions (X^- = PF_6^- (**11**), BF_4^- (**12**), Tf_2N^- (**13**) (Scheme 3.7) was not successful due to contamination of TSILs (**11-13**) with both counterions.

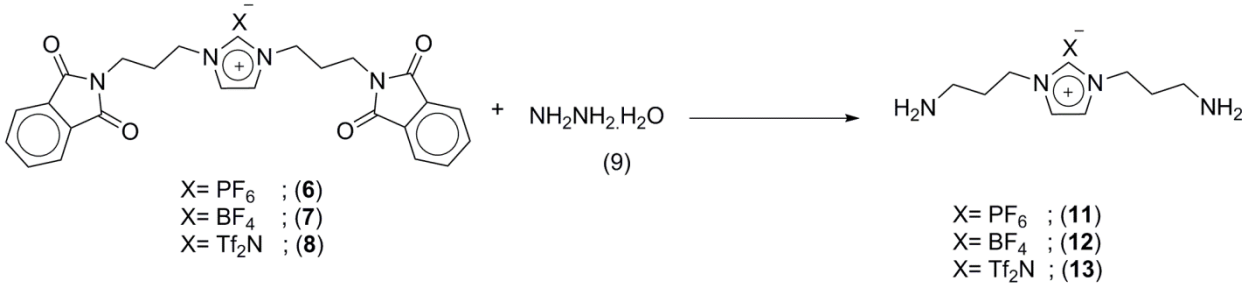

Scheme 3.7. Attempted hydrolysis of the TSIL precursors (**6-8**) to yield TSIL-PF_6 (**11**), TSIL-BF_4 (**12**) and TSIL-Tf_2N (**13**)

3.3.5 Imidazolium-based TSIL and their Oligo(ionic liquids) (OILs) and CO_2 capturing.

TSIL (**10**) or similar structures with different alkyl chain (lengths) was prepared in the literature by many other research groups. As a rule of thumb, all of them use a protecting group for the primary amine terminal to eliminate any other undesired side reaction within the starting material (alkyl halides) that may occur during synthesis. If not protected, this might give multiple nucleophilic substitutions as a result of the high reactivity of the resulting product which does not facilitate both cleanliness and ease of separation. In our work, we used a phthaloyl-protecting group that is easy to cleave off upon hydrolysis.

The first research group to report the structure was Tan *et al.*,[123] They reported on the use of a TSIL as a comonomer for a material being prepared to produce a heterogeneous catalyst for immobilizing a Mn(III)-based catalyst for enantioselective epoxidation of styrene (Scheme 3.8), where they synthesize TSIL starting from imidazole and 3-bromopropylamine (non-existent as a chemical material) unless the authors made a typo and meant the use of its hydrobromide salt.

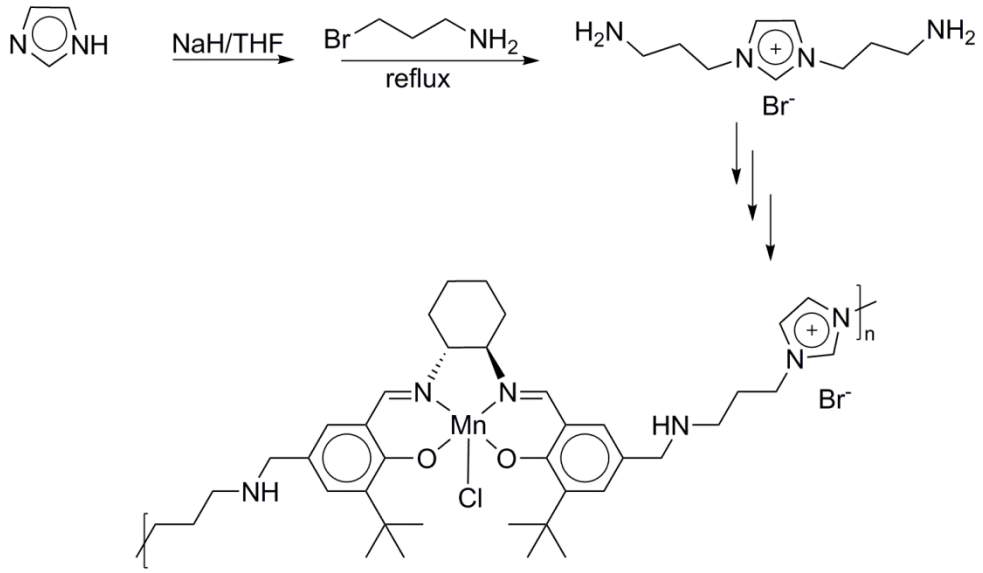

Scheme 3.8. Preparation of TSIL (**10**) and their use as a comonomer for the production of oligomeric Mn(III)-based heterogeneous catalyst for the enantioselective epoxidation of styrene.[123]

Within their experimental procedure, he should have written an extra additional step for use of a base to neutralize the acidic moiety (hydrobromic acid) to yield the free amine groups (the experimental procedure for preparing the TSIL (**10**) was not written precisely).

Moreover, Coleman and coworkers,[124] managed to synthesize (**10**) in a much more pure, sophisticated, multi-step synthesis (Scheme 3.9). The starting material synthesis requires further three-step synthesis that was tedious and time-consuming.

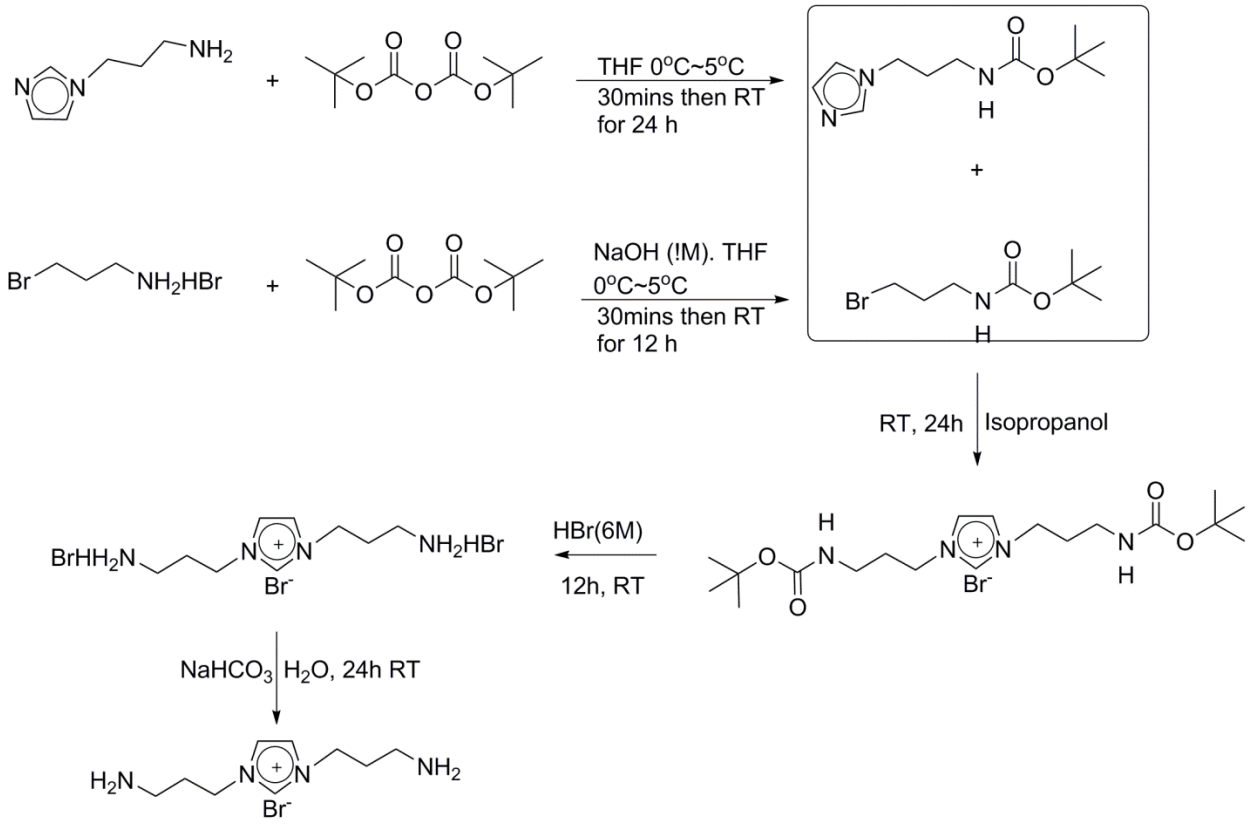

Scheme 3.9. Multi-Step synthesis carried out by Coleman and coworkers.[124]

Very recently, a new protocol that came along with a very less demanding step was reported by Zhang *et al.*,[125] In this protocol 3-bromopropylamine hydrobromide was treated with a protecting group, *viz.*, Triphenylmethyl chloride (TrCl), (Scheme 3.10). So far, this report is considered to be the best among other experimental procedures for the preparation of (**10**). The

CO_2 capture capacity in aqueous solution was estimated as 1.05 mol CO_2 per mol of TSIL at 303.15 K, (18.5 wt %) with good thermal stability (T_d *ca.* 250 °C).

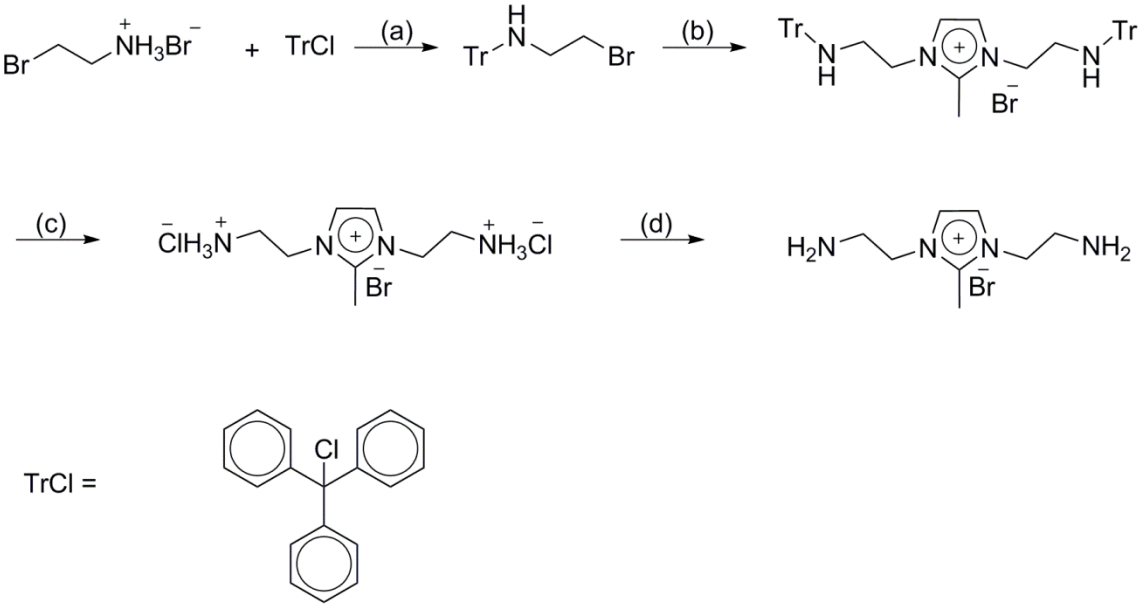

Scheme 3.10. Synthesis of (**10**) reported by Zhang *et al*.[125]

TSIL-Br (**10**) was synthesized using a new approach of protected amine terminals. This TSIL is considered to have a dual function as a capturing agent as well as a co-monomer to be used for the oligomerization/polymerization (Scheme 3.11). A neat sample of (**10**) was submitted for CO_2 capturing purposes using a Setaram microbalance. The sample was activated at 100.0 °C for 1 h (*in vacuuo*), sorption took place at 35.0 °C. Surprisingly, CO_2 sorption was 1.7 wt%. Presumably, it can be attributed to the high viscosities associated with TSIL and its H-bonding network. Such low sorption values, were observed by Davis and coworkers who used a mono-substituted, amine-tethered TSIL (Scheme 1.5).[46]

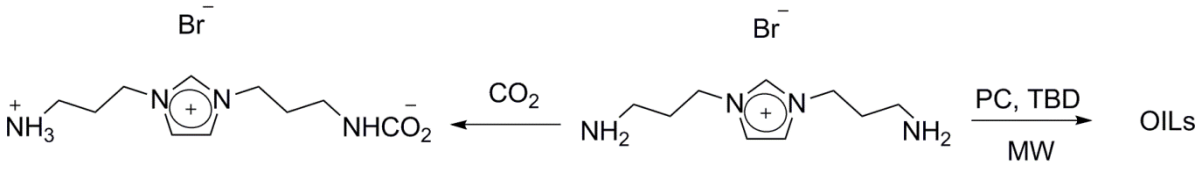

Scheme 3.11. TSIL (**10**) dual function as a capturing agent, OILs: Oligo(ionic liquids).

On the other hand, the oligomeric form can be synthesized *via* two basic strategies: Firstly, chemical modification of existing polymers *e.g.* transplantation of IL functionalities, which is not the followed methodology in this work. Secondly, direct polymerization of IL monomers,[55] *e.g.* synthesis of PILs through polyurea formation.

Recently,[119] we discovered a pathway for the synthesis of OILs using a novel approach which is based on a microwave assisted, organocatalyzed, solvent-free synthesis starting from propylene carbonate and diamines. Therefore, our approach was to design an IL-based imidazolium diamine moiety for the purpose of oligomerization/polymerization to yield the corresponding OILs/PILs, respectively. It is noteworthy that these materials are novel for the synthesis of these OILs (if any, Scheme 3.12).

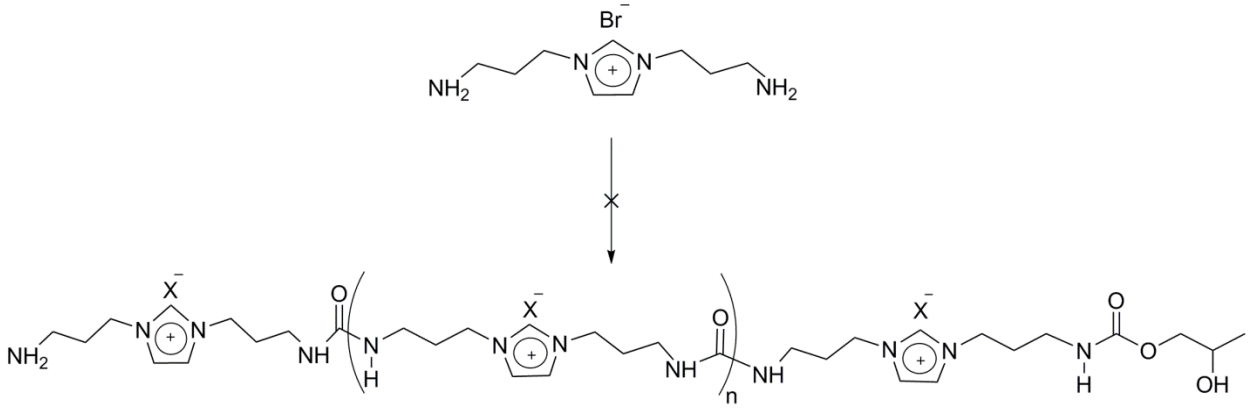

Scheme 3.12. Presumed Synthesis of the Oligo(ionic liquids) (**OILs**). Conditions applied: 1:1 (**10**):PC, 2.0 mol% TBD, 50.0 ºC, 200.0 W.

All reactions were carried out under air, following up a previously published protocol.[119] The reaction was heating very rapidly due to the ionic nature of the TSIL, but the reaction did not show any produced oligomers as shown by 1H NMR. The same reaction was repeated, and materials were prepared inside the glovebox, and the same result was obtained as the former experiment excluding the possibility of poisoning of the materials due to air. Failure to obtain OILs was achieved presumably due to high viscosity of TSIL which might prevent the diffusion of TSIL (**10**) towards PC. Application of the same reaction using polar solvents, *e.g.* DMF, DMSO was also carried out. No materials were achieved, presumably due to poisoning of the organocatalyst by the presence of the solvent.

3.4 Aliphatic [*n*]-Oligoureas, [*n*]-OUs

3.4.1 Optimization conditions with 1,6-hexamethylenediamine (HMDA)

3.4.1.1 Dynamic control mode

As a model, the dynamic mode (Section 4.3.1.1) was used in order to optimize the conditions for the oligomerization a set of parameters were studied using an equimolar ratio of 1,6-hexamethylenediamine (**HMDA**) and PC as a model reaction to yield the **[*6*]-OU**. The parameters were chosen as a function of catalyst loading, microwave energy, temperature and time. The optimized conditions are: 2.0 mol% TBD, 50.0 °C, 10.0 min and 200.0 W.

3.4.1.2 Fixed-Power mode

During optimization, the microwave effect was investigated in the dynamic mode (Section 4.3.1.1). In addition, after optimization, **[*6*]-OU** synthesis was further tested using the fixed mode (Section 4.3.1.2) as shown in Table 3.1. Using fixed power almost quantitative yields were obtained as a function of time, Table 3.2. Best microwave power was at 10.0 W with a yield of 96.0%. It is noteworthy that 1.0 and 2.0 W runs did not yield any collected products.

1H NMR shows a proportional increase in yield upon increasing the power till a maximum is reached at 10.0 W (run 4, Table 3.1). The decrease in yield is presumably due to decomposition of the prepared **[*6*]-OU** due to focused microwave energy. Therefore, it was concluded to have the power input (10.0 W) as an optimal power. The DP value is equal to 12 for the obtained **[*6*]-OU** within plausible error from NMR.[119] Upon fixing the microwave power to see the effect of time on conversion of the oligourea it would be plausible to think that upon increasing time an increase in DP values would be seen. The results came in accordance to the expected hypothesis.

Table 3.1. Percentage yield as a function of Microwave energy using the fixed mode.

Run	Power (W)	Yield (%) [a]
1	5.0	0
2	8.0	30.0
3	9.0	28.0
4	10.0	96.0
5	12.0	95.0

[a] Conditions applied (optimized): 1:1diamine:PC; 2.0 mL PC; 2.0 mol% TBD, t = 20.0 min.

Table 3.2 shows percentage yield as a function of time. At time t = 10 min, There was no product formed. A DP for the **[*6*]-OU** is = 16 after one hour, with a yield of 97.0% and equals 20 after two hours with a 98.0% yield. Results are reproducible, and almost quantitative conversion can be obtained upon tuning the appropriate time.[119]

Table 3.2. Percentage yield as a function of time (*min*) using the fixed mode

Run	Time, *t* (*min*)	Yield (%)[a]
1	10.0	0
2	15.0	94.0
3	20.0	96.0
4	60.0	97.0
5	120.0	98.0

[a] Conditions applied (*optimized*): 1diamine:1 PC; 2.0 mL PC; 2.0 mol% TBD, 10.0W.

3.4.2 Screening and testing different variables

The production of the **[*6*]-OU** was a solvent-free, transition-metal free, microwave-assisted, eco-friendly synthesized, low catalyst loading, lower toxicity of chemicals involved, less time and energy consuming. All of these are considered as good merits that enhance the efficiency of the whole process. To the best of our knowledge, regarding polyurea synthesis, the temperature of the reaction conducted was as low as 50.0 °C, which is considered to be the lowest temperature for the preparation of polyurea based-materials, using condensation polymerization starting from a *non-isocyanate* route.[93,126] This makes the process itself much more attractive under the applied conditions. For the purification purposes, five different workup-procedures were used: Soxhlet extraction, methanol/boiling water, methanol soaking/washing, and trifluoroacetic acid (TFA) solubilization followed by precipitation in either Et_2O or methanol. Regarding TFA-containing methods, traces or leftovers of the acid, might give failure during analysis of the oligomers while performing thermal analyses. The easiest workup-procedure was "soaking in methanol" method; it was the most efficient among others in purity and processing time.

3.4.2.1 Organocatalysts Screening

In this study, organocatalysts 1,5,7-triazabicyclo[4.4.0]dec-5-ene (**TBD**, **a**), 1,8-diazabicyclo[5.4.0]undec-7-ene (**DBU**, **b**), Schreiner's thiourea based catalyst (**c**), 1,5-diazabicyclo[4.3.0]non-5-ene (**DBN**, **d**), 1,1,3,3-tetramethylguanidine (**TMG**, **e**), 1,4-diazabicyclo[2.2.2]octane (**DABCO**, **f**) and 4-dimethylaminopyridine (**DMAP**, **g**) were used. *Other than TBD (**a**)-catalyzed processes, which gave an off-white solid paste, all other* catalyzed-*processes using organocatalysts* (**b-g**) *gave oily products.* The arbitrary parameters were 3.1 mol% cat., 220.0 W, 100.0 °C, 10.0 min, and solvent-free conditions. It was shown that it is superior in catalysis to give the aforementioned oligomers.[119]

The guanidine super base TBD (**a**) is one of the most effective commercially-available organocatalysts for the oligomerization process when compared to other organocatalysts.[106] It was reported to have an activity in condensing propylene glycol with CO_2 to produce PC[127] besides its superior activity in more than 15 different organic and polymeric processes.[128]

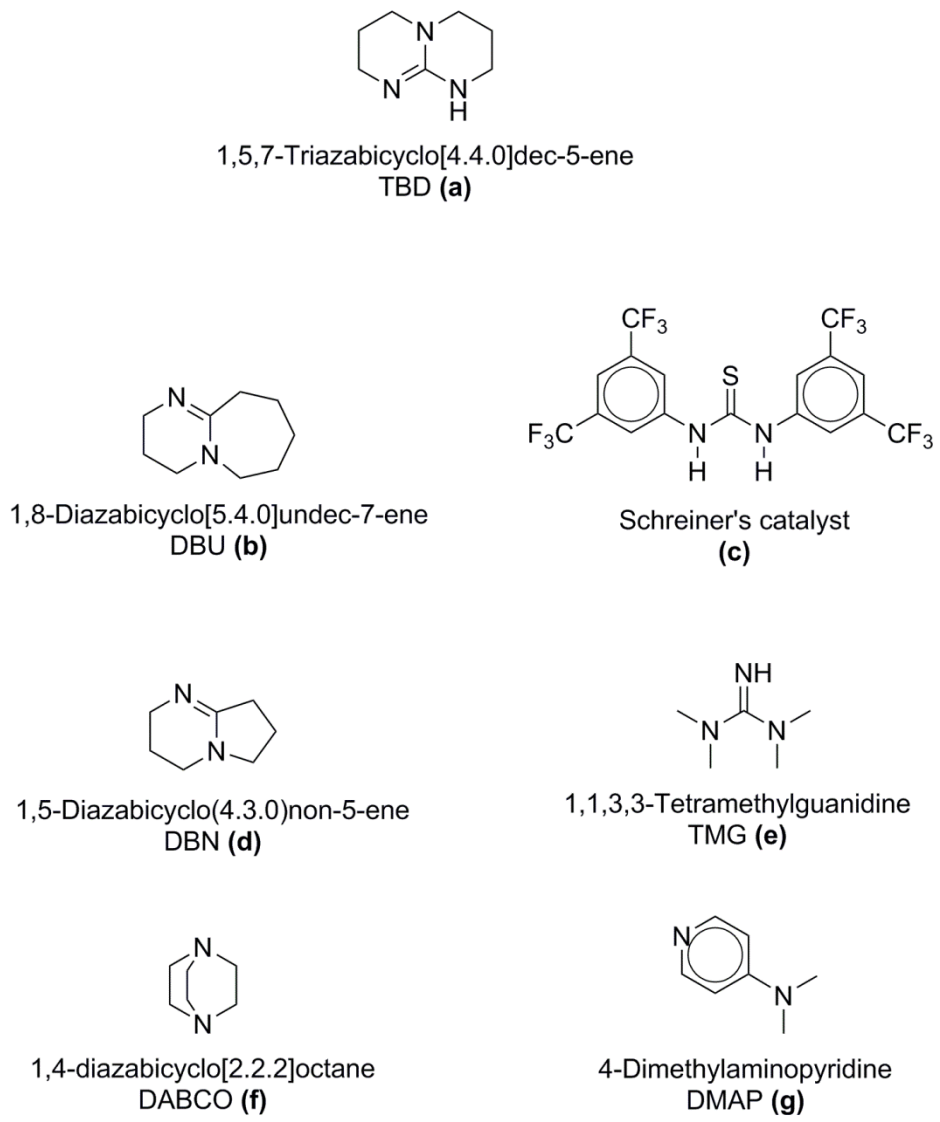

Figure 3.6. Structural formula for the catalysts used in the study (**a-f**).[119]

3.4.2.2 Carbonylating agents

Among the non-phosgene carbonylating agents, PC, EC and DMC were used to see the reactivity of each one of them within the oligomerization process. PC gave the best yields, *viz.*, of 65.0% (run 1, Table 3.3), followed by EC with a 54.0% (run 2, Table 3.3). On the other hand, unexpectedly, DMC showed almost no reactivity towards oligomerization, this might be due to methanol is not a strong microwave absorber, *viz.*, methanol has low energy dissipation factor

($tan\delta$) once compared to ethylene glycol/propylene glycol.[129] Table 3.3 shows the yields obtained under the same conditions.

A control experiment showed that the ring opening of PC *via* TBD to give polycarbonate was not feasible under the same applied conditions. IR and NMR spectroscopy showed that there was no change in the reaction under the applied conditions, only peaks/signals for the starting materials can be observed.

Table 3.3. Yield as a function of Carbonylating agents.[119]

Run	Carbonylating Agent[a]	Yield (%)
1	PC	65.0
2	EC	54.0
3	DMC	< 1.0

[a] Conditions applied: 3.1 mol% TBD, 100.0 °C, 220.0 W, 10.0 min.

3.4.2.3 Thermal *vs.* Microwave control

To show the importance of a microwave reactor and its role in enhancing the reaction to yield **[*n*]-OUs** under the appropriate conditions, a thermal control experiment was carried out in an ATR-FTIR autoclave (Section 4.1) applying thermal energy only using the same conditions, the reactor itself is heated to the desired temperature, *viz.* 50.0 °C, and components were added in the same manner when using the microwave reactor. The gradual decrease in the intensity of propylene carbonate at 1790 cm^{-1} as a result of consumption accompanied with an increase in the absorption band of urethane functionality assigned at 1696 cm^{-1}, is the result of the catalyzed nucleophilic attack of the diamine at the carbonyl carbon of the propylene carbonate as shown in Figure 3.7. Workup after 10.0 min showed only viscous material, 1H NMR analysis of the product revealed the formation of urethane protected diamine. These experiments proved that the reaction is not successful unless microwave energy is applied.[119]

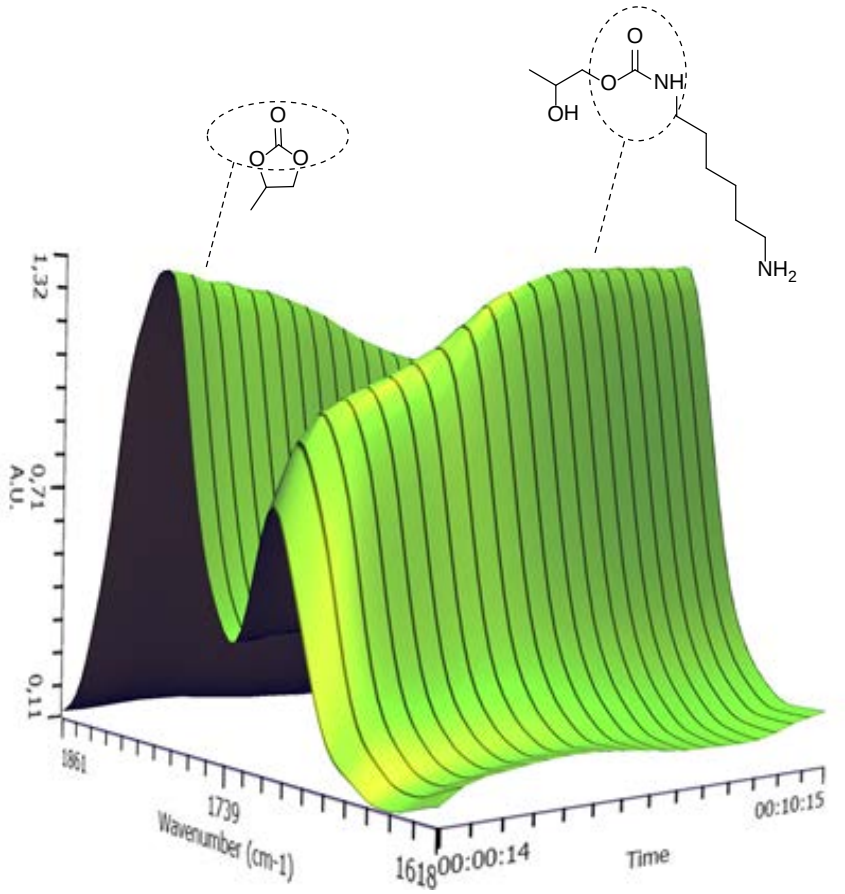

Figure 3.7. *In-situ* ATR-FTIR spectrum of the oligomerization process under thermal conditions. (Only spectra from 1477 to 1861 cm^{-1} over 10.0 minutes are shown for clarity).

3.4.2.4 Solubility Tests and Organic Solvents.

The solubility behavior of **[*6*]-OU** using polar solvents as in N,N-dimethylacetamide (DMAc), DMSO, DMF, and NMP was not successful. Even upon mixing with a 5.0 wt % LiCl, neither cold nor hot solubilization (100.0 °C) was capable of dissolving the aforementioned oligomers. On the other hand, room temperature solubilization was feasible through the use of perflourinated protic solvents such as, 1,1,1,3,3,3-Hexafluoroisopropanol (HFIP), trifluoroacetic acid (TFA), or formic acid. Such trend is presumably due to strong intermolecular hydrogen bonding formed upon dissolution. TFA was chosen for solubilization of the **[*6*]-OU** due to being the least hazardous.[119]

3.4.2.5 Screening with aromatic diamines and amino alcohols

Using a microwave-assisted reactor, the same reaction with the aromatic diamines did not show any reactivity presumably due to the low nucleophilicity of the aromatic diamine compared to aliphatic diamines (Scheme 3.13). Furthermore, no oligomer formation concerning the reaction of amino alcohols with PC under the same applied conditions was formed. On the other hand, Bis(hydroxyalkyl)urea was formed, which is in accordance to the literature as synthesized and patented by Yasuji *et al.*[130] which cannot undergo further reactions because the hydroxyl group is not nucleophilic enough to ring open the PC.[119]

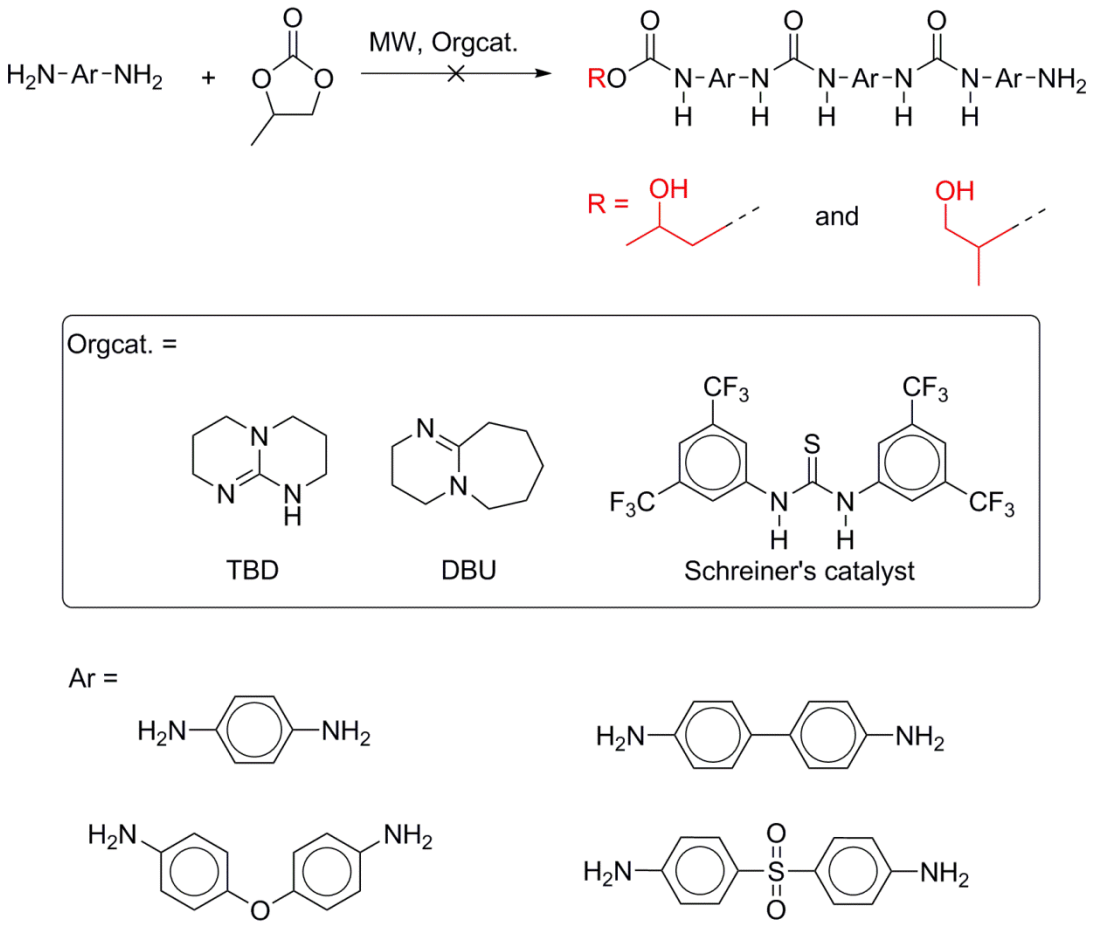

Scheme 3.13. Failed oligoemerization experiments of aromatic diamines with PC.

3.4.3 [*6*]-Oligourea ([*6*]-OU) Results

Upon assigning the DP value from the 1H NMR spectra, the total mass of the prepared oligomers was calculated. Elemental analysis is based on the total mass of the oligomer including the end groups.[119] The elemental analysis is to a great extent close to the proposed structures. Figure 3.8 shows the ATR-FTIR spectra of the HMDA and the [*6*]-oligourea, (**[*6*]-OU**). The band at 1614 cm^{-1} (**C**) can be assigned to carbonyl stretching of a urea functional group, as well as the band at 1571 cm^{-1} (**D**) which is ascribed to (CO–NH) amide stretching. Also, the formation of a band at 3318 cm^{-1} (**A**) which is ascribed to a secondary amine peak as well as the disappearance of the two bands of the antisymmetric stretching (**B_1**) and symmetric (**B_2**) of the primary amine corresponding the starting material centered at 3328 cm^{-1}, 3254 cm^{-1}, and 3165 cm^{-1}. These assignments confirm the aforementioned assumption. This indicates that the material was transformed into the presumed **[*6*]-OU**. X stands for the secondary amine of carbamate upon capturing atmospheric CO_2. This can be cleaved upon applying the reaction conditions.[119]

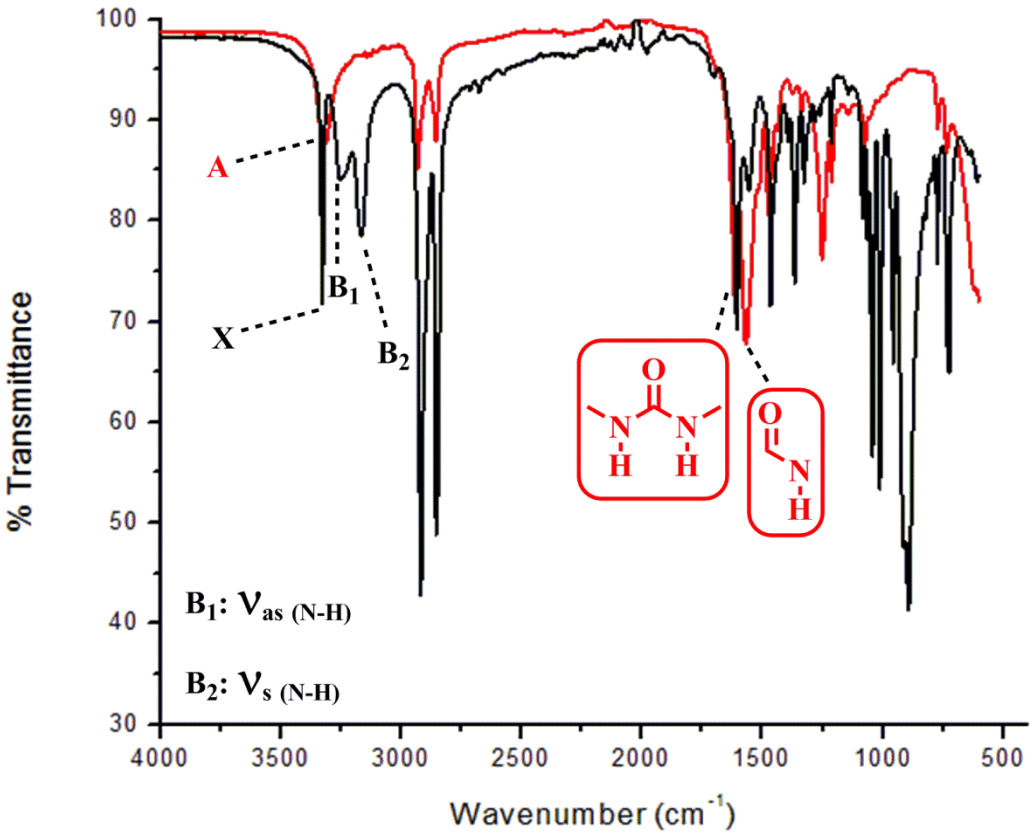

Figure 3.8. The FTIR-Spectrum of the corresponding **[*6*]-OU** (**Red**) and its corresponding 1,6-Hexamethylenediamine (**HMDA**) (**Black**). (Reproduced from Ref. [119] with permission from The Royal Society of Chemistry).

Figure 3.9 shows the 1H NMR of the **[*6*]-OU**, a triplet is shown at 3.30 ppm representing the methylene group closest to the urea functional group, *i.e.* **2**, Figure 3.9, and two definite singlets at 1.63, 1.31 representing protons of the main skeleton of the repeating unit. **3** and **4**, Figure 3.9. The urethane end group (**a**, **a′**, **b**, **b′**, **c**, and **c′**) is distinguished by a set of multiplets assigned at (3.85-4.27), the reason for such complex pattern is attributed to the existence of isomeric hydroxopropyl carbamate end groups as a result of the regio-unselective ring opening of PC. The peaks assigned at around 6.7, and 7.0 ppm (**1**, Figure 3.9), are attributed to the proton to deuterium exchange at the amine end group of **[*6*]-OU**, since the signal of -NH_2 utterly vanishes after 48 h in TFA due to H-D exchange (Figure 3.10). The degree of polymerization (DP) is equal to 12 and the molecular weight of the oligomers is *ca.* 2.0 kDa within the plausible error.

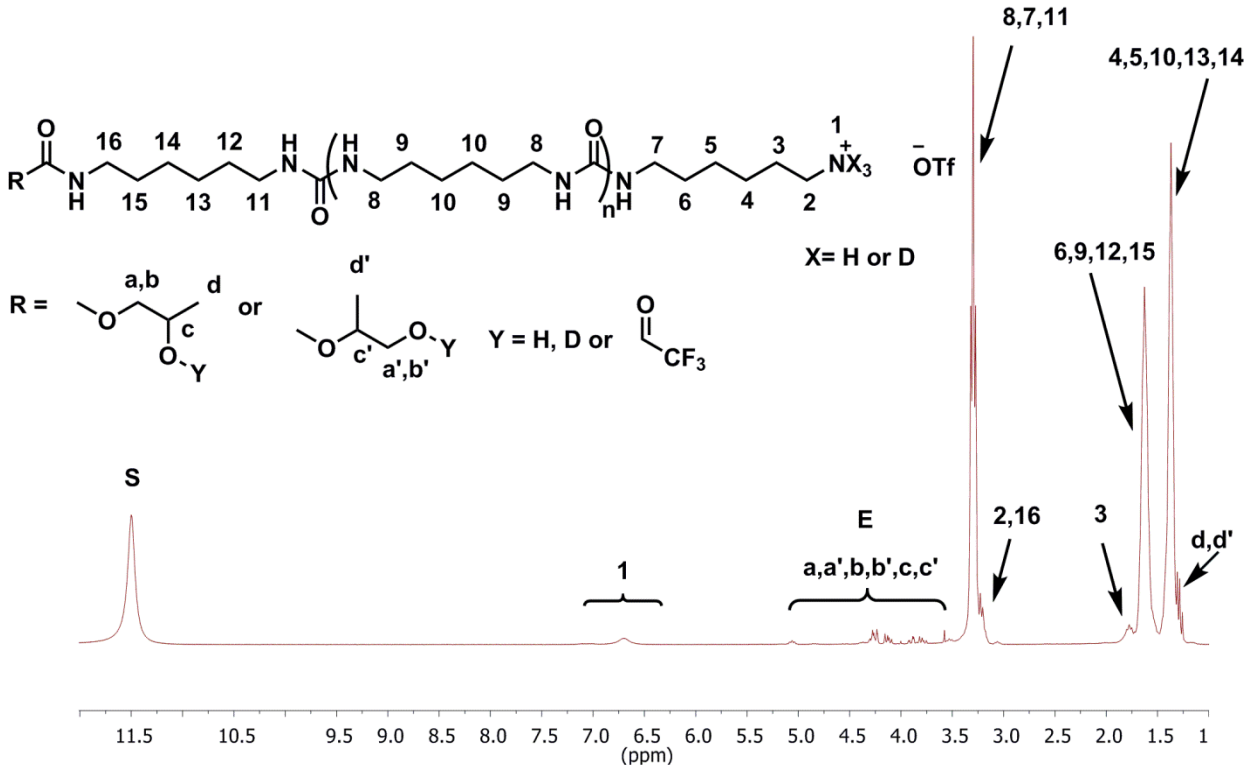

Figure 3.9. 1H NMR of the **[*6*]-OU** in TFA-*d*, **S**: Solvent, **E**: End group (Reproduced from Ref. [119] with permission from The Royal Society of Chemistry).[119]

On the one hand, solutions of the oligomers in TFA-*d*, were stable over a long period of time as a function of the urea backbone. On the other hand, shifts in peaks of the urethane end group as a result of esterification in highly acidic solution, *viz.*, TFA-*d*. Figure 3.10 shows the stability study up to 48h. For consistency and precision of analysis, fresh samples were prepared before measuring any 1H NMR spectrum. The peaks in the right rectangular region, (**E**, Figure 3.10) in the range (3.85-4.27) ppm shows the transformation for the urethane end group into the propylene glycol upon hydrolysis of the oligomer's end group. A detailed assignment of the signals from the hydroxopropyl carbamate end group is tangled by its reactions with TFA. Moreover, another exchange of the –OH proton with deuterium occurs (middle rectangular region, Figure 3.10), followed by the reaction with TFA to form a trifluoroacetic ester (TFA-PG, Figure 3.10).[119] Clearly, the other peaks associated to the urea backbone show its extreme stability over prolonged acidic treatment, this explains why polyurea are used in coating industry.[93]

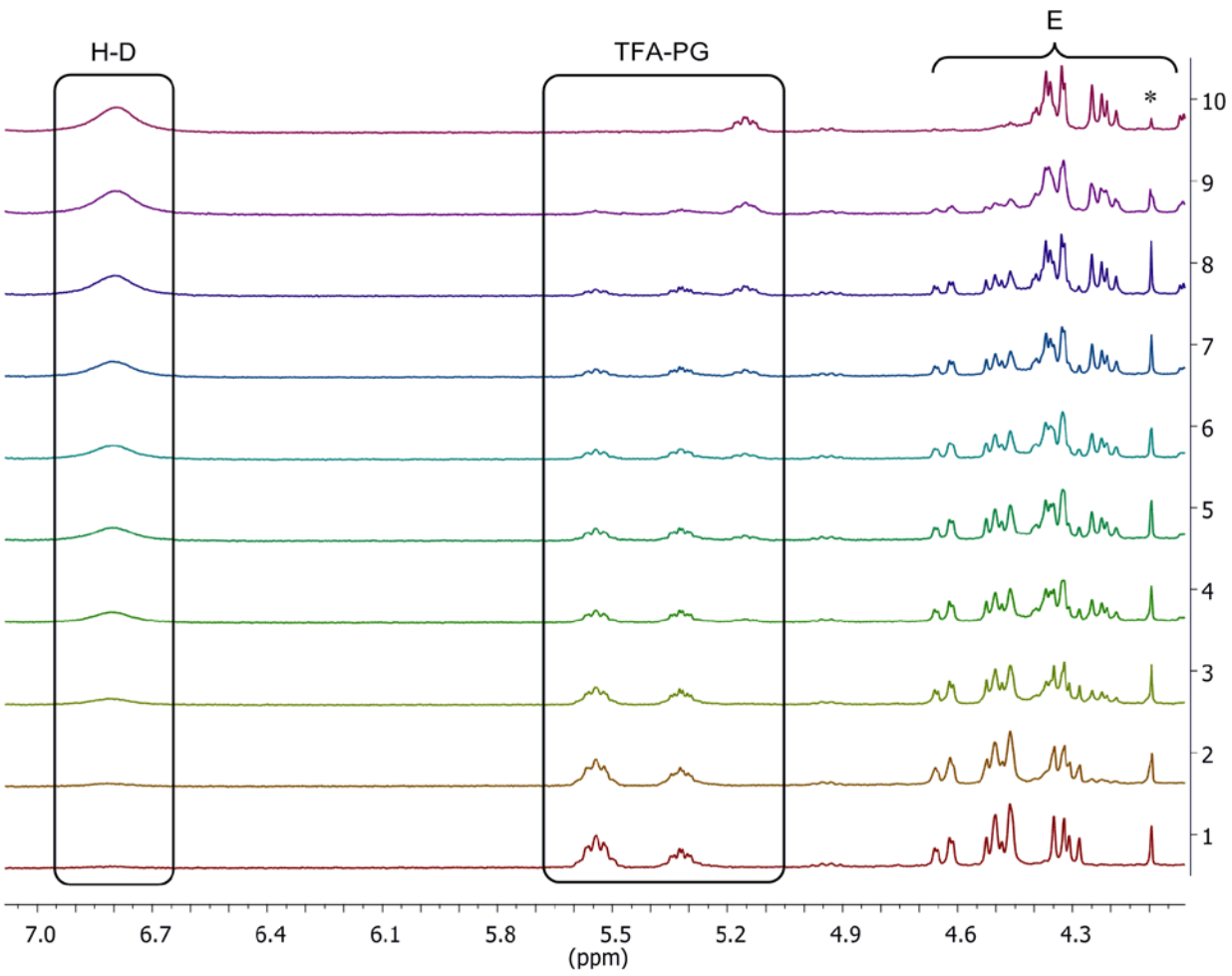

Figure 3.10. Stability study of the **[*6*]-OU** in TFA-*d* after 1.0 h, 2.0 h, 3.0 h, 4.0 h, 5.0 h, 6.0 h, 12.0 h, 24.0 h and 48.0 h (from top to bottom, respectively). *: MeOH traces.[119]

Figure 3.11 shows the 13C NMR of **[*6*]-OU**, which further confirms the presumed structure. The peak at 161.4 ppm (**1**, Figure 3.11) is assigned to the carbonyl group of the urea functionality. Further peaks, *viz.* **2**, **3** and **4** at 44.2, 30.7 and 28.0 ppm, respectively; correspond to the carbon atoms forming the backbone skeleton of the repeating unit.[119] The urethane end group could not be seen within the spanned time for a 13C experiment due to hydrolysis.

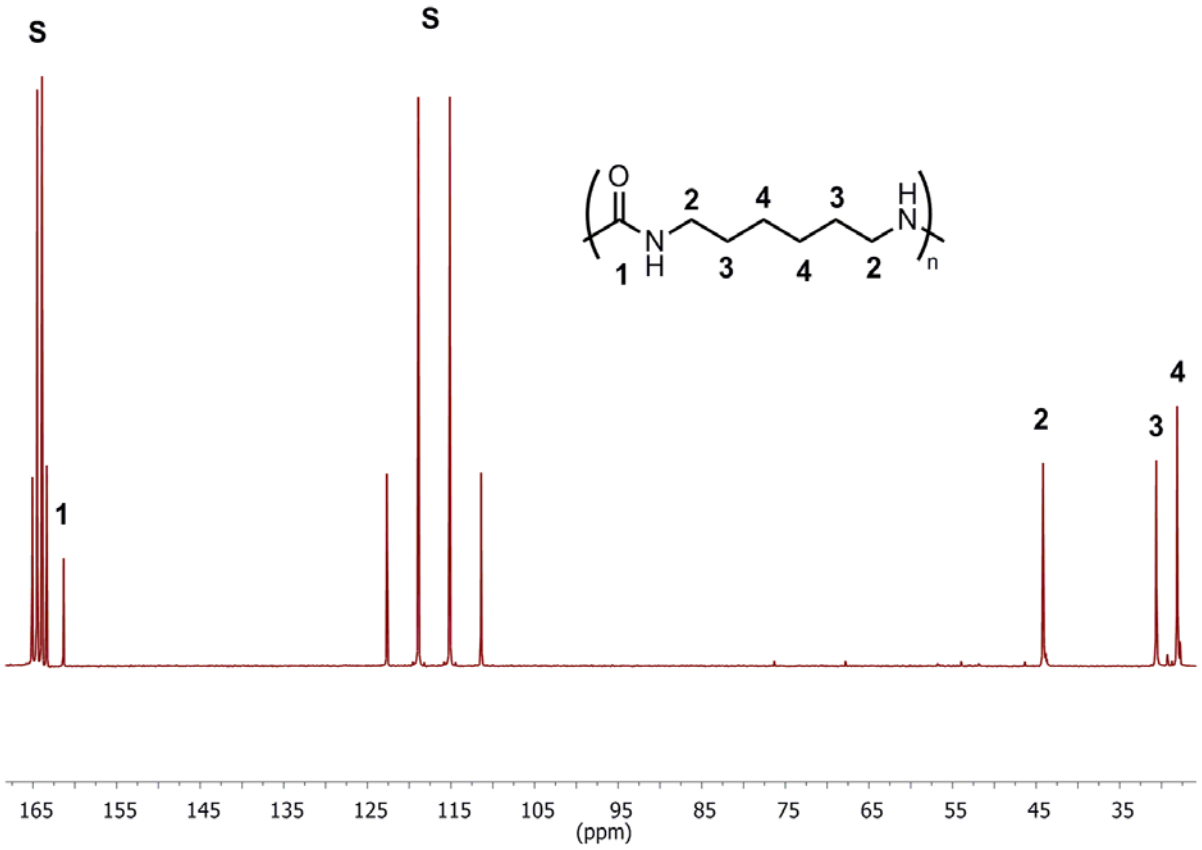

Figure 3.11. 13C NMR of the **[*6*]-OU** in TFA-*d*, S: Solvent.[119]

3.4.3.1 Synthesis of other candidates of [*n*]-OUs

Similarly, **[*n*]-OUs**-based solid sorbents were prepared through a TBD-organocatalyzed reaction with the use of a microwave, mono-modal system in a dynamic mode similarly to a procedure that was previously optimized and reported for the synthesis of **[*6*]-OU** by Qaroush *et al*. (Scheme 3.14).[119]

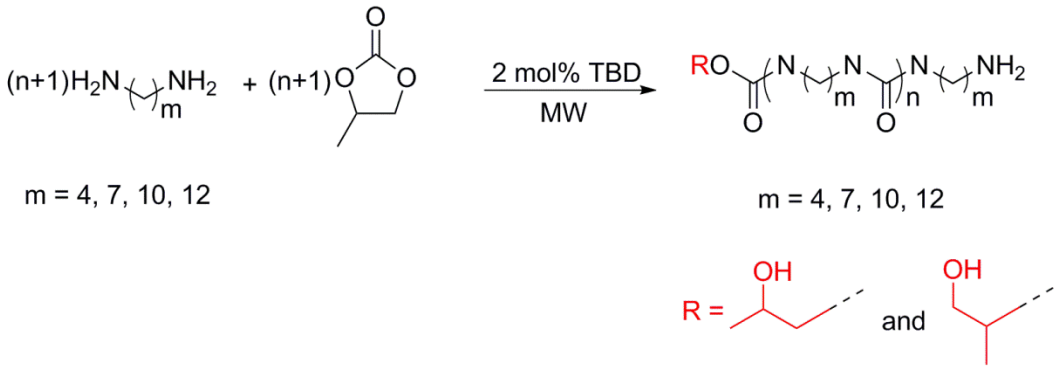

Scheme 3.14. General representation for the organocatalyzed microwave-assisted oligomerization of primary diamines with propylene carbonate (PC) (TDB: 1,5,7-triazabicyclo[4.4.0]dec-5-ene; MW: microwave).[131]

The dynamic mode was selected for the synthesis in order to reach mild temperatures and avoid excessive thermal microwave effects, which could affect the reaction yields.[65] Under these conditions, equimolar amounts of homologous diamines and PC afforded the desired **[*n*]-OUs** as white-colored powders upon drying. Table 3.4 summarizes the degree of polymerization (DP), yields, and elemental analyses of the oligomers, *viz.*, **[*4*]-**, **[*7*]-**, **[*10*]-**, and **[*12*]-OUs**. [131]

The obtained yields were very good in comparison with values reported by a similar condensation method conducted *via* a thermal approach at very high temperatures and vacuum for prolonged times.[126] According to our procedure, DP varies significantly as a function of spacer, *i.e.* the shorter the spacer in the diamine moiety the higher the DP value. This is presumably due to a solubility issue. The elemental analysis results were in good agreement with the calculated formula for each oligomer, where the DP and a statistical distribution of 1:1 molar ratio of amine:urethane end groups were taken into consideration. In all cases (**[*n*]-OU**, ***n*** = ***4***, ***7***, ***10***, and ***12***), the presence of some traces of methanol affected the microanalyses, as observed by 1H NMR and TGA, this result was consistent to a previously reported study.[119, 131]

Table 3.4. Summary of results for the synthesized **[*n*]-OUs** [131]

[*n*]-OU.MeOH	DP[b]	Yield (%)[c]	EA (Total mass)[d]	
			Calculated	Found
[*4*]-OU.H_2O	9	82.0	C: 51.29 H: 9.05 N: 22.30	C: 51.51 H: 8.95 N: 22.09
[*7*]-OU.H_2O	10	76.0	C: 60.03 H: 10.38 N: 16.80	C: 60.56 H: 10.42 N: 16.33
[*10*]-OU	7	78.0	C: 65.35 H: 11.18 N: 13.32	C: 65.64 H: 11.38 N: 13.21
[*12*]-OU	6	86.0	C: 67.73 H: 11.58 N: 11.59	C: 67.59 H: 11.64 N: 11.54

[a] Conditions: 1:1 molar ratio of diamine:PC, 2.0 mol% TBD, 50.0 ºC, 10.0 min, 200.0 W; [b] Obtained from 1H NMR; [c] Isolated yields; [d] The total formula weight is accounted with the inclusion of end groups.

A clear evidence of the formation of the urea functional group was observed by using Attenuated Total Reflectance-Fourier Transform Infrared Spectroscopy (ATR-FTIR). For instance, [***10***]**-OU** showed two definite new peaks at 1615 cm^{-1} (amide I, C=O; **C**) and 1570 cm^{-1} (amide II, CO-NH; **B**) in comparison to the spectrum of the starting material as shown in Figure 3.12.[119] A small peak at 1691 cm^{-1} (**D**) related to the formation of a urethane end group was also detected.[132] The single broadened band centered at 3321 cm^{-1} (**H**) is related to the presence of an amine group of a urea moiety. In this region, a similar peak can be also observed in the ATR-FTIR spectrum of the starting material (1,10-diaminodecane, **1,10-DAD**) at 3329 cm^{-1} (**I**) but this signal corresponds to a secondary amine peak in a carbamate functional group.[133] The latter is formed while performing the ATR-FTIR measurement under air. However, the formation of urea

group in [***10***]**-OU** was confirmed by a peak at 1251 cm^{-1} (**A**), which is assigned to the single bond C-N.[134] The latter peak is determinant to differentiate between the existence of urea group or a carbamate. Moreover, the formation of the **[*10*]-OU** can be proved by the disappearance of the one symmetric (3162 cm^{-1}, **F**) and one asymmetric (3252 cm^{-1}, **G**) vibration band of **1,10-DAD**. In addition, signals corresponding to the aliphatic backbone of both materials were also seen. Accordingly, $\mathbf{E_{amine}}$ (2917 and 2848 cm^{-1}) blue shifted to $\mathbf{E_{urea}}$ (2932 and 2856 cm^{-1}).[131]

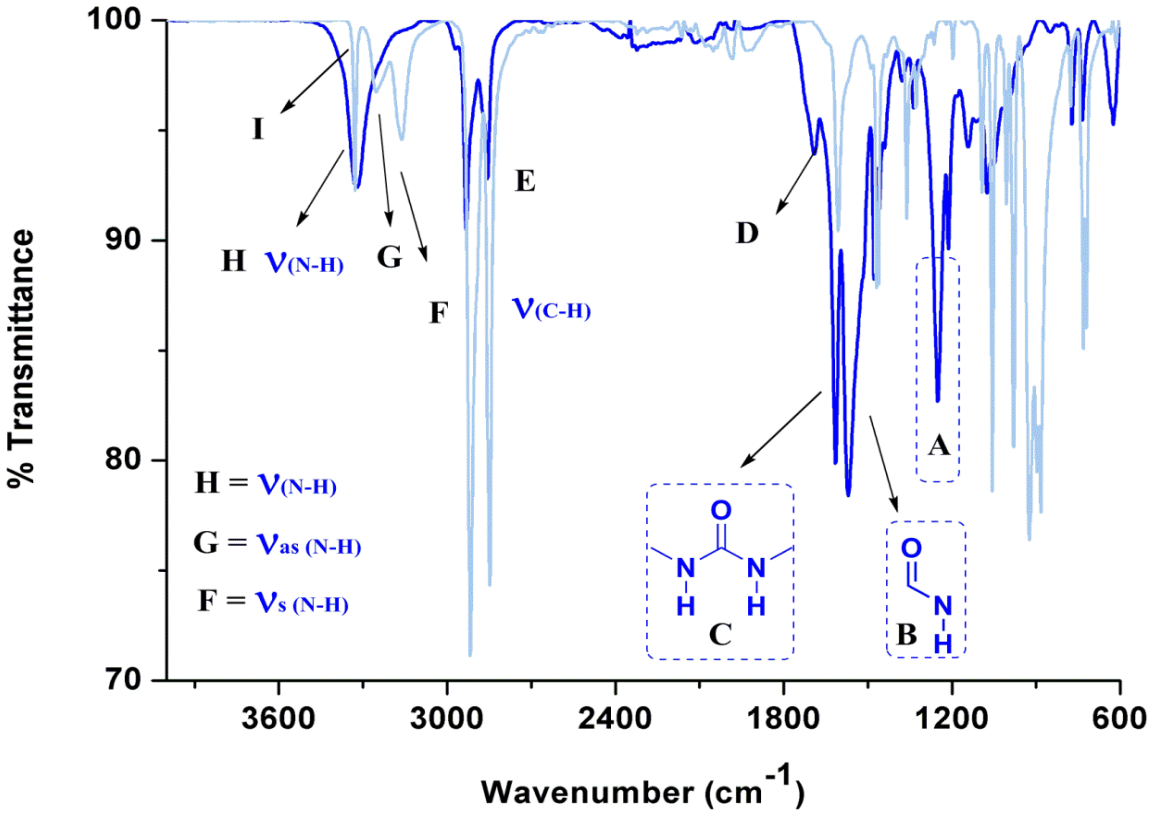

Figure 3.12. ATR-FTIR spectra of **[*10*]-OU** (dark blue) and its diamine comonomer (light blue).[131]

The DP of the obtained oligomers can be estimated by end-group analysis *via* 1H NMR spectroscopy in deuterated trifluoroacetic acid (TFA-*d*), as recently demonstrated by our research group.[119] Figure 3.13 shows a descriptive 1H NMR spectrum for one of the oligomers, *viz.* **[*10*]-OU**. Integration of the protons related to the α-carbon of the ammonium end group (**2'**), which is formed after addition of TFA-*d* to the [***n***]**-OUs**, relative to the protons on the α-carbon close to the urea repeating unit (**2**) gives the DP. For **[*10*]-OU**, the 1H NMR spectrum shows a triplet at

3.28 ppm representing the methylene group closest to the urea functional group in the backbone of the repeating unit (methylene group **2**) and multiplets between 1.80 and 1.20 ppm related to the methylene protons of the main skeleton of the repeating unit (methylene groups **3** to **6**). This is in agreement with the proposed structure for **[*10*]-OU**.[131]

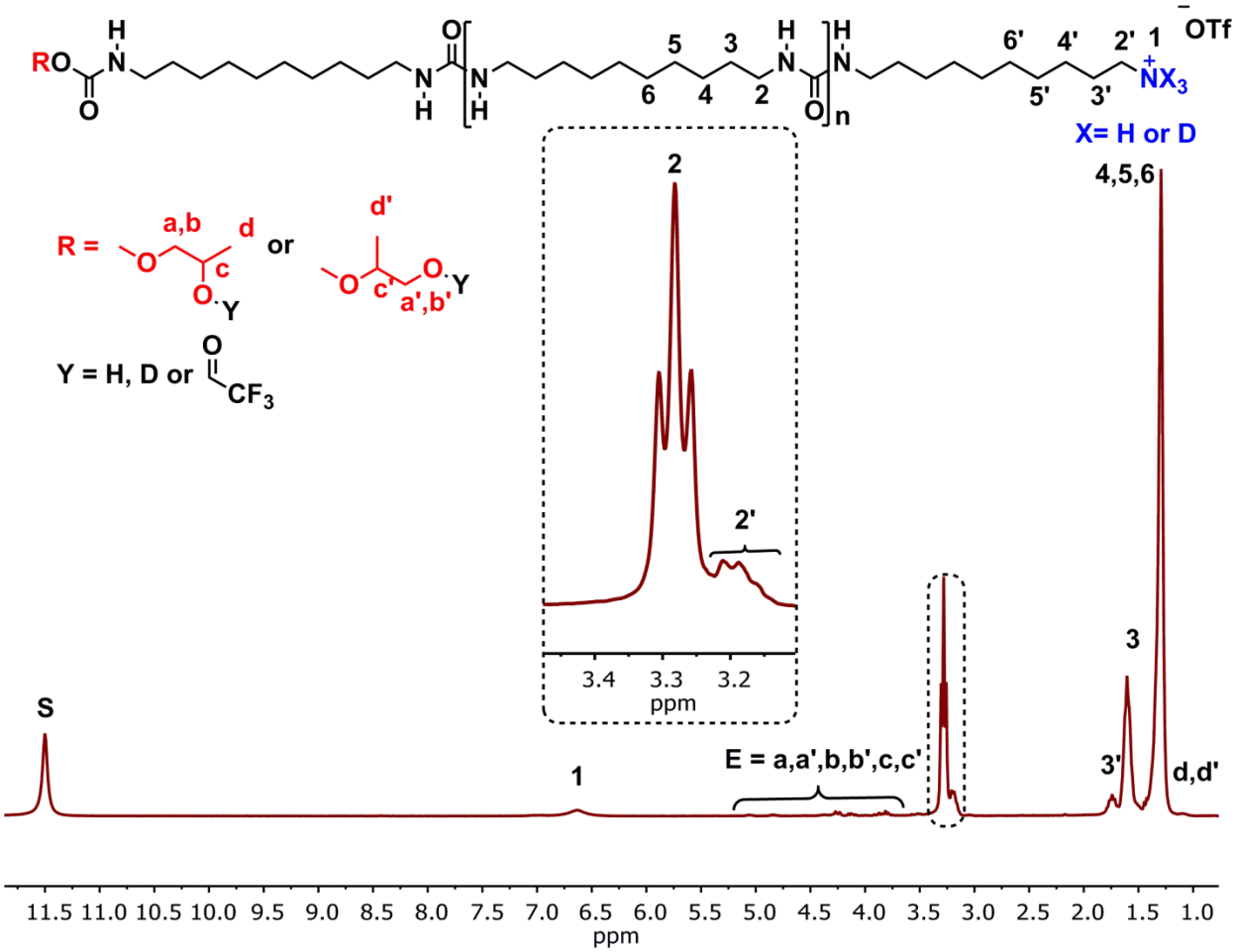

Figure 3.13. 1H NMR spectrum for the prepared **[*10*]-OU** in TFA-*d* at room temp.[131]

Moreover, Figure 3.14 shows the ^{13}C NMR of **[*10*]-OU** which revealed the presence of a urea group at 161.2 ppm. [131]

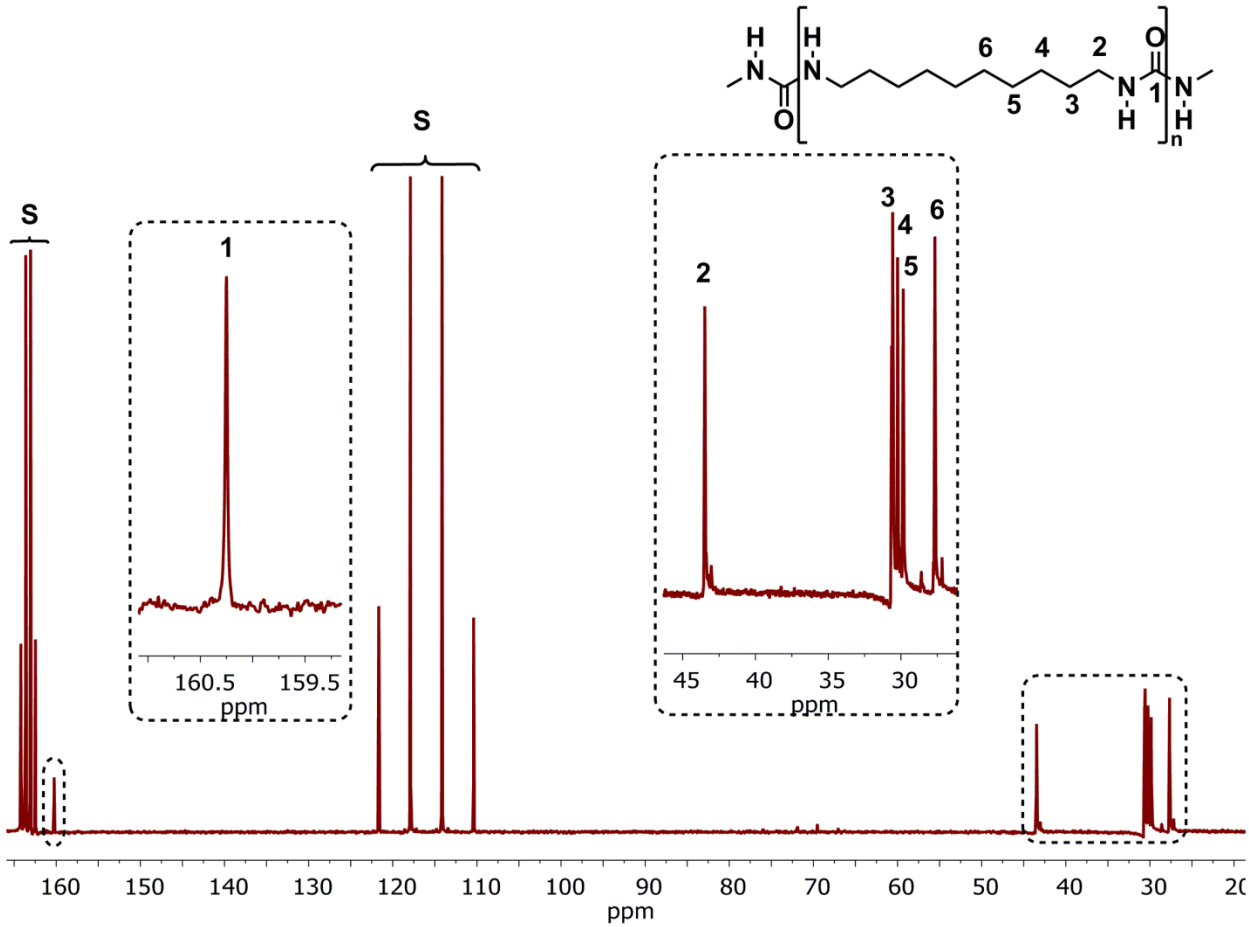

Figure 3.14. 13C NMR of **[*10*]-OU** in TFA-*d*.[131]

3.4.3.2 Thermal Analysis

Thermogravimetric analysis (TGA) was conducted on the new oligomeric materials to study their thermal stability (Figure 3.15). For comparison reasons, TGA from the previously prepared **[*6*]-OU** is also shown.[119] In particular, two thermal transitions are observed. Firstly, a gradual decomposition occurs after *ca.* 200.0 ºC in all **[*n*]-OUs**, which can be explained by the formation of PC as a result of backbiting of the urethane end group.[119] Thermal stability of the backbone remains intact till about 300.0 ºC as observed in similar compounds.[119] A second decomposition step was detected for all **[*n*]-OUs** as a result of an arbitrarily isocyanate formation rather than backbiting or zip mechanism to form cyclic ureas (as in the case of oligomers with short methylene chains). In this regard, a very significant difference is detected in the TGA trace of the **[*4*]-OU** due to the presumed formation of seven membered ring cyclic urea.[126] For all

oligomers, T_{d50} (decomposition temperatures at 50.0 % weight loss) is *ca*. 350.0 ºC (Table 3.5).[131]

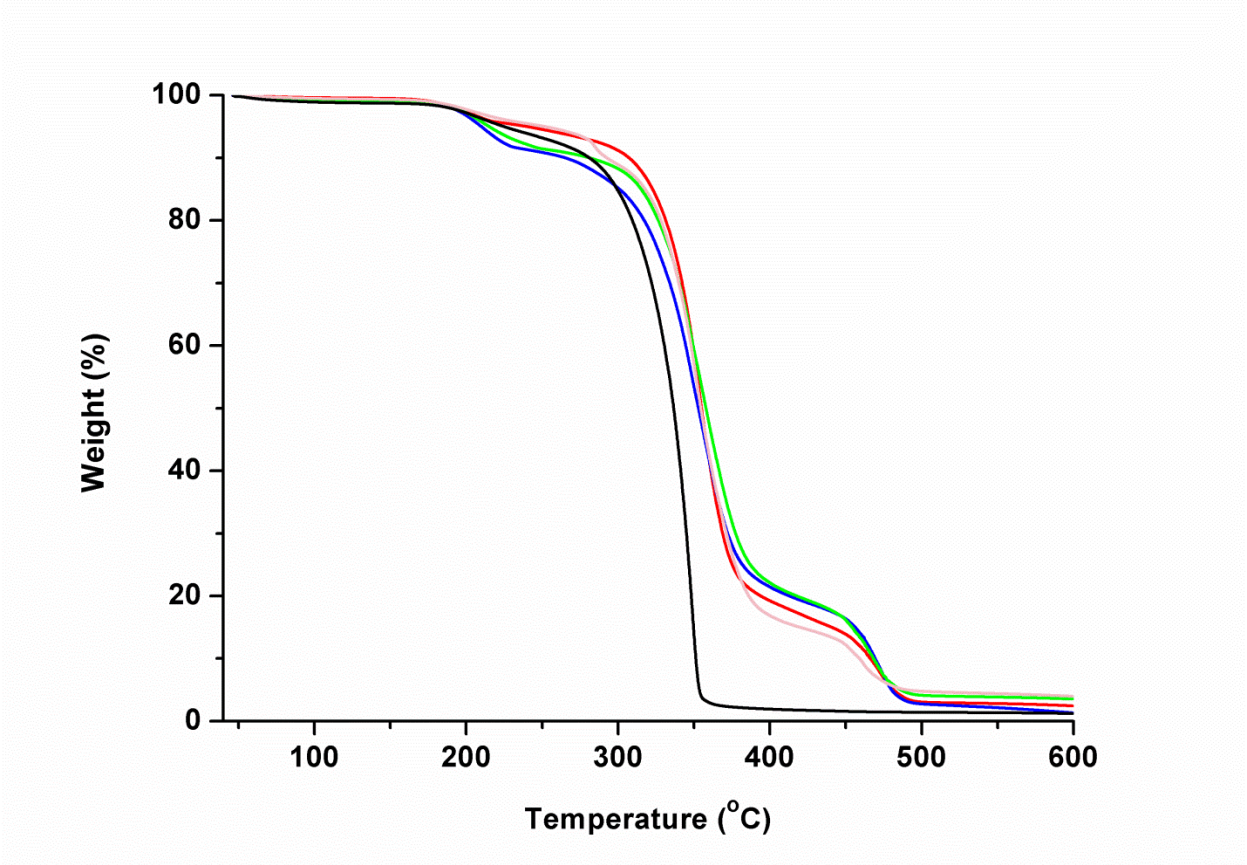

Figure 3.15. TGA traces of **[*n*]-OUs**, (***n*** = **12** (red ——), **10** (blue ——), **7** (green ——), **6** (Magenta ——), and **4** (black ——)).[131]

Further thermal properties of **[*n*]-OUs** were studied using differential scanning calorimetry (DSC, Table 3.5). No thermal transitions were observed when performing a full scan from room temperature till 200.0 ºC at different heating rates (5.0 or 10.0 K/min). The scan was prolonged till 300.0 ºC with the loss of the end group (*vide infra*). On cooling, an exothermic crystallization peak could be observed at 205.0, 192.0, and 165.0 ºC for **[*7*]-**, **[*10*]-**, and **[*12*]-OUs**, respectively. In addition, melting temperatures (T_m) were detected at 229.0, 215.0, and 204.0 ºC for those materials, respectively. These are spacer-dependent, *viz.* the longer the spacer between the urea groups, the lower T_m. Due to the high crystallinity of the produced **[*n*]-OUs** (*vide infra*), T_g values could not be determined. % Crystallinity was measured using DSC (Table 3.5).[135]

Table 3.5. Thermal properties of the studied **[*n*]-OUs**.[131]

[*n*]-OU	**Enthalpy of fusion ΔH_{fus} (J/g)**	**% Crystallinity[a]**	**T_{d50} [b]**	**T_m (°C)**	**T_{cr} [c]**
[*4*]-OU	n.a	n.a	348.0	n.a	n.a
[*6*]-OU[d]	n.a	n.a	352.0	282.0	252.0
[*7*]-OU	109.0	81.0	357.0	229.0[e]	205.0
[*10*]-OU	100.0	74.0	349.0	215.0[f]	192.0
[*12*]-OU	95.0	70.0	353.0	204.0	165.0

[a] % Crystallinity[135] = ΔH_{fus}(sample)/ΔH_{fus}(urea); [b] Decomposition temperature at 50.0% weight loss obtained from TGA; [c] Crystallization temperature; [d] Taken from a previously-reported study.[119] An additional thermal transition was observed for the **[*n*]-OU** samples at [e] T_m= 241.0 °C and [f] T_m= 223.0 °C. n.a: Not Available.

The overall behavior show that materials are highly crystalline relative to urea in the range of 81.0, 74.0, and 70.0 % crystallinity for **[*7*]-**, **[*10*]-**, and **[*12*]-OU**, respectively. Regarding **[*6*]-OU**, T_m is close to the decomposition temperature and, therefore, heat of fusion (ΔH_{fus}) cannot be obtained.[131]

3.4.3.3 Powder X-ray diffraction patterns (PXRD) patterns

Powder X-ray diffraction patterns (PXRD) gave another proof towards the presence of crystallinity of the prepared **[*n*]-OU**s. Urea functionality forms the crystalline domains through bidentate hydrogen bonds; on the other hand, the carbon chains constituting the backbone form the amorphous domains, the amorphous domains increased with the chain length as shown in (Figure 3.16), leading to the decrease of the crystallinity.[131] This is the same trend as seen for the [*n*]-polyurea, **[*n*]-PU** prepared from *s*CO_2.[102]

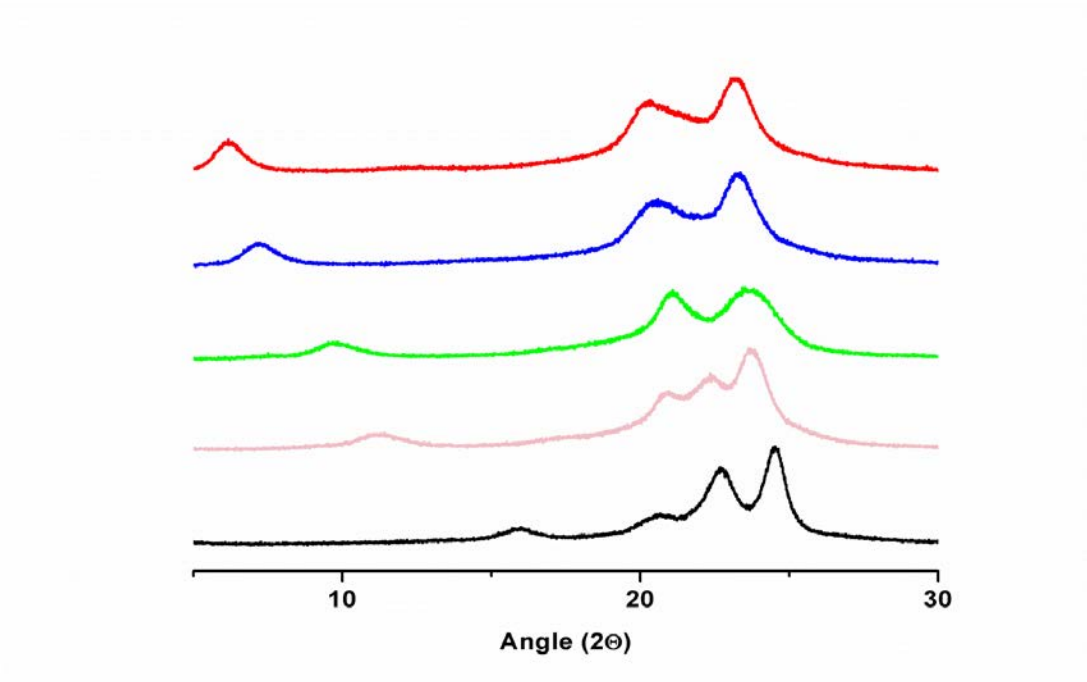

Figure 3.16. XRD pattern of the studied **[*n*]-OUs**, (***n*** = **12** (red ——), **10** (blue ——), **7** (green ——), **6** (Magenta ——), and **4** (black ——)).[131]

3.4.4 CO_2 Sorption experiments of [*n*]-OUs

As the new synthesized materials contain a terminal amino group (Scheme 3.14), it was presumed that this moiety would react with CO_2 and, therefore, the **[*n*]-OUs** could be employed as solid sorbents for CO_2 capture. Preliminary CO_2 sorption tests at 35.0 ºC were made using a microbalance, which also allows the activation of the samples under vacuum at 60.0 ºC before the sorption measurements, as described in the experimental section. Figure 3.17 shows moderate to good sorption capacities (7.76 to 18.90 $mg_{CO2}/g_{sorbent}$) of the different **[*n*]-OUs**. Very fast sorption kinetics were observed for all samples.[131]

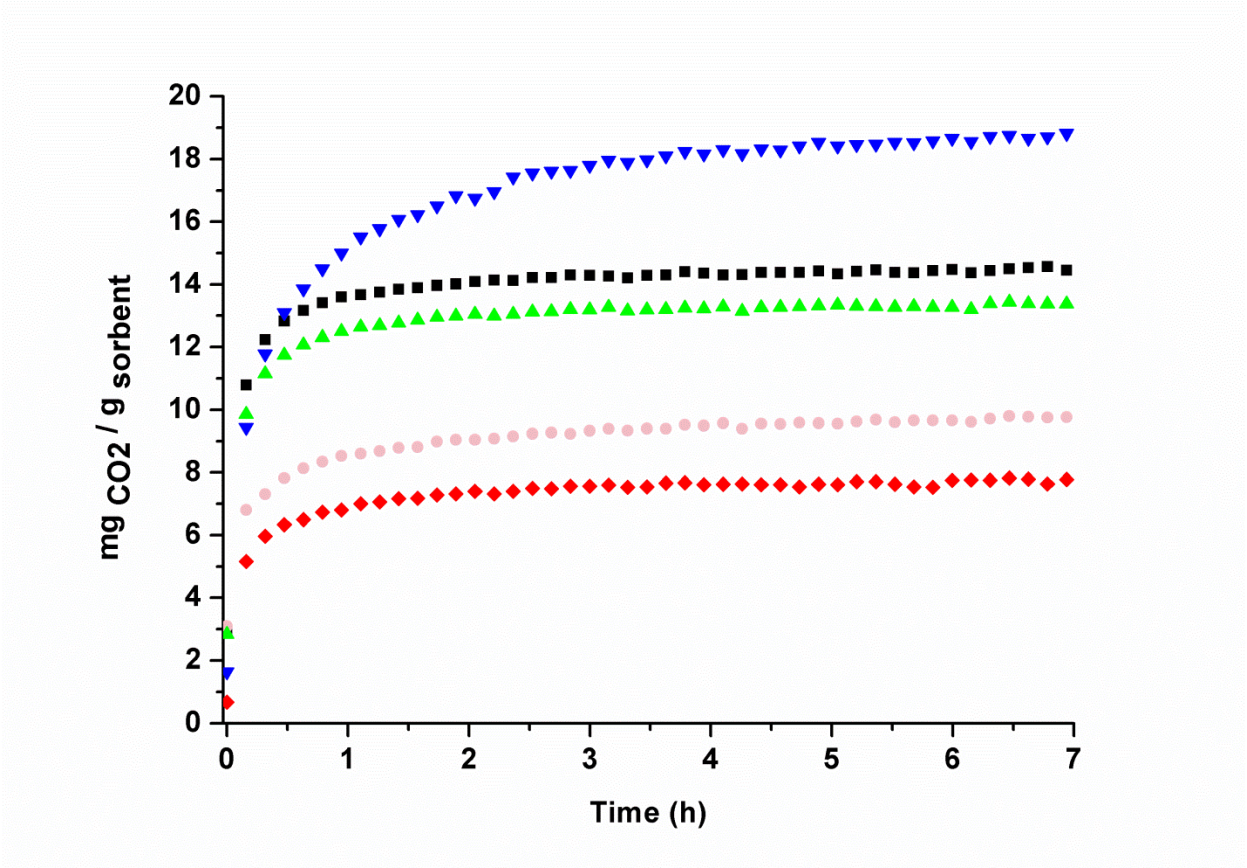

Figure 3.17. CO_2 sorption isotherms for the **[*n*]-OUs** activated under vacuum at 60.0 ºC (***n*** = **12** (red ♦), **10** (blue▼), **7** (green▲), **6** (Magenta ●), and **4** (black ■)).[131]

The sorption equilibrium was reached for most of the **[*n*]-OUs** within minutes of exposure to CO_2. For **[*10*]-OUs**, this equilibrium was not present and further CO_2 uptake was detected, probably due to some diffusion limitation to internal -NH_2 moieties. To study the effect of the activation step on the sorption capacities, sorption measurements were also run for all **[*n*]-OUs** upon activation at 100.0 ºC under vacuum. Higher sorption values (10.12 to 22.70 $mg_{CO2}/g_{sorbent}$) were determined for the **[*n*]-OUs** (Figure 3.18).[131]

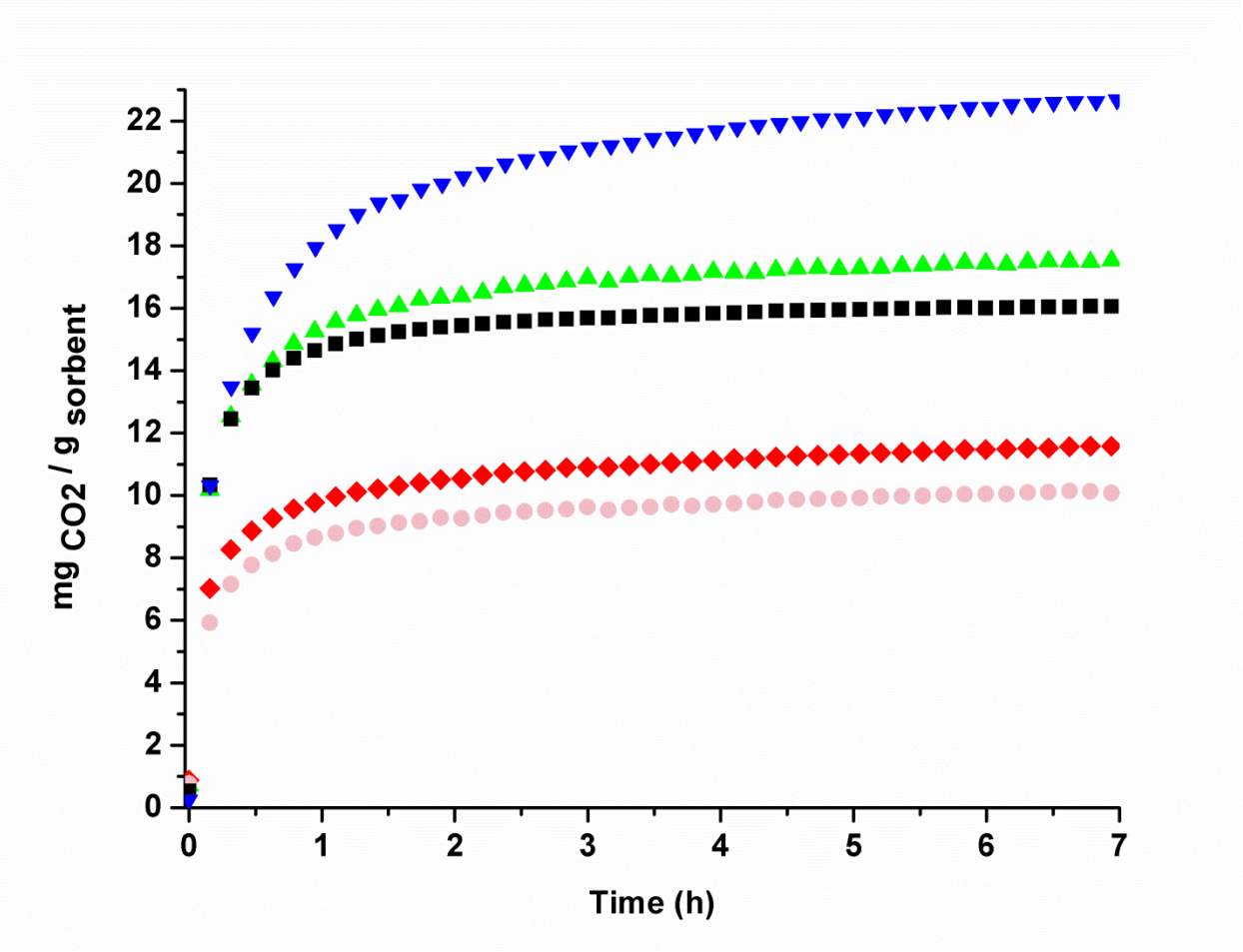

Figure 3.18. CO_2 sorption isotherms for the synthesized **[*n*]-OUs** activated under vacuum at 100.0 ºC (***n*** = **12** (red ♦), **10** (blue▼), **7** (green▲), **6** (Magenta ●), and **4** (black ■)).[131]

Among all the oligomers, **[*10*]-OU** gave the highest sorption capacity and the sorption equilibrium was not reached up to 7.0 h. In all samples, no significant N_2 sorption was detected. There is no clear trend between the CO_2 sorption capacity, the DP, and the methylene chain length (between two consecutive urea groups). In order to investigate a possible dependence of the sorption properties of the oligomeric materials with their macrostructure, Brunauer-Emmett Teller (**BET**) analysis was used. All oligomeric materials have a very small specific surface area and are nonporous (Table 3.6).[131]

Table 3.6. Sorption capacities and specific surface area of the studied **[*n*]-OUs**-based sorbents. [131]

[*n*]-OU	**Specific Surface area (m^2/g)[a]**	**N wt% Elemental analysis**	**NH_2:NH[b]**	**Theoretical sorption capacity ($mg_{CO2}/g_{sorbent}$)**	**Sorption Capacity[c] ($mg_{CO2}/g_{sorbent}$)**	
					60.0 ºC	**100.0 ºC**
[*4*]-OU	3.42	22.09	1:21	31.6	14.54	16.07
[*6*]-OU	0.85	17.77[d]	1:22	25.4	9.86	10.12
[*7*]-OU	0.35	16.33	1:23	21.4	13.35	17.51
[*10*]-OU	n.a	13.21	1:17	23.1	18.90	22.70
[*12*]-OU	1.60	11.54	1:15	22.7	7.76	11.60

[a] Specific surface area as measured by the BET model; [b] Calculated from the DP values of each **[*n*]-OU**; [c] Sorption capacities were recorded at 35.0 ºC and 1.0 bar with different activation temperatures; [d] Reference 119; n.a: Not available.

The theoretical sorption capacity of CO_2 for each oligomer was calculated based on the NH_2:NH ratio (calculated from the DP values of each **[*n*]-OU**), the found nitrogen weight percent (N wt%, Table 3.4), and considering a maximum 1:1 reaction ratio between CO_2 and NH_2 in the presence of water (wet conditions, Scheme 3.15, **Path A**). A comparison between the experimental and theoretical sorption capacities of **[*10*]-OU** indicates that this oligomer almost reaches the theoretical value when activation is conducted at 100.0 ºC. However, other oligomers did not show such any similar behavior which means that other factors may affect the accessibility of CO_2 for the -NH_2 end group moieties (*vide infra*).[131]

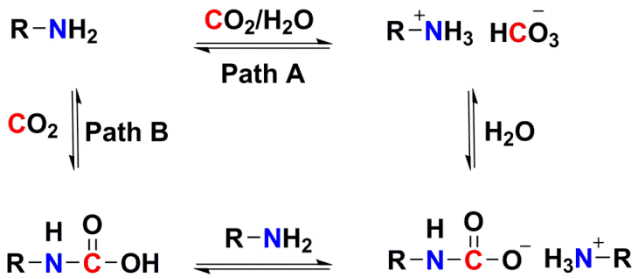

Scheme 3.15. The reversible formation of a **[*n*]-OUs**- containing bicarbonate zwitterion (**Path A,** *1:1 Mechanism*) or carbamate (**Path B,** *1:2 Mechanism*) as a result of CO_2 sorption by the amine-terminated **[*n*]-OUs** in the presence or absence of water, respectively.[131]

3.4.5 Labeling experiments

In order to confirm the formation of bicarbonate during the first CO_2 sorption period in **[*10*]-OU**, a series of 13C cross polarization-magic angle spin (CP-MAS) solid state NMR experiments were performed (Figure 3.19).[131]

After activation at 60.0 ºC and exposure to $^{13}CO_2$ (99.0 atom % 13C, <3 atom % 18O), **[*10*]-OU** shows two peaks in the low-field region of the 13C CP-MAS solid state NMR spectrum (164.8 ppm and 160.6 ppm, Figure 3.19, **a**). The latter peak corresponds to the carbonyl groups as compared with the 13C solid state NMR spectrum of activated **[*10*]-OU** (Figure 3.19, **b**). The second peak (164.8 ppm) indicates the formation of bicarbonate in **[*10*]-OU**. This is confirmed by the 13C CP-MAS NMR spectra of $NaH^{13}CO_3$ and $Na_2{}^{13}CO_3$ standards (Figure 3.19; **e** and **d**, respectively) as the latter one showed a prominent peak at 171.2 ppm (presumably, another signal corresponding to a bicarbonate contaminant as received from the manufacturer was also observed). This indicates that bicarbonate species are formed during the CO_2 sorption measurements with **[*10*]-OU** due to the presence of water molecules (Scheme 3.15, **Path A**) Water might be adsorbed on the oligomers as a result of humidity.[131]

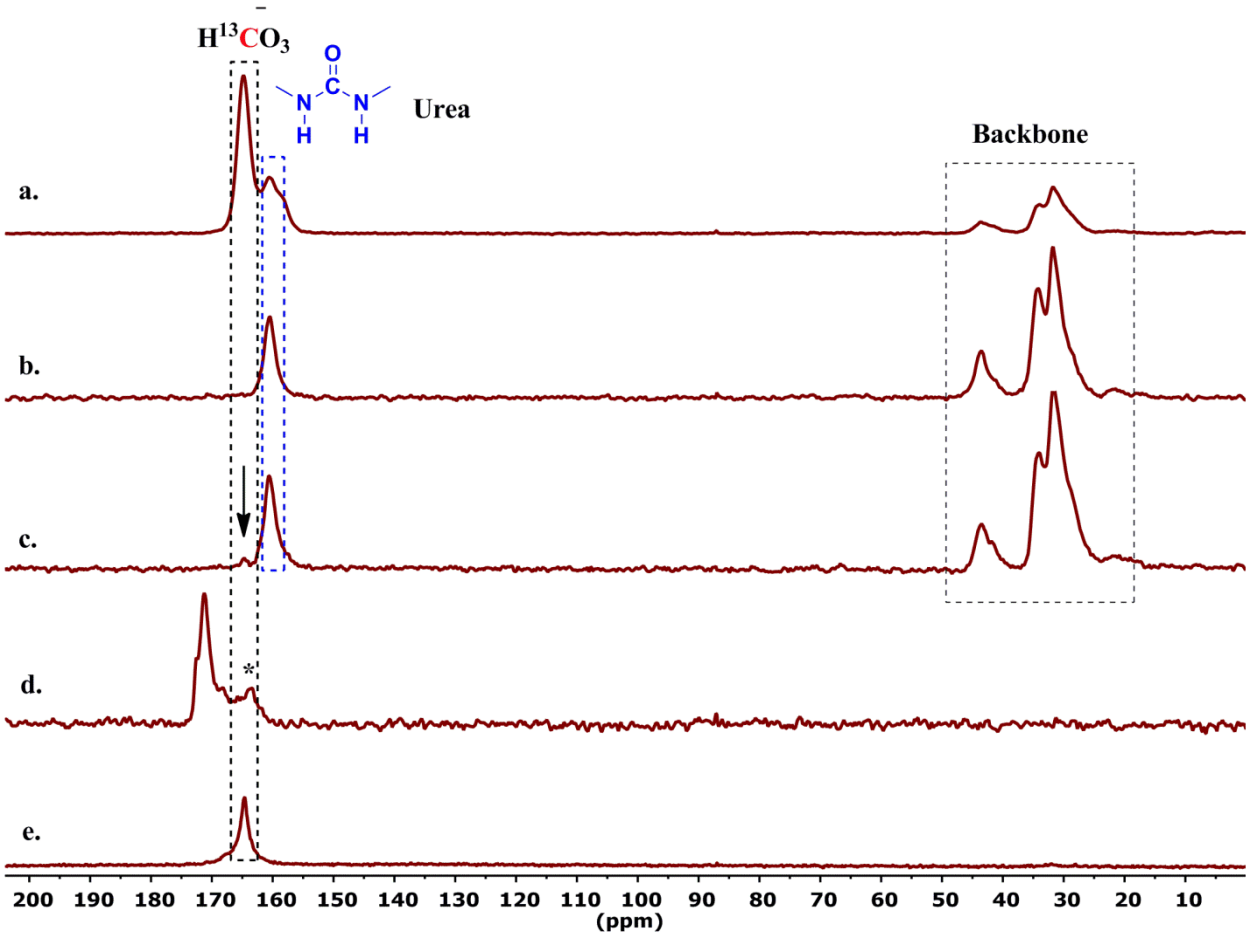

Figure 3.19. Different 13C CP-MAS NMR spectra of **[*10*]-OU**: **a**. After activation at 60.0 ºC and treatment with $^{13}CO_2$; **b**. After activation at 60.0 ºC; **c**. Without activation; **d**. ^{13}C-labeled sodium carbonate ($Na_2{}^{13}CO_3$) standard (*signal corresponding to a presumable bicarbonate contaminant from the manufacturer); **e**. ^{13}C-labeled sodium bicarbonate ($NaH^{13}CO_{3)}$ standard.[131]

The decomposition of **[*n*]-OUs**-containing bicarbonates to form **[*n*]-OUs** requires a higher amount of energy than the corresponding carbamates, which required us to go beyond 60.0 ºC (*in vacuuo*) to activate the samples completely.[136]

3.4.6 Testing of sorption capacities at different temperatures

As **[*10*]-OU** showed the highest sorption capacity, it was considered as model for further tests. Sorption capacities of **[*10*]-OU** upon increasing the sorption temperature from 35.0 to 65.0 and 95.0 ºC on the same experimental run were determined. As depicted in Figure 3.20, the sorption capacities decreased in the order 22.0, 20.0, and 14.0 $mg_{CO2}/g_{sorbent}$, respectively.[131] Presumably, the decrease in sorption is presumably due to decomposition of the formed carbamate/bicarbonate as shown in TGA-MS experiments (*vide infra*).

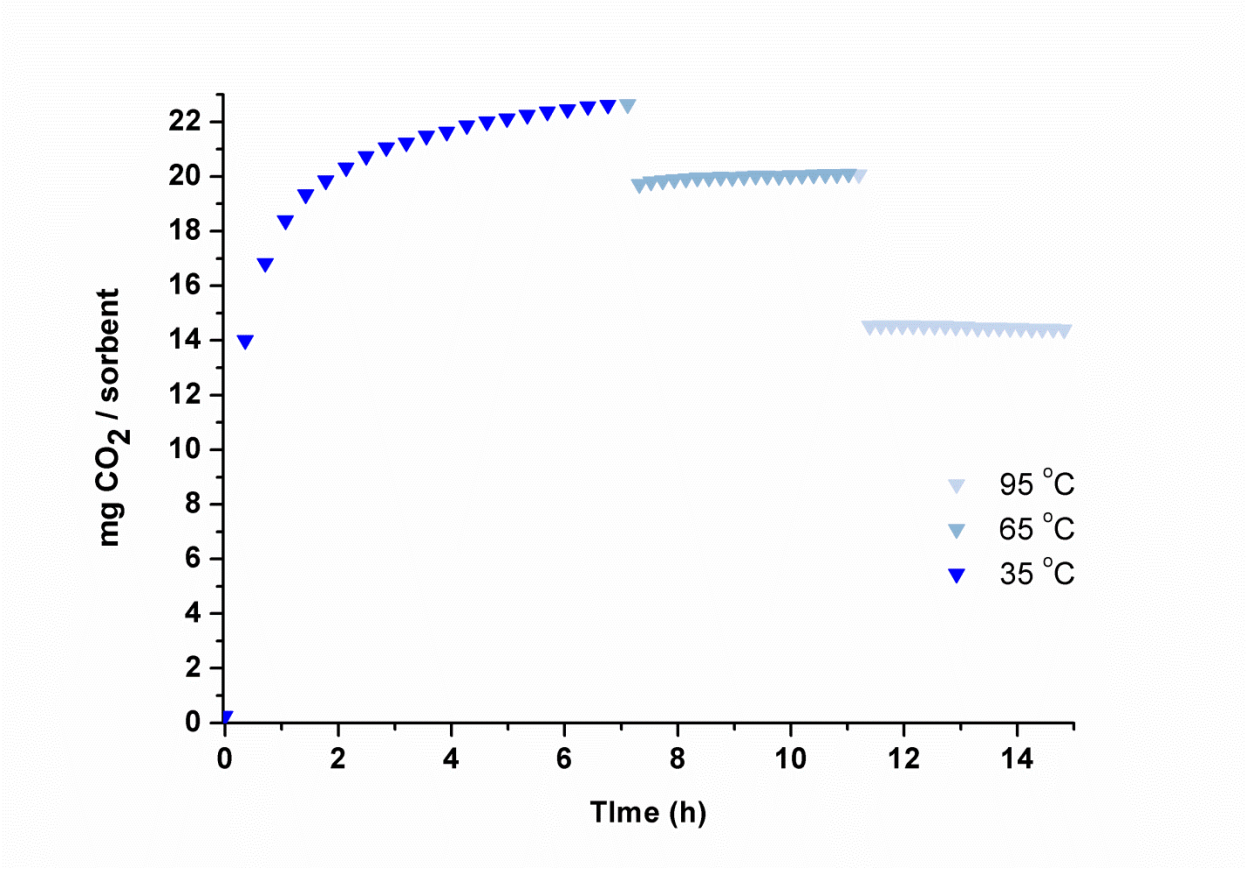

Figure 3.20. Sorption capacities of **[*10*]-OU** activated under vacuum at 100.0 ºC as a function of time at different temperatures.[131]

3.4.7 Cyclic sorption/desorption experiments

[*10*]-OU was further investigated under a series of CO_2 sorption/desorption periods to test its recyclability. Samples were activated for 30.0 minutes at either 60.0 ºC (A′) or 100.0 ºC (A) (*in vacuuo*), sorption was carried out at 35.0 ºC (**S**, **S′**), and desorption was set for 60.0 minutes, at 60.0 ºC (**D′**) or 100.0 ºC (D) (*in vacuuo*). A profile with conditions/steps is provided in Scheme 3.16.[131]

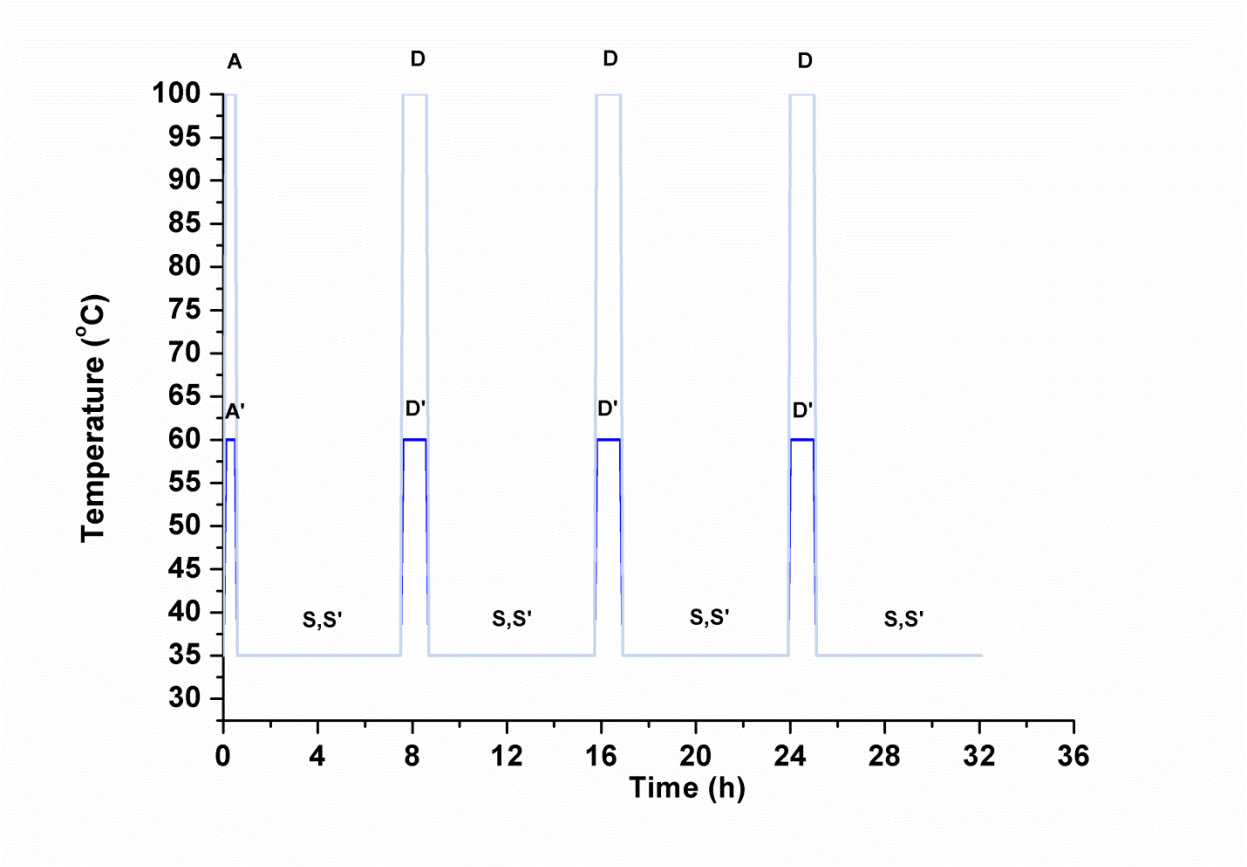

Scheme 3.16. Schematic representation for the sorption/desorption for the **[*10*]-OU** applied at either activation /regeneration temperature at 60.0 ºC (A′, S′, and D′) or at 100.0 ºC (A, S, and D) as the **A**: activation at the desired temperature, **S**: sorption at 35.0 ºC, and **D**: desorption at the desired temperature, respectively. A prime marking implies conditions applied at 60.0 ºC.

3.4.8 Cyclic Sorption/Desorption at 60.0 ºC

Figure 3.21 shows that the first CO_2 sorption step is in agreement with the former sorption capacity for **[*10*]-OU** (Figure 3.17) but the sorption capacity decreases in the latter three CO_2 sorption periods. However, the sorption capacity for **[*10*]-OU** is similar in the latter three. This suggests a partial reversible sorption-desorption mechanism. It was thought to make desorption with longer times in order to make the hypothesis tested.[131]

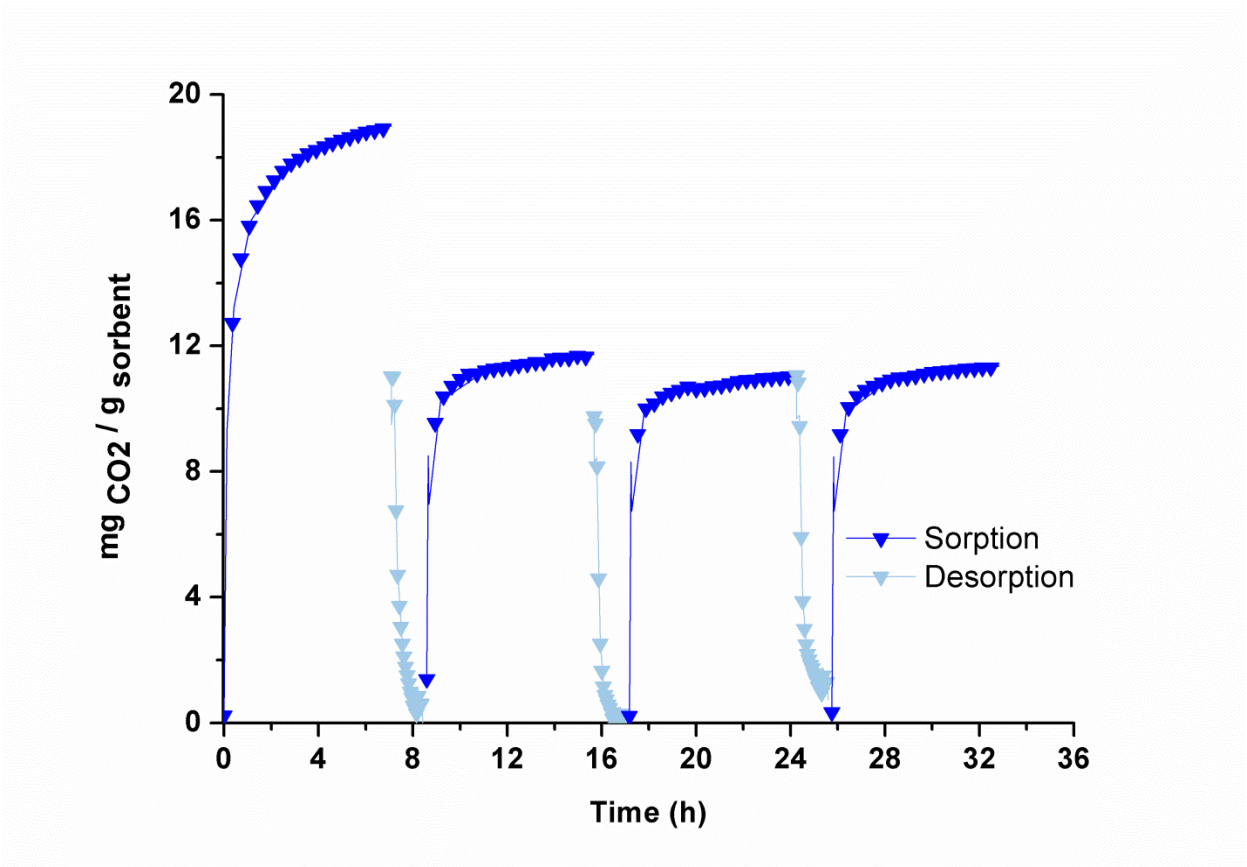

Figure 3.21. Cyclic CO_2 sorption/desorption of **[*10*]-OU** activated at 60.0 ºC.[131]

On the one hand, longer desorption periods (2 h) improved only slightly the CO_2 sorption capacity of **[*10*]-OU** after the first sorption period (Figure 3.22). This led us to go beyond 60.0 ºC to study the effect of obtaining stable cycles along the regeneration of the solid sorbent.

When performing the cyclic sorption/desorption measurement at 60.0 ºC (desorption was under vacuum) the pattern of cycles generated differs upon changing the desorption temperature (*vide infra*). While performing the first cycle, (Figure 3.21), 18.90 $mg_{CO2}/g_{sorbent}$ was achieved. Upon running the second sorption cycle, a behavior similar to the first one would be expected. On the other hand, *ca.* 12.0 $mg_{CO2}/g_{sorbent}$ were achieved (almost one half). The species formed upon sorption is expected to be carbamate ions as a result of a **1:2 mechanism** (*vide supra*), (Scheme 3.15, **Path A**). Therefore, the substance was heated to a higher temperature to make sure that anhydrous conditions can be achieved to eliminate the presence of water.

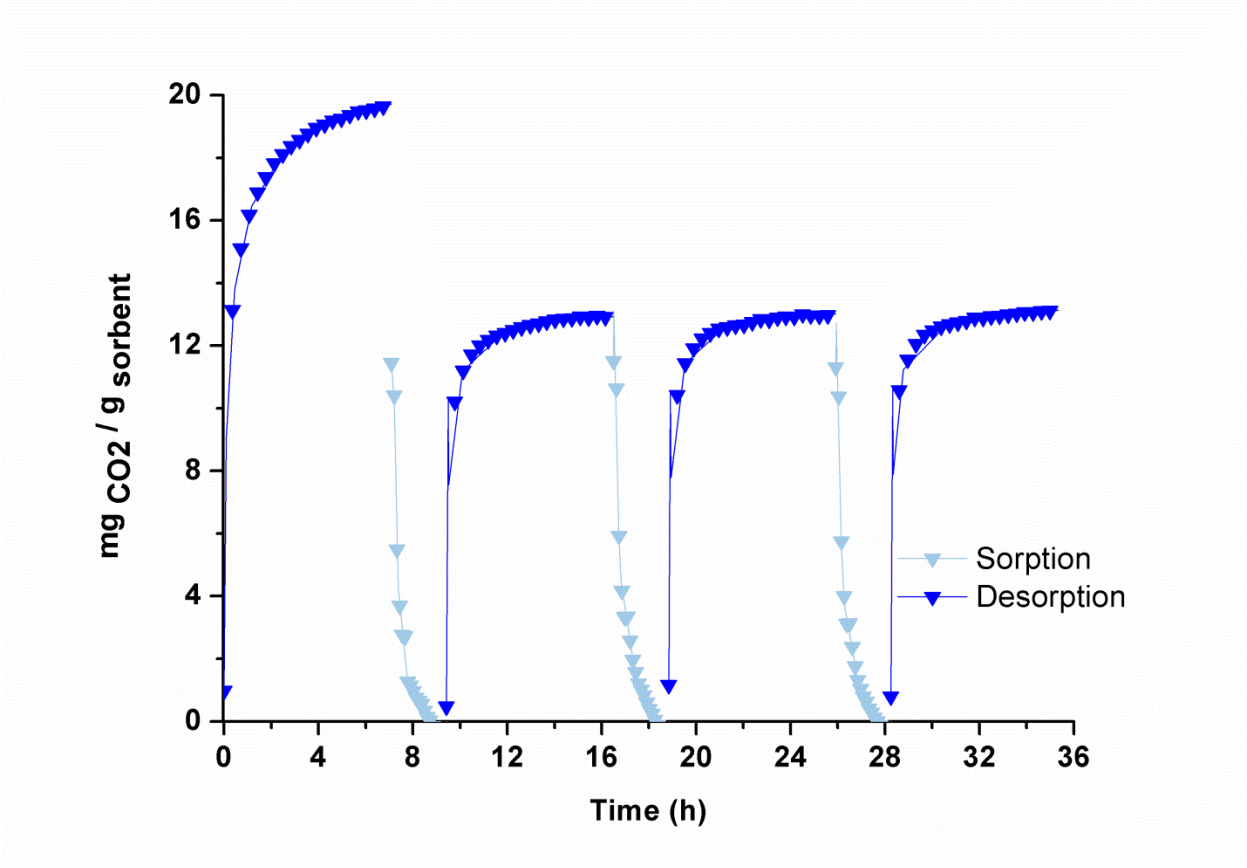

Figure 3.22. Cyclic sorption/desorption for the **[*10*]-OU** at 60.0 ºC with longer desorption times. Sorption was carried out at 35.0 ºC at 1.0 bar.[131]

3.4.9 Cyclic Sorption/Desorption at 100.0 ºC

Due to the increased sorption capacity at higher activation/desorption temperature, another planned cyclic sorption/desorption at 100.0 ºC was taken into consideration. Subsequently, CO_2 sorption/desorption cyclic measurements with a high activation temperature (100.0 ºC) but with different desorption temperatures (60.0 ºC and 100.0 ºC, respectively) were conducted and the expected outcome was exactly the same as previously depicted in Figure 3.21 (Scheme 3.16, with the codes A, S, and D).[137]

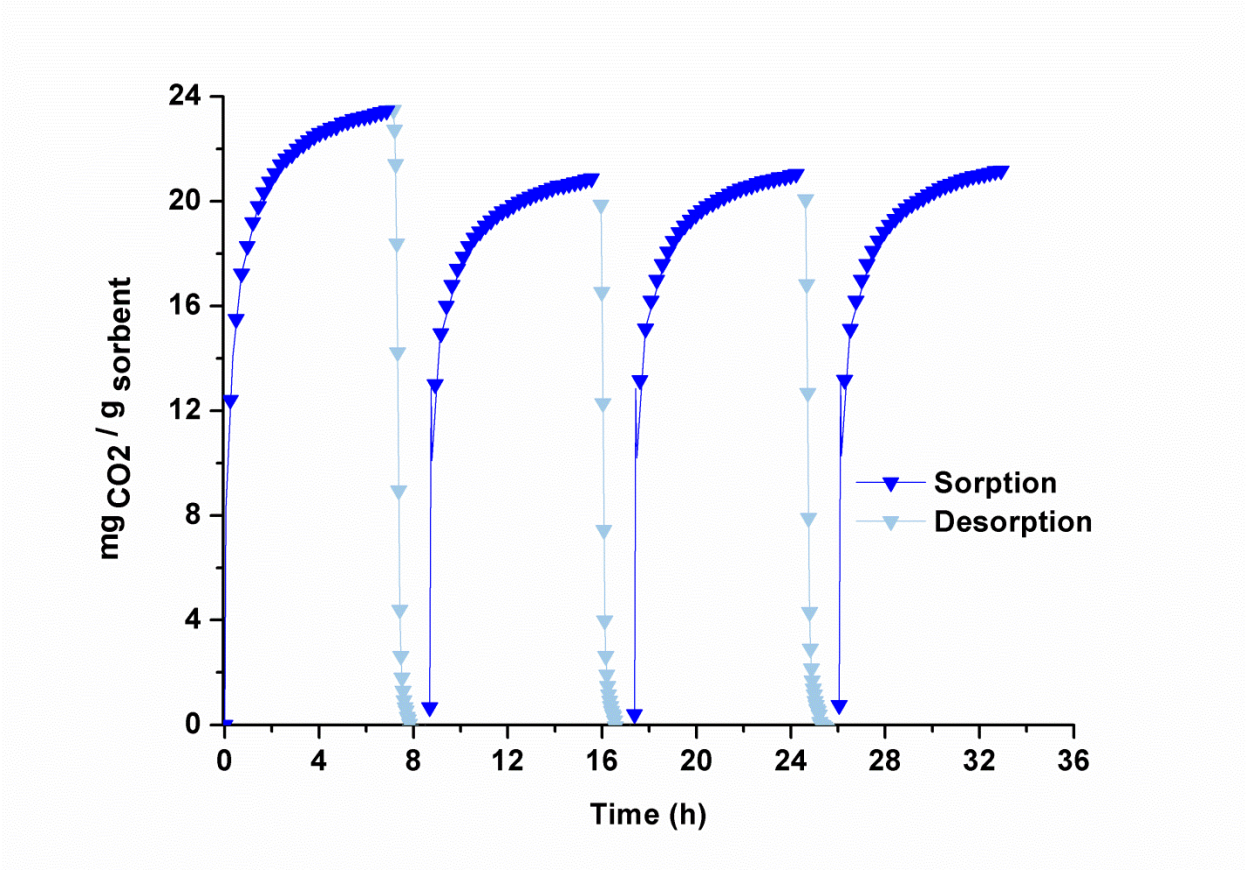

Figure 3.23. Cyclic CO_2 sorption/desorption of **[*10*]-OU** activated at 100.0 ºC, sorption was carried out at 35.0 ºC at 1.0 bar, desorption was carried out at 100.0 ºC (under vacuum).[137]

A new designed experiment was carried out by activating/desorping the **[*10*]-OU** at 100.0 ºC (*in vacuuo*, Figure 3.23). Clearly, a new trend that was not seen in the previous cyclic sorption/desorption (Figure 3.21 and Figure 3.22). Almost equivalent cycles are obtained. In the

first cycle, the same trend of fast kinetics as seen in Figure 3.18, the latter three achieved stable, higher-valued cycles. Moreover, when the substance is heated to a 100.0 ºC (*under vacuum*), the sorption capacity improved in the first cycle, sorption was recorded up to 22.70 $mg_{CO2}/g_{sorbent}$, the theoretical sorption following a **1:1 mechanism** is 23.10 $mg_{CO2}/g_{sorbent}$, presumably due to activating the amino groups at the terminal, it means that almost 98.3% (Table 3.6) of the total primary amines were loaded with CO_2.[137]

Surprisingly, the second cycle (Figure 3.23) was almost below the first cycle by a small difference, *viz.*, 20.0 $mg_{CO2}/g_{sorbent}$. Initially, that was a bit hard to understand at that instance when anhydrous conditions can be achieved at such harder conditions. The possibility for the formation of bicarbonates *via* a **1:1 mechanism** *is almost zero*, due to the exclusion of water. On the other hand, if water was present in the system, it would be excluded at such high temperature, *viz.*, 60.0 ºC and 100.0 ºC (*under vacuum*), respectively. This means that the increased sorption in the latter three cycles is due to another unknown factor away from a **1:1 mechanism**.[137]

Regarding the thermal history of the **[*10*]-OU**, the material showed a thermal stability up to 200.0 ºC (*ca.* 100.0 ºC, *in vacuuo*). After 200.0 ºC, a first step loss presumably due to a backbiting step occurs, the urethane end group backbites to form PC which can be lost during heating as a result of unzipping (Scheme 3.17).[119] That might be the logical reasoning for the almost doubled amount of chemisorbed CO_2 in the latter three cycles (Figure 3.23). [137]

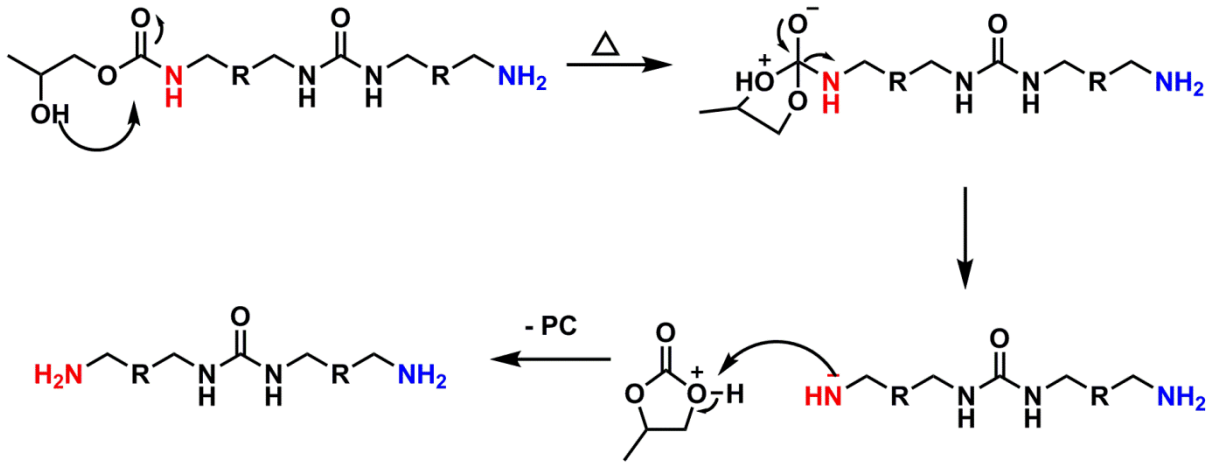

Scheme 3.17. *In-situ* formation of a new amine (**red**) arm due to an induced thermal backbiting of the urethane end group.

On the other hand, Table 3.7 shows two oligomers; *viz.*, **[*7*]-**, and **[*10*]-OU** which possess almost complete CO_2 capturing efficiency (sorption capacity at 100.0 ºC/theoretical sorption capacity) with values of 81.8 and 98.3 %, respectively. Further, the rest of the **[*n*]-OUs** series are almost one half of the overall efficiency (**[*10*]-OU > [*7*]-OU > [*12*]-OU ≈ [*4*]-OU > [*6*]-OU**). Fortunately, this corresponds to the same order of urethane cleavage that can be seen within the magnified rectangular area of the TGA profile in the region above 200.0 ºC (Figure 3.24). It explains the reason why for the unexpected behavior of both **[*7*]-**, and **[*10*]-OU** materials in the previous study.[137]

Table 3.7. Efficiency of capturing CO_2 of the **[*n*]-OU**-based sorbents[137]

[*n*]-OU	**Theoretical sorption capacity ($mg_{CO2}/g_{sorbent}$)[a]**	**Sorption Capacity[c] ($mg_{CO2}/g_{sorbent}$) at 100.0 ºC[a]**	**Efficiency of capturing CO_2 (%)**
[*4*]-OU	31.6	16.07	50.9
[*6*]-OU	25.4	10.12	39.8
[*7*]-OU	21.4	17.51	81.8
[*10*]-OU	23.1	22.70	98.3
[*12*]-OU	22.7	11.60	51.1

a: Taken from reference [131].

Presumably, The latter oligomers have had the highest efficiency in sorbing CO_2 due to having the ease of loss of the urethane end group both terminals as amino groups (Scheme 3.17) as evidenced by the TGA experiment (first step after 200.0 ºC, Figure 3.15). It means that carbamates should be formed instead of bicarbonates because under these conditions no water was present.[137]

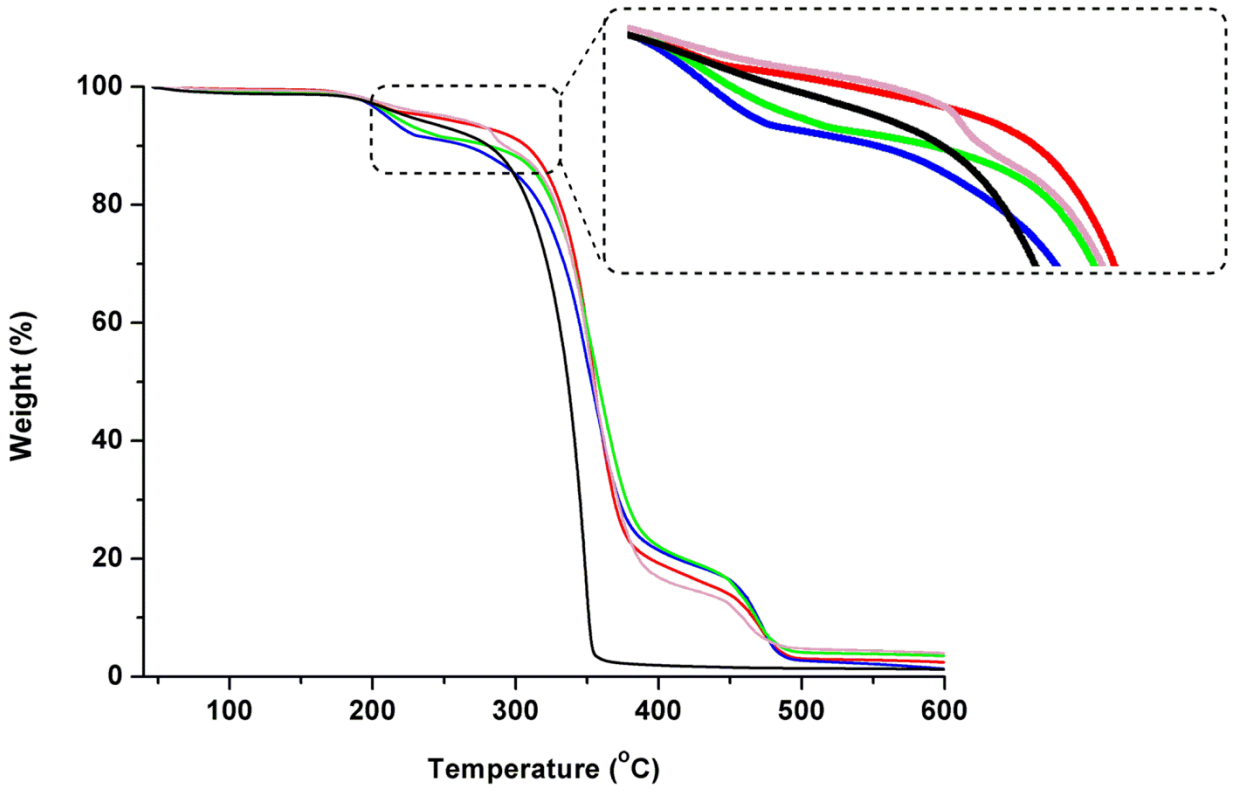

Figure 3.24. TGA traces of **[*n*]-OUs**, (***n*** = **12** (red ——), **10** (blue ——), **7** (green ——), **6** (magenta ——), and **4** (black ——)). Magnification of the rectangular area corresponding to a loss of a PC molecule as a result of activating samples at 100.0 ºC (*in vaccuo*) ≈ 200.0 ºC (at atmospheric pressure). (**[*10*]-OU > [*7*]-OU > [*12*]-OU ≈ [*4*]-OU > [*6*]-OU**).[137]

Accordingly, another mechanism would apply, *viz.*, **1:2 mechanism** of CO_2:amine, this explained the so-called almost the same loading (Figure 3.23) of the three cycles relative to the first cycle which was observed due to capturing of CO_2 by both arms (Scheme 3.18). The difference between the first cycle and the consecutive three is due to the loss of PC (Figure 3.25), together with adsorbed H_2O and MeOH which were contained in the original samples before activation.[137]

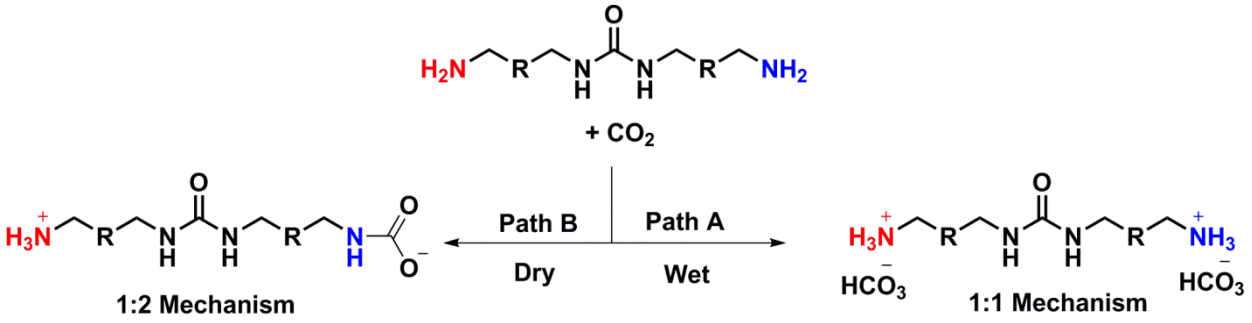

Scheme 3.18. CO_2-chemisorbed *via* 1:2 (**Path B**) or 1:1 (**Path A**) mechanisms upon measuring under dry or wet conditions, respectively. **R** = condensed formula for the **[*10*]-OU,** for viewing purposes of the full structure, see Figure 3.13.[137]

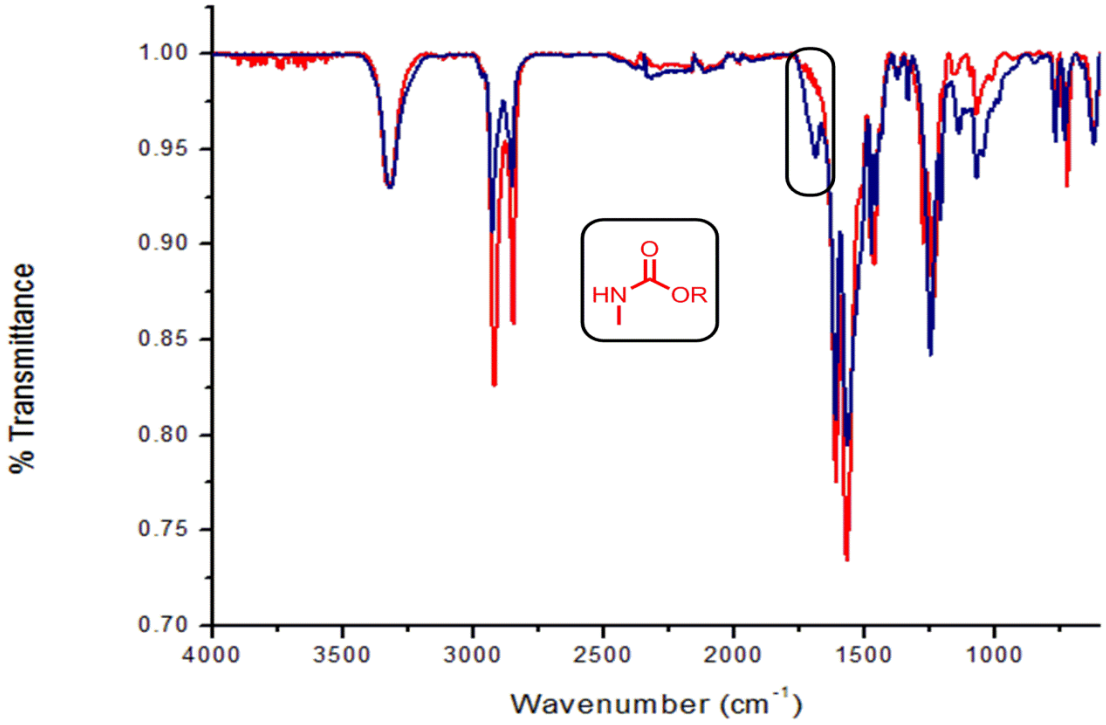

Figure 3.25. FTIR-Spectrum of **[*10*]-OU** before (**blue**) and after activation (**red**) at 100.0 ºC (*in vacuuo*). Loss of a urethane group (blue peak in the rectangle area) due to activation of the materials at 100.0 ºC (*in vacuuo*).

To show the proof-of-principle for the cleavage of urethane upon activation at 100.0 ºC (*in vacuuo*), ATR-FTIR was carried out on the activated **[*10*]-OU** (red spectrum, Figure 3.25) sample after being activated at 100.0 ºC, the pre-assigned peak at 1691 cm^{-1} (blue-colored peak in the rectangular area, Figure 3.25) disappeared due to loss of urethane end group due to backbiting. It is noteworthy, small traces of a urethane end group can be seen, this explains the incomplete experimental sorption capacity (98.3%, Table 3.7) due to presence of traces of urethane end-capping functional group.[137]

Moreover, to further support the above mentioned hypothesis, an *in-situ* TGA-MS experiment for the **[*10*]-OU** was carried out and the temperature profile was added carefully to see at which temperature the urethane end group loss occurs. The experiment did not show any losses for PC under the applied conditions. It did not show any change in the ion current of PC under the same conditions applied in the experiment, *viz.*, 100.0 ºC. Presumably, loss of the urethane end group as a result of activation of the **[*10*]-OU** might be a plausible explanation for the trend. Also this might explain the absence of the presumed peaks or even the detection is lower than the detection limit of machine due to the signal to noise (S/N) of the baseline. On the other hand, other members of the **[*n*]-OUs** were also tested to verify the hypothesis. In this experiment, the weakest absorber was taken into consideration, and a careful design was deployed to show the dislodging of the end group under the same temperature of activation, *viz*., **[*6*]-** and **[*12*]-OU** at 100.0 ºC (*in vacuuo*).[137]

On the one hand, a TGA-MS profile of **[*6*]-OU** shows that there is no total loss of PC during activation (Figure 3.26). That was a bit misleading because in theory, **[*6*]-OU** should have its urethane end group which can be seen from the TGA profile (Figure 3.24) as well as its low sorption compared to **1:1 mechanism** (Table 3.6). On the other hand, in the last region of activation, *viz.*, 100.0-120.0 ºC, an abnormal broadened peak is shown for CO_2. The experiment chosen was giving evidence that there might be another source of CO_2 within the sorbent that is being fragmented. The rational explanation was PC. If successful, it should fragment and give CO_2 as well as a propylene moiety. Due to limited amount of the material, the same experiment was carried out with another candidate, *viz.* **[*12*]-OU**. It is noteworthy, that PC has a low relative

intensity of the parent molecular ion, upon fragmentation, a prominent molecular ion peak at m/z = 57 is well observed.[138]

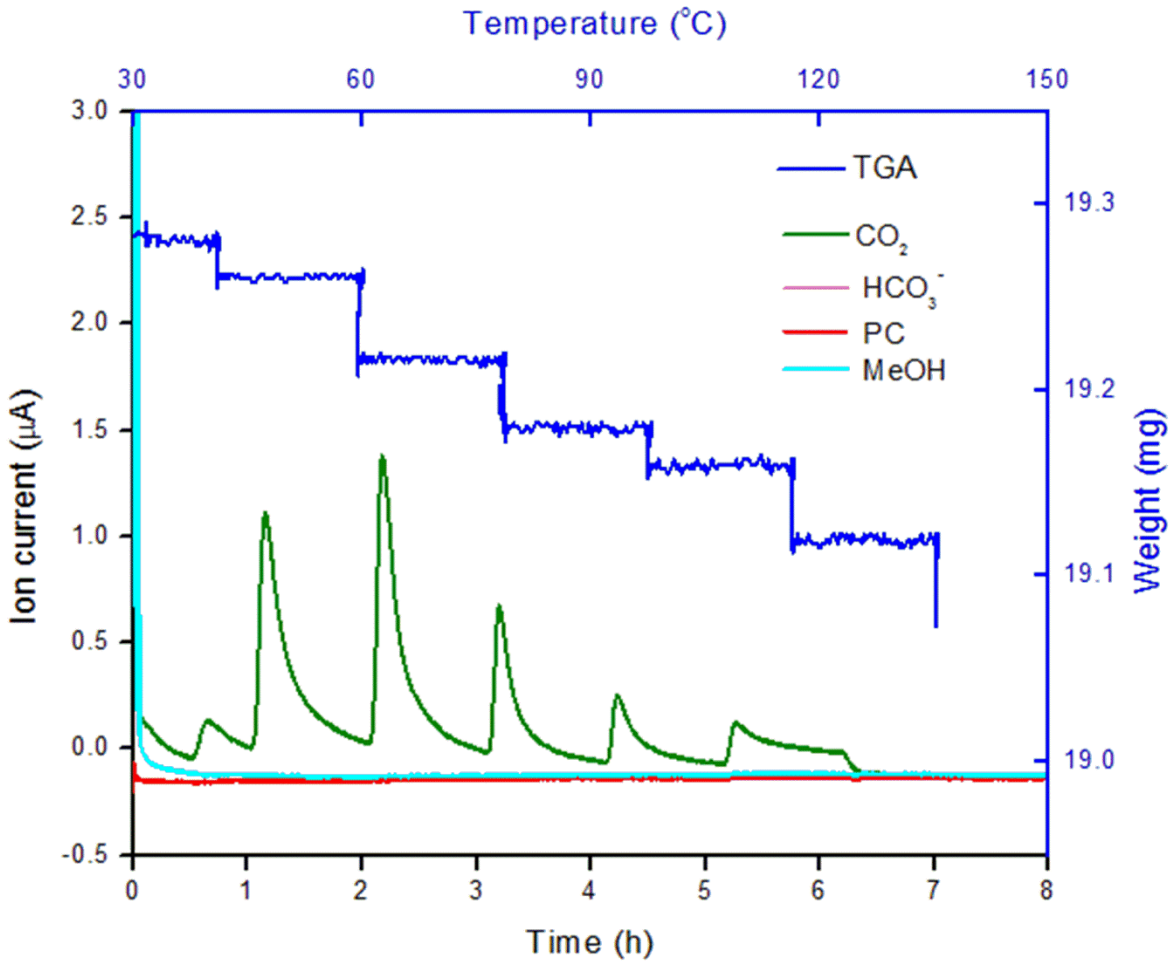

Figure 3.26. TGA-MS profile of **[*6*]-OU** experiment under a step-wise rise of temperature. PC: Propylene carbonate, Water peak was eliminated due to higher intensity. TGA profile (*in vaccuo*): 30.0 ºC (30 min), (30.0-40.0) ºC (1 h), (40.0-60.0) ºC (1 h), (60.0-80.0) ºC (1 h), (80.0-100.0) ºC (1 h), (100.0-120.0) ºC (1 h), and (120.0-1350.0) ºC (1 h). Heating rate: 10.0 K/min.[137]

Figure 3.27 shows a TGA-MS profile for the activated **[*12*]-OU**, it shows two prominent facts regarding the CO_2-loss behavior upon a stepwise rise of temperature. Firstly, the CO_2 loss at every step under vacuum indicates two active species involved, at lower vacuum (below 40.0 ºC)

as well as high vacuum (above 60.0 ºC). Most probably, carbamates and bicarbonate in the presence of a humid environment might equilibrate, Scheme 3.15. Secondly, an interesting broadening of CO_2 peak is the last step in the range of (100.0-120.0) ºC. As an assumption that there is an additional source of CO_2 at this point that might be the result of the broadening of the last peak. Most presumably, under mass spectrometric conditions, fragmentation pattern of PC to give CO_2 and propylene radical moiety might explain the reason why for the tendency of broadening.[138]

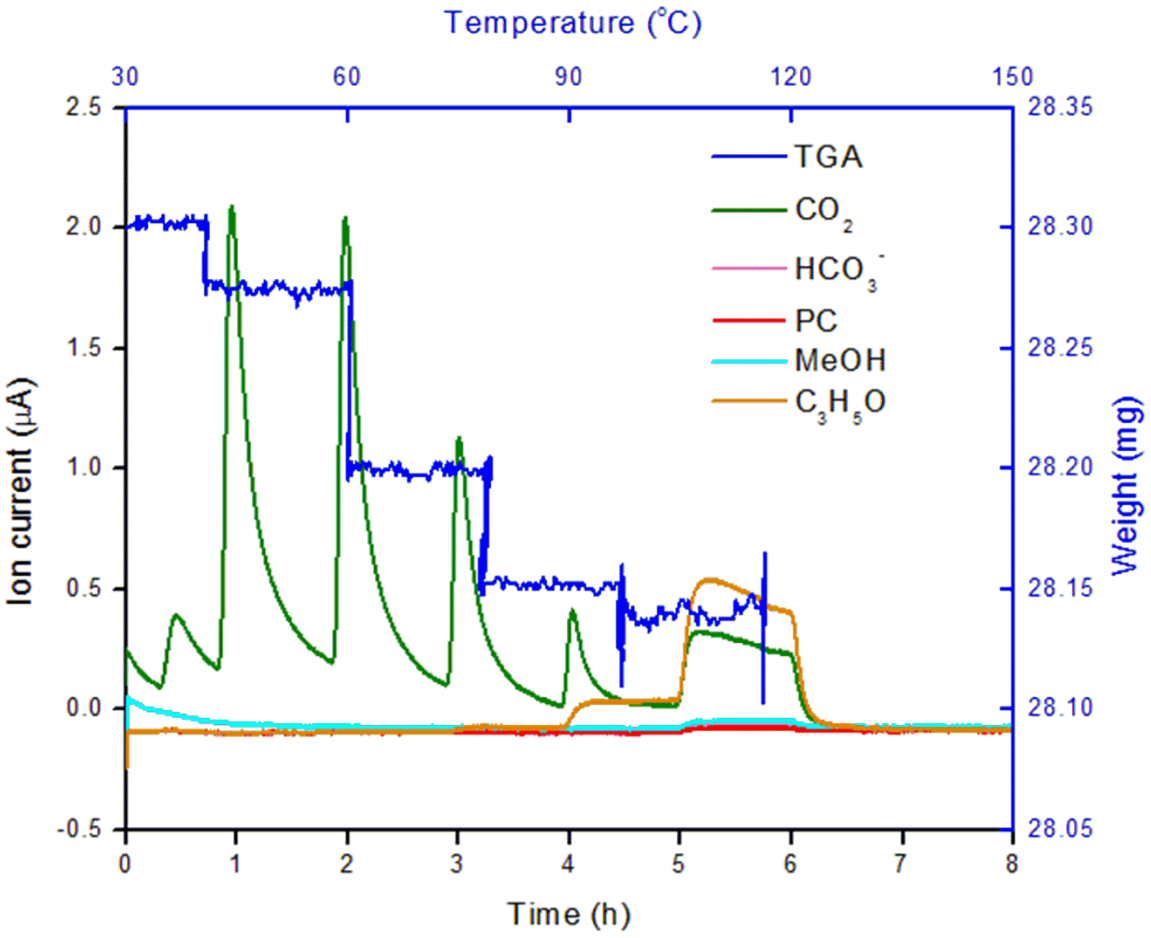

Figure 3.27. TGA-MS profile of **[*12*]-OU** experiment under a step-wise addition of temperature. PC: Propylene carbonate, C_3H_5O: fragmented PC moiety. Water peak was eliminated due to higher intensity. TGA profile (*in vaccuo*): 30.0 ºC (30 min), (30.0-40.0) ºC (1 h), (40.0-60.0) ºC (1 h), (60.0-80.0) ºC (1 h), (80.0-100.0) ºC (1 h), and (100.0-120.0) ºC (1 h). Heating rate: 10.0 K/min.

Further, ^{13}C CP-MAS NMR spectroscopy (Figure 3.28) was carried out to confirm the presence of carbamates under the applied condition. Due to the sensitivity of carbamates and to prevent further hydrolysis from the atmosphere, the preparation of the sample was carried out inside the glovebox. The formation of Urea (**C**), carbamate (**B**), and bicarbonate (**A**) was assigned at 160.6, 161.7, and 164.9 ppm, respectively. ^{13}C CP-MAS NMR paved another proof for the presence of two species within the sample as a result of humidity during sample preparation.[137]

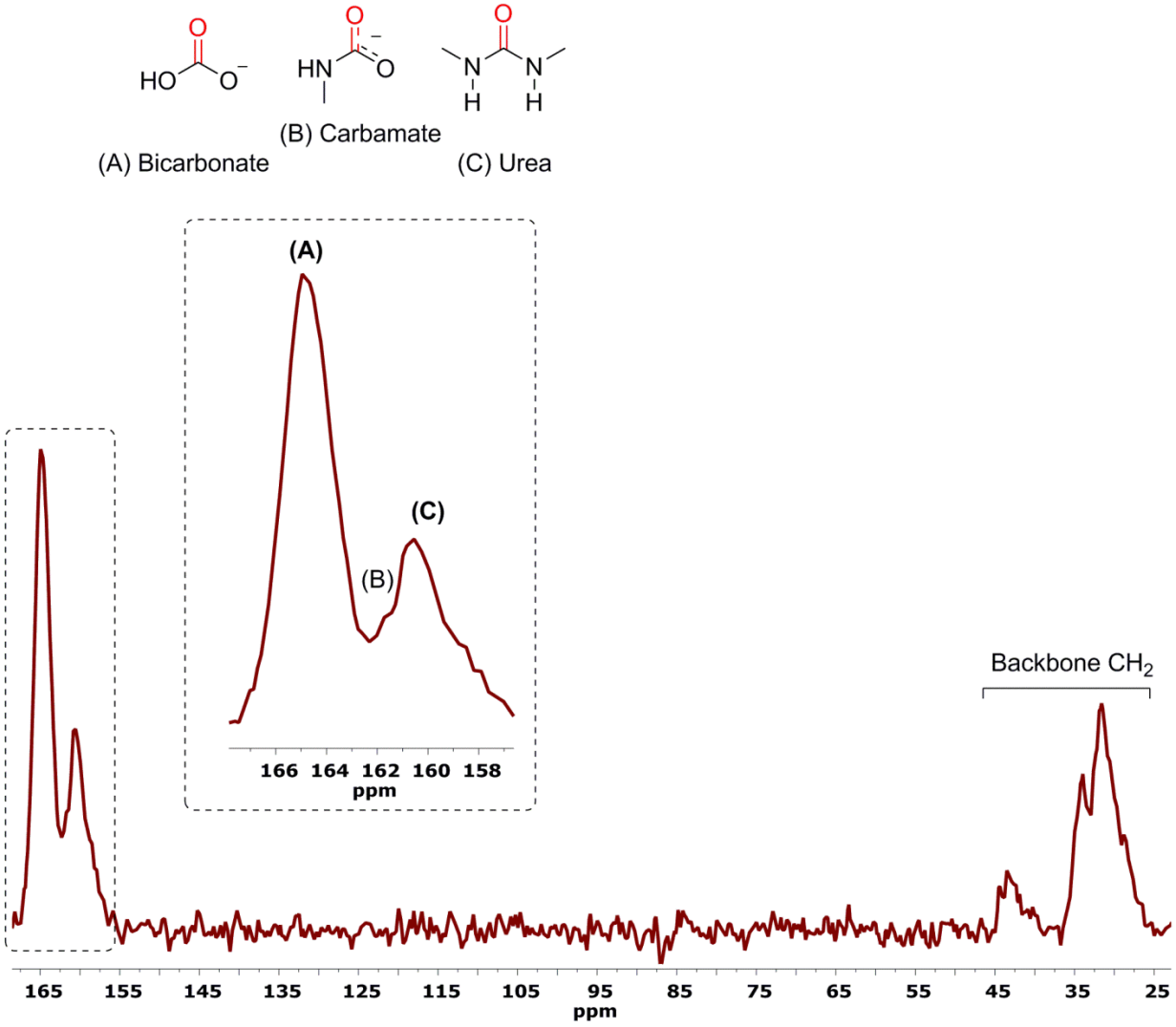

Figure 3.28. Partial 13C CP-MAS NMR spectrum for the **[*10*]-OU-**$^{13}CO_2$ activated at 100.0 ºC (*in vacuuo*).[137]

3.4.10 High-pressure, thermogravimetric analysis (HP-TGA) sorption measurements.

To see the predominant effect of either physisorption or chemisorption in **[*10*]-OU**, high-pressure thermogravimetric apparatus (HP-TGA) was used. Additional CO_2 sorption capacity values for **[*10*]-OU** at different pressures were recorded. The resulting sorption capacities were similar to the previously recorded sorption capacity and they were characterized by a very fast sorption profile with a value of 20.11 $mg_{CO2}/g_{sorbent}$ at 1.033 bar and a maximum sorption capacity of 23.63 $mg_{CO2}/g_{sorbent}$ at 10.55 bar (Figure 3.29). Expectedly, there is no significant increase of sorption capacity as a function of increasing pressure, indicating only chemisorption as the principal mechanism for sorption.[131]

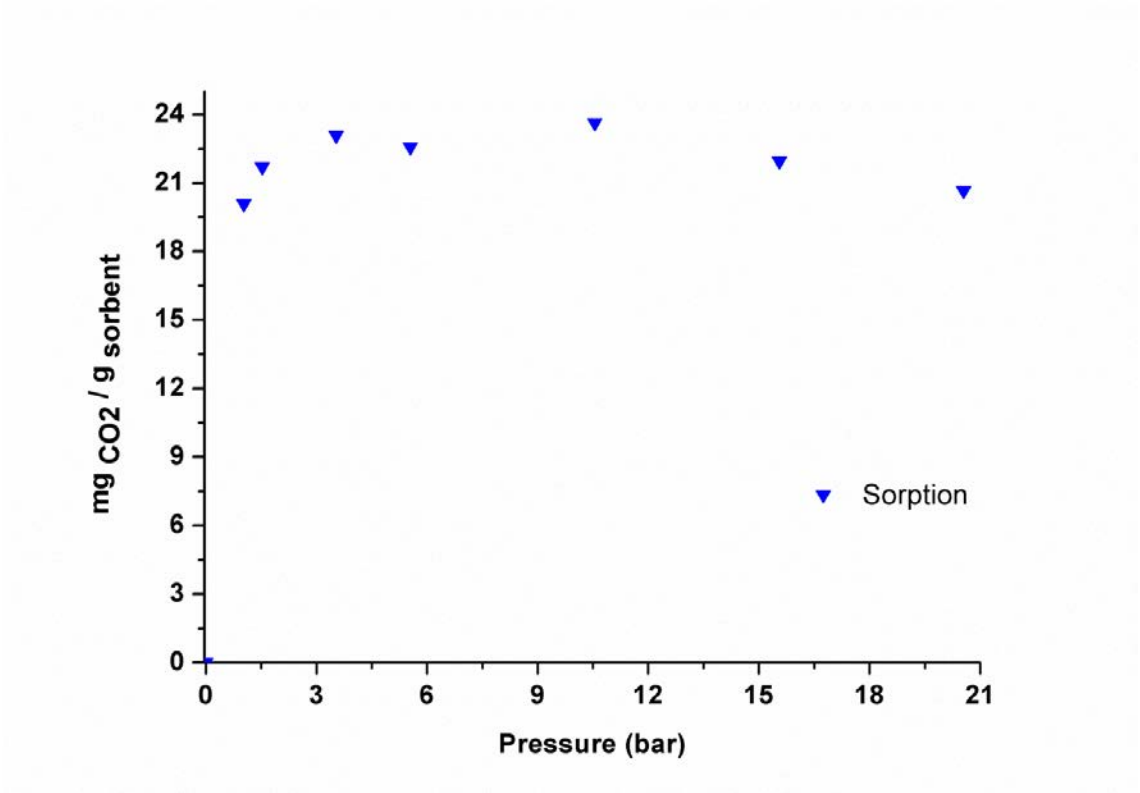

Figure 3.29. CO_2 sorption isotherm capacities from **[*10*]-OU** at 35.0 ºC and different CO_2 pressures.[131]

3.4.11 Comparison of [*n*]-OUs-based sorbents with other sorption systems.

The presence of different measurement units (*e.g.* mol%, wt%, $mmol_{CO2}/g_{sorbent}$, or $mg_{CO2}/g_{sorbent}$) and conditions (*e.g.* temperature and pressure) to describe and determine the CO_2 sorption capacity of new materials in the literature impedes a direct comparison with our results.[139] On the other hand, the use of diverse methods (***volumetric*** or ***gravimetric***) can afford contradicting results. As an example, Cooper[140] and coworkers reported on the synthesis of porous organic solids. One of these synthesized materials showed an interesting character by changing the recrystallization solvent. *i.e.* from permanently porous polymorph cages upon changing into a nonporous material once dissolved into ethyl acetate (surface area, SA_{BET} = 24.0 m^2/g, 1.03 $mmol_{CO2}/g_{sorbent}$ at 16.0 ºC and 1.0 bar CO_2) using a volumetric method. However, no sorption was detected using a gravimetric method.

Although having differences with our measurement system; *viz.*, gravimetric *vs.* volumetric, the **[*n*]-OUs** are competitive with reported CO_2 sorption capacities of known porous and non-porous sorbents bearing in mind the ecofriendly and easy approach for the synthesis, cost-effectiveness of the starting materials, fast kinetics regarding CO_2 sorption/desorption, and resistance of the oligomers to humidity. Moreover, our measuring conditions are closer to those required in industrial facilities.[85] Concerning porous materials, Antonietti and coworkers reported on the preparation of a mesoporous poly(ionic liquid) (***mp*PIL**), which was made upon the reaction of equivalent amounts of 4-vinylbenzene chloride together with 1-vinylimidazole. The resulting polymers gave a maximum CO_2 sorption of 0.46 $mmol_{CO2}/g_{sorbent}$ (Table 3.8).[141]

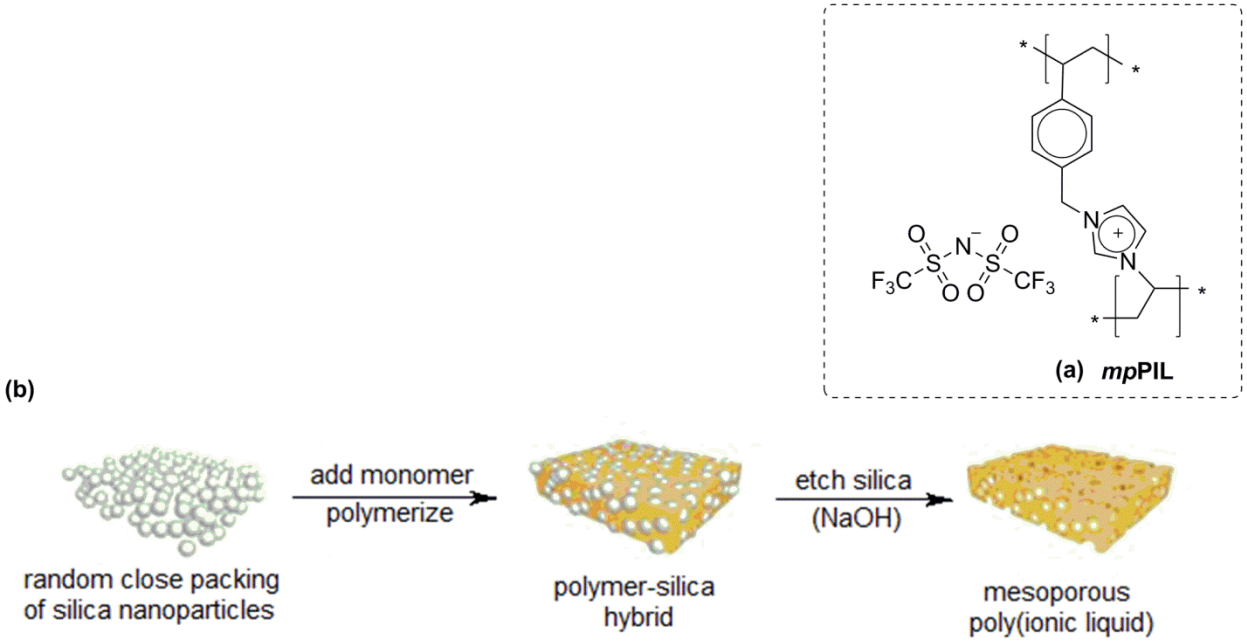

Scheme 3.19. **a)** Structural representation of mesoporous poly(ionic liquids) (***mp*PILs**) representation. **b)** Schematic overview of the employed hard-templating pathway.[141]

In addition, Qiu and coworkers studied porous aromatic frameworks (Scheme 3.20, **X = , PAF-3; X = , PAF-4**) for the capture of CO_2.[142] They showed that adsorption occurs at room temperature and atmospheric CO_2 pressures with an overall uptake of 1.09 $mmol_{CO2}/g_{sorbent}$.

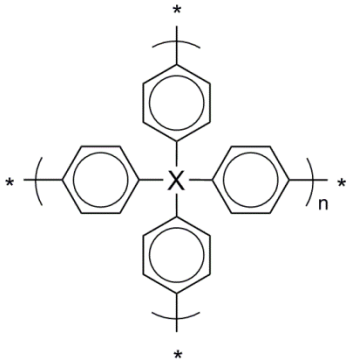

Scheme 3.20. Structural representation of the porous aromatic frameworks, X = Si (PAF-3) and X = Ge (PAF-4).[142]

Moreover, under the same conditions, Jiang and his coworkers implemented the use of MOP networks (Figure 3.30).[144] These sorbents gained a total of 1.18 $mmol_{CO2}/g_{sorbent}$ at 0 ºC and atmospheric pressures.

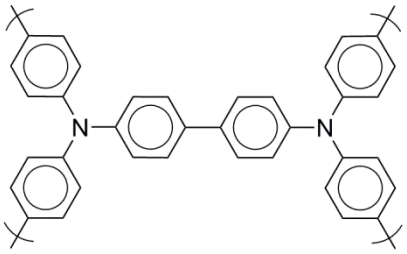

Figure 3.30. Structural representation for YPTPA.[144]

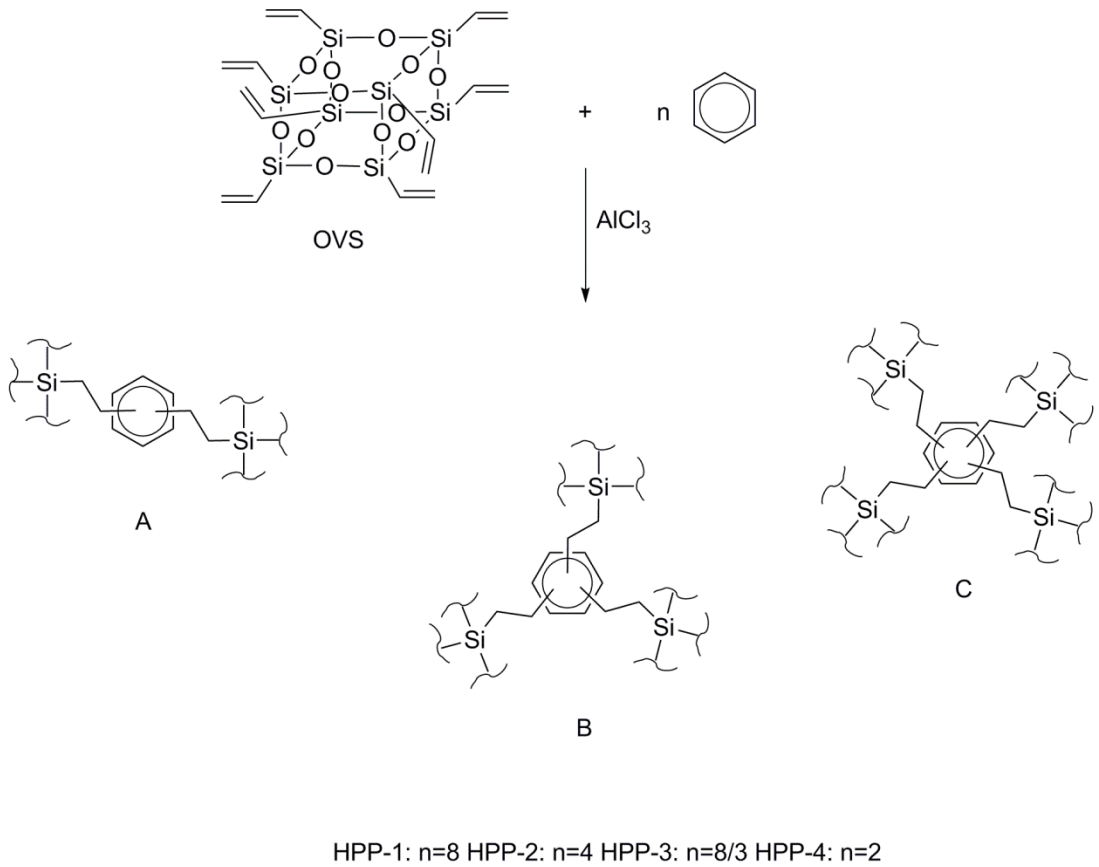

Scheme 3.21. Synthetic routes to HPP-1 to HPP-4. Some fragments are shown as a possibility to be formed; OVS: Octavinylsilsesquioxane.[146]

Wu *et al.*[146] reported on the synthesis of hybrid porous polymers (**HPP**, Scheme 3.21) that were constructed from octavinylsilsesquioxane (OVS) and benzene *via* a Friedel-Crafts reaction, among the synthesized materials, HPP-3 had the highest S_{BET} , which gave 0.62 $mmol_{CO2}/g_{sorbent}$ at 25.0 ºC and 1.0 bar.

Table 3.8. Comparison of the CO_2 sorption capacity of **[*10*]-OU** with different sorbents.[131]

Sorbent	T (^{o} C)	P (bar)	Sorption capacity ($mmol_{CO2}/g_{sorbent}$)	Reference
[*10*]-OU[a]	35.0	1.0	0.52	[131]
***mp*PIL (mesoporous)**	25.0	1.0	0.46	[141]
PAF-3	25.0	1.0	1.82	[142]
MOP, CMP-1	25.0	1.0	1.18	[143]
YPTPA	0.0	1.13	1.56	[144]
P6 [BIEMMA][Br]	25.0	1.0	0.08	[145]
HPP	25.0	1.0	0.62	[146]

[a] As measured by a TGA-DSC instrument.

Regarding nonporous materials, the CO_2 sorption value of **[*10*]-OU** is higher than those reported for ILs and comparable or even higher than those evaluated for PILs. In 2005, Tang *et al.*[147] introduced PILs (*e.g.* poly[(*p*-vinylbenzyl)trimethylammonium tetrafluoroborate]; P[[VBTMA][BF_4], Figure 3.31) as solid sorbents to capture CO_2. Those non-porous sorbents gave an adsorption of 10.22 mol% (22.0 °C, 0.78 atm CO_2). Under our measuring conditions (35.0 °C and 1.0 bar CO_2), higher CO_2 equilibrium capacity was reached (*ca.* 11.0 mol%).[131]

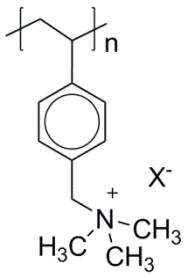

Figure 3.31. Structural representation of poly[(*p*-vinylbenzyl)trimethylammonium tetrafluoroborate] P[VBTMA][BF_4], [147] or its hexafluorophosphate P[VBTMA][PF_6][36] PILs. X: BF_4^-, PF_6^-.

A similar PIL (P[VBTMA][PF_6], Figure 3.31) was studied by Supasitmongkol and Styring[36] adsorbs up to 77.0 wt%, upon the use of a scaled-up adsorber that was constructed from a Radley's carousel synthesizer. However, this polymer absorbed only 2.47 wt% as determined by TGA, while **[*10*]-OU** absorbed 2.36 wt% under TGA conditions. In addition, there is no clear correlation between crystallinity and CO_2 sorption.[131]

3.5 Synthesis of Other Candidates of Aromatic/Aliphatic *ter*-Oligoureas.

Ter-oligomerization trials using aromatic diamines, Hexamethylenediamine (HMDA) and propylene carbonate (PC) were not successful. On the other hand, co-oligomers were obtained, *viz.*, **[*6*]-OU′**. These oligomers differed from those synthesized in Section 4.6.6.2, the discrepancy is represented by both the degree of polymerization (DP) as well as end groups. DP values are less, and urethane end groups are end-capping both terminals. The rational explanation for such trend was due to the 1:2 ratio of aliphatic diamine to PC which would give the same DP no matter aromatic diamine was used (Scheme 3.22).

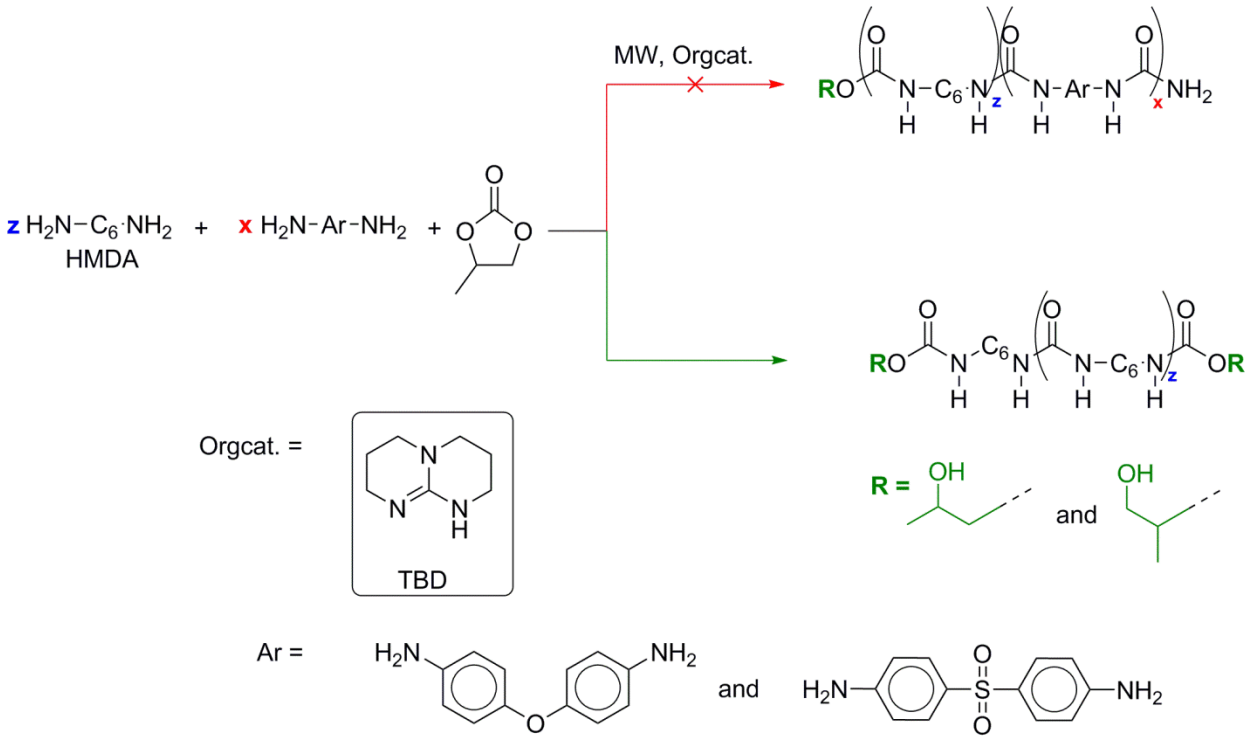

Scheme 3.22. Oligomerization of aliphatic/aromatic diamines with PC organocatalyzed by TBD.

Those materials were characterized by both 1H NMR and IR spectroscopy. Using 1H NMR, a clear evidence for the failure of preparation of the teroligomers was the absence of the aromatic hydrogens in the NMR spectrum (Section 4.6.7). According to NMR, DP for the formed materials was 4.0, the materials produced were methanol insoluble, and therefore, TFA was used as NMR solvent. IR spectroscopy confirmed the presence of a urea bond formation as seen by the formation of a carbonyl stretching at 1617 cm^{-1} as well as an extra pronounced peak associated with amide formation at 1752 cm^{-1}. Peaks assigned above 3000 cm^{-1} were observed at 3318 cm^{-1} which can be attributed to the secondary amine formation due to urea bondage.[119] Urethane group was identified with a medium intensity peak at 1685 cm^{-1}.[132]

Chapter 4

EXPERIMENTAL PART

4 EXPERIMENTAL PART.

4.1 Instruments used.

Nuclear Magnetic Resonance (NMR)

Solution NMR spectra were collected at room temperature using a Bruker ARX300 spectrometer and trifluoroacetic acid (TFA-*d*) as deuterated solvent. 1H and 13C NMR spectra were referenced to the residual solvent signal (1H: CF_3COOH, 11.50 ppm; 13C: CF_3COOD, 116.6 ppm).

Cross Polarization-Magic Angle Spin- Nuclear Magnetic Resonance (13C CP-MAS NMR)

Solid State NMR experiments were performed using a Bruker Avance 300 (1H: 300.0 MHz, 13C: 75.0 MHz) equipped with a 4.0 mm- ZrO_2 rotor, which was spun at a rate of 12.0 KHz. Adamantane was used as an external standard.

Differential Scanning Calorimetry (DSC)

DSC measurements were performed on a DSCQ2000 from TA Instruments in the temperature range from 25.0 to 300.0 °C. Samples were sealed in T-zero hermetic aluminum pans under Argon and scanned at a rate of 10.0 K/min under a N_2 atmosphere.

Thermogravimetric Analysis (TGA)

TGA analyses were performed using Q5000 from TA instruments under N_2 with a flow rate of 10.0 mL/min and a heating rate of 10.0 K/min.

Thermogravimetric Analysis –Mass Spectrometry (TGA-MS)

The gravimetric and calorimetric measurements were performed in a modified SETARAM TG DSC 111 instrument with a BARATRON 122A pressure transducer. For precise measurements, a sample (about 20 mg) was filled inside a glass vial, activated at 30.0 °C for 30 min (under

vacuum), then stabilized to 40.0 °C for another 30 min, afterwards, temperature was raised gradually to reach 60.0 °C, 80.0 °C, 100.0 °C, 120.0 °C and 140.0 °C (*in vacuuo*). After setting the TGA measurement, the mass spectrometric recording started with a delay of 10 seconds to ensure that all experiments with unified parameters.

Attenuated Total Reflectance-Fourier Transform Infra-red Spectroscopy (ATR-FTIR)

ATR-FTIR Infrared spectra were recorded on a Bruker Vertex 70-FT-IR spectrometer with an MCT detector at room temperature coupled with a Vertex Pt-ATR accessory. Materials (*ca.* 5 mg), were dried in a vacuum oven prior to use. Sample manipulation was carried out under air very rapidly.

***In-situ* Attenuated Total Reflectance-Fourier Transform Infra-red Spectroscopy (*in-situ* ATR-FTIR).**

In-situ ATR-FTIR measurements were carried out using a 50.0 mL stainless steel reactor a Mettler-Toledo MMIR45m RB04-50 with an MCT Detector; *DiComp* (Diamond) probe connected *via* Pressure Vessel; Sampling 4000 to 650 cm^{-1} at 8 wavenumber resolution; Scan option: 64; Gain: 1x. The drying and preparation of the autoclave required cleaning with DCM, acetone, then rinsed with toluene. Heated at 110.0 °C (*in vacuuo*) overnight to make sure that the autoclave is dry. Upon starting the material, the vacuum pump was closed and Argon valve was opened by which the opening of the reactor was ensured by an argon blanket.

Elemental Analysis

Elemental analyses were performed on a HEKAtech EuroEA elemental analyzer. Regarding air sensitive materials, all sample preparation involved was carried out under standard glovebox.

Powder X-ray diffraction (PXRD)

PXRD patterns were measured using a Bruker D8 Advance X-ray diffractometer (Bruker AXS, Karlsruhe, Germany) with Bragg-Brentano geometry, equipped with a two-dimensional detector (Vantec-1®, Bruker AXS, Karlsruhe, Germany).

4.2 Methods

4.3 Oligomerization experiments

4.3.1.1 Microwave-assisted reactions in the dynamic-mode

The working principle of the dynamic mode is based on a sensor feedback; it controls the temperature upon varying the microwave power automatically. All **[*n*]-OU** applied in the study were synthesized using this mode unless otherwise stated. *Catalysts used, catalysts loading, temperature, and time were optimized using the dynamic mode.* Optimized conditions were: parameters used: Microwave power 200.0 W, 2.0 mol% TBD, 50.0 °C, and a time of 10 *min*. The reaction temperature was measured with an IR-sensor.

4.3.1.2 Microwave-assisted reactions in the fixed-mode

The fixed mode applies a specified amount of energy (fixation of microwave power) for a specified amount of time. *Along with the dynamic mode,* **[*6*]-OU** *was fully optimized using this mode as a function of time, and microwave power.* The reaction temperature was measured with an IR-sensor.

4.3.2 Optimization Conditions

In order to find out the right conditions (set of optimized parameters) for the oligomerization recipe, different variables were taken into consideration, *i.e.* Temperature, pressure, time, microwave power (MW), solvent, organocatalysts used, Microwave method (*dynamic- vs. fixed-*

mode). Moreover, *1,6-Hexamethylenediamine (**HMDA**) was taken as a model compound to be optimized*. In the following sub-section, a careful study will be shown elsewhere (*vide infra*).[119]

4.3.2.1 As a Function of Organocatalyst.

The organocatalysts applied in the study were: 1,5,7-triazabicyclo[4.4.0]dec-5-ene (**TBD**, **a**), 1,8-diazabicyclo[5.4.0]undec-7-ene (**DBU**, **b**), Schreiner's thiourea based catalyst (**c**), 1,5-diazabicyclo[4.3.0]non-5-ene (**DBN**, **d**), 1,1,3,3-tetramethylguanidine (**TMG**, **e**), 1,4-diazabicyclo[2.2.2]octane (**DABCO**, **f**) and 4-dimethylaminopyridine (**DMAP**, **g**). Among all chosen candidates (**b-g**, *vide supra*), only TBD (**a**) Gave solid **[*6*]-OU** upon applying the same conditions.

4.3.2.2 As a Function of Organocatalyst's Loading (mol%).

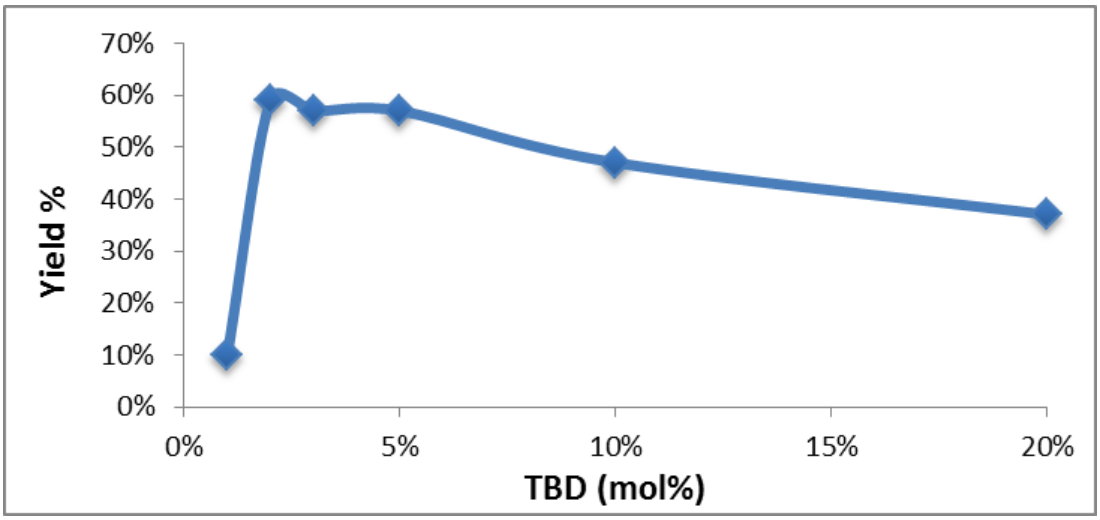

Figure 4.1. Yield as a function of catalyst loading (*mol %*); parameters used: TBD (mol%), 220.0 W, 50.0 °C, 10.0 *min* and solvent-free conditions, *dynamic mode*. HMDA was used as a model compound.

As shown in Figure 4.1, optimal catalyst loading was **2.0 mol%**.

4.3.2.3 As a Function of Oligomerization Time (min).

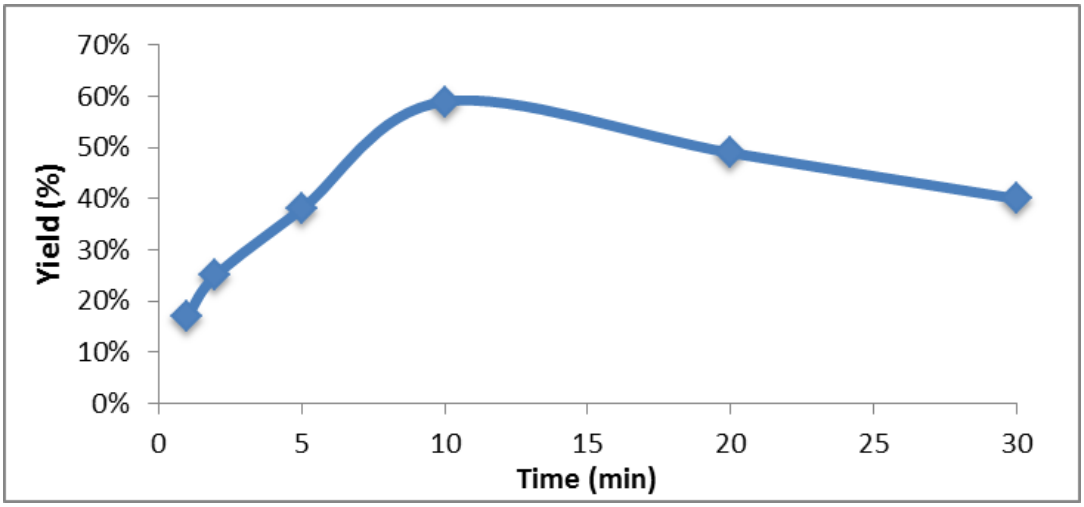

Figure 4.2. Yield as a function of time (*min*), parameters used: time (*min*), 3.1 mol% TBD, 220.0 W, 50.0 °C and solvent-free conditions, *dynamic mode*. HMDA was used as a model compound.

As shown in Figure 4.2, time for performing the oligomerization was t = **10.0 minutes**.

4.3.2.4 As a Function of Temperature.

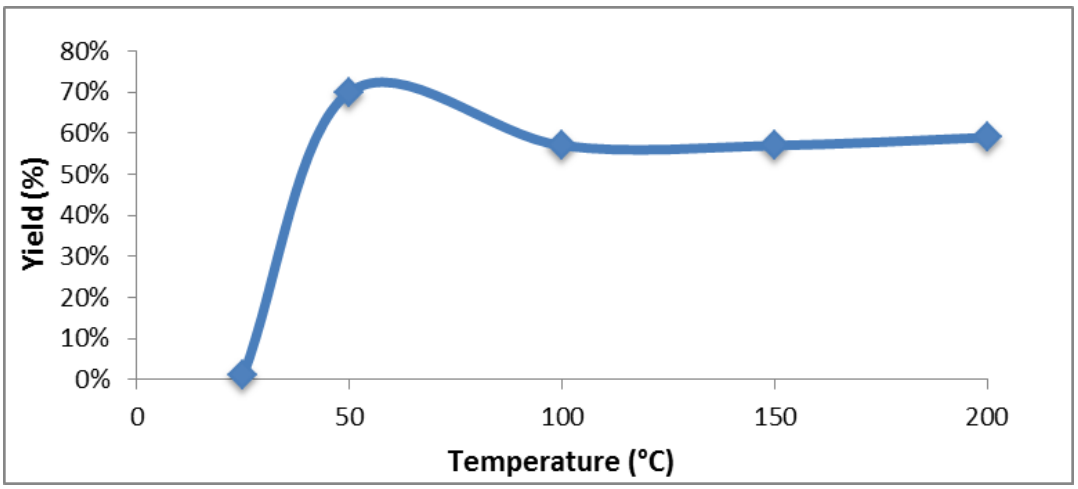

Figure 4.3. Yield as a function of temperature (°C), parameters used: Temp (°C), 3.1 mol% TBD, 220.0W, time 10.0 min and solvent-free conditions, *dynamic mode*. HMDA was used as a model compound.

As shown in Figure 4.3, optimal temperature was **50.0 °C**.

4.3.2.5 As a Function of Microwave Power.

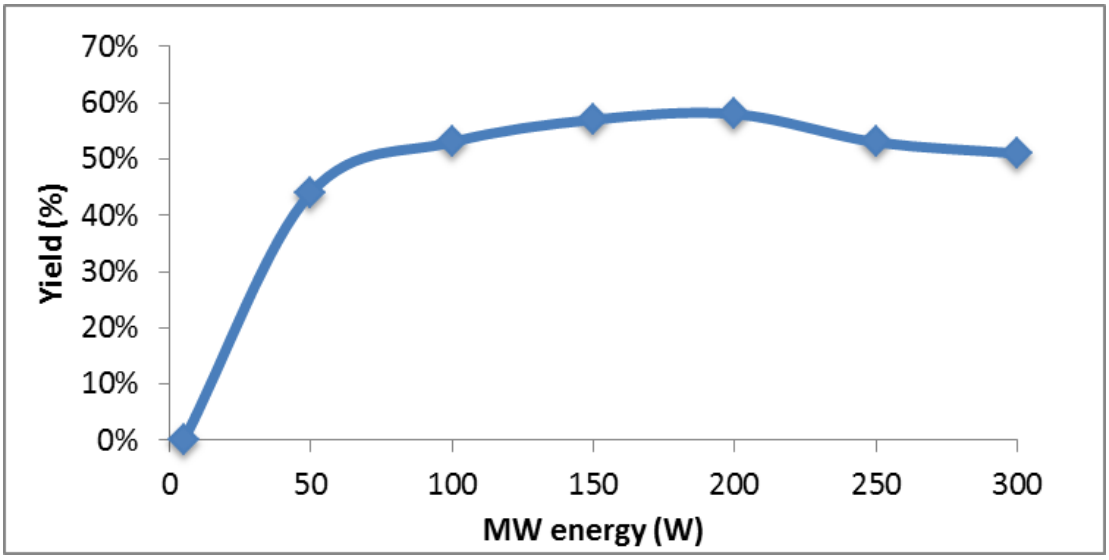

Figure 4.4. Yield as a function of MW energy (W), parameters used: Microwave power 220.0 W, 3.1 mol% TBD, 50.0 °C, time 10.0 *min* and solvent-free conditions, *dynamic mode*. HMDA was used as a model compound.

By default, increasing the microwave power will increase the yields obtained till a plateau is reached. After this point, no more pronounced effect for more power is observed. As shown in Figure 4.4, optimal microwave power was **200.0 W**.

4.4 Oligomerization Recipe

Unless otherwise stated, representative oligomerization recipe: In a 35.0 mL CEM reactor vessel containing a mini-stirring bar, an equimolar ratio of the aliphatic diamines was mixed with propylene carbonate catalyzed by 2.0 mol% TBD. Upon optimization, the oligomerization procedure was carried out at 50.0 °C, 200.0 W, 10.0 minutes using 2.0 mol% of the super base TBD under solvent–free conditions (Scheme 4.1). Upon completion, off-white to pale yellow paste was formed. To purify the oligomers; the paste was soaked and washed in MeOH, crushed using a mortar and pestle, washed with copious amounts of MeOH, then filtered on a preweighed filter paper, dried overnight in a vacuum oven at 80.0 °C. Quantification of the oligomeric material was gravimetric.

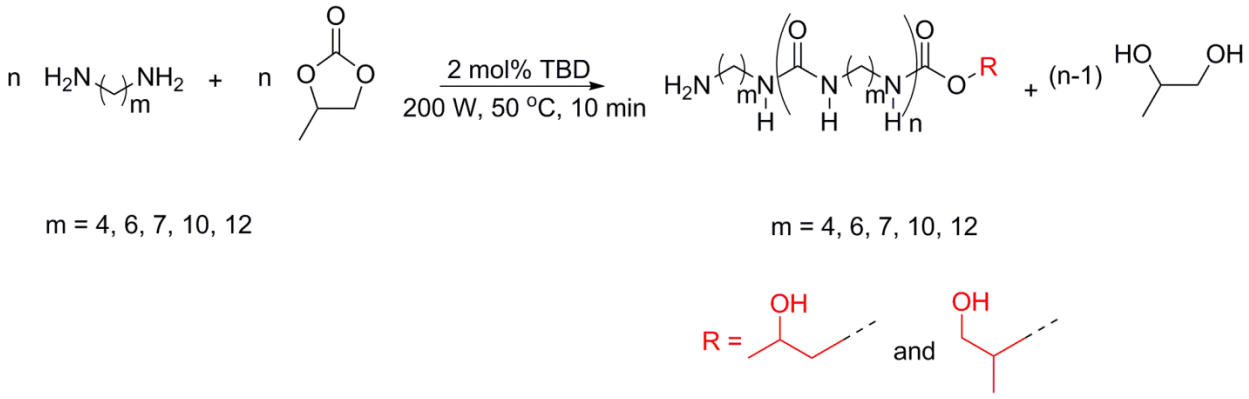

Scheme 4.1. General representation for the organocatalyzed solvent-free microwave-assisted oligomerization process

4.5 Sorption Experiments

Gravimetric CO_2/N_2 sorption measurements of the **[*n*]-OUs** were performed using a Setaram®-Labsys evo TG/DSC-apparatus in a continuous flow mode (0.98 atm at *Garching b. München, Germany*). In a general gravimetric CO_2-sorption experiment, *ca.* 20.0 mg of sample was filled into a platinum crucible (140.0 µL, diameter = 5.0 mm) and kept in the apparatus under high vacuum for 30.0 min at either 60.0 °C or 100.0 °C in order to activate the sample then the sample was allowed to cool down to 35.0 °C. Then, the apparatus was filled for five minutes with CO_2 or N_2 (flow rate = 200.0 mL/min) and kept under a steady flow (16.0 mL/min) for 7.0 h at 35.0 °C under atmospheric pressure. A schematic representation of the temperature profiles at 60.0 °C or 100.0 °C of the measurement is provided in Figure 4.5 and Figure 4.6, respectively (*vide infra*). The sample weight is recorded once every second throughout the experiment. Buoyancy effects on the weight signal were corrected *via* subtraction relative to a blank measurement.

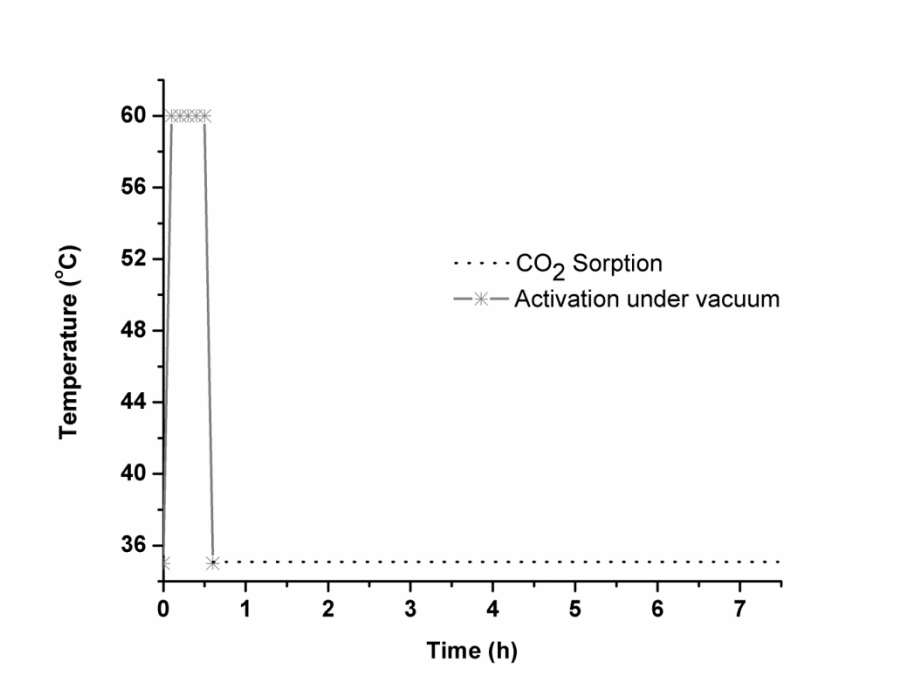

Figure 4.5. Schematic representation of the activation under vacuum (60.0 ºC) and CO_2 sorption profile for all **[*n*]-OUs**.

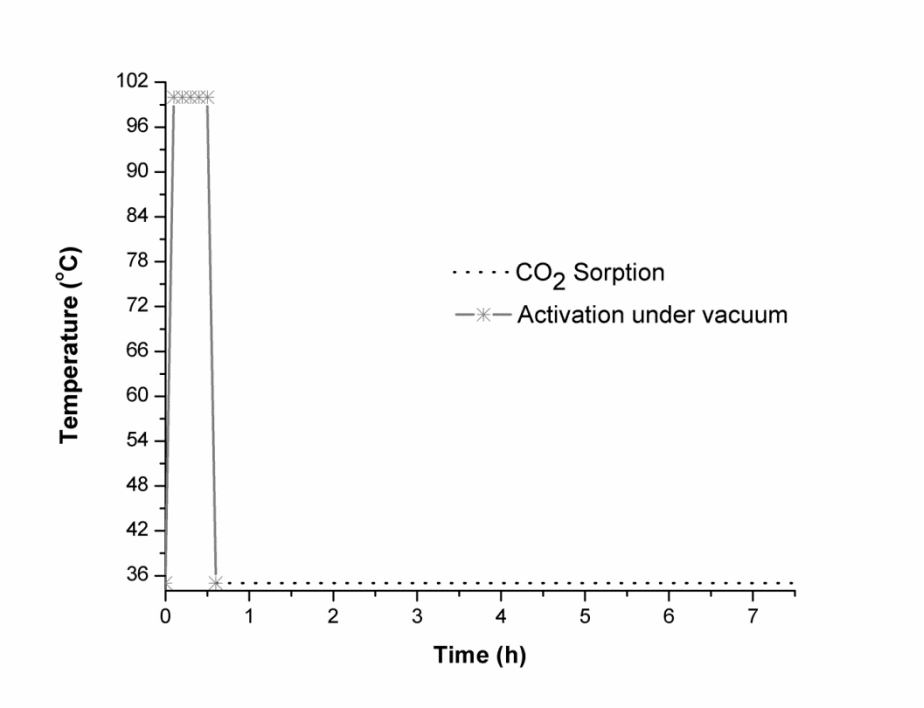

Figure 4.6. Schematic representation of the activation under vacuum (100.0 ºC) and CO_2 sorption profile for all **[*n*]-OUs**.

4.6 Materials

All reactions were performed under inert Argon using standard Schlenk techniques unless otherwise stated. 1,5,7-triazabicyclo[4.4.0]dec-5-ene (TBD) (**a**) 1,8-diazabicyclo[5.4.0]undec-7-ene (DBU) (**b**), 1,5-diazabicyclo[4.3.0]non-5-ene (DBN) (**d**), 1,1,3,3-tetramethylguanidine (TMG) (**e**), 1,4-diazabicyclo[2.2.2]octane (DABCO) (**f**) and 4-dimethylaminopyridine DMAP (**g**), (Figure 3.6) were purchased from Aldrich in the highest purity grade possible and used as received unless otherwise stated. Schreiner's thiourea based catalyst (**c**) was synthesized by us using a novel procedure (Section 4.6.1). *N-(3-bromopropyl)phthalimide* 98%, sodium hydride (60% mineral oil dispersion), imidazole 99.5%, anhydrous Magnesium sulfate ($MgSO_4$), *Lithium bis(trifluoromethylsulphonyl)imide*, *Hydrazine* and Acetonitrile were all purchased from Sigma-Aldrich and Potassium hexafluorophosphate (KPF_6), Sodium tetrafluoroborate ($NaBF_4$) and *lithium bis(trifluoromethylsulphonyl)imide*, $LiTf_2N$ were purchased from ACROS. All chemicals were used as received without further purification; hexane and dichloromethane (DCM) were commercially available solvents (technical grade solvents). Dried tetrahydrofuran (THF) was

obtained from a solvent purification system (SPS). The mono-substituted precursor *2-(3-(1H-imidazol-1-yl)propyl)isoindoline-1,3-dione* (**3**) was prepared following a literature procedure.[122]

4.6.1 Synthesis of 1,3-bis(3,5-bis(trifluoromethyl)phenyl)thiourea (Schreiner's catalyst, c)

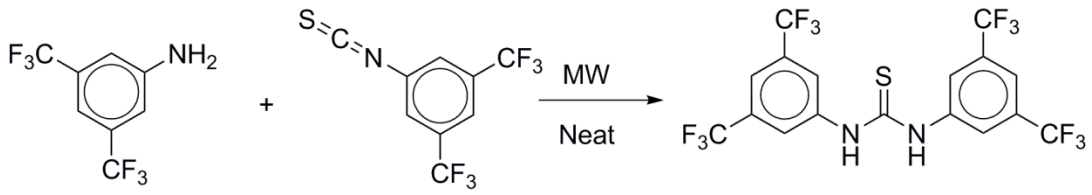

Scheme 4.2. Synthesis of Schreiner's thiourea-based organocatalyst (**c**).

Under air conditions, using a CEM Discover® (*S-Class*) focused microwave synthesizer, and applying a dynamic mode. A 35-mL CEM reactor vessel containing a mini-stirring bar, 3,5-bis(trifluoromethyl)aniline (0.63 mL, 0.004 mol) was added to neat 3,5-bis(trifluoromethyl)-phenyl isothiocyanate (1.0 g, 0.0039 mol), prestirred for two minutes and allowed to heat at 55.0 °C, 300.0 W and 20.0 minutes. Upon cooling, the product was filtered and washed with cold ethyl acetate (3 × 5.0 mL). It is noteworthy that the thiourea synthesis applied in this report is the highest yielding synthesis reported in literature with a new preparative procedure to give almost quantitative yields.

Yield: 98.0%. (Literature values were 60.0-85.0 % that spanned from 4-5 days, under room temperature.[148]

1H NMR: (300.0 MHz, Acetone-d^6) = 9.92 (s, 2H), 8.29 (s, 4H), 7.84 (s, 2H)

EA ($C_{17}H_8F_{12}N_{22}S$) ***Calc.*:** C: 40.81, H: 1.61, N: 5.60, S: 6.41.
***Found*:** C: 40.71, H: 1.59, N: 5.53. , S: 6.22.

4.6.2 Synthesis of Alkylammonium Carbamates

Method A:

Under schlenk conditions, to a 100-mL schlenk flask containing 0.05 mol solution of the diamine in 50 mL dichloromethane (DCM). CO_2 was added by bubbling into the solution for 30.0 minutes under ambient temperature and pressure. CO_2 was left to bubble; a white suspension appeared upon bubbling. Upon completion, the precipitate was filtered through a glass frit (no. 4), and washed with DCM (3 × 15 mL). The precipitate was dried *in vacuuo* at room temperature.

Method B:

In a prestirred 100-mL steel autoclave (prepared in an oven at 150 C)containing 0.05 mol solution of the diamine in 50 mL dichloromethane (DCM). CO_2 was added through bubbling into the solution for 30.0 minutes under ambient temperature. Upon stirring, introduction of 5 bar CO_2 was left to equilibrate for 10 minutes, the reaction was left to stir for 30 min. Upon completion, the precipitate was filtered through a glass frit (no. 4), and washed with DCM (3 × 15 mL). The precipitate was dried *in vacuuo* at room temperature.

Method C: A small modification for method B

In a 50-mL steel autoclave containing 0.025 mol solution of the diamine in 50 mL dichloromethane (DCM). CO_2 was added through bubbling into the solution for 30.0 minutes under ambient temperature. Upon stirring, introduction of 5.0 bar CO_2 was left to equilibrate for 10 minutes, the reaction was left to stir for 30 min. Upon completion, the precipitate was filtered through a glass frit (no. 4), and washed with DCM (3 × 15 mL). The precipitate was dried *in vacuuo* at room temperature. In this method, the highest yields were obtained due to the use of a built-in mechanical stirrer.

(**Note**: All products were only water-soluble; as a result, these compounds decompose. Therefore, solid state analysis was performed to characterize the products, *e.g.* ATR-FTIR and EA).

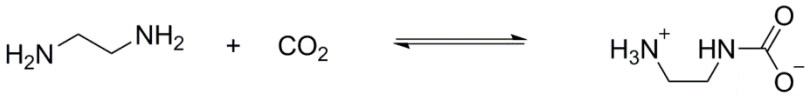

Scheme 4.3. Synthesis of ethylenediammonium carbamate using CO_2 and ethylenediamine

Yield of applied methods (A, B and C): 76-93%.

EA ($C_3H_8N_2O_2 \bullet H_2O$) ***Calc.*:** C: 29.51, H: 8.25, N, 22.94.
***Found*:** C: 29.43, H: 8.03, N: 22.76.

ATR-IR (cm^{-1}): 3287, 2923, 2877, 2703, 2650, 2559, 2164, 2145, 1561, 1466, 1377, 1298, 1153, 971, 815, 698.

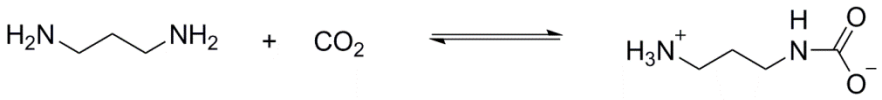

Scheme 4.4. Synthesis of 1,3-propylenediammonium carbamate using CO_2 and 1,3-propylenediamine

Yield of methods (A, B and C): 83-92%.

EA ($C_4H_{10}N_2O_2 \bullet H_2O$) ***Calc.*:** C: 35.29, H: 8.88, N, 20.58.
***Found*:** C: 35.08, H: 8.95, N: 20.18.

ATR-IR (cm^{-1}): 3329, 2958, 2934, 2853, 2783, 2705, 2653, 2553, 2163, 2145, 1638, 1560, 1460, 1420, 1343, 1273, 1167, 1130, 1060, 1034, 1007, 980, 936, 832, 816, 777, 671.

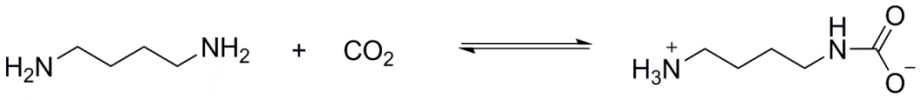

Scheme 4.5. Synthesis of 1,4-butylenediammonium carbamate using CO_2 and 1,4-butylenediamine

Yield of methods (A, B and C): 73-84%.

EA ($C_5H_{12}N_2O_2 \bullet H_2O$) ***Calc.***: C: 39.99, H: 9.40, N, 18.65.

Found: C: 39.67, H: 9.73, N: 18.29.

ATR-IR (cm^{-1}): 3316, 2923, 2856, 2759, 2660, 2560, 2338, 2324, 2163, 1554, 1469, 1394, 1303, 1154, 1049, 1001, 958, 936, 912, 884, 819, 738, 685.

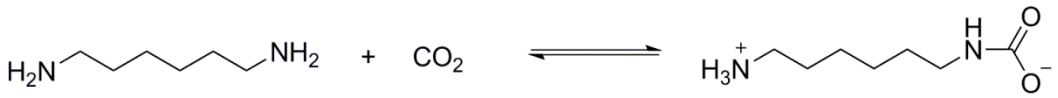

Scheme 4.6. Synthesis of 1,6-hexamethylenediammonium carbamate using CO_2 and 1,6-hexamethylenediamine (**HMDA**)

Yield of methods (A, B and C): 81-95%.

EA ($C_7H_{16}N_2O_2$) ***Calc.***: C: 52.48, H: 10.07, N, 17.49.

Found: C: 52.43, H: 9.95, N: 17.29.

ATR-IR (cm^{-1}): 3315, 2926, 2854, 2667, 2576, 2336, 2325, 2164, 2123, 1630, 1559, 1475, 1384, 1309, 1266, 1075, 1007, 959, 816, 730, 699.

4.6.3 Synthesis of Arylammonium Carbamates

Arylammonium carbamates were not obtained under the three methods that were discussed in section 3.1. Therefore, more focus was going towards the synthesis of aliphatic correspondents.

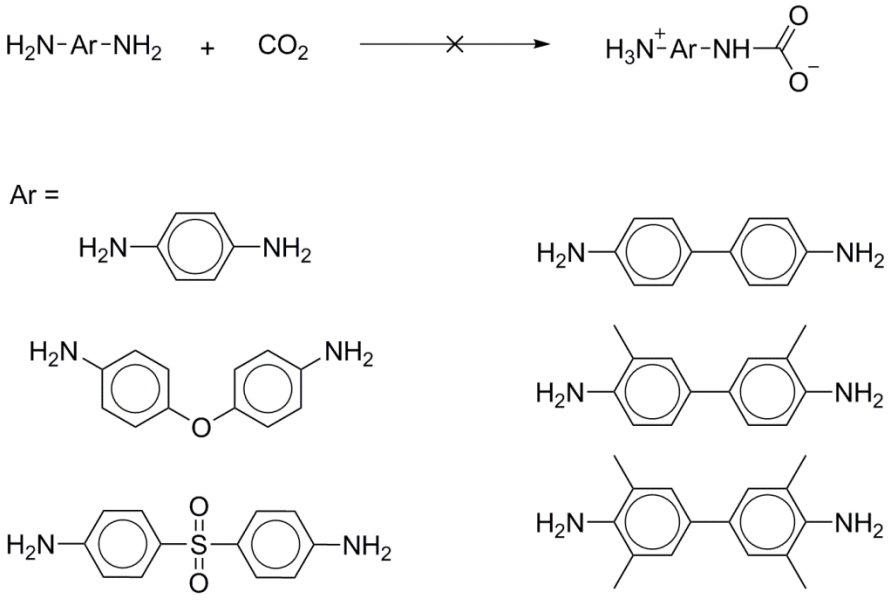

Scheme 4.7. Failed synthesis of aromatic carbamates.

4.6.4 Synthesis of Task specific ionic liquids (TSILs)

4.6.4.1 2-(3-(1H-imidazol-1-yl)propyl)isoindoline-1,3-dione (**3**)

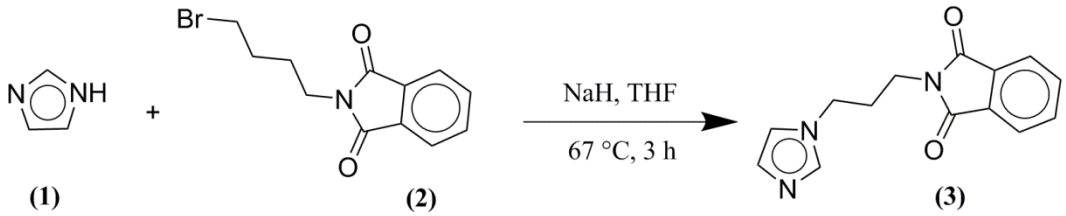

Scheme 4.8. Ternerization reaction of the mono-substituted TSIL-precursor (**3**)

Mono-substituted precursor IL was prepared in one-step by a ternerization reaction according to a previously reported method prepared by Harjani *et al.*[122] to a well stirred suspension of sodium hydride (4.200 g, 7.000 g of the 60.0% mineral oil dispersion, 175.0 mmol) in THF (500 mL), under Argon atmosphere, maintained at 0 °C, the solution of imidazole (**1**) (13.09 g, 192.5 mmol) in THF (200.0 mL) was added, over a period of 30.0 min. After an additional 30.0 min of stirring at 0 °C, the solution of *N-(3-bromopropyl)phthalimide* (**2**) (46.90 g, 175 mmol) in THF (200 mL) was added to it gradually at 0 °C. The reaction mixture was stirred at room temperature

for 1 h and finally refluxed at 67.0 °C for 3 h. The work up involved filtration and washing the residual NaBr with THF and evaporation of the combined organics to yield a syrupy mass, which was dissolved in DCM (250 mL), washed with water, dried over anhydrous $MgSO_4$ and treated with hexanes (1000 mL) under cold conditions to precipitate a white solid. (Harjani *et al.* Yield: 80.0 %; our Yield: 60.0 %). A slight modification in the last step yielded a crystalline product.

1H NMR: (300.0 MHz, $CDCl_3$-d^3) = 7.76-7.85 (m, 1H), 7.70 (s, 1H), 7.17 (s, 1H), 6.92 (s,1H), 4.09 (t, 1H), 3.68 (t, 1H), 2.17 (p, 1H).

13C NMR: (75.0 MHz, $CDCl_3$-d^3) = 168.4, 137.2, 134.3, 132.0, 129.3, 123.4, 118.9, 44.6, 44.6, 35.2, 30.2.

EA ($C_{14}H_{13}N_3O_2$) ***Calc.*:** C: 65.87, H: 5.13, N, 16.46.
***Found*:** C: 65.66, H: 5.10, N: 16.25.

4.6.4.2 1,3-bis(3-(1,3-dioxoisoindolin-2-yl)propyl)-1H-imidazol-3-ium bromide (**4**)

The TSIL-precursor *1,3-bis(3-(1,3-dioxoisoindolin-2-yl)propyl)-1H-imidazol-3-ium bromide* (**4**) preparation was not reported before. It was synthesized *via* two pathways, *viz.*, a) Thermal approach. b) microwave-assisted approach.

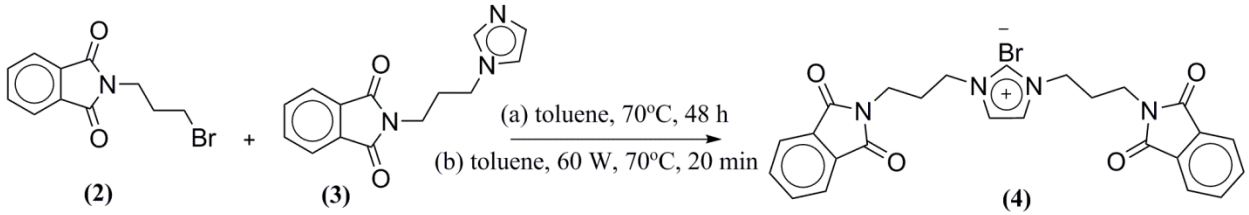

(a) Thermal approach
(b) Microwave approach

Scheme 4.9. Quaternization reaction of the di-substituted TSIL-precursor (**4**)

4.6.4.2.1 *Thermal approach:*

In a 250 mL Schlenk tube equipped with a magnetic stirring bar, N-(3-bromopropyl)phthalimide (**2**) (4.183 g, 0.015 mol) was added to a stirred solution of the of 2-(3-(1H-imidazol-1-yl)propyl)isoindoline-1,3-dione (**3**) (0.40g, 0.0015mol) in 50.0 mL toluene. The solution was set to reflux in an oil bath at 70.0 °C with continuous stirring; upon refluxing, a white turbid solution was observed and left to reflux for 48 hours. Upon finishing, the reaction was cooled to room temperature; the white precipitate was filtered, washed with copious amounts of toluene, and dried in a vacuum oven at 60.0 °C for 4 hours.

4.6.4.2.2 *Microwave-assisted approach*

In a 35 mL microwave vessel containing a mini-stirring bar, *N-(3-bromopropyl) phthalimide* (**2**) (7.24 g, 0.027 mol) was added to a pre-stirred solution of *2-(3-(1H-imidazol-1-yl)propyl)isoindoline-1,3-dione* (**3**) (0.70g, 0.0027 mol) which was dissolved in toluene (20 mL), mixed at room temperature till no further solids were observed, and then introduced to the microwave reactor. The solution was heated to 70.0 °C for 20.0 minutes, and 60.0 W. Upon finishing the reaction, a white precipitate formed. The product was filtered, washed with toluene (5×20 mL), and subsequently dried in a vacuum oven at 60.0 °C for 4 hours to obtain an amorphous white powder.

Yield: 60.0%

1H NMR: (300.0 MHz, $CDCl_3$-*d*) = 7.85-7.76 (m, 1H), 7.70 (s, 1H), 7.17 (s, 1H), 6.92 (s,1H), 4.09 (t, 1H), 3.68 (t, 1H), 2.17 (p, 1H).

13C NMR: (75.0 MHz, $CDCl_3$-*d*) = 168.4, 137.2, 134.3, 132.0, 129.3, 123.4, 118.9, 44.6, 44.6, 35.2, 30.2.

EA ($C_{25}H_{23}BrN_4O_4$) ***Calc.*:** C: 57.37, H: 4.43, N, 10.70.
***Found*:** C: 57.63, H: 4.43, N: 10.33.

4.6.4.3 Metathesis reaction of the TSIL precursors

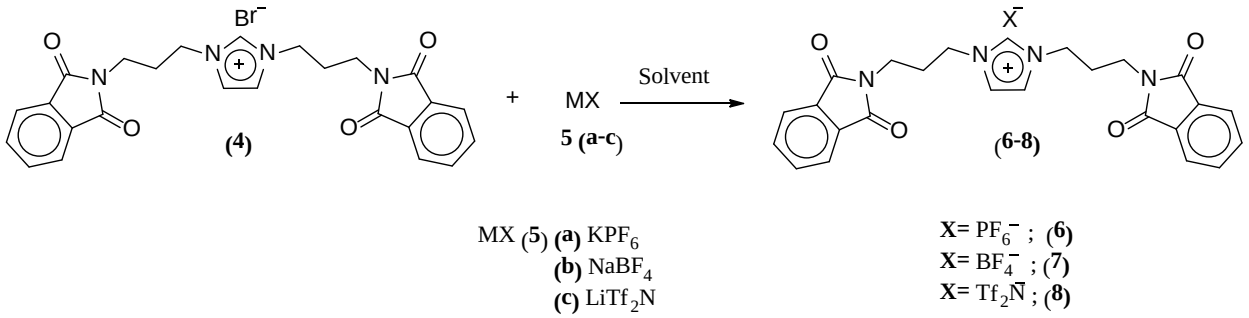

Scheme 4.10. Metathesis of IL precursor (**4**) using different Metal salts (**MX**)

4.6.4.3.1 1,3-bis(3-(1,3-dioxoisoindolin-2-yl)propyl)-1H-imidazol-3-ium hexafluorophosphate (**6**)

In a 100 mL round bottom flask equipped with a magnetic stirring bar, (**4**) (0.5 g, 0.000955 mol) was added to (50 mL) deionized water. After dissolution, Potassium hexafluorophosphate, KPF_6 (**5a**) (0.1760 g, 0.000955 mol) was added. The solution was stirred for 40.0 hours at room temperature. The reaction workup involved filtration and then evaporation of water under reduced pressure to yield a white precipitated powder.

Not successful.

4.6.4.3.2 1,3-bis(3-(1,3-dioxoisoindolin-2-yl)propyl)-1H-imidazol-3-ium tetrafluoroborate (**7**)

In a 100 mL round bottom flask equipped with a magnetic stirring bar, a solution of (**4**) (0.5 g, 0.000955 mol) in 50 mL Acetonitrile (CH_3CN) at room temperature was added. After dissolution, Sodium tetrafluoroborate, $NaBF_4$ (**5b**) (0.10489 g, 0.000955 mol) was added. Upon addition, a white precipitate formed. The solution was stirred for 40.0 hours at room temperature. The reaction workup involved filtration and then evaporation of CH_3CN under reduced pressure to yield a white precipitated powder.

Not successful.

4.6.4.3.3 1,3-bis(3-(1,3-dioxoisoindolin-2-yl)propyl)-1H-imidazol-3-ium bis((trifluoro-methyl)-sulfonyl)imide (**8**)

In a 250 mL round bottom flask equipped with a magnetic stirring bar, a solution (**4**) (0.5 g, 0.000955 mol) in a 150 mL mixture of 1:1 (by volume), deionized H_2O/MeOH was dissolved. Upon dissolution, *lithium bis(trifluoromethylsulphonyl)imide*, $LiTf_2N$ (**5c**) (0.274 g, 0.000955 mol) was added. The solution was stirred for 40.0 hours at room temperature. The reaction workup involved evaporation of methanol and then the deionized water under reduced pressure to yield a white precipitated powder, which was re-dissolved in methanol and then filtered. Afterwards, methanol was evaporated under reduced pressure to give a white precipitate.

Not successful.

4.6.4.4 Hydrolysis of TSIL-precursors

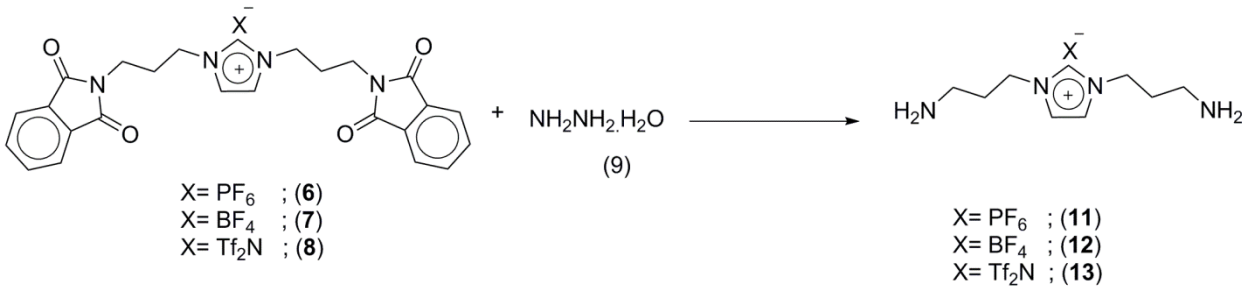

Scheme 4.11. Failed hydrolysis of the TSIL-precursors (**6**-**8**) to yield TSIL-PF_6 (**11**), TSIL-BF_4 (**12**), and TSIL-Tf_2N (**13**).

4.6.4.4.1 1,3-bis(3-aminopropyl)-1H-imidazol-3-ium Bromide, IL-Br (**10**)

In a 250 mL Schlenk equipped with a stirring bar, hydrazine monohydrate (**9**) (1.30 mL, 0.026 mol) was added to a 100 mL solution of (**4**) (0.5g, 0.000955 mol) in absolute ethanol. The well stirred solution was refluxed in an oil bath at 78.0 °C for 48h. Upon completion, the reaction workup involved double filtration using a filter paper followed by a microfilter to ensure non-turbid mother liquor. Afterwards, evaporation of the filtrate under reduced pressure to get a pale yellow syrupy product. The IL-Br (**10**) was placed in a 50 mL round bottom flask and heated in

an oil bath for 7 days under vacuum to eliminate any contamination *via* water or CO_2 during the manipulation.

Yield: 96.0%, Purity (84% according to 1H NMR).

4.6.4.4.2 1,3-bis(3-aminopropyl)-1H-imidazol-3-ium hexafluorophosphate, (**TSIL-PF_6)** (**11**)

In a 250 mL Schlenk equipped with a stirring bar, hydrazine monohydrate (**9**) (1.19 mL, 0.02459 mol) was added to a 100 mL solution of (**6**) (0.53 g, 0.000911 mol) in CH_3CN. The well stirred solution was refluxed in an oil bath at 78.0 °C for 48h. The reaction workup involved double filtration using a filter paper followed by a microfilter to ensure non-turbid mother liquor. Afterwards, evaporation of the filtrate under reduced pressure to get pale yellow syrupy product. (**11**) was placed in a 50 mL round bottom flask and heated in an oil bath for 7 days under vacuum to eliminate any contamination *via* water or CO_2 during the manipulation.

Not successful.

4.6.4.4.3 1,3-bis(3-aminopropyl)-1H-imidazol-3-ium tetrafluoroborate, (**IL-BF_4)** (**12**)

In a 250 mL Schlenk equipped with a stirring bar, hydrazine monohydrate **(9)** (1.28 mL, 0.02647 mol) was added to a 100 mL solution of (**7**) (0.50 g, 0.00094 mol) in CH_3CN. The solution was refluxed in an oil bath at 82.0 °C for 48h. The reaction workup involved double filtration using a filter paper followed by a microfilter to ensure a clear mother liquor. Afterwards, evaporation of the filtrate under reduced pressure was performed to yield a pale yellow precipitate. The IL-BF_4 (**12**) was placed in a 50 mL round bottom flask and heated in an oil bath for 7 days under vacuum to eliminate any contamination *via* water or CO_2 during the manipulation.

Not successful.

4.6.4.4.4 1,3-bis(3-aminopropyl)-1H-imidazol-3-ium bis((trifluoromethyl)sulfonyl)amide, (**TSIL-Tf_2N**) (**13**)

In a 250 mL Schlenk equipped with a stirring bar, hydrazine monohydrate (**9**) (2.0 mL, 0.041 mol) was added to a 100 mL of crude product (**8**) in CH_3CN. The well stirred solution was refluxed in an oil bath at 82.0 °C for 48h. No further workup was feasible.

Not successful.

4.6.5 Synthesis of Aromatic Oligourea

The aromatic diamines applied in the study did not show any activity towards applied conditions in the dynamic mode. The recipe is the same applied for the aliphatic correspondents.

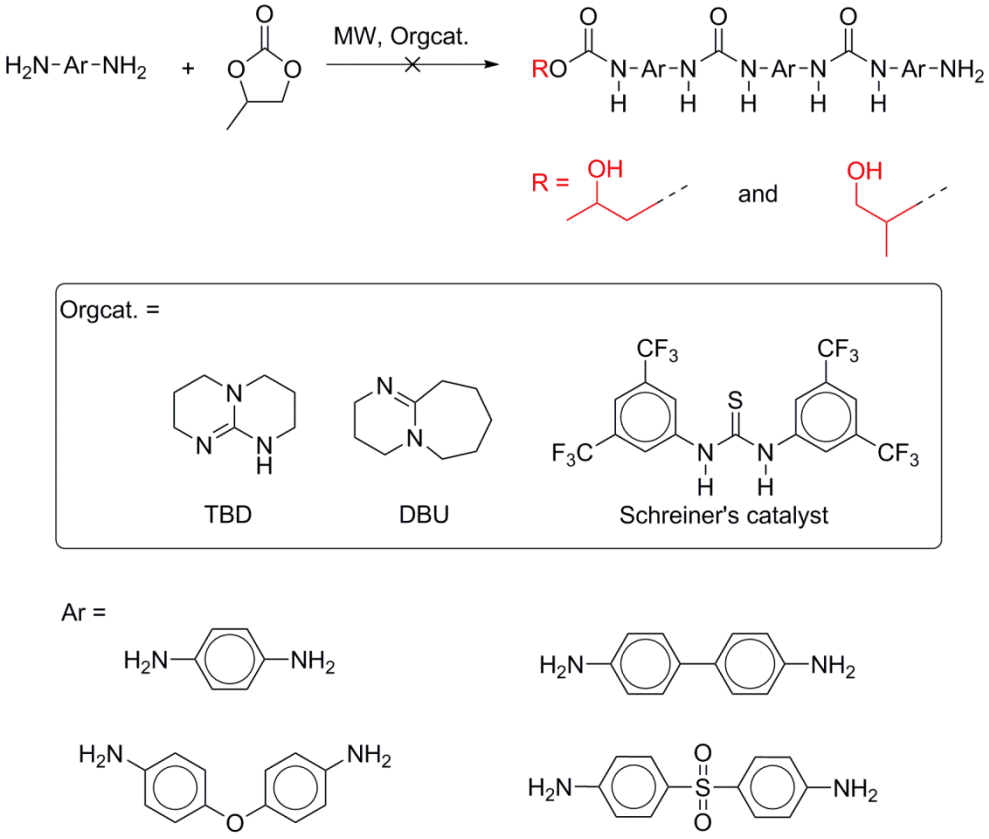

Scheme 4.12. Failed oligoemerization experiments of aromatic diamines with PC.

The oligomerization recipe: In a 35.0 mL CEM reactor vessel containing a mini-stirring bar, an equimolar ratio of the aliphatic diamines was mixed with propylene carbonate catalyzed by 2.0 mol% of the organocatalyst (Orgcat.), *viz.*, TBD, DBU, and Schreiner's catalyst (*vide infra*). Upon optimization, the oligomerization procedure was carried out at 50.0 °C, 200.0 W, 10.0 minutes using 2.0 mol% of the superbase TBD under solvent–free conditions. Upon completion, no precipitate was formed. 1H NMR showed the presence of the peaks for the starting materials.

Not Successful.

4.6.6 Synthesis of [*n*]-Oligourea analysis, ([*n*]-OUs)

*Synthesis of **[n]-OUs** was carried out under air conditions.* elemental analysis values were corrected relative to the presence of tracews of methoanol and H_2O as seen by the NMR and TGA experiments (Table 3.4).

4.6.6.1 [*4*]-Oligourea, ([*4*]-OU)

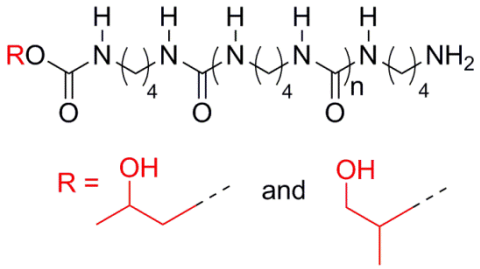

Figure 4.7. Structural representation of the **[*4*]-OU**

Yield: 82%. Degree of Polymerization (**DP = 9**).

1H NMR: (300.0 MHz, TFA-*d*) = 7.15 (1 H, s), 6.83 (1 H, s), 5.06 (1 H, s), 4.27 (1 H, t, *J* =10.8), 3.98 - 4.21 (1 H, m), 3.58 - 3.95 (1 H, m), 3.59 (1 H, s), 3.35 (2H, s), 3.11 (1 H, s), 1.69 (2 H, s), 1.46 (1 H, d, *J* = 6.3), 1.39 (1 H, d, *J* = 6.3), 1.29 (1 H, dd, *J* = 10.1, 6.6).

13C NMR: (75.0 MHz, TFA-*d*) = 160.9, 72.0, 69.7, 67.3, 42.6, 42.5, 42.1, 27.8, 27.6, 27.1, 18.1, 16.2.

EA ($C_{59}H_{124}N_{22}O_{15}$) ***Calc.*:** C: 51.29, H: 9.05, N: 22.30.
***Found*:** C: 51.51, H: 8.95, N: 22.09.

ATR-IR (cm^{-1}): 3318, 2940, 2862, 1614, 1569, 1516, 1476, 1456, 1378, 1274, 1224, 1145, 1078, 1055, 776, 750, 637, 620.

4.6.6.2 [*6*]-Oligourea, ([*6*]-OU)

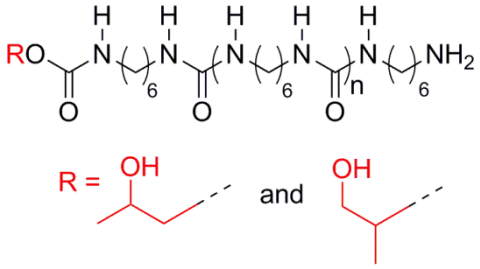

Figure 4.8. Structural representation of the **[*6*]-OU**

Yield: 79.0%. (**DP = 12**).

1H NMR: (300.0 MHz, TFA-*d*) = 6.70 (1 H, s), 4.20 - 4.32 (1 H, m), 4.08-4.17 (1 H, m), 3.75 - 3.94 (1 H, m), 3.58 (1 H, s), 3.30 (2 H, t, *J* 7.1), 3.22 (1 H, d, *J* 7.0), 1.63 (2 H, s), 1.25 - 1.46 (3 H, m).

13C NMR: (75.0 MHz, TFA-*d*) = 161.4, 72.6, 70.1, 67.1, 44.2, 43.4, 31.2, 30.7, 29.2, 28.2, 27.4, 18.6, 16.8.

EA ($C_{101}H_{204}N_{28}O_{16}$) ***Calc.*:** C: 58.69, H: 9.95, N: 18.97.
Found: C: 58.14, H: 10.04, N: 17.77.

ATR-IR (cm^{-1}): 3307, 2931, 2856, 1614, 1561, 1477, 1460, 1375, 1337, 1250, 1213, 1146, 1077, 772, 735, 615, 607.

4.6.6.3 [*7*]-Oligourea, ([*7*]-OU)

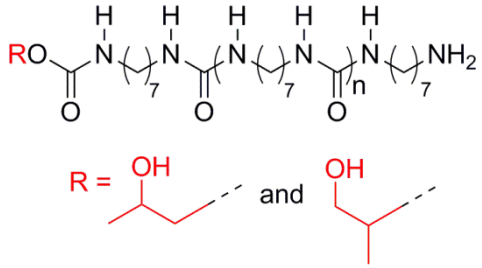

Figure 4.9. Structural representation of the **[*7*]-OU**

Yield: 76%. (**DP = 10**).

1H NMR: (300.0 MHz, TFA-*d*) = 6.67 (1 H, s), 5.00 - 5.13 (1 H, m), 4.84 (1 H, dd, *J* = 13.8, 7.5), 4.58 (1 H, d, *J* = 8.6), 4.36 (1 H, s), 4.20 - 4.30 (1 H, m), 4.12 (1 H, dd, *J* = 11.8, 7.5), 4.00 (1 H, s), 3.87 (1 H, d, *J* = 2.7), 3.74 - 3.85 (1 H, m), 3.57 (1 H, s), 3.29 (2 H, t, *J* = 7.1), 3.20 (1 H, d, *J* = 6.9), 2.42 (1 H, t, *J* = 7.0), 1.72 - 1.81 (1 H, m), 1.61 (2 H, s), 1.34 (3 H, s).

13C NMR: (75.0 MHz, TFA-*d*) = 161.3, 72.8, 70.4, 67.8, 44.3, 44.2, 44.08, 43.9, 30.7, 29.4, 28.5, 28.0.

EA ($C_{100}H_{206}N_{24}O_{16}$) ***Calc.*:** C: 60.03, H: 10.38, N: 16.80.
***Found*:** C: 60.56, H: 10.42, N: 16.33.

ATR-IR (cm^{-1}): 3325, 2929, 2853, 1611, 1570, 1476, 1460, 1374, 1312, 1243, 1208, 1146, 1128, 1078, 768, 728, 639, 613.

4.6.6.4 [*10*]-Oligourea, ([*10*]-OU)

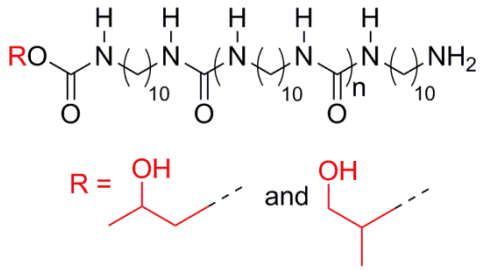

Figure 4.10. Structural representation of the **[*10*]-OU**

Yield: 78%. (**DP = 7**).

1H NMR: (300.0 MHz, TFA-*d*) = 6.61 (1 H, s), 5.02 - 5.10 (1 H, m), 4.84 (1 H, dd, *J* = 14.6, 6.9), 4.56 (1 H, t, *J* = 7.5), 4.38 (1 H, d, *J* = 30.8), 4.25 (1 H, dd, *J* = 11.5, 2.0), 4.12 (1 H, dd, *J* = 11.6, 7.4), 3.84 (1 H, dd, *J* = 16.7, 9.2), 3.46 - 3.61 (1 H, m), 3.28 (2 H, t, *J* = 7.1), 3.05 (1 H, s), 2.17 (1 H, s), 1.17 - 1.84 (9 H, m).

13C NMR: (75.0 MHz, TFA-*d*) = 161.2, 76.3, 72.9, 70.5, 46.7, 31.4, 31.3, 31.2, 31.1, 30.9, 30.8, 29.5, 28.6, 28.1.

EA ($C_{103}H_{210}N_{18}O_{12}$) ***Calc.*:** C: 65.35, H: 11.18, N: 13.32.
***Found*:** C: 65.64, H: 11.38, N: 13.21.

ATR-IR (cm^{-1}): 3321, 2932, 2855, 1691, 1615, 1570, 1478, 1461, 1441, 1377, 1337, 1251, 1213, 1143, 1113, 1075, 1051, 875, 844, 819, 772, 735, 618.

4.6.6.5 [*12*]-Oligourea, ([*12*]-OU)

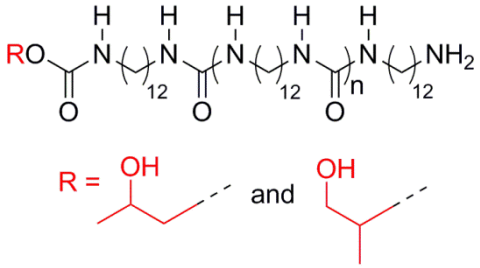

Figure 4.11. Structural representation of the **[*12*]-OU**

Yield: 86%. (**DP = 6**).

1H NMR: (300.0 MHz, TFA-*d*) = 6.63 (1 H, s), 5.10 - 5.01 (1 H, m), 4.21 - 4.33 (1 H, m), 4.12 (1 H, dd, *J* = 11.7, 7.4), 3.73 - 3.93 (1 H, m), 3.28 (1 H, t, *J* = 7.2), 3.15 - 3.22 (1 H, m), 1.56 - 1.65 (1 H, m), 1.29 (7 H, s).

13C NMR: (75.0 MHz, TFA-*d*) = 161.1, 76.8, 72.8, 70.5, 44.4, 31.5, 31.4, 31.1, 30.7, 29.4, 28.5, 28.0.

EA ($C_{109}H_{222}N_{16}O_{11}$) ***Calc.*:** C: 67.73, H: 11.58, N: 11.59.
***Found*:** C: 67.59, H: 11.64, N: 11.54.

ATR-IR (cm^{-1}): 3333, 2920, 2849, 1690, 1612, 1571, 1477, 1465, 1374, 1310, 1263, 1233, 1149, 1105, 1075, 777, 723, 610.

4.6.7 Synthesis of Aromatic/Aliphatic Teroligoureas

Ter-oligomerization trials using aromatic diamines, Hexamethylenediamine (HMDA), and propylene carbonate (PC) were not successful. On the other hand, co-oligomers were obtained, *viz.*, **[*6*]-OU**. These oligomers differed from those synthesized in section 4.6.6.2, the discrepancy is represented by both the degree of polymerization (DP) as well as end groups. DP values are less, and urethane end groups are end-capping both terminals. The rational explanation for such

trend was due to the 1:2 ratio of aliphatic diamine to PC which would give the same DP no matter aromatic diamine was used.

Not successful as teroligomer.

Co-oligomer formation with double-capped urethane end groups, (**[*6*]-OU′).**

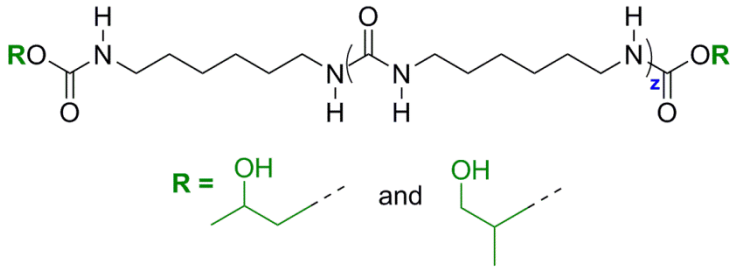

Figure 4.12. Structural representation of the double-end capped urethanated **[*6*]-OU** as a result of failed *ter*-oligomerization.

Yield: 66%. (**DP = 4**).

1H NMR: (300.0 MHz, TFA-*d*) = 5.13 – 5.20 (m, 1H), 5.03 – 5.11 (m, 1H), 4.19 – 4.33 (m, 6H), 4.06 – 4.17 (m, 3H), 3.72 – 3.96 (m, 5H), 3.29 (t, *J*=7.2, 67H), 3.14 – 3.24 (m, 14H), 1.61 (s, 53H), 1.53 – 1.56 (m, 39H), 1.37 (t, *J*=4.0, 72H), 1.29 (t, *J*=6.9, 20H).

ATR-IR (cm^{-1}): 3318, 2932, 2855, 1685, 1617, 1572, 1541, 1478, 1461, 1440, 1377, 1338, 1251, 1213, 1142, 1074, 1050, 1015.

Chapter 5

SUMMARY

5 SUMMARY

In the current work, alternatives for the amine-based scrubbing agent monoethanolamine (**MEA**) were synthesized and used for CO_2 capturing purposes. Problems associated with MEA involve, degradation, oxidation, and crosslinking. MEA absorption in aqueous solutions is highly energetic to regenerate due to the high heat capacity of water. Therefore, search for other alternatives was the main goal of this PhD thesis. Several candidates have been synthesized as a function of nitrogen content. Capturing agents ranged forming Amino-tethered, multi-armed ammonium bromides salts (**$(NH_2)_3$-N^+-R-N^+-$(NH_2)_3$,**), imidazolium-based TSIL and their new route for synthesis and the manipulation of oligomerization to yield oligo(ionic liquid)s (**OILs**). In addition, the most successful generation of green sorbents, *viz.* [*n*]-Oligoureas (**[*n*]-OUs**). Unfortunately, the ammonium-based amine tethered synthesis were not successfully prepared due to having decomposition during prepration or after modification

A new eco-friendly, isocyanate-free, energy-saving method for the production of **[*6*]-OUs** utilizing a green carbonylating agent, *viz.* propylene carbonate (PC), is reported. It comprises an organocatalyzed, microwave-assisted, solvent-free synthesis. Two modes of microwave-assisted synthesis, *viz.* dynamic and fixed energy modes were applied. Upon optimization, the dynamic mode gave 79.0 % yields of **[*6*]-OU**. On the other hand, almost quantitative yields were obtained using the fixed mode, within 20.0 min, 10.0 W, and same catalyst loading. Combination of both organocatalysis and microwave energy input appears to be a key issue for the efficiency of the reaction, with the fixed energy mode being best suited for **[*6*]-OU**. It should be noted that all data reported are reproducible (due to the homogeneous microwave technology used by CEM discover S-Class of microwave reactors). To the best of our knowledge, this is the best synthetic approach for the preparation of the title oligomers with an eco-friendly approach. It paves the way to use more of the biorenewable and sustainable chemicals as a feedstock for the production of polyureas. The oligomer produced was analyzed by EA, ATR-FTIR, XRD, 1H and 13CNMR. Furthermore, thermal properties of the resulting **[*6*]-OU** were analyzed using TGA and DSC.

Moreover, further candidates of the same family were also synthesized for the purpose of CO_2 capturing. The degree of polymerization (DP) of the oligomers was determined by end-group

analysis *via* 1H NMR spectroscopy. Thermal stabilities and % crystallinity were further investigated through TGA, DSC, and XRD. Decomposition temperatures at 50% weight loss (T_{d50}) were *ca.* 350 ºC for all prepared oligomers. The CO_2 capturing capacities were determined at 35.0 ºC by a gravimetric method. Accordingly, **[*10*]-OU** had the highest CO_2 sorption capacity at two different activation temperatures (60.0 or 100.0 ºC) with a maximum equilibrium sorption of 18.90 or 22.70 $mg_{CO2}/g_{sorbent}$ (1.0 bar, 35.0 ºC), respectively. Chemisorption was the principal mechanism for CO_2 capture in **[*n*]-OUs**. This was supported by 13C CP-MAS NMR experiments of **[*10*]-OU** with $^{13}CO_2$, which indicated the formation of bicarbonates (**1:1 mechanism**) as a result of the reaction with amine-terminated oligomers in the presence of humidity. Furthermore, the sorption capacity of **[*10*]-OU** did not change significantly as a function of pressure as studied by high pressure thermogravimetric (HP-TGA) analysis. Cyclic CO_2 sorption/desorption measurements were carried out to test the recyclability of **[*10*]-OU**. Activating the sample at 60.0 ºC, three stable CO_2 sorption cycles were achieved after the first cycle. The difference between the first and the latter cycles is presumably explained by the absence of water, which affords carbamates through a **1:2 mechanism**. Moreover, an induced urethane cleavage was reported during the activation of **[*10*]-OU** at 100.0 ºC. This cleavage increases the sorption capacity of the sorbent in order to capture CO_2. ATR-FTIR, TGA-MS, and solid state 13C CP-MAS NMR were used to confirm the aforementioned urethane cleavage.

Chapter 6

ZUSAMMENFASSUNG

6 ZUSAMMENFASSUNG

In der vorliegenden Arbeit wurde eine gründliche Studie bezüglich der Alternativen für den aminbasierten Gaswäscher Monoethanolamin (MEA) durchgeführt. Bei der Anwendung des Monoethanolamins treten in der Regel mehrere unerwünschte Degradationsprozesse auf. Diese sind z. B. partielle Zersetzung, Oxidation und Vernetzung des Reagens. Als eine alternative Lösung zur Verbesserung der Stabilität des Gaswaschmittels können stabile ammoniumreiche oligomere Substanzen maßgeschneiderter Komposition betrachtet werden. Der Fokus dieser Arbeit liegt dabei auf der Syntheseentwicklung von aminterminierten Ammoniumbromide ($(NH_2)_3$-N^+-R-N^+-$(NH_2)_3$), imidazoliumbasierten aufgabenspezifischen ionischen Flüssigkeiten (**TSILs**), oligomeren ionischen Flüßigkeiten (**OILs**), sowie [*n*]-Oligoharnstoffen (**[*n*]-OUs**). Im Zuge der Arbeit stellte sich heraus, dass die aminterminierten Ammoniumbromide synthetisch nicht zugänglich sind. Die im Rahmen dieser Forschung synthetisierten Substanzen wurden auf ihr CO_2-Absorptionsverhalten untersucht.

Eine neue umweltfreundliche isocyanatfreie energieeffiziente Methode für die Produktion von **[*6*]-OUs** bei der Anwendung von einem „grünen“ Carbonylierungsreagens (Propylencarbonat (PC)) wurde entwickelt. Die Methode basiert sich auf einer organokatalysierten mikrowellenunterstützten lösungsmittelfreien Synthese. Die Prozessführung wurde sowohl in einem dynamischen als auch in einem konstanten Energiemodus studiert. Die Optimierung der Reaktionsführung lieferte eine maximale Ausbeute der **[*6*]-OU** in Höhe von 79.0 % für einen dynamischen Modus und einen quantitativen Umsatz für die konstante Betriebsart (20.0 min, 10.0 W). Eine Kombination aus passenden organischen Katalysatorspezies mit der richtigen Auswahl der Zufuhrart der Mikrowellenenergie war ein Schlüsselelement für effiziente **[*6*]-OU** Produktion.

Zusätzlich wurden die anderen **[*n*]-OUs** mit den Linkern unterschiedlicher Länge synthetisiert und ihr CO_2-Absorptionsverhalten untersucht. Es muss darauf hingewiesen werden, dass die Synthesen mittels einem „CEM discover S-Class“-Mikrowellenreaktor durchgeführt wurden und sind voll reproduzierbar. Die erhaltenen **[*n*]-OUs** wurden mittels EA, ATR-FTIR, XRD, ^{1}H und ^{13}C NMR analysiert. Der Polymerisationsgrad (DP) von Oligomeren wurde mittels ^{1}H NMR-Endgruppenanalyse ermittelt. Die thermischen Eigenschaften, die Stabilität und der

Kristallinitätsgrad der **[*n*]-OUs** wurden anhand TGA, DSC und XRD bestimmt. Ein Zersetzungspunkt aller getesteten Oligomere beim 50% Massenverlust (T_{d50}) wurde bei ca. 350 ºC beobachtet. CO_2-Absorptionskapazitäten wurden bei 35.0 ºC, 1.0 bar durch gravimetrische Analyse bestimmt. Dabei stellte sich heraus, dass **[*10*]-OU** über die höchste Absorptionskapazität für zwei unterschiedlichen Aktivierungstemperaturen mit einer maximalen Gleichgewichtssorption von 18.90 $mg_{CO2}/g_{sorbent}$ für 60.0 ºC und 22.70 $mg_{CO2}/g_{sorbent}$ für 100.0 ºC verfügt. Der prinzipielle Mechanismus für Kohlendioxidbindung ist die Chemosorption. Dies wurde durch eine Reihe der 13C CP-MAS NMR Experimente von **[*10*]-OU** mit $^{13}CO_2$ bewiesen. Das Experiment zeigte die Bildung von Bicarbonaten in der feuchten Umgebung als Ergebnis der Reaktion der aminterminierten Oligomere nach dem **1:1 Mechanismus**. Darüber hinaus, wie es aus hochdruck-thermogravimetrischen Analyse (HP-TGA) ersichtlich ist, wurden keine signifikanten Änderungen der Sorptionskapazität von **[*10*]-OU** als Funktion des Drucks beobachtet. Eine zyklische CO_2 Sorption/Desorption-Messung wurde für die Abschätzung der Recyclingfähigkeit von **[*10*]-OU** eingesetzt. Nach der Aktivierung der Probe bei 60.0 ºC und 100.0 ºC wurden mindestens drei stabile Sorptionszyklen erreicht. Der Unterschied zwischen dem ersten Initiierungszyklus und weiteren Sorptionszyklen lässt sich durch die Abwesenheit des Wassers in der Umgebung erklären. Die wasserfreien Bedingungen begünstigen die Bildung der Carbamate und bestimmen somit den Sorptionsprozess durch einen **1:2 Mechanismus**. Außerdem wurde eine thermisch induzierte Urethandegradation **[*10*]-OU** während der Aktivierung bei 100.0 ºC durch ATR-FTIR, TGA-MS, sowie 13C CP-MAS Festkörper-NMR Techniken nachgewiesen. Diese Zersetzung erhöht die Sorptionskapazität des Sorbers und begünstigt dadurch die CO_2 Sorption.

Anhand der gründlichen Literaturrecherche lässt sich behaupten, dass die von uns entwickelte Herstellung von **[*n*]-OUs** die umweltfreundlichste Synthesealternative darstellt. Diese Methode erschließt die Möglichkeit Polyharnstoffe durch eine nachhaltige Nutzung der erneuerbaren biologischen Rohstoffe zu erhalten.

Chapter 7

CONCLUSION AND OUTLOOK

7 CONCLUSION AND OUTLOOK

In this humbled work, an eco-friendly approach for the synthesis of [*n*]-oligourea, **[*n*]-OU; n = 4, 6, 7, 10, 12)** was proposed. The method had the following merits: it follows an isocyanate-free, phosgene-free, organocatalyzed, microwave-assisted, solvent-free synthesis. As an outlook for the current work proposed in the thesis, much more chemisorption can be enhanced by increasing the amino groups which can be introduced in the backbone itself. The method was optimized following a dynamic-power mode, using HMDA as a representative candidate for the family produced (Organocatalysts used, catalyst loading (mol%), power (W), temperature (ºC), and time (min)). Further, it was studied as a function of power, and time in the fixed mode. After optimization, the other members of the **[*n*]-OUs** were synthesized in the same fashion. These materials were fully analyzed and characterized in solution and solid-state analyses, *viz.*, 1H, and 13C NMR, EA, ATR-FTIR. Thermal properties and stabilities were characterized using TGA, and DSC, the latter was used to determine % crystallinity relative to a urea as a standard. Along with DSC, XRD was used to confirm crystallinity present in the **[*n*]-OUs**. CO_2-sorption experiments were carried out at 35.0 ºC, and 1.0 bar. Prior to sorption, the materials were activated either at 60.0 ºC or 100.0 ºC (*under vacuum*). Among the whole homologous series, **[*10*]-OU** was the most active in CO_2 sorption. The sorption was much better attained at the latter temperature due to an *in-situ* CO_2 capture as a result of generation of a new amino group due to backbiting of the urethane end group and forming PC. The **[*10*]-OU** was further tested at different sorption temperatures, *viz.*, 35.0, 65.0, and 95.0 ºC. Further testing included the stability of sorption/desorption cycles at both 60.0 ºC or 100.0 ºC temperatures. It was shown that the active species in CO_2-sorption was bicarbonate following a thorough ^{13}C CP-MAS NMR study. On the one hand, At 60.0 ºC, the material was partially activated, water was not taken out till the second cycle was applied, and that is why it followed **1:1 mechanism**. On the other hand, the second, third, and fourth cycles formed with equivalent, half-sorbed values of the first cycle are attributed to elimination of water out of the system (dry conditions). Therefore, carbamates would be formed due to a **1:2 mechanism**.

For the Task specific ionic liquids (TSILs), the new synthetic route for the brominated TSIL made a new perspective towards the ease of the synthesis of these interesting molecules to be used as templates or co-monomers. This can be utilized to capture CO_2 in a polymeric material

rather than its monomeric form to overcome problems associated with viscosity. Therefore, other alternative pathways for the synthesis of poly(ionic liquids) (PILs) using solvents to allow the diffusion of the highly viscous TSIL towards the carbonylating agent to produce PILs were thought of to overcome those limitations.

Still to do by concluding this work, is to increase the chemisorption values for the produced family throughout the functionalization of the [*n*]-diamines forming functionalized co-oligomers, or simply by mixing with previous diamines b by forming either random or even more organized alternating *ter*-oligomer. Expectedly, the latter would be much more efficient by forming an ordered structure which might be a good tool to diffuse CO_2 effectively. This can be done when multiple secondary or tertiary amines can be introduced when choosing the primary diamines, chosen examples are reported (*vide infra*, Figure 7.1).

On the other hand, more ^{15}N CP-MAS NMR solid-state studies can be carried out to clarify more on the chemistry of CO_2 and amine-based sorbent. In the literature, there has been only one study that was published in 1999.[149]

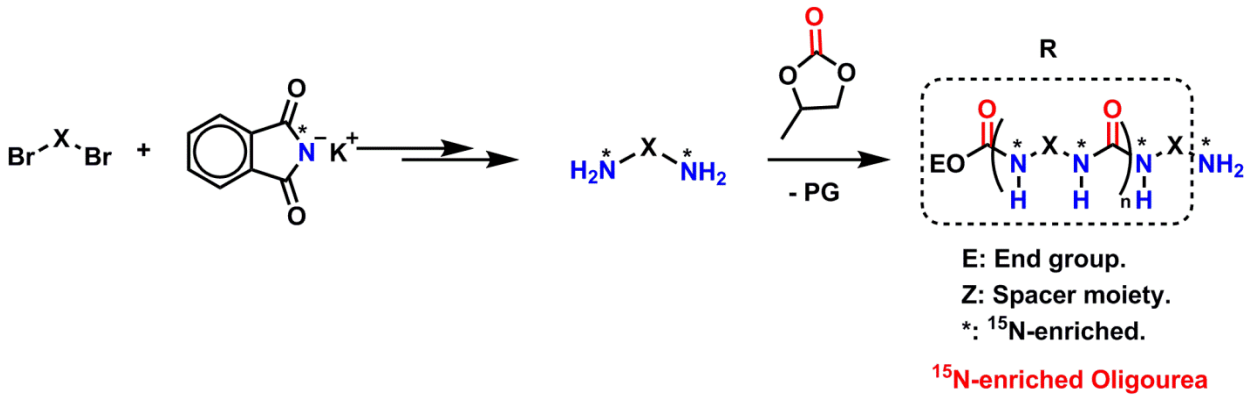

Scheme 7.1. ^{15}N-labeling experimnets for the synthesis of labeled-amines, X = -$(CH_2)_m$-

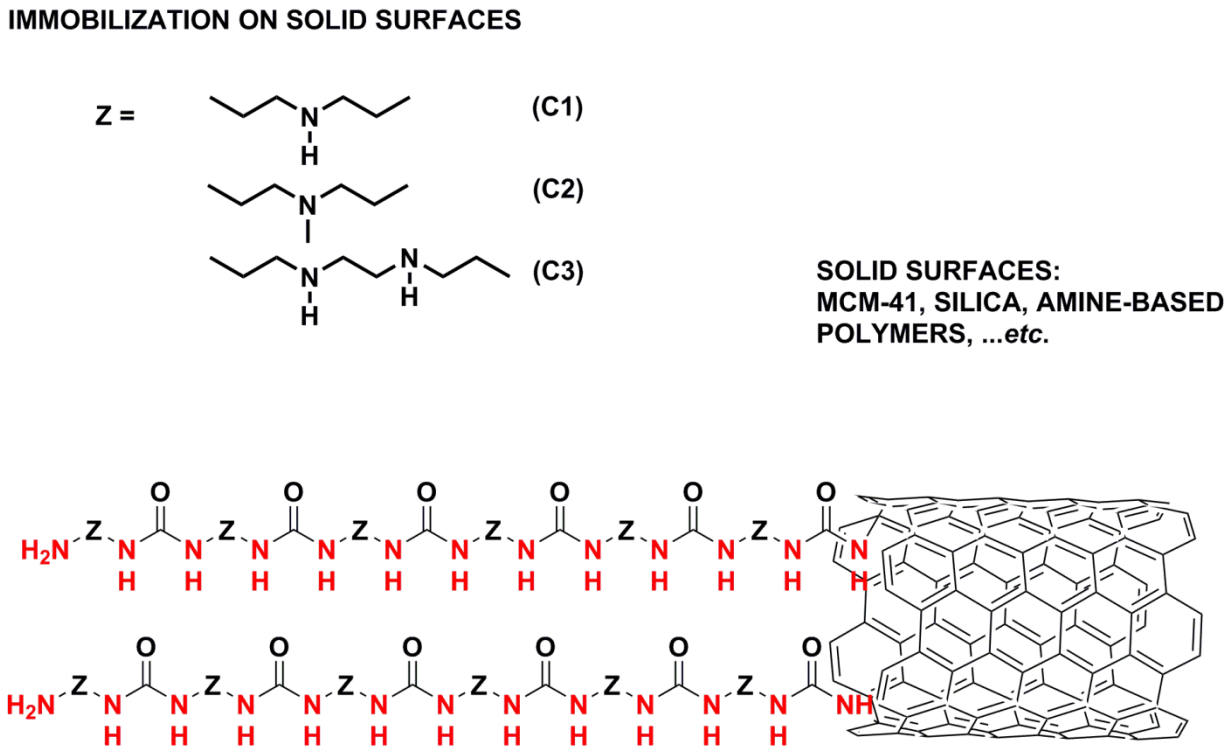

Figure 7.1. Immobilization of functionalized oligourea over solids and their use as solid sorbents as a proposed future work.

Urea introduction can be a good reason for increasing the chemical stability towards other routes for impregnation under post-combustion conditions. The extra stability is governed by the extensive H-bonding network that can be formed along the urea.

Chapter 8

REFERENCES

8 REFERENCES

[1] G. A. Olah, G. K. S. Prakash, and A. Goeppert. *J. Am. Chem. Soc.,* **2011**, *133*, 12881-12898.

[2] R. S. Haszeldine. *Science*, **2009**, *325*, 1647-1652.

[3] F. M. Orr, Jr. Science, *Science*, **2009**, *325*, 1656-1658.

[4] R. K. Pachauri, A. Reisinger. IPCC Fourth Assessment Report, Intergovernmental Panel on Climate Change, **2007**.

[5] M. Aresta, A. Dibenedetto, and A. Angelini. *Chem. Rev.*, **2014**, *114*, 1709-1742.

[6] M. R. Allen, D. J. Frame, C. Huntingford, C. D. Jones, J. A. Lowe, M. Meinshausen, and N. Meinshausen. *Nature*, **2009**, *458*, 1163-1166.

[7] P. Luis, T. V. Gerven, and B. V. Bruggen. *Prog. Energy Combust. Sci.*, **2012**, *38*, 419-448.

[8] C. Stewart and M. A. Hessami. *Energy Convers. Manage.*, **2005**, *46*, 403-420.

[9] **(a)** D. Keith, *Science*, **2009**, *325*, 1654-1655. **(b)** A. J. Hunt, E. H. K. Sin, R. Marriott, and J. H. Clark, *ChemSusChem*, **2009**, *3*, 306-322.

[10] M. Pera-Titus. *Chem. Rev.*, **2014**, *114*, 1413-1492.

[11] R. J. Allam, R. Bredesen, and E. Drioli, Carbon Dioxide Separation Technologies. *In* "Carbon Dioxide Recovery and Utilization", M. Aresta (*Ed.*), Kluwer Academic Publishers: Dordrecht, the Netherlands, **2003**.

[12] K. Sumida, D. L. Rogow, J. A. Mason, T. M. McDonald, E. D. Bloch, Z. R. Herm, T.-H. Bae, and J. R. Long. *Chem. Rev.*, **2012**, *112*, 724-781.

[13] E. J. Granite and H. W. Pennline, *Ind. Eng. Chem. Res.*, **2002**, *41*, 5470-5476.

[14] A. Goeppert, M. Czaun, G. K. Prakash, and G. A. Olah. *Energy & Environ. Sci.*, **2012**, *5*, 7833-7853.

[15] R. R. Bottoms, US 1783901, (Girdler Corp.), 1930.

[16] J. D. Figueroa, T. Fout, S. Plasynski, H. McIlvried, and R. D. Srivastava. *Int. J. Greenhouse Gas Control*, **2008**, *2*, 9-20.

[17] G. T. Rochelle. *Science*, **2009**, *325*, 1652-1654.

[18] M. Abu-Khader. *Energy Sources, A*, **2006**, *28*, 1261-1279.

[19] A. L. Kohl, and R. Nielsen, Gas Purification, *5th ed.*, Gulf Publishing Company, Houston, TX, USA, **1997**.

[20] W. Li, B. S. Turk, S. K. Gangwal, T. O. Nelson, R. P. Gupta, S. Park, and S. Tamhankar. **2005**. High temperature carbon dioxide removal from syngas using lithium silicate-based sorbents. *In*: Proceedings of the 22nd International Pittsburgh Coal Conference, Pittsburgh, PA.

[21] Vattenfall's Project on carbon capture and sequestration (CCS), (oxyfuel-process), http://corporate.vattenfall.com/Global/corporate/investors/interim_reports/2008/q3_report_2008.pdf. Accessed on June, 2014.

[22] A.-H. Liu, R. Ma, C. Song, Z.-Z. Yang, A. Yu, Y. Cai, L.-N. He, Y.-N. Zhao, B. Yu, and Q.-W. Song. *Angew. Chem. Int. Ed.*, **2012**, *51*, 11306-11310.

[23] N. V. Plechkova, R. D. Rogers, and K. R. Seddon. *ACS Symp. Ser.*, Washington DC, [*In*: *ACS Symp. Ser.*, **2009**; 1030], doi: 10.1021/bk-2009-1030.

[24] S. Gabriel and J. Weiner. *Ber.* **1888**, *21*, 2669-2679.

[25] H. L. Chum, V. R. Koch, L. L. Miller, and R. A. Osteryoung. *J. Am. Chem. Soc.*, **1975**, *97*, 3264-3265.

[26] J. S. Wilkes, J. A. Levisky, R. A. Wilson, and C. L. Hussey. *Inorg. Chem*., **1982**, *21*, 1263-1264.

[27] **(a)** P. Wasserscheid, and T. Welton. *Ionic Liquids in Synthesis*, Wiley-VCH, Weinheim **2003**. **(b)** H. Zhao, and S.V. Malhotra. *Aldrichimica Act*a, **2002**, *35*, 75-83. **(c)** I. Kimaru, Ionic Liquids - An Odyssey, G. I. T. Lab. J., 9-10/**2011**, 13-17. *Accessed online: April, 2014*.

[28] N. V. Plechkova and K. R. Seddon. *Chem. Soc. Rev.*, **2008**, *37*, 123-150.

[29] G. W. Meindersma, M. Maase, and A. B. De Haan, "Ionic Liquids" *Ullmann's Encyclopedia of Industrial Chemistry*, **2007**, Wiley-VCH, Weinheim, DOI: 10.1002/14356007.l14 l01.

[30] T. Welton. *Coord. Chem. Rev.*, **2004**, *248*, 2459-2477.

[31] K. P. Doyle, C. M. Lang, K. Kim, and P. A. Kohl. *J. Electrochem. Soc.*, **2006**, *153*, A1351-A1357.

[32] **(a)** A. Berthod, M. J. Ruiz-Angel, and S. Carda-Broch. *J. Chromatogr. A.* **2008**, *1184*, 6-18. **(b)** S. Chun, S. V. Dzyuba, and R. A. Bartsch. *Anal. Chem.* **2001**, *73*, 3737-3741. **(c)** M.-C. Tseng, M.-J. Tseng, and Y.-H. Chu. *Chem. Commun.* **2009**, 7503-7505.

[33] D. W. Armstrong, L. Zhang, L. He, and M. L. Gross. *Anal. Chem.*, **2001**, *73*, 3679-3686.

[34] S. Liangliang, T. Dingyin, H. Bin, M. Junfeng, Z. Guijie, L. Zhen, S. Yichu, Z. Lihua, and Z. Yukui. *Anal. Bioanal. Chem.*, **2011**, *399*, 3387-3397.

[35] P. Sun, and D. W. Armstrong. *Anal. Chim. Acta*, **2010**, *661*, 1-16.

[36] S. Supasitmongkol and P. Styring. *Energy & Environ. Sci.*, **2010**, *3*, 1961-1972.

[37] J. Bara, D. Camper, D. L. Gin, and R. D. Noble. *Acc. Chem. Res.*, **2010**, *43*, 152-159.

[38] L. M. Sánchez, G. W. Meindersma, and A. B. de Haan. *Chem. Eng. J.*, **2011**, *166*, 1104-1115.

[39] Z. Zhang, S. Hu, J. Song, W. Li, G. Yang, and B. Han. *ChemSusChem*, **2009**, *2*, 234-238.

[40] P. M. Dean, J. M. Pringle, and D. R. MacFarlane. *Phys. Chem.*, **2010**, *12*, 9144-9153.

[41] **(a)** T. Welton. *Chem. Rev.*, **1999**, *99*, 2071-2083. **(b)** G. Fitzwater, W. Geissler, R. Moulton, N. V. Plechkowa, A. Robertson, K. R. Seddon, J. Swindall, and K. Wan Joo, Ionic liquids: sources of innovation, Report Q002, QUILL, Belfast, **2005**.

[42] **(a)** R. D. Rogers, and K. R. Seddon. *ACS Symp. Ser.*, **2003,** *856*. **(b)** R. D. Rogers, and K. R. Seddon, (*Ed.*), Ionic Liquids IIIB: Fundamentals, Progress, Challenges, and Opportunities: Transformations and Processes. *ACS Symp. Ser.*, **2005,** *902*. **(c)** R. D. Rogers, K. R. Seddon, and S. Volkov. Green Industrial Applications of Ionic Liquids. *NATO Science Series*. **2002**, *92*, Kluwer Academic Publishers, Netherlands.

[43] J. H. Davis Jr., and K. J. Forrester. *Tetrahedron Lett.*, **1999**, *40*, 1621-1622.

[44] J. H. Davis Jr., *Chem. Lett.* **2004**, *33*, 1072-1077.

[45] A. D. Sawant, D. G. Raut, N. B. Darvatkar, and M. M. Salunkhe. *Green Chem. Lett. Rev.*, **2011**, *4*, 41-54.

[46] E. D. Bates, R. D. Mayton, I. Ntai, and J. H. Davis. *J. Am. Chem. Soc.*, **2002**, *124*, 926-927.

[47] **(a)** L. A. Blanchard, D. Hancu, E. J. Beckman, and J. F. Brennecke, *Nature*, **1999**, *399*, 28-31. **(b)** L. A. Blanchard, Z. Gu, and J. F. Brennecke. *J. Phys. Chem. B*, **2001**, *105*, 2437-2344.

[48] J. M. Zhang, S. J. Zhang, K. Dong, Y. Q. Zhang, Y. Q. Shen, and X. M. Lv. *Chem.-Eur. J.*, **2006**, *12*, 4021-4026.

[49] Y. Zhang, S. Zhang, X. Lu, Q. Zhou, W. Fan, and X. Zhang. *Chem.- Eur. J.*, **2009**, *15*, 3003-3011.

[50] C. Wang, S. M. Mahurin, H. Luo, G. A. Baker, H. Li, and S. Dai. *Green Chem.*, **2010**, *12*, 870-874.

[51] Z. Xue, Z. Zhang, J. Han, Y. Chen, and T. Mu. *Int. J. Greenhouse Gas Control*, **2011**, *5*, 628-633.

[52] Z.-Z. Yang, Y.-N. Zhao, and L.-N. He. *RSC Adv.*, **2011**, *1*, 545-567.

[53] X. Zhang, X. Zhang, H. Dong, Z. Zhao, S. Zhang, and Y Huang. *Energy Environ. Sci.*, **2012**, *5*, 6668-6681.

[54] S. Hanioka, T. Maruyama, T. Sotani, M. Teramoto, H. Matsuyama, K. Nakashima, M. Hanaki, F. Kubota, and M. Goto. *J. Membr. Sci.*, **2008**, *314*, 1-4.

[55] **(a)** O. Green, S. Grubjesic, S. Lee, and M. A. Firestone. *Polym. Rev.*, **2009**, *49*, 339-360. **(b)** J. Lu, F. Yan, and J. Texter. *Prog. Polym. Sci.*, **2009**, *34*, 431-448. **(c)** D. Mecerreyes. *Prog. Polym. Sci.*, **2011**, *36*, 1629-1648. **(d)** J. Yuan, and M. Antonietti. *Polymer*, **2011**, *52*, 1469-1482. **(e)** M. D. Green, and T. E. Long. *Polym. Rev.*, **2009**, *49*, 291-314. (**e**) J. Yuan, and M. Antonietti. *Prog. Polym. Sci.*, **2013**, *38*, 1009-1036.

[56] M. F. Hoover. *J. Macromol. Sci.-Chem.*, **1970**, *4*, 1327-1418.

[57] Y. B. Xiong, H. Wang, Y. J. Wang, and R. M. Wang. *Polym. Adv. Technol.*, **2011**, *23*, 835-840.

[58] J. Yuan, H. Schlaad, C. Giordano, and M. Antonietti. *Europ. Polym. J.*, **2011**, *47*, 772-781.

[59] X. He, W. Yang, and X. Pei. *Macromolecules*, **2008**, *41*, 4615-4621.

[60] W. Li, J. Fang, M. Lv, C. Chen, X. Chi, Y. Yang, and Y. Zhang. *J. Mater. Chem.*, **2011**, *21*, 11340-11346.

[61] Y. Zhang, X. Chen, J. Lan, J. You, and L. Chen. *Chem. Bio. Drug Des.*, **2009**, *74*, 282-288.

[62] J. Tang, H. Tang, W. Sun, M. Radosz, Y. Shen. *J. Polym. Sci. A: Polym. Chem.*, **2005**, *43*, 5477-5489.

[63] J. Tang, H. Tang, W. Sun, H. Plancher, M. Radosz, and Y. Shen. *Chem. Commun.*, **2005**, 3325-3327.

[64] R. Gedye, F. Smith, K. Westaway, H. Ali, L. Baldisera, L. Laberge, and J. Rousell. *Tetrahedron Lett.*, **1986**, *27*, 279-282.

[65] A. de la Hoz, A, Diaz-Ortiz, and A. Moreno. *Chem. Soc. Rev.*, **2005**, *34*, 164-178, and references therein.

[66] P. Lidström, J. Tierney, B. Wathey, and J. Westman. *Tet. Lett.*, **2001**, *57*, 9225-9283.

[67] M. Baghbanzadeh, L. Carbone, P. D. Cozzoli, and C. O. Kappe. *Angew. Chem. Int. Ed.*, **2011**, *50*, 11312-11359.

[68] (**a**) D. Bogdal, P. Penczek, J. Pielichowski, and A. Prociak. *Adv. Polym. Sci.*, **2003**, *163*, 193-263. (**b**) L. Zong, S. Zhou, N. Sgriccia, M. C. Hawley, and L. C. Kempel. *J. Micro. Pow. Electromag. Rad.*, **2003**, *38*, 49-74.

[69] For more reviews see: (**a**) C. Ebner, T. Bodner, F. Stelzer, and F. Wiesbrock. *Macromol. Rapid Commun.*, **2011**, *32*, 254-288. (**b**) S. Mallakpour, and Z. Rafiee. *Iran. Polym. J.*, **2008**, *17*, 907-935.

[70] C. O. Kappe, D. Dallinger, and S. S. Murphree, Practical microwave synthesis for organic chemists: Strategies, instruments and protocols, Weinheim, Wiley-VCH, **2009**.

[71] M. I. Malik, B. Trathnigg, and C. O. Kappe. *Macromol. Chem. Phys.*, **2007**, *208*, 2510-2524.

[72] C. O. Kappe. *Angew. Chem. Int. Ed.*, **2004**, *43*, 6250-6284.

[73] A. Banihashemi, H. Hazarkhani, and A. Abdolmaleki. *J. Pol. Sci. A: Polym. Chem.*, **2004**, *42*, 2106-2111.

[74] P. D. Vaidya, and E. Y. Kenig. *Chem. Eng. Technol.*, **2007**, *30*, 1467-1474.

[75] A. Dibenedetto, M. Aresta, C. Fragale, and M. Narracci. *Green Chem.*, **2002**, *4*, 439-443.

[76] D. M. D'Alessandro, B. Smit, and J. R. Long. *Angew. Chem. Int. Ed.*, **2010**, *49*, 6058-6082.

[77] X. Xu, Ch. Song, J. M. Andresen, B. G. Miller, and A. W. Scaroni. *Energy & Fuels*, **2002**, *16*, 1463-1469.

[78] C. Pevida, C. E. Snape, and T. C. Drage. *Energy Proced.*, **2009**, *1*, 869-874.

[79] A. Brunettia, F. Scuraa, G. Barbieria, E. Drioli. *J. Mem. Sci.*, **2010**, *359*, 115-125.

[80] N. Du, H. Bum Park, M. M. Dal-Cin, and M. D. Guiver. *Energy Environ. Sci.*, **2012**, *5*, 7306-7322.

[81] S. Choi, J. H. Drese, and C. W. Jones. *ChemSusChem*, **2009**, *2*, 796-854.

[82] B. Li, Y. Duan, D. Luebke, and B. Morreale. *Appl. Energy*, **2013**, *102*, 1439-1447.

[83] J. Alauzun, E. Besson, A. Mehdi, C. Reyé, and R. J. P. Corriu. *J. Am. Chem. Soc.*, **2005**, *127*, 11204-11205.

[84] K. S. Walton, A. R. Millward, D. Dubbeldam, H. Frost, J. J. Low, O. M. Yaghi, and R. Q. Snurr. *J. Am. Chem. Soc.*, **2008**, *130*, 406-407.

[85] R. Dawson, A. I. Cooper, and D. J. Adam. *Polym. Int.*, **2013**, *62*, 345-352.

[86] N. D. Hutson. *Chem. Mater.*, **2004**, *16*, 4135-4143.

[87] D. P. Bezerra, R. S. Oliveira, R. S. Vieira, and C. L. Cavalcante Jr., D. C. S. Azevedo. *Adsorption*, **2011**, *17*, 235-246.

[88] Y. Yang, H. Li, S. Chen, Y. Zhao, and Q. Li. *Langmuir*, **2010**, *26*, 13897-13902.

[89] P. Li, B. Ge, S. Zhang, S. Chen, Q. Zhang, and Y. Zhao. *Langmuir*, **2008**, *24*, 6567-6574.

[90] H. Mark, and G. S. Whitby, (*Eds.*), "Collected Papers of Wallace Hume Carothers on High Polymeric Substances", Interscience Publishers, Inc., **1940**, New York.

[91] O. Bayer. *Angew. Chem.*, **1947**, *59A*, 257-288.

[92] P. Y. S. Lam, P. K. Jadhav. C. J. Eyermann, C. N. Hodge, Y, Ru. L. T. Bacheler, J. L. Meek, M. J. Otto, M. M. Rayner, Y. N. Wong, C.-H. Chang, P. C. Weber, D. A. Jackson, and T. R. Sharpe, S. Erickson-Viitanen. *Science*, **1994**, *263*, 380-384.

[93] C. I. Chiriac and F. Tanasã. In *Ullmann's Encyclop. Indust. Chem.*, **2012**, Wiley-VCH, Wienheim. DOI: 10.1002/ 14356007.d21_d01.

[94] **(a)** M. Sadeghi, M. A. Semsarzadeh, M. Barikani, and B. Ghalei. *J. Memb. Sci.*, **2010**, *354*, 40-47. **(b)** H. Li, B. D. Freeman, and O. M. Ekiner. *J. Memb. Sci.*, **2011**, *369*, 49-58.

[95] **(a)** B. J. Habgood, D. A. Harper, and R. J. W. Reynolds. *GB* 580524, (Imperial College Corp.), **1946**. **(b)** E. L. Wittbecker, *US* 2816879, (Dupont Corp.), **1957**.

[96] N. Chau, M. Uatanabe, and Y. J. Iwakura. *Polym. Sci. Polym. Chem. Ed.*, **1981**, *19*, 1279-1282.

[97] S. Boileau, L. Bouteiller, F. Laupretre, and F. Lortie. *New J. Chem.*, **2000**, *24*, 845-848.

[98] **(a)** R. J. Cooter, *US* 3131167, (Union Carbide Corp.), **1964**. **(b)** *GB* 902134, (Union Carbide Corp.), **1962**.

[99] B. Bruchmann, J.-F. Stumbe, and E. Wagner. *US* 7645855, (BASF Aktiengesellschaft, DE). **2005**.

[100] H.-J. Knolker, T. Braxmeier and G. Schlechtingen, *Angew. Chem., Int. Ed.*, **1995**, *34*, 2497-2500.

[101] N. Yamazaki, F. Higashi, and T. Iguchi. *Polym. Lett. Ed.*, **1974**, *12*, 517-521.

[102] C. Wu, J. Wang, P. Chang, H. Cheng, Y. Yu, Z. Wu, D. Dong, and F. Zhao. *Phys. Chem. Chem. Phys.*, **2012**, *14*, 464-468.

[103] **(a)** J. S. Nowick. *Acc. Chem. Res.*, **1999**, *32*, 287-296. **(b)** V. Semetey, D. Rognan, C. Hemmerlin, R. Graff, J.-P. Briand, M. Marraud, and G. Guichard. *Angew. Chem. Int. Ed.*, **2002**, *41*, 1893-1895. **(c)** C. Aisenbrey, N. Pendem, G. Guichard, and B. Bechinger, *Org. Biomol. Chem.*, **2012**, *10*, 1440-1447. **(d)** J. Fremaux, L. Fischer, T. Arbogast, B. Kauffmann, and G. Guichard. *Angew. Chem. Int. Ed.*, **2011**, *50*, 11382-11385. **(e)** K. Burgess, J. Ibarzo, D. S. Linthicum, D. H. Russell, H. Shin, A. Shitangkoon, R. Totani, and A. J. Zhang. *J. Am. Chem. Soc.*, **1997**, *119*, 1556-1564. **(f)** K. Burgess, D. S. Linthicum, and H. W. Shin. *Angew. Chem., Int. Ed.*, **1995**, *34*, 907-909.

[104] **(a)** M. Aresta (*Ed.*), *Carbon Dioxide as Chemical Feedstock*, Wiley-VCH, Weinheim, **2010**, and references therein. **(b)** J. Clements. *Ind. Eng. Chem. Res.*, **2003**, *42*, 663-674.

[105] Y. Xie, Z. Zhang, T. Jiang, J. He, B. Han, T. Wu, and K. Ding. *Angew. Chem. Int. Ed.*, **2007**, *46*, 7255-7258.

[106] D. Enders, O. Niemeier, and A. Henseler. *Chem. Rev.*, **2007**, *107*, 5606-5655, and references therein.

[107] M. M. Guchok, V. M. Guchok, and V. K. Mazalov. [Abstract] *Kriobiolog. Kriomed.*, **1981**, *9*, 36-43.

[108] J. Shang, S. Liu, X. Ma, L. Lu, and Y. Deng. *Green Chem.*, **2012**, *14*, 2899-2906.

[109] P. R. Edwards, J. R. Hiscock, and P. A. Gale. *Tetrahedron Lett.*, **2009**, *50*, 4922-4924.

[110] P. R. Edwards, J. R. Hiscock, P. A. Gale, and M. E. Light. *Org. Biomol. Chem.*, **2010**, *8*, 100-106.

[111] N. Busschaert, P. A. Gale, C. J. E. Haynes, M. E. Light, S. J. Moore, C. C. Tong, J. T. Davis, and J. W. A. Harrell. *Chem. Commun.*, **2010**, *46*, 6252-6254.

[112] S. K. Dey, Chutia, and R. G. Das. *Inorg. Chem.*, **2012**, *51*, 1727-1738.

[113] P. Bose, R. Dutta, S. Santra, B. Chowdhury, and P. Ghosh. *Eur. J. Inorg. Chem.*, **2012**, 5791-5801.

[114] I. Ravikumar and P. Ghosh. *Chem. Commun.*, **2010**, *46*, 1082-1084.

[115] A. Pramanik, M. E. Khansari, D. R. Powell, F. R. Fronczek, and M. A. Hossain. *Org. Lett.*, **2014**, *16*, 366-369.

[116] S.-Y. Moon, E. Jeon, J.-S. Bae, M. Byeon, and J.-W. Park. *Polym. Chem.*, **2014**, *5*, 1124-1131.

[117] B. E. Gurkan, J. C. de la Fuente, Elaine M. Mindrup, L. E. Ficke, B. F. Goodrich, E. A. Price, W. F. Schneider, and J. F. Brennecke. *J. Am. Chem. Soc.*, **2010**, *132*, 2116-2117.

[118] W. A. Eger, A. Genest, B. Rieger, N. Roesch. *ChemSusChem*, **2012**, 5, 1967-1973.

[119] A. K. Qaroush, A. S. Al-Hamayda, Y. K. Khashman, S. I. Vagin, C. Troll, and B. Rieger, *Catal. Sci. Tech.*, **2013**, *3*, 2221-2226.

[120] C. Cadena, J. L. Anthony, J. K. Shah, T. I. Morrow, J. F. Brennecke, and E. J. Maginn. *J. Am. Chem. Soc.*, **2004**, *126*, 5300-5308.

[121] J. Yuan, D. Mecerreyes, and M. Antonietti. *Prog. Polym. Sci*., **2013**, *38*, 1009-1036.

[122] J. R. Harjani, T. Friščič, L. R. MacGillivray and R. D. Singer. *Dalton Trans.*, **2008**, 4595-4601.

[123] R. Tan, D. Yin, N. Yu, H. Zhao, and D. Yin. *J. Catal.*, **2009**, *263*, 284-291.

[124] P. Li, Q. Zhao, J. L. Anderson, S. Varanasi, And M. R. Coleman. *J. Polym. Sci. A: Polym. Chem.*, **2010**, *48*, 4036-4046.

[125] J. Zhang, C. Jia, H. Dong, J. Wang, X. Zhang, and S. Zhang. *Ind. Eng. Chem. Res.*, **2013**, *52*, 5835-5841.

[126] L. Ubaghs. PhD dissertation, RWTH Aachen University, **2005**.

[127] S.Y. Huang, J. Ma, J.P. Li, N. Zhao, W. Wei, and Y. H. Sun. *Catal. Commun.*, **2008**, *9*, 276-280.

[128] A. Huczynski and B. Brzezinski, *e-EROS Encyclo. of Reag. Org. Synt.*, John Wiley & Sons, Ltd, **2008**, DOI:10.1002/047084289X.rn00786.

[129] C. Oliver Kappe, D. Dallinger, and S. Shaun Murphree (*Ed.*), Practical Microwave Synthesis for Organic Chemists: Strategies, Instruments, and Protocols. **2009**, Wiley-VCH Verlag, Weinheim.

[130] M. Yasuji, H. Koji, and K. Masato. JP 06293727A19941021, **1994**.

[131] A. K. Qaroush, D. A. Castillo-Molina, C. Troll, M. A. Abu-Daabes, H. M. Alsyouri, A. S. Abu-Surrah, and B. Rieger. *ChemSusChem*, to be submitted.

[132] **(a)** K. K. Jena, D. K. Chattopadhyay, and K. V. S. N. Raju. *Europ. Polym. J.*, **2007**, *43*, 1825-1837. **(b)** A. K. Mishra, D. K. Chattopadhyay, B. Sreedhar, and K. V. S. N. Raju. *Prog. Org. Coat.*, **2006**, *55*, 231-243.

[133] D. Fernandes, W. Conway, R. Burns, G. Lawrance, M. Maeder, and G. Puxty. *J. Chem. Thermodynamics*, **2012**, *54*, 183-191.

[134] R. M. Silverstein, G. C. Bassler, and T. C. Morrill. Spectrometric identification of organic compounds, *5th Ed.*, **1991**, ISBN 0471634042, Wiley, New York.

[135] Degree of crystallinity was calculated relative to urea with an enthalpy of fusion of ΔH_{fus} = 135.0 J/g, which was considered to be 100% crystalline. For more detailed information, see: **(a)** B. Wunderlich, *Thermal Analysis of Polymeric Materials*, Springer-Verlag, **2005**. **(b)** I. Groves. T. Lever, and N. Hawkins of TA Instruments, Ltd. (UK), Thermal Analysis Application Brief. Determination of Polymer Crystallinity by DSC, TA-123A.

[136] P. Jackson, K. J. Fischer, M. I. Attalla. *J. Am. Soc. Mass Spectrom.*, **2011**, *22*, 1420-1431.

[137] A. K. Qaroush, D. A. Castillo-Molina, C. Troll, M. A. Abu-Daabes, H. M. Alsyouri, A. S. Abu-Surrah and B. Rieger. *ChemSusChem*, to be submitted.

[138] Spectral database for organic compounds, SDBS No.: 486. Accessed online: June, 2014. http://sdbs.db.aist.go.jp.eaccess.ub.tum.de/sdbs/cgi-bin/direct_frame_top.cgi

[139] L. Espinal, D. L. Poster, W. Wong-Ng, A. J. Allen, and M. L. Green. *Environ. Sci Tech.*, **2013**, *47*, 11960-11975.

[140] T. Tozawa, J. T. A. Jones, S. I. Swamy, S. Jiang, D. J. Adams, S. Shakespeare, R. Clowes, D. Bradshaw, T. Hasell, S. Y. Chong, C. Tang, S. Thompson, J. Parker, A. Trewin, J. Bacsa, A. M. Z. Slawin, A. Steiner, and A. I. Cooper. *Nat. Mater.*, **2009**, *8*, 973-978.

[141] A. Wilke, J. Yuan, M. Antonietti, and J. Weber. *ACS Macro Lett.*, **2012**, *1*, 1028-1031.

[142] T. Ben, C. Pei, D. Zhang, J. Xu, F. Deng, X. Jing, and S. Qiu. *Energy & Environ. Sci.*, **2011**, *4*, 3991-3999.

[143] R. Dawson, D. J. Adams, and A. I. Cooper. *Chem. Sci.*, **2011**, *2*, 1173-1177.

[144] X. Yang, S. Yao, M. Yu, and J.-X. Jiang. *Macromol. Rapid Commun*., **2014**, DOI: 10.1002/marc.201300864.

[145] E. I. Privalova, E. Karajalainen, M. Nurmi, P. Mäki-Arvela, K. Eränen, H. Tenhu, D. Y. Murzin, and J.-P. Mikkola. *ChemSusChem*, **2013**, *6*, 1500-1509.

[146] Y. Wu, D. Wang, L. Li, W. Yang, S. Feng, and H. Liu. *J. Mater. Chem. A*, **2014**, *2*, 2160-2167.

[147] J. Tang, H. Tang, W. Sun, H. Plancher, M. Radosz, and Y. Shen. *Chem. Commun.*, **2005**, 3325-3327.

[148] H. Y. Kim, and K. Oh. *Org. Lett.*, **2011**, *13* (6), 1306-1309.

[149] V. Schimming, C.-G. Hoelger, G. Buntkowsky, I. Sack, J.-H. Fuhrhop, S. Rocchetti, and H.-H. Limbach. *J. Am. Chem. Soc.*, **1999**, *121*, 4892-4893.